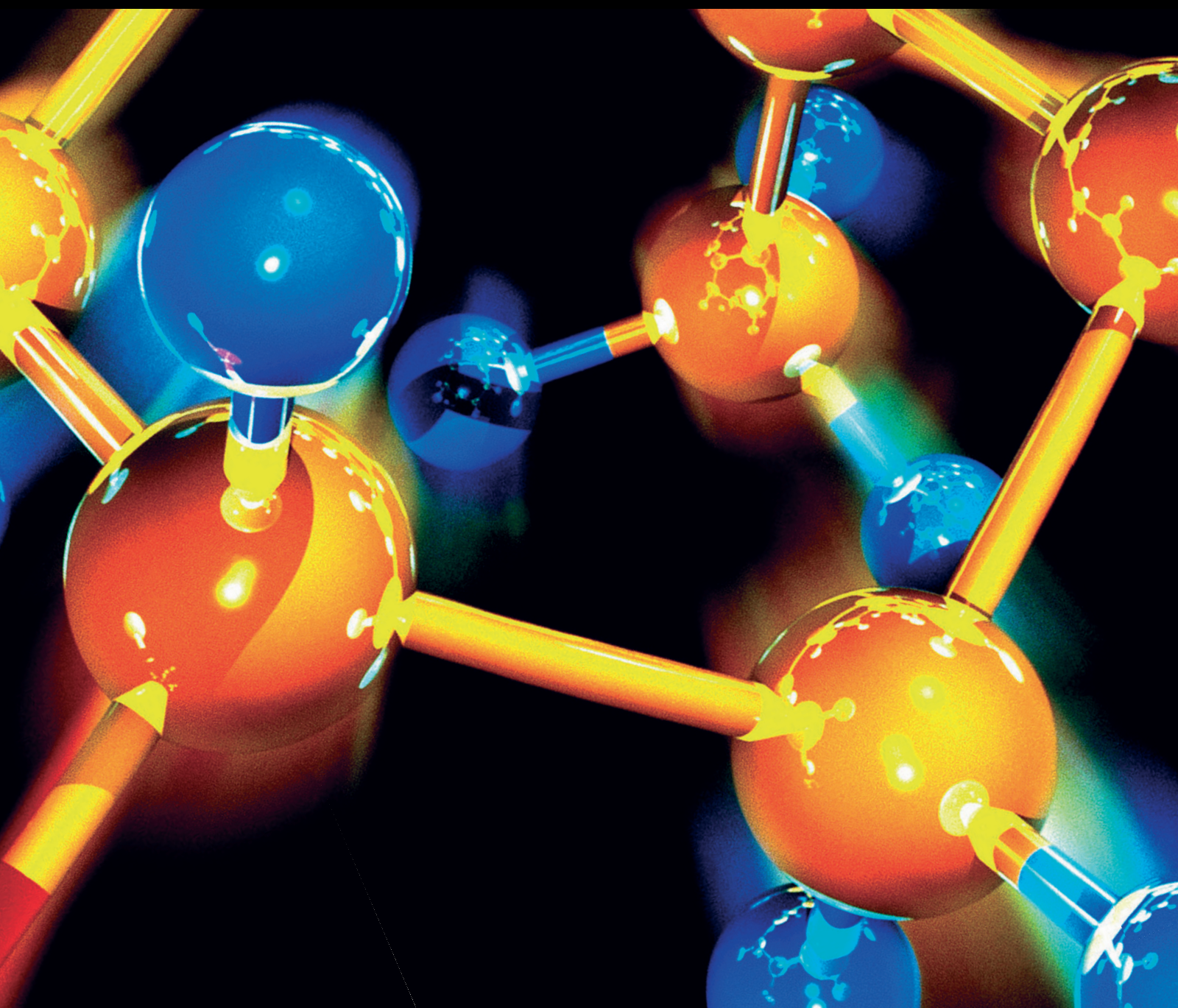


New Trends in Monitoring and Removing the Pollutants from Water

Lead Guest Editor: Alina Barbulescu

Guest Editors: Narcis Duteanu, Adina Negrea, and Makarand M. Ghangrekar





New Trends in Monitoring and Removing the Pollutants from Water

New Trends in Monitoring and Removing the Pollutants from Water

Lead Guest Editor: Alina Barbulescu

Guest Editors: Narcis Duteanu, Adina Negrea,
and Makarand M. Ghangrekar




Copyright © 2018 Hindawi. All rights reserved.



This is a special issue published in "Journal of Chemistry." All articles are open access articles distributed under the Creative Commons Attribution License, which permits unrestricted use, distribution, and reproduction in any medium, provided the original work is properly cited.

Contents



New Trends in Monitoring and Removing the Pollutants from Water

Alina Barbulescu , Narcis Duteanu, Adina Negrea, and Makarand M. Ghangrekar
Editorial (2 pages), Article ID 8394086, Volume 2018 (2018)


New Sustainable Biosorbent Based on Recycled Deoiled Carob Seeds: Optimization of Heavy Metals Remediation

M. Farnane, A. Machrouhi, A. Elhalil, M. Abdennouri, S. Qourzal, H. Tounsadi , and N. Barka 
Research Article (16 pages), Article ID 5748493, Volume 2018 (2018)


Atmospheric Nitrogen Deposition Associated with the Eutrophication of Taihu Lake

Xi Chen , Yan-hua Wang , Chun Ye, Wei Zhou, Zu-cong Cai, Hao Yang, and Xiao Han
Research Article (10 pages), Article ID 4017107, Volume 2018 (2018)



Spatial and Temporal Variations of Water Quality of Mateur Aquifer (Northeastern Tunisia): Suitability for Irrigation and Drinking Purposes

Besma Tlili-Zrelli , Moncef Gueddari, and Rachida Bouhlila
Research Article (15 pages), Article ID 2408632, Volume 2018 (2018)

Assessment of the Trophic Status of the South Lagoon of Tunis (Tunisia, Mediterranean Sea): Geochemical and Statistical Approaches

Myriam Abidi , Rim Ben Amor, and Moncef Gueddari
Research Article (17 pages), Article ID 9859546, Volume 2018 (2018)


Removal of Colored Organic Pollutants from Wastewaters by Magnetite/Carbon Nanocomposites: Single and Binary Systems

Simona Gabriela Muntean , Maria Andreea Nistor, Eliza Muntean , Anamaria Todea, Robert Ianoş, and Cornelia Păcurariu
Research Article (16 pages), Article ID 6249821, Volume 2018 (2018)

Water Pollution and Water Quality Assessment of Major Transboundary Rivers from Banat (Romania)

Andreea-Mihaela Dunca 
Research Article (8 pages), Article ID 9073763, Volume 2018 (2018)

Impact Assessment of Phosphogypsum Leachate on Groundwater of Sfax-Agareb (Southeast of Tunisia): Using Geochemical and Isotopic Investigation

Samira Melki  and Moncef Gueddari
Research Article (10 pages), Article ID 2721752, Volume 2018 (2018)

Editorial

New Trends in Monitoring and Removing the Pollutants from Water

Alina Barbulescu¹ ,¹ Narcis Duteanu,² Adina Negrea,² and Makarand M. Ghangrekar³

¹*Ovidius University of Constanta, Constanta, Romania*

²*Politehnica University of Timisoara, Timisoara, Romania*

³*Indian Institute of Technology, Kharagpur, India*

Correspondence should be addressed to Alina Barbulescu; emma.barbulescu@yahoo.com

Received 24 October 2018; Accepted 5 December 2018; Published 30 December 2018

Copyright © 2018 Alina Barbulescu et al. This is an open access article distributed under the Creative Commons Attribution License, which permits unrestricted use, distribution, and reproduction in any medium, provided the original work is properly cited.

The objectives of this special issue were to address new trends in monitoring and removing the pollutants from water by different electrochemical and biological methods, as well as modelling the process of the adsorption of these pollutants from aqueous solutions. Twenty articles were submitted, and after the peer review process, seven papers were selected for inclusion in the present special issue.

This special issue is a complex one because some of the published papers are dealing with the monitoring of water quality and the other part of the published articles cover the preparation and utilisation of cheap and environmental friendly materials for removal of different pollutants. We believe that the research papers published in this special issue highlight the important topics represented by water quality monitoring by removal of different pollutants by using cheap, cost effective, and environmental friendly adsorbents, presenting the latest advances into the field.

The article by M. Farnane et al., entitled “New sustainable biosorbent based on recycled deoiled carob seeds: Optimization of heavy metals remediation” presents the development and usage of a new and efficient bioadsorbent” is dealing with the production and testing of new bioadsorbent materials. This new adsorbent was prepared by using deoiled carob seeds, an agroindustry waste. Prepared adsorbent was used for removal of cadmium and cobalt ions from aqueous solutions in order to obtain the optimum conditions for removal of these ions. Optimal conditions for the removal of studied ions were represented by using 0.1 g of adsorbent for 1 L of solution with an initial metal concentration of 50 mg·L⁻¹. Process optimisation was

possible by using the full-factorial experimental design. It was found that the adsorption capacity of the produced adsorbent can be improved by treating carob seeds with sodium hydroxide.

The article by X. Chen et al., entitled “Atmospheric nitrogen deposition associated with the eutrophication of Taihu Lake” is presenting the results regarding the effect of excessive amount of nitrogen deposition and its contribution to water eutrophication in Taihu basin. Comparing the data with those collected in 2007, it was observed that the contribution of nitrogen deposition to Taihu Lake increased in the last period. Accordingly, this phenomenon can accelerate the eutrophication process of Taihu Lake.

The article entitled “Spatial and temporal variations of water quality of Mateur aquifer (Northeastern Tunisia): Suitability for irrigation and drinking purposes” by B. Tlili-Zrelli et al. present the spatial and temporal variations of the hydrochemical characteristics of Mateur aquifer groundwater, which represent a critical water resource in the northeast of Tunisia. The aquifer study is important due to the water quality deterioration provoked by the salinization and the augmentation of the nitrate contamination. Experimental study shows that the highest water quality was found in the northwest and southeast part of the aquifer, areas corresponding to the recharge zone. Also, the raining season have a little influence on water quality, mainly due to the dilution.

The article entitled “Assessment of the trophic status of the South Lagoon of Tunis (Tunisia, Mediterranean Sea): Geochemical and statistical approaches” by M. Abidi et al. is

presenting the water quality on South Lagoon of Tunis after its restoration. This lagoon had during time severe environmental quality issues. To solve these problems, a large restoration project was conducted. During this process, the sediments were dredged, leading at an improvement of water circulation by removing the areas of water stagnation. Experimental results have shown the high level of nutrients due to the natural and anthropogenic factors. So, the lagoon remains eutrophic, presenting a poor water quality and requiring a serious intervention.

The article entitled "Removal of colored organic pollutants from wastewaters by magnetite/carbon nanocomposites: Single and binary systems" by S. G. Muntean et al. is presenting the development of a methodology for the selective removal of industrial dyes from wastewaters by using an adsorption technology based on magnetic adsorbents. Magnetic nanoparticles embedded with activated carbon matrix were tested as adsorbents for industrial dyes removal from aqueous solutions. The regeneration capacity of adsorbent materials was tested by performing seven adsorption/desorption cycles. These materials represent a viable alternative by considering the low-cost characteristics of the synthesis, higher efficiency for the magnetic separation, and higher stability and reusability.

The article entitled "Water pollution and water quality assessment of major transboundary rivers from Banat (Romania)" by A.-M. Dunca is focused on the water management on the Timiș-Bega hydrographical basin. To assess the water quality, the water quality index was computed by taking in account the maximum, minimum, and the average annual values of physical, chemical, and biological parameters. For protecting and preserving the water quality, especially of Banat transboundary rivers, it is necessary to implement adequate wastewater management, through the construction of modern and efficient waste water treatment plants.

The article entitled "Impact assessment of phosphogypsum leachate on groundwater of Sfax-Agareb (southeast of Tunisia): Using geochemical and isotopic investigation" by S. Melki and M. Gueddari reports the results of the spatiotemporal variation of the conductivity and concentrations of major elements on groundwater of Sfax-Agareb (Southeast of Tunisia), for the period October 2013 and October 2014. It was shown that contents of ^{18}O and ^2H showed that the water of the Sfax-Agareb aquifer undergoes a large-scale evaporation process originated from recent rainfall. Experimental data proved that the groundwater was deteriorated in the downstream part of the Sfax-Agareb aquifer. The study will be helpful for the proper water development and for applying the proper remediation strategies to reduce the pollution.

Conflicts of Interest

The Guest Editor and Guest Co-editors declare that there are no conflicts of interest or agreements with private companies that will prevent us working impartially in the editorial process.

Acknowledgments

The editors thank all the authors for their contributions.

*Alina Barbulescu
Narcis Duteanu
Adina Negrea
Makarand M. Ghangrekar*

Research Article

New Sustainable Biosorbent Based on Recycled Deoiled Carob Seeds: Optimization of Heavy Metals Remediation

M. Farnane,¹ A. Machrouhi,¹ A. Elhalil,¹ M. Abdennouri,¹ S. Qourzal,² H. Tounsadi ^{1,3} and N. Barka ¹

¹Laboratoire des Sciences des Matériaux, des Milieux et de la Modélisation (LS3M), FPK, Univ Hassan 1, B.P. 145, 25000 Khouribga, Morocco

²Equipe de Catalyse et Environnement, Département de Chimie, Faculté des Sciences, Université Ibn Zohr, B.P. 8106 Cité Dakhla, Agadir, Morocco

³Université Sidi Mohamed Ben Abdellah, Faculté des Sciences Dhar Elmehraz, Laboratoire d'Ingénierie, d'Electrochimie, de Modélisation et d'Environnement, Fès, Morocco

Correspondence should be addressed to N. Barka; barkanouredine@yahoo.fr

Received 6 April 2018; Accepted 5 August 2018; Published 9 October 2018

Academic Editor: Adina Negrea

Copyright © 2018 M. Farnane et al. This is an open access article distributed under the Creative Commons Attribution License, which permits unrestricted use, distribution, and reproduction in any medium, provided the original work is properly cited.

In this study, an efficient biosorbent was developed from deoiled carob seeds, a agroindustrial waste. The biosorption efficiency was evaluated for cadmium and cobalt ions removal from aqueous solution under various parameters such as treating agent, solution pH, biosorbent dosage, contact time, initial metal ions concentration, and temperature. The effect of some major inorganic ions including Na^+ , K^+ , Ca^{2+} , Mg^{2+} , and Al^{3+} on the biosorption was also established. Based on this preliminary study, four independent variables including solution pH, biosorbents dosage, initial metal concentration, and treating agent were chosen for the optimization of the process using full-factorial experimental design. It was found that chemical pretreatment of the raw deoiled carob seeds with NaOH strongly enhances its biosorption potential. Thus, the optimal conditions for high biosorption of cadmium(II) and cobalt(II) were achieved at pH of 6, biosorbent dosage of 1 g/L, and initial metal concentration of 50 mg/L. The biosorbents were characterized by Fourier transform infrared spectroscopy (FT-IR), scanning electron microscopy (SEM), energy dispersive X-ray (EDX), Boehm titration, and the point of zero charge (pH_{PZC}).

1. Introduction

Heavy metal pollution imposes ecological and public health problems according to hazardous and irrecoverable effects of metal ions on the environment and aquatic ecosystems [1]. Besides, the toxic and harmful effects to organisms living in water, heavy metals also accumulate throughout the food chain and may affect human beings [2]. In this way, the removal and recovery of heavy metals from aqueous effluents before being disposed in the environment is required [3].

Various methods have been used to remove heavy metal ions such as chemical precipitation [4], membrane filtration [5], ion exchange [6], solvent extraction [7], flotation [8],

and electrochemical treatment [9]. Among all these mentioned methods, sorption is an effective and eco-friendly method for the removal of heavy metal ions from wastewaters due to its simple design, easy operation handling, and availability of different sorbents with large efficacy to remove a wide range of heavy metals [10–12]. Activated carbons are widely used as adsorbents in wastewater treatment because of their high surface areas and active functional groups, but their high cost inhibits sometimes their use [13]. Therefore, there is a need to develop other biosorbents from alternative low-cost raw materials for the same role as activated carbon. Recently, low-cost precursors have become the focus of researchers for example, chitosans [14], bark of *Pinus elliottii* [15], *Jatropha curcas* [16],

sugarcane bagasse [17], *Eichornia crassipes* [18], coconut [19], agricultural peels [20–22], sunflower stalks [23], raw carob shells and chemically treated carob shells [24], *Diploaxis harra*, and *Glebionis coronaria* L [25].

The aim of this study is to assess the applicability of chemically treated deoiled carob seeds for the removal of cadmium(II) and cobalt(II) ions from aqueous solution. Biosorption studies were carried out under various parameters such as solution pH, biosorbents dosage, contact time, initial metal ions concentration, and temperature. The biosorption kinetic data were tested by pseudo-first-order and pseudo-second-order kinetic models. The equilibrium data were analyzed using Langmuir and Freundlich models. This paper also discussed the combined effect of the most influencing parameters, which are solution pH, biosorbent dosage, concentration of the solution, and the treating agent. Full-factorial experimental design with two levels (2^4) and surface response methodology were used to acquire the optimal parameters for high removal of Cd(II) and Co(II) ions.

2. Experimental

2.1. Materials. All the chemicals used in the preparation and the biosorption studies were of analytical grade. Cd ($(\text{NO}_3)_2 \cdot 4\text{H}_2\text{O}$ (98%), $\text{Co}(\text{NO}_3)_2 \cdot 6\text{H}_2\text{O}$ (98%), NaCl (99.5%), $\text{Al}(\text{NO}_3)_3 \cdot 9\text{H}_2\text{O}$ ($\geq 98\%$), HCl (37%), Na_2CO_3 , and NaHCO_3 were obtained from Sigma-Aldrich (Germany). Mg ($(\text{NO}_3)_2 \cdot 6\text{H}_2\text{O}$ (97%) was provided from SDS (France), Ca ($(\text{NO}_3)_2 \cdot 4\text{H}_2\text{O}$ and HNO_3 (65%) from Scharlau (Spain), and NaOH (98%) was provided from Merck (Germany).

2.2. Preparation of the Biosorbents. The deoiled residue was obtained as a by-product from the hydrodistillation process of carob seeds from the region of Khenifra in Morocco. The biomass was repeatedly washed with demineralized water and then oven dried at about 120°C for 24 h min in order to remove excess moisture. The dried biomass was then grounded using mortar and pestle and sieved to get a size fraction lower than $160\ \mu\text{m}$, referred as Raw-seeds. For the chemical treatment, 10 g of the Raw-seeds was treated with 100 mL of 1 M solution of HCl or NaOH for 2 h. The biosorbents were then filtered and washed with distilled water until neutral pH. The pretreated biosorbents were then dried in an oven at 120°C for 24 h and stored in glass bottles under following names HCl-seeds and NaOH-seeds for further use.

2.3. Characterisation. FTIR transmittance spectra of the biosorbents were recorded in the region of $4000\text{--}400\ \text{cm}^{-1}$ using a Scottech-SP-1 spectrophotometer. Basic and oxygenated acidic surface groups were assessed by Boehm titrations [26]. About 0.1 g of each sample was mixed with 50 mL of 0.01 M aqueous reactant solution (NaOH, Na_2CO_3 , NaHCO_3 , or HCl). The mixtures were stirred at 500 rpm for 24 h at room temperature. Then, the suspensions were filtrated by a $0.45\ \mu\text{m}$ membrane filter. To determine the oxygenated groups content, back titrations of the filtrate (10 mL) were achieved with standard 0.01 M-HCl solution.

Basic groups contents were also determined by back titration of the filtrate with 0.01 M-NaOH solution. The morphological characteristics were analyzed by scanning electron microscopy (SEM). Small amount of each sample was finely powdered and mounted directly onto aluminum sample holder using the two-sided adhesive carbon model. Energy dispersive X-ray (EDX) was also performed to determine the elemental composition of the raw carob seeds and the both treated samples. The point of zero charge (pH_{PZC}) was determined by the pH drift method according to the method proposed by Noh and Schwarz [27]. The pH of NaCl aqueous solution (50 mL at 0.01 mol/L) was adjusted to successive initial values in the range from 2.0 to 12.0 by addition of HNO_3 (0.1 N) and/or NaOH (0.1 N). Furthermore, 0.05 g of each biosorbent was added in 50 mL of solution and stirred for 6 h. The final pH was measured and plotted against the initial pH. The pH_{PZC} was determined at the value for which $\text{pH}_{\text{final}} = \text{pH}_{\text{initial}}$.

2.4. Batch Biosorption Procedure. Stock solutions were prepared by dissolving desired weight of each metal ion in distilled water, and necessary concentrations were obtained by dilution. Biosorption experiments were investigated in a series of beakers containing 100 mL of the metal ion solution at desired concentration and desired weight of the biosorbent. The mixtures were stirred for 2 h at 500 rpm using a magnetic stirrer. The influence of pH was performed by varying the pH from 2.0 to 7.0 at an initial metal concentration of 100 mg/L. The pH of the solutions was adjusted with either 0.1 M of HCl or 0.1 M of NaOH and using a SensION + PH31 pH meter. The biosorbent dosage was varied from 0.5 to 5 g/L. The contact time was varied between 5 and 210 min at room temperature with initial pH solution. Biosorption equilibrium was established for different metal ion concentration between 20 and 200 mg/L. The effect of temperature was tested from 10 to 50°C using a thermostatically controlled incubator. The effect of some major inorganic ions including Na^+ , K^+ , Mg^{2+} , Ca^{2+} , and Al^{3+} on the biosorption was studied for each heavy metal at a constant initial metal concentration of 100 mg/L. The concentration of each ion was varied from 10 to 100 mg/L.

After each biosorption experiment completed, the solid phase was separated from the liquid phase by centrifugation at 3000 rpm for 10 min. Metal ions concentration was determined using a PerkinElmer atomic absorption spectrophotometer (Analyst 200).

The biosorption capacity and biosorption removal efficiency were calculated using the following equations:

$$q_{t,e} = \frac{(C_0 - C_{t,e})}{R}, \quad (1)$$

$$\% \text{ removal} = \frac{(C_0 - C)}{C_0} * 100, \quad (2)$$

where $q_{t,e}$ (mg/g) is the biosorbed quantity at any time or at equilibrium, C_0 (mg/L) is the initial metal ion concentration, $C_{t,e}$ (mg/L) is the metal ion concentration at a time t or at

equilibrium, and R (g/L) is the mass adsorbents per liter of solution.

Kinetic and equilibrium parameters were estimated with the aid of the nonlinear regression method using Origin 6.0 software.

2.5. Design of Experiment for the Optimization of Cd(II) and Co(II) Biosorption. The methodology of experimental design was used for modeling and optimization of the biosorption processes of Cd(II) and Co(II) ions from aqueous solutions. The four most influencing factors are solution pH (A), biosorbents dosage (B), initial metals concentration (C), and treating agent (D). The values of variable levels are presented in Table 1. The experiments were made according to a full-factorial design at two levels (2^4), with 16 experiments.

In addition, a first-order polynomial model was also used for modeling sorption of Cd(II) or Co(II) ions. The general equation of the first-order polynomial model is presented in

$$Y = b_0 + b_1A + b_2B + b_3C + b_4D + b_{12}AB + b_{13}AC + b_{14}AD + b_{23}BC + b_{24}BD + b_{123}ABC + b_{124}ABD + b_{134}ACD + b_{234}BCD + b_{1234}ABCD, \quad (3)$$

where Y (mg/g) is the responses of interest (adsorption capacity of Cd(II) (Y_1) and adsorption capacity of Co(II) (Y_2)).

The results were analyzed using the Trial software Design Expert 10.0.0.

3. Results and Discussion

3.1. Characterization

3.1.1. FT-IR Analysis of the Biosorbents. The infrared spectra of Raw-seeds, NaOH-seeds, and HCl-seeds are illustrated in Figure 1. The figure shows broad absorption band for Raw-seeds at $3200\text{--}3600\text{ cm}^{-1}$ due to the stretching of the N-H bond of amino groups and indicative of bonded hydroxyl group [11], and this band was separated into more resolute three bands after the chemical pretreatments with NaOH and HCl. Two bands at around $3200\text{--}3400\text{ cm}^{-1}$ indicate the presence of carboxylic acid and amino groups, and the other one near 3500 cm^{-1} is related to the OH stretching vibration mode in alcohol and phenol groups. The band at 2930 cm^{-1} corresponds to the symmetrical and asymmetrical-CH-vibrations in lipids. The peaks located at 1620 cm^{-1} are characteristics of C=O stretching for aldehydes and ketones, which can be conjugated or nonconjugated to aromatic rings [28]. The C-O, C-C, and C-OH stretching vibrations can be attributed to peaks in the region of $1180\text{--}1048\text{ cm}^{-1}$. The spectra showed bands located at 630 cm^{-1} , assigned to OH- ions.

3.1.2. Boehm Titration of the Biosorbents. The oxygen functional groups are very important characteristics of the biosorbents because they determine the surface properties

TABLE 1: Process factors and their levels.

Factors	Levels	
	Low (-)	High (+)
A. pH	4	6
B. Biosorbent dose (g/l)	1	3
C. Initial concentration (mg/l)	50	100
D. Treating agent	HCl	NaOH

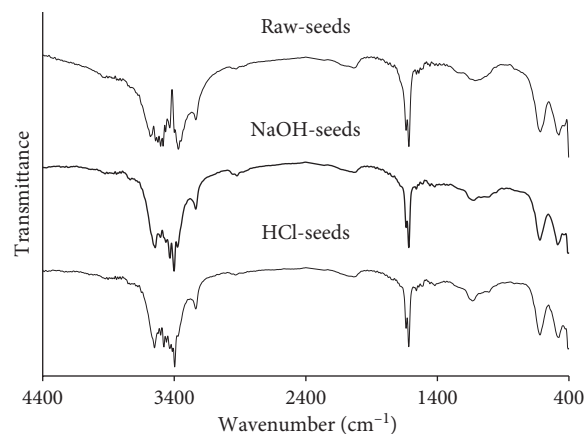


FIGURE 1: FT-IR spectra of Raw-seeds, HCl-seeds, and NaOH-seeds biosorbents.

and hence their quality as biosorbents. These functional groups are mainly divided as acidic or basic, which affect the surface charge and consequently the biosorption capability of the biosorbents. The Boehm's titration method provides qualitative and quantitative information regarding the total amount of basic groups and the amounts of acidic functional groups such as carboxylic, lactonic, and phenolic. From Table 2, it can be seen that Raw-seeds, HCl-seeds, and NaOH-seeds' surface constituted mainly of acidic groups, which are due to phenolic, lactonic, and carboxylic groups and a less quantity of basic groups. So, the surface of these biosorbents is acidic. The biosorbents having greater surface acid groups have higher cation exchange properties. According to the experimental data, the HCl-seeds had an important amount of acidic groups than Raw-seeds followed by NaOH-seeds. The use of chemical reagents acid in the treatment process produces an increase in the amount of acid groups present in the biosorbent surface. It was observed that the concentration of lactonic and phenolic groups in HCl-seeds is higher than those of carboxylic groups.

3.1.3. Morphology of the Biosorbents. The surface texture and morphology of biosorbents were analyzed by SEM in order to compare the morphology of raw and chemically treated carob seeds. The SEM images of these biosorbents are depicted in Figure 2. As it is clearly shown, there is a significant difference among the tree samples. In fact, no obvious pores can be seen for Raw-seeds. Then, for the HCl-seeds, the surface morphology does not have well-defined pores. However, the NaOH-seeds' surface indicates some

TABLE 2: Chemical groups on the surface of the biosorbents.

Biosorbent	Carboxylic groups (meq/g)	Lactonic groups (meq/g)	Phenolic groups (meq/g)	Total acid groups (meq/g)	Total basic groups (meq/g)
Raw-seeds	0.4070	0.4880	0.4900	1.3850	0.3750
HCl-seeds	0.3810	0.5150	0.5240	1.4200	0.3650
NaOH-seeds	0.4090	0.4830	0.4990	1.3910	0.3870

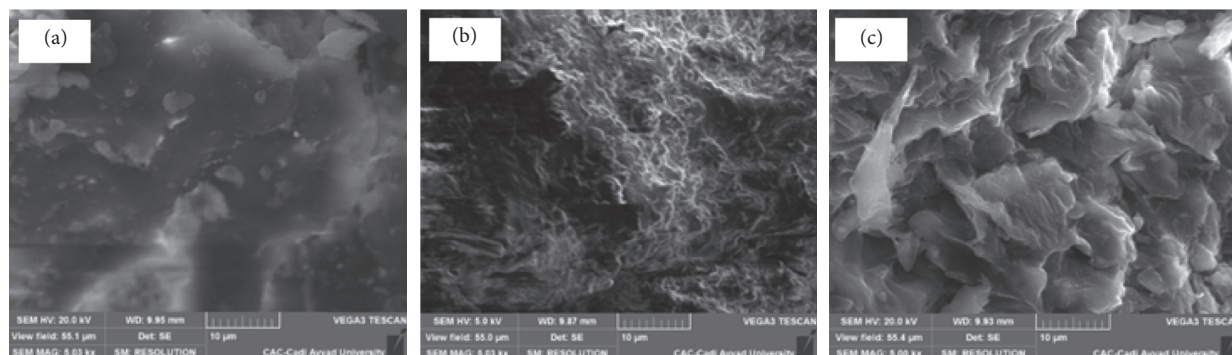


FIGURE 2: SEM images of (a) Raw-seeds, (b) HCl-seeds, and (c) NaOH-seeds.

irregular cavities and a changing in the external texture as a result of the reaction between the raw material and the treating agent. These different characteristics allow NaOH-seeds to contribute a high adsorption performance of heavy metals. These results suggest that the NaOH is an effective agent for creating well-developed pores on the surface of the raw material, which is already shown for the alkaline-treated carob shells [24].

3.1.4. EDX Analysis. EDX is an analytical technique to identify the element presence on the material surface based on its characteristic X-ray energy. This technique is normally coupled with SEM analysis to gain more complete result. The elemental compositions of Raw-seeds, NaOH-seeds, and HCl-seeds are tabulated in Table 3. In addition, the elemental compositions are presented under peaks in Figure 3. The major components of the raw carob seeds were set up to be carbon (56.13 weight%) and oxygen (35.31 weight%). However, these Raw-seeds also contain a small percentage of phosphorus, sulfur, chlorine, potassium, and calcium. After the HCl treatment, a small reduction in the percentage of carbon (54.71 weight%) and a significant rise in the quantity of oxygen (45.10 weight%) was seen. An extinction of potassium and calcium was noticed. However, for NaOH-seeds, it can be also seen that the percentage of carbon decreases (48.32 weight%), and the oxygen content increased to acquired 40.35 weight%. A change in the elemental composition was noticed after the NaOH treatment which mainly falls within an appearance of new elements, including sodium, magnesium, and aluminum and a disappearance of other elements such as phosphorus, sulfur, and chlorine. As a result, it might be concluded that the alkaline treatment increases the percentage of oxygen in HCl-seeds followed by NaOH-seeds and reduced the amount of carbon for both biosorbents as the same order.

3.1.5. pH of Zero Charge. The pH_{PZC} is an important characteristic for the biosorbent as it indicates its acidity-basicity and the net surface charge of the biosorbent in solution. The pH_{PZC} was 5.9, 2.3, and 6.9, respectively, for Raw-seeds, HCl-seeds, and NaOH-seeds. We can see that the Raw-seeds have an acidic surface. After the treatment by HCl, we found an increase in the acidity of the biomaterial at 2.3. But, after NaOH treatment, an increase in the pH_{PZC} appears. The low pH_{PZC} is in agreement with the predominance of surface acid groups. This result indicates that, for pH lower than 5.9, 2.3, and 6.9, the surfaces of the Raw-seeds, HCl-seeds, and NaOH-seeds are positively charged. Then at these pH, the biosorption of the studied metals was inhibited, due to the electronic repulsion between metal ions and positively charged functional groups. Inversely, for pH superior of 5.9, 2.3, and 6.9, the number of negatively charged sites on the Raw-seeds, HCl-seeds, and NaOH-seeds' surface increases, and metal biosorption becomes more important.

3.2. Biosorption Performance

3.2.1. Effect of Solution pH on the Biosorption. The pH of the solution has a significant impact on the uptake of heavy metals, since it indicates the surface charge of the adsorbent and the degree of ionization and speciation of the adsorbate [29]. The pH of the solution controls the electrostatic interactions between the sorbent and the sorbate [30]. However, the dependence of heavy metal biosorption on pH was different for each metal. Figure 4 shows the effect of pH on biosorption of Cd(II) and Co(II) onto Raw-seeds, HCl-seeds, and NaOH-seeds. It can be seen that the metal biosorption increases with increasing solution pH, and it is strongly dependent on pH solution. It is known generally that the percent removal of the heavy

TABLE 3: Elemental composition of Raw-seeds, HCl-seeds, and NaOH-seeds.

Element	Raw-seeds		HCl-seeds		NaOH-seeds	
	Weight %	Atomic %	Weight %	Atomic %	Weight %	Atomic %
C	56.13	65.81	54.71	61.72	48.32	58.11
O	35.31	31.09	45.10	38.19	40.35	36.43
Na	—	—	—	—	4.13	2.59
Mg	—	—	—	—	0.90	0.53
Al	—	—	—	—	0.34	0.18
P	0.23	0.11	0.10	0.05	—	—
S	0.23	0.10	0.07	0.03	—	—
Cl	0.21	0.08	0.02	0.01	—	—
K	4.94	1.78	—	—	0.17	0.17
Ca	2.95	1.04	—	—	1.98	1.98

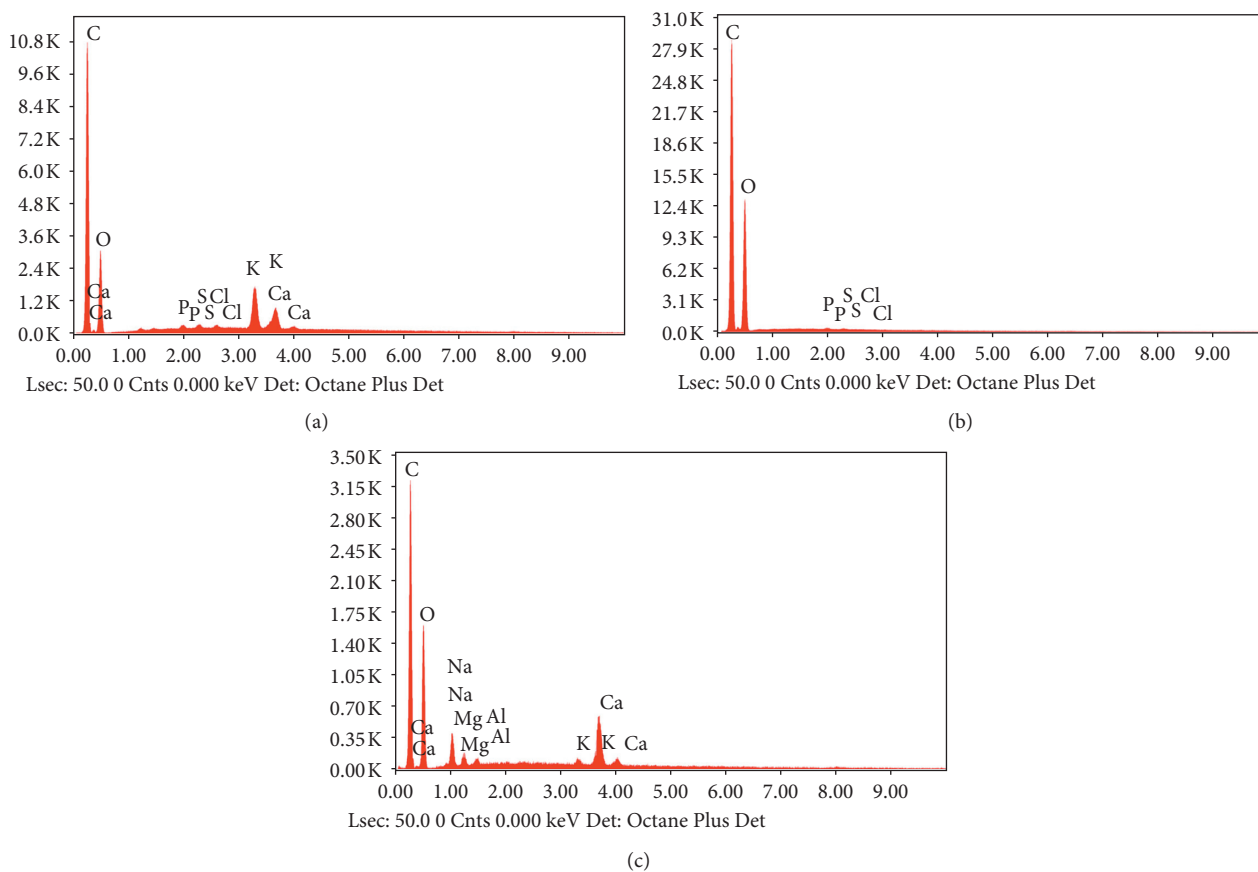


FIGURE 3: EDX analysis of (a) Raw-seeds, (b) HCl-seeds, and (c) NaOH-seeds.

metal ions increases with pH. At low pH, the cations compete with the H^+ ions in the solution for the sorption sites and therefore biosorption declines. In contrast, as pH increased, the competition between proton and metal cation decreases which means that there are more negative groups available for the binding of metal ions which results a greater metal uptake. On the other hand, at higher pH, metal cations start to form hydroxide complexes or precipitate as their hydroxides, which decrease the biosorption of metal ions [31, 32]. The pH_{PZC} values indicate that the biosorbent acquires a positive charge below a pH of 5.9, 2.3, and 6.9, respectively, for Raw-seeds, HCl-seeds,

and NaOH-seeds. Above these values, the biosorbents' surface becomes negatively charged [33]. Therefore, the ionic sorbent-sorbate interaction becomes progressively significant for pH higher than 5.9, 2.3, and 6.9. As shown in the figure, the sorption capacities for Cd(II) and Co(II) by NaOH-seeds are greater than those biosorbed by Raw-seeds and HCl-seeds. This may be related to the properties of biosorbent and metal sorbate.

3.2.2. Effect of Biosorbents Dosage. The biosorbent dosage is an important parameter because this parameter determines

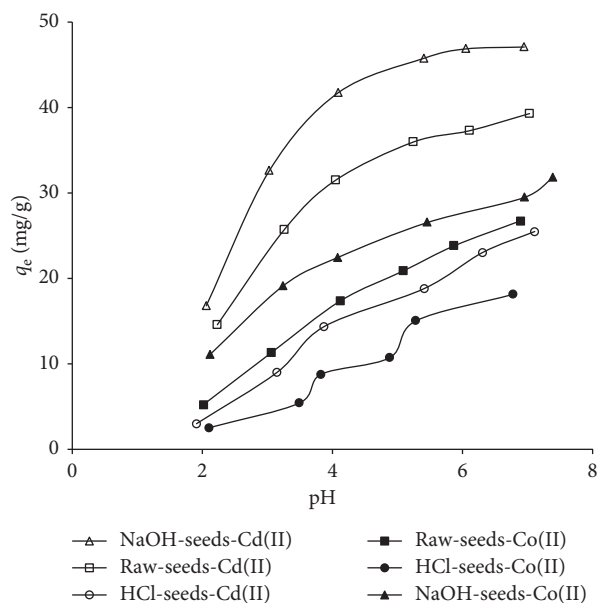


FIGURE 4: Effect of pH on the biosorption of Cd(II) and Co(II) onto the biosorbents: $C_0 = 100$ mg/L, contact time = 120 min, $R = 2$ g/L, and $T = 25^\circ\text{C}$.

the capacity of biosorbent for a given Cd(II) and Co(II) concentration and also determines sorbent-sorbate equilibrium of the system. Figure 5 represents the Cd(II) and Co(II) removal efficiencies for the study biosorbents. This figure indicates that the percentage removal of Cd(II) and Co(II) increased with increasing biosorbent dose due to the increase in the total available surface area and the number of active sites for biosorption of the biosorbent particles [32]. The percentage removal of Cd(II) increased from 20.70 to 76.06%, from 10.60 to 23.65%, and from 32.20 to 99.91% when the biosorbents dosage was increased from 0.5 to 5 g/L, respectively, for Raw-seeds, HCl-seeds, and NaOH-seeds. For Co(II), the biosorption yield increased from 12.73 to 36.94%, from 3.34 to 13.50%, and from 17.02 to 55.69% when the biosorbents dosage was increased from 0.5 to 5 g/L, respectively, for Raw-carob, HCl-carob, and NaOH-carob. Therefore, the biosorption yield was almost the same when the biosorbent dosage was higher than 3 g/L. This trend could be explained as a consequence of a partial aggregation of biosorbent at higher sorbent dosage, which results in the decrease in effective surface area for the [34] biosorption [35].

3.2.3. Biosorption Kinetics. The effect of contact time on the biosorption of Cd(II) and Co(II) metal ions is reported in Figure 6. The evolution of the biosorbed amount of metal ions with the contact time indicates that the equilibrium was relatively fast and was totally reached in about 45 min for the biosorption of Cd(II) by both the biosorbents and was 60 min in the case of Co(II). This equilibrium time is very short in comparison with other literature results [36–38], which is one of the advantages of our biosorbents. In Figure 4, two kinetic regions can be observed: the first one is characterized by a high biosorption rate, which is due to the

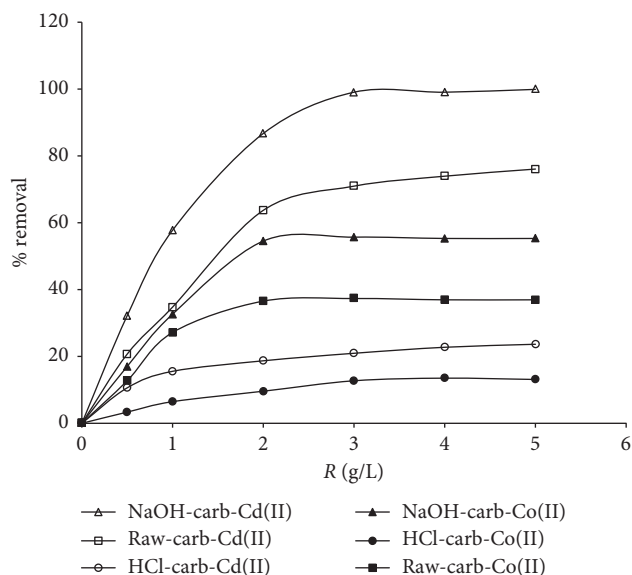


FIGURE 5: Effect of biosorbents dosage on the removal of Cd(II) and Co(II) by the biosorbents: $C_0 = 100$ mg/L, contact time = 120 min, initial pH, and temperature = 25°C .

fact that initially the number of sites of available biosorbent is higher and the driving force for mass transfer is greater. Metal ions easily access first the biosorption sites. As time progresses, the number of free sites of Raw-seeds, HCl-seeds, and NaOH-seeds decreases and the nonbiosorbed cations in solution are assembled on the surface, thus limiting the biosorption capacity.

In order to determine the biosorption efficiency of Cd(II) and Co(II) on three biosorbents, two kinetic models are used; the pseudo-first-order and the pseudo-second-order kinetic models. Kinetic data were analyzed on the basis of the regression coefficient (r^2) and the amount of metal biosorbed per unit weight of the biosorbent.

The Lagergren first-order rate expression based on solid capacity is generally expressed as follows [39]:

$$q = q_e(1 - e^{-k_1 t}), \quad (4)$$

where q_e and q (both in mg/g) are, respectively, the amounts of metal biosorbed at equilibrium and at any time t (min) and k_1 (1/min) is the rate constant of biosorption.

The pseudo-second-order equation is expressed as [40]

$$q = \frac{k_2 q_e^2 t}{1 + k_2 q_e t}, \quad (5)$$

where k (g/mg min) is the pseudo-second order rate constant.

The obtained data and the correlation coefficients, r^2 , are listed in Table 4. The results show that the calculated equilibrium values using pseudo-first-order model kinetic were very close to the experimental ones (q_{exp}) than the others calculated from the pseudo-second-order model and also showed the best fit to the experimental data with the highest correlation coefficients ($r^2 = 0.999$) for the both metal ions. From these results, it was concluded that

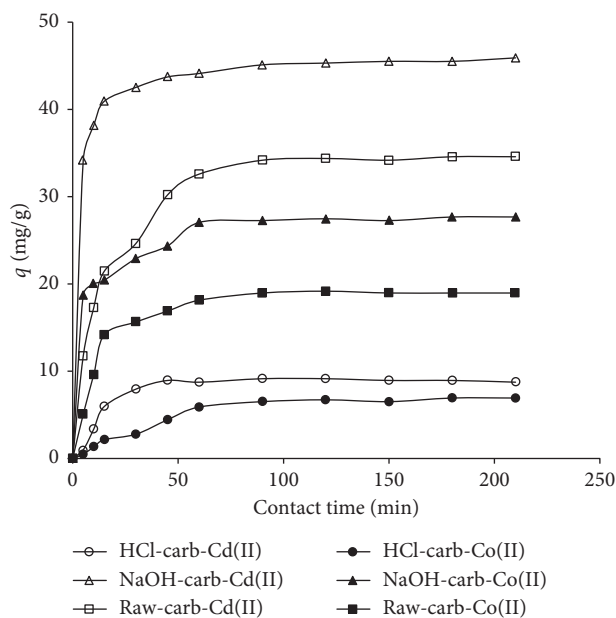


FIGURE 6: Kinetics of Cd(II) and Co(II) biosorption by the biosorbents: $C_0 = 100$ mg/L, $R = 2$ g/L, initial pH, and temperature = 25°C.

TABLE 4: Pseudo-first-order and pseudo-second-order kinetic parameters for the biosorption of Co(II) and Cd(II).

Metal	Biosorbent	q_e (mg/g)	Pseudo-first-order			Pseudo-second-order		
			q_e (mg/g)	k_1 (1/min)	r^2	q_e (mg/g)	k_2 (g/mg·min)	r^2
Cd(II)	Raw-seeds	34.578	34.159	0.071	0.996	37.230	0.002	0.992
	HCl-seeds	8.942	9.076	0.043	0.991	10.380	0.005	0.972
	NaOH-seeds	45.905	45.863	0.296	0.992	42.649	0.009	0.994
Co(II)	Raw-seeds	18.963	18.964	0.064	0.998	20.697	0.004	0.993
	HCl-seeds	6.929	7.090	0.022	0.984	8.907	0.002	0.973
	NaOH-seeds	27.676	27.605	0.051	0.999	28.741	0.005	0.997

the biosorption of Cd(II) and Co(II) onto Raw-seeds, HCl-seeds, and NaOH-seeds could be better described by the pseudo-first-order model. This may be due to rapidity transfer speed of Cd and Co molecules to the surface of the biosorbent and the availability of active sites.

3.2.4. Biosorption Isotherms. The biosorption isotherms describe how the sorbate molecules are distributed between the liquid phase and solid phase when the system reaches the equilibrium. The analysis of isotherm data by fitting them to different models is important to find a sustainable model that can be used [41]. The biosorption isotherms are illustrated in Figure 7. It is obvious that the amount of metal biosorbed increases as its equilibrium concentration increased. This trend may be due to the high driving force for mass transfer at a high initial heavy metal concentration. In addition, if the heavy metal concentration in solution is higher, the active sites of biosorbent are surrounded by much more ions, and the biosorption phenomenon occurs more efficiently. Thus, biosorption amount increases with

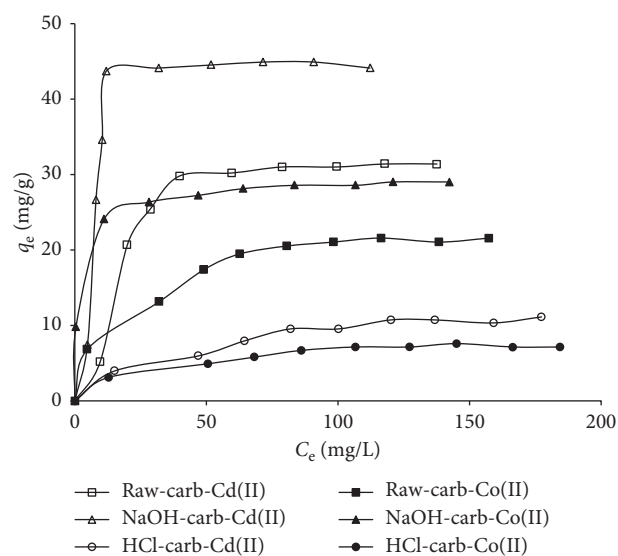


FIGURE 7: Adsorption isotherms of Cd(II) and Co(II) biosorption by the biosorbents: $R = 2$ g/L, initial pH, contact time = 120 min, and temperature = 25°C.

the increase of initial ion concentration [42]. The isotherms' form was type L for Raw-seeds, HCl-seeds, and NaOH-seeds according to Giles classification [43].

Several biosorption isotherms can be used to correlate the biosorption equilibrium in heavy metals biosorption on several biosorbents. Some well-known isotherms are Langmuir and Freundlich models.

(1) *Langmuir Model*. Langmuir isotherm assumes two main points in the biosorption process. First, the biosorption happens at specific homogeneous biosorption sites in the biosorbent. Second, the monolayer biosorption and maximum biosorption occurs when biosorbed molecules form a saturated layer on the surface of adsorbent. All biosorption sites involved are energetically identical, and the intermolecular force decreases as the distance from the biosorption surface increases [44].

$$q_e = \frac{q_m K_L C_e}{1 + K_L C_e}, \quad (6)$$

where q_m (mg/g) is the maximum monolayer biosorption capacity, K_L (L/mg) is the Langmuir equilibrium constant related to the biosorption affinity, and C_e is the equilibrium concentration.

(2) *Freundlich Model*. Freundlich isotherm is an empirical equation assuming that the biosorption process takes place on heterogeneous surfaces, and biosorption capacity is related to the concentration of biosorbed metal ions at equilibrium. Freundlich isotherm is suitable in treating metal ions' biosorption at higher concentrations. However, this isotherm is not suitable for low concentration range.

Freundlich isotherm model is represented by the following equation [45]:

$$q_e = K_F C_e^{1/n}, \quad (7)$$

where K_F ($\text{mg}^{1-1/n}/\text{g/L}^n$) is the Freundlich constant and n is the heterogeneity factor. The K_F value is related to the biosorption capacity, while $1/n$ value is related to the biosorption intensity.

(3) *Analysis of Adsorption Isotherms*. The calculated isotherm parameters for each model and correlation coefficients analyzed by nonlinear regression method are presented in Table 5. This table shows that the Langmuir model indicates higher values of correlation coefficients ($r^2 > 0.993$) in the biosorption of Co(II) than Cd(III) biosorption onto the three biosorbents. For these reasons, it can be approved that Langmuir equilibrium isotherm describes the metal biosorption process using the studied biosorbents well. This process is occurred by the formation of metal ion monolayer onto the biosorbent surface with finite number of identical sites, which are homogeneously distributed over the biosorbent surface [46]. The q_{max} values were 34.85, 14.08, and 49.11 mg/g for Cd(II) and 24.74, 7.65, and 28.18 mg/g in the case of Co(II) respectively, for Raw-seeds, HCl-seeds, and NaOH-seeds. We can also conclude that NaOH-seeds' biosorption capacity is superior than that of

Raw-seeds and HCl-seeds. On the other hand, the biosorption of Cd(II) on the three biosorbents is greater in comparison to that of the Co(II) biosorption. This may be due to the nature of the interaction between each sorbate and biosorbent. However, the Freundlich model provides two parameters: k_f and n . k_f is related to the biosorption capacity and biosorption intensity of the metal ions on the different biosorbents and represents the quantity of metal ions biosorbed onto biosorbent at equilibrium concentration. n represents the strength of metal ions' biosorption on the biosorbent. n value from 1 to 10 indicates relatively strong biosorption. The obtained n values in the studied biosorbents were more than 1, which indicates relatively a strong biosorption of the metal ions on the biosorbents [47].

Table 6 presents a comparison of the maximum adsorption capacity of Raw-seeds, HCl-seeds, and NaOH-seeds with various adsorbents reported in the literature for the adsorptive removal of Cd(II) and Co(II). Though there were variations in some experimental conditions, the table shows that the biosorption capacity of Raw-seeds, HCl-seeds, and NaOH-seeds for the both heavy metals is most higher compared to other adsorbents used in previous studies. This can be explained by the nature of functional groups present in the surface of Raw-seeds, HCl-seeds, and NaOH-seeds.

3.2.5. *Effect of Temperature*. The variation of sorption efficiencies of Cd(II) and Co(II) on Raw-seeds, HCl-seeds, and NaOH-seeds as function of solution temperature is shown in Figure 8. It was observed that the temperature does not have significant influence on the biosorption capacity in the studied range. The variation in temperature had two major effects on the sorption process. An increase in the temperature is known to increase the rate of diffusion of the adsorbate molecules across the external boundary layer and in the internal pores of the adsorbent particles as a result of reduced viscosity of the solution [61]. In addition, several authors have shown that further increases in the temperature may lead to a decrease in the metal removal percentage. This may be attributed to an increase in the relative desorption of the metal from the solid phase to the liquid phase, deactivation of the biosorbent surface owing to bond disruption [62], or weakness of the sorbent active site binding forces and the sorbate species and also between the adjacent molecules of the sorbed phase [63].

3.2.6. *Effect of Inorganic Ions*. Industrial effluents often contain more than one metal ion. Consequently, biosorption becomes competitive, in which several metal ions compete for a limited number of binding sites [64]. Figure 9 shows the effect of Na^+ , K^+ , Mg^{2+} , Ca^{2+} , and Al^{3+} ions on the biosorption of Cd(II) and Co(II). From this figure, we can conclude that the monovalent cations K^+ and Na^+ have less influence on the biosorption. On the other hand, divalent and trivalent ions inhibit the biosorption on the both biosorbents. The degree of inhibition by the inorganic ions followed the sequence: $\text{K}^+ < \text{Na}^+ < \text{Mg}^{2+} < \text{Ca}^{2+} < \text{Al}^{3+}$ for the both metals. The monovalent cations Na^+ and K^+ are

TABLE 5: Model isotherm constants for the biosorption of Cd(II) and Co(II) biosorption onto Raw-seeds, HCl-seeds, and NaOH-seeds.

Isotherms	Parameters	Raw-seeds		HCl-seeds		NaOH-seeds	
		Cd(II)	Co(II)	Cd(II)	Co(II)	Cd(II)	Co(II)
Langmuir	q_m (mg/g)	34.85	24.74	14.08	7.65	49.11	28.18
	K_L (L/mg)	0.082	0.054	0.021	0.086	0.150	1.100
	r^2	0.996	0.997	0.992	0.999	0.999	0.993
Freundlich	N	5.176	5.890	3.352	12.082	4.564	6.091
	K_F (mg ^{1-1/n} /g/Ln)	12.61	9.47	2.40	13.97	17.53	4.68
	r^2	0.988	0.994	0.988	0.999	0.991	0.973

TABLE 6: Comparison of biosorption capacity (q_m) of Raw-seeds, HCl-seeds, and NaOH-seeds for Cd(II) and Co(II) with different other biosorbents.

Adsorbent	q_m (mg/g) Cd(II)	q_m (mg/g) Co(II)	References
Pine bark	28.00	—	[48]
Peat	22.50	—	[49]
Hazelnut shells	5.42	—	[50]
Waste tea leaves	31.48	—	[51]
Aquatic plant <i>Najas graminea</i>	28.00	20.6	[52]
Black carrot residues	—	5.35	[53]
Coir pith	—	12.82	[54]
<i>J. rubens</i> (red algae)	30.50	32.6	[55]
Saw dust	26.73	—	[56]
Neem bark	25.57	—	[57]
Mangosteen shell	3.15	0.34	[11]
Areca catechu	10.66	—	[58]
	—	27.15	[59]
Rose waste biomass	—	20.63	[60]
	31.35	17.41	[24]
<i>Sargassum wightii</i>	14.90	10.46	[24]
Raw-carob	49.63	30.04	[24]
HCl-carob			
NaOH-carob			
Raw-seeds	31.35	17.41	Present study
HCl-seeds	14.90	10.46	Present study
NaOH-seeds	49.63	30.04	Present study

bound by ionic attraction and therefore do not compete directly with the binding of heavy metals by the biosorbents. However, divalent and trivalent ions prevent the biosorption on the both biosorbents. The decreasing of Al^{3+} with high concentrations may be attributed to favorable electrostatic effects due to the increased number of positively charged surface binding sites arising from Al^{3+} . However, the effect of ionic strength is explained as the result of competition of ions with the heavy metals for electrostatic binding to the surface of Raw-seeds, HCl-seeds, and NaOH-seeds. Because, the functional groups are negatively charged, they will electrostatically attract any cation, be it inorganic or heavy metal ions of interest [65].

3.3. Optimization of Biosorption Conditions

3.3.1. Experimental Design. Table 7 shows the adsorption conditions and experimental results for the two responses of cadmium and cobalt removal. As can be seen, there was a considerable variation in the removal efficiency of cadmium and cobalt at different values of the already selected

factors. Consequently, the maximum sorption capacities of cadmium and cobalt were 85.73 and 51.90 mg/g, respectively. These greater capacities were obtained for the initial concentration of 50 mg/l, pH = 6, biosorbent dose of 1 g/l with carob seeds treated by NaOH agent. The regression analysis was performed to adjust the response functions with the experimental data. The values of regression coefficient estimated are presented in Table 8. From the table, the biosorbent dose and initial concentration present a negative effect on cadmium and cobalt ions removal, while the pH and treating agent have a positive effect on elimination of two heavy metals. The analysis of the interaction effects shows a significant interaction between biosorbent dose and treating agent for cadmium removal ($b_{24} = -6.09$) with a negative impact and a significant interaction between biosorbent dose and initial concentration for cobalt removal with a positive effect ($b_{23} = 2.58$).

3.3.2. Analysis of Variance (ANOVA). Analysis of variance (ANOVA) was carried out to justify the adequacy of the models. After discarding the insignificant terms, the

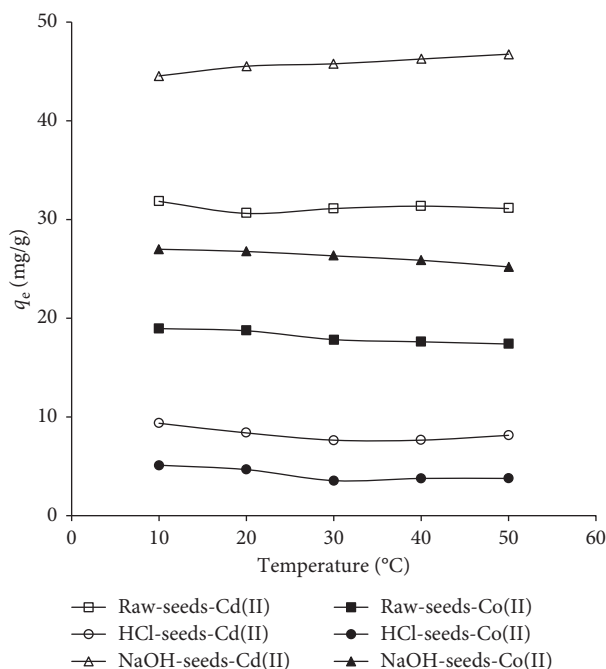


FIGURE 8: Effect of temperature on Cd(II) and Co(II) biosorption by the biosorbents: $R = 2$ g/L, initial pH, contact time = 120 min, and $C_0 = 100$ mg/L.

ANOVA data for the coded quadratic models for the two responses at a confidence level of 95% are reported in both Tables 9 and 10. The quality of the model developed was evaluated based on correlation coefficient, R^2 , and standard deviation. Data given in Tables 9 and 10 demonstrate that the two models were significant at p values < 0.05 . The closer the R^2 to unity and the smaller the standard deviation, the more accurate the response could be predicted by the model. The regression equations, in terms of their coded factors, are expressed by the following second-order polynomial equations:

$$Y1 = 38.93 + 5.23A - 12.86B - 4.42C + 11.89D - 2.41AB - 1.57AD + 1.95BC - 6.09BD + 1.66BCD, \quad (8)$$

$$Y2 = 23.24 + 2.15A - 4.93B - 6.32C + 7.83D - 0.95AB + 2.58BC - 2.48BD. \quad (9)$$

According to these equations, it is revealed that the pH and treating agent have a positive effect on cadmium ions removal. Moreover, the removal of the cadmium decreased if biosorbents dosage and initial metals concentration increases. Additionally, the interactions pH (A)–biosorbents dosage (B), pH (A)–treating agent (D), biosorbents dosage (B)–initial concentration (C), biosorbents dosage (B)–treating agent (D), and biosorbents dosage (B)–initial concentration (C)–treating agent (D) also had a significant effect on cadmium sorption. The interactions AB, AD, and BD presented a negative effect on cadmium ions removal. Then, the interactions BC and BCD presented a positive

effect on cadmium removal. When this interaction is in the high level, the removal of cadmium increased. It is the same in the case of cobalt. Furthermore, the interactions pH de la solution (A)–biosorbents dosage (B), biosorbents dosage (B)–initial metals concentration (C), and biosorbents dosage (B)–treating agent (D) also had a significant effect on cobalt sorption. In fact, the interaction BC had a positive effect on cobalt sorption proving an increase in this response. On the other hand, the interaction AB and BD present a negative effect for cobalt sorption.

3.3.3. Response Surface Analysis. The three-dimensional (3D) response surface of the tested factors is presented for identifying the type of interaction between the studied factors. For biosorption of cadmium, there are significant interactions between pH and biosorbent dose and another one between biosorbent dose and initial concentration. Figure 10 presents response surfaces plots for these significant interactions. This figure indicates that the sorption of cadmium increased with increasing of pH and and decrease of biosorbent dose with a fixed initial concentration at 50 mg/l with NaOH treating carob (Figure 10(a)). Furthermore, the sorption of Cd(II) increased with decreasing of biosorbent dose and initial concentration (Figure 10(b)). A maximal sorption cadmium response is observed at pH=6 and initial concentration of 50 mg/l at a biosorbent dose of 1 g/l with NaOH treating carob.

Figure 11 presents the significant interaction between pH and biosorbent dose and another one between biosorbent dose and initial concentration, for the sorption of cobalt. Figure 11(a) shows that the biosorption of Co(II) increased with increasing of pH and decreasing of biosorbent dose with a fixed initial concentration at 50 mg/l

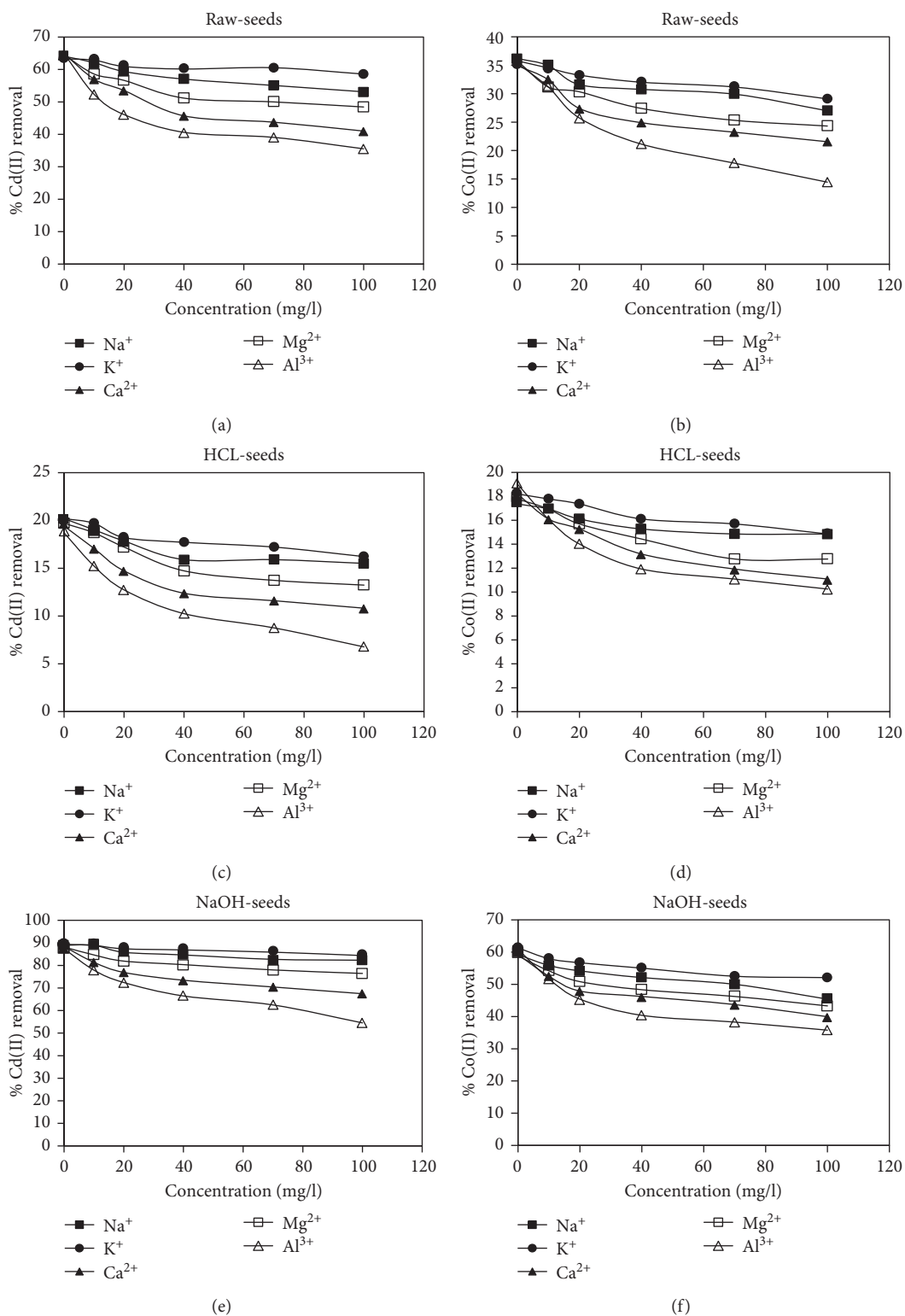


FIGURE 9: Effect of Na⁺, K⁺, Ca²⁺, Mg²⁺, and Al³⁺ concentration on the inhibition of the biosorption of Cd(II) and Co(II) onto biosorbents.

with NaOH treating carob. Moreover, when the initial concentration and the biosorbent dose decrease, the sorption of cobalt increases at pH = 6 with NaOH treating carob (Figure 11(b)). So, the best cobalt biosorption was obtained with pH = 6, biosorbent dose of 1 g/l, concentration of 50 mg/l, and NaOH treating carob.

3.3.5. Optimization. The two responses were optimized simultaneously by using the desirability function approach. The response variable was 1.00. Hence, " R^2 " is in consistent enough with the " R^2_{Adj} ." Thus, $R^2 = 0.9979$, $R^2 = 0.9955$ and $R^2_{Adj} = 0.9947$, $R^2_{Adj} = 0.9916$ for Cd(II) and Co(II) sorption responses. The model F -value of the

TABLE 7: Factorial experimental design matrix coded, real values, and experimental results of the responses.

Run	Coded values				Actual values				Responses	
	A	B	C	D	A	B	C	D	Cd(II)	Co(II)
1	-1	-1	-1	-1	4	1	50	HCl	30.59	24.22
2	+1	-1	-1	-1	6	1	50	HCl	46.21	29.30
3	-1	+1	-1	-1	4	3	50	HCl	19.23	14.48
4	+1	+1	-1	-1	6	3	50	HCl	29.34	18.05
5	-1	-1	+1	-1	4	1	100	HCl	19.56	5.58
6	+1	-1	+1	-1	6	1	100	HCl	38.86	12.36
7	-1	+1	+1	-1	4	3	100	HCl	11.57	8.64
8	+1	+1	+1	-1	6	3	100	HCl	20.92	10.71
9	-1	-1	-1	+1	4	1	50	NaOH	70.11	42.86
10	+1	-1	-1	+1	6	1	50	NaOH	85.73	51.90
11	-1	+1	-1	+1	4	3	50	NaOH	32.10	26.53
12	+1	+1	-1	+1	6	3	50	NaOH	33.48	29.17
13	-1	-1	+1	+1	4	1	100	NaOH	56.32	27.61
14	+1	-1	+1	+1	6	1	100	NaOH	66.89	31.56
15	-1	+1	+1	+1	4	3	100	NaOH	30.11	18.81
16	+1	+1	+1	+1	6	3	100	NaOH	31.80	20.13

TABLE 8: Values of model coefficients of the two responses.

Main coefficients	Y1	Y2
b_0	38.93	23.24
b_1	5.23	2.15
b_2	-12.86	-4.93
b_3	-4.42	-6.32
b_4	11.89	7.82
b_{12}	-2.41	-0.95
b_{13}	-0.11	-0.39
b_{14}	-1.57	-0.03
b_{23}	1.95	2.58
b_{24}	-6.09	-2.48
b_{34}	-0.11	-0.22
b_{123}	0.06	0.03
b_{124}	-0.49	-0.18
b_{134}	-0.49	-0.41
b_{234}	1.66	-0.22
b_{1234}	0.61	0.43

TABLE 9: Analysis of variance for sorption of cadmium ions.

Source	Sum of squares	df	Mean square	F value	p value; prob > F	
Model	6488.97	9	720.99	313.12	<0.0001	Significant
A	437.22	1	437.22	189.88	<0.0001	
B	2645.07	1	2645.072	1148.73	<0.0001	
C	313.043	1	313.04	135.95	<0.0001	
D	2262.37	1	2262.37	982.524	<0.0001	
AB	93.14	1	93.14	40.445	0.0007	
AD	39.45	1	39.45	17.13	0.0061	
BC	61.03	1	61.03	26.51	0.0021	
BD	593.24	1	593.24	257.64	<0.0001	
BCD	44.40	1	44.40	19.28	0.0046	
Residual	13.81	6	2.30			
Cor. total	6502.796	15				

$$R^2 = 0.9979; R_{adj}^2 = 0.9947.$$

both responses is greater, in order of 313.12 and 255.37 for Cd(II) and Co(II) sorption, respectively. Further, these results explain that the models are suitable. Then, it was found that there was good agreement between experimentally and model predicted response factor which confirms the adequacy and the significance of the proposed model. The optimal conditions for high sorption of cadmium(II) and cobalt(II) were achieved at pH = 6, biosorbent dose of 1 g/l, and initial concentration = 50 mg/l with carob seeds treated by NaOH. The greater sorption capacities were 85.73 mg/g for Cd(II) and 51.90 mg/g for Co(II).

4. Conclusion

During this study, raw carob seeds and chemically treated carob seeds were used as low-cost natural biosorbents for the removal of Cd(II) and Co(II) from aqueous solutions.

The biosorption productivity was tested by using different biosorption conditions. According to these studies, it was found that the biosorption yield increases with the increase of biosorbent dosage with an optimum at 0.1 g/L. The optimum sorption was obtained at basic pH medium. The sorption process was very rapid, since the equilibrium time was obtained at 90 min for Cd(II) and 60 min for Co(II). Biosorption kinetics data were properly fitted with the pseudo-first-order kinetic model. The equilibrium biosorption was increased with an increase in the initial ions concentration in solution. The biosorption isotherm could be well fitted by the Langmuir equation. The temperature does not have much influence on the biosorption performance. Other tests show that the presence of inorganic ions had specific effects on Cd(II) and Co(II) biosorption onto biosorbents, with the inhibition effect observing the following sequence: $K^+ < Na^+ < Mg^{2+} < Ca^{2+} < Al^{3+}$. From these studies, it can be also seen that chemical pretreatment the raw carob shell with NaOH strongly enhances its

TABLE 10: Analysis of variance for sorption of cobalt ions.

Source	Sum of squares	df	Mean square	F value	p value; prob > F	
Model	2302.19	7	328.88	255.37	<0.0001	Significant
A	74.23	1	74.23	57.64	<0.0001	
B	388.97	1	388.97	302.03	<0.0001	
C	639.204	1	639.20	496.33	<0.0001	
D	980.24	1	980.24	761.14	<0.0001	
AB	14.54	1	14.54	11.29	0.0099	
BC	106.31	1	106.31	82.55	<0.0001	
BD	98.69	1	98.69	76.63	<0.0001	
Residual	10.30	8	1.29			
Cor. total	2312.50	15				

$R^2 = 0.9955$; $R^2_{adj} = 0.9916$.

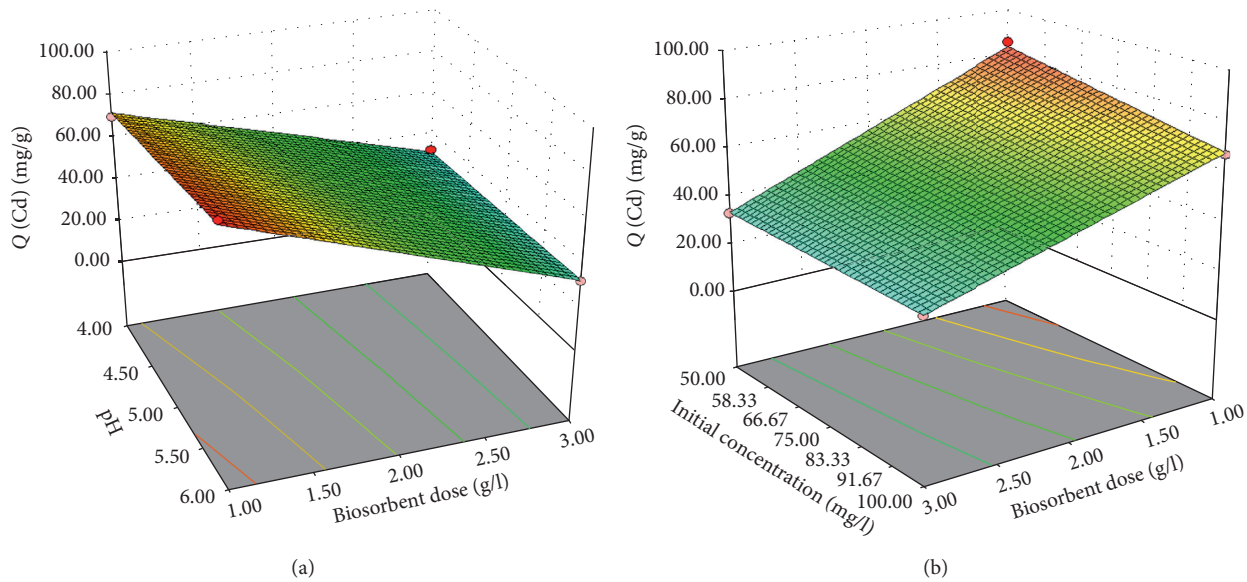


FIGURE 10: Surface response plots for the cadmium ions removal.

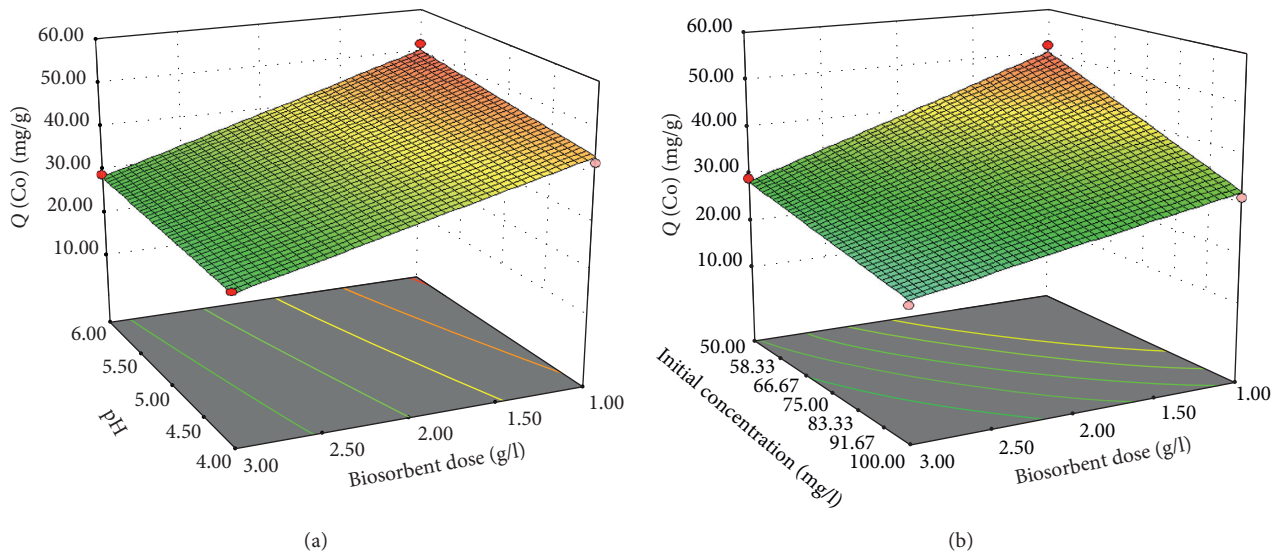


FIGURE 11: Surface response plot for the cobalt ions removal.

biosorption potential for the cadmium(II) and cobalt(II) ions. Full-factorial experimental design was used to determine the optimum conditions of different variables which affect the removal of Cd(II) and Co(II) ions. In order to achieve approximately the greater values of biosorption capacities of treated carob shell for Cd(II) and Co(II) ions, the optimum values of different process parameters were found to be 85.73 mg/g for Cd(II) and 51.90 mg/g for Co(II). These higher sorption efficiencies are obtained at pH = 6, biosorbent dose of 1 g/l, and initial concentration = 50 mg/l with carob shell treated by NaOH.

Data Availability

The data used to support the findings of this study are available from the corresponding author upon request.

Conflicts of Interest

The authors declare that they have no conflicts of interest.

Supplementary Materials

In summary, efficient biosorbents were developed from deoiled carob seeds. The biosorption efficiency was evaluated for cadmium and cobalt ions removal from aqueous solution under various parameters. Based on this preliminary study, four independent variables including solution pH, biosorbents dosage, initial metal concentration, and treating agent were chosen for the optimization of the process using full-factorial experimental design. It was found that chemical pretreatment of the raw deoiled carob seeds with NaOH strongly enhances its biosorption potential. The optimal conditions for high biosorption of cadmium(II) and cobalt (II) were achieved at pH of 6, biosorbent dosage of 1 g/L, and initial metal concentration of 50 mg/L. (*Supplementary Materials*)

References

- [1] S. H. Abbas, I. M. Ismail, T. M. Mostafa, and A. H. Sulaymon, "Biosorption of heavy metals: a review," *Journal of Chemical Science and Technology*, vol. 3, no. 4, pp. 74–102, 2014.
- [2] M. Jaishankar, T. Tseten, N. Anbalagan, B. B. Mathew, and K. N. Beeregowda, "Toxicity, mechanism and health effects of some heavy metals," *Interdisciplinary Toxicology*, vol. 7, no. 2, pp. 60–72, 2014.
- [3] H. M. Zwain, M. Vakili, and I. Dahlan, "Waste material adsorbents for zinc removal from wastewater: a comprehensive review," *International Journal of Chemical Engineering*, vol. 2014, Article ID 347912, 13 pages, 2014.
- [4] M. J. González-Muñoz, M. A. Rodríguez, S. Luque, and J. R. Álvarez, "Recovery of heavy metals from metal industry waste waters by chemical precipitation and nanofiltration," *Desalination*, vol. 200, no. 1–3, pp. 742–744, 2006.
- [5] H. Bessbousse, T. Rhlalou, J. F. Verchère, and L. Lebrun, "Removal of heavy metal ions from aqueous solutions by filtration with a novel complexing membrane containing poly (ethyleneimine) in a poly(vinyl alcohol) matrix," *Journal of Membrane Science*, vol. 307, no. 2, pp. 249–259, 2008.
- [6] R. Kiefer, A. I. Kalinitchev, and W. H. Höll, "Column performance of ion exchange resins with aminophosphonate functional groups for elimination of heavy metals," *Reactive and Functional Polymers*, vol. 67, no. 12, pp. 1421–1432, 2007.
- [7] J. Konczyk, C. Kozłowski, and W. Walkowiak, "Lead(II) removal from aqueous solutions by solvent extraction with tetracarboxyl- resorcin [4] arene," *Physicochemical Problems of Mineral Processing*, vol. 49, no. 1, pp. 213–222, 2013.
- [8] H. Polat and D. Erdogan, "Heavy metal removal from waste waters by ion flotation," *Journal of Hazardous Materials*, vol. 148, no. 1–2, pp. 267–273, 2007.
- [9] A. Hamid Sulaymon, A. Obaid Sharif, and T. K. Al-Shalch, "Removal of cadmium from simulated wastewaters by electrodeposition on stainless steel tubes bundle electrode," *Desalination and Water Treatment*, vol. 29, no. 1–3, pp. 218–226, 2011.
- [10] K. Vijayaraghavan, K. Palanivelu, and M. Velan, "Biosorption of copper(II) and cobalt(II) from aqueous solutions by crab shell particles," *Bioresource Technology*, vol. 97, no. 12, pp. 1411–1419, 2006.
- [11] P. Chakravarty, N. Sen Sarma, and H. P. Sarma, "Biosorption of cadmium(II) from aqueous solution using heartwood powder of Areca catechu," *Chemical Engineering Journal*, vol. 162, no. 3, pp. 949–955, 2010.
- [12] I. Anastopoulos and Z. George Kyzas, "Progress in batch biosorption of heavy metals onto algae," *Journal of Molecular Liquids*, vol. 209, pp. 77–86, 2015.
- [13] K. A. Adegoke and O. S. Bello, "Dye sequestration using agricultural wastes as adsorbents," *Water Resources and Industry*, vol. 12, pp. 8–24, 2015.
- [14] S. Y. Bratskaya, A. V. Pestov, Y. G. Yatluk, and V. A. Avramenko, "Heavy metals removal by flocculation/precipitation using N-(2-carboxyethyl)chitosans," *Colloids and Surfaces A: Physicochemical and Engineering Aspects*, vol. 339, no. 1–3, pp. 140–144, 2009.
- [15] A. C. Gonçalves Jr., L. Strey, C. A. Lindino, H. Nacke, D. Schwantes, and E. P. Seidel, "Applicability of the Pinus bark (*Pinus elliottii*) for the adsorption of toxic heavy metals from aqueous solutions," *Acta Scientiarum Technology*, vol. 34, no. 1, pp. 79–87, 2012.
- [16] H. Nacke, A. C. Gonçalves Jr., G. F. Coelho, L. Strey, and A. Laufer, "Renewable energy technologies: removal of cadmium from aqueous solutions by adsorption on Jatropha biomass," in *Green Design, Materials and Manufacturing Processes*, H. Bártolo and J. P. Duarte, Eds., pp. 367–37, CRC Press Taylor & Francis Group, Boca Raton, 1st edition, 2013.
- [17] V. C. G. Dos Santos, C. R. T. Tarley, J. Caetano, and D. C. Dragunski, "Assessment of chemically modified sugarcane bagasse for lead adsorption from aqueous medium," *Water Science and Technology*, vol. 62, no. 2, pp. 457–465, 2010.
- [18] A. C. Gonçalves Jr., C. Selzlein, and H. Nacke, "Uso de biomassa seca de aguapé (*Eichornia crassipes*) visando à remoção de metais pesados de soluções contaminadas," *Acta Scientiarum Technology*, vol. 31, no. 1, pp. 103–108, 2009.
- [19] A. Bhatnagar, V. J. P. Vilar, C. M. S. Botelho, and R. A. R. Boaventura, "Coconut-based biosorbents for water treatment a review of the recent literature," *Advances in Colloid and Interface Science*, vol. 160, no. 1–2, pp. 1–15, 2010.
- [20] E. Njikam and S. Schiewer, "Optimization and kinetic modeling of cadmium desorption from citrus peels: a process for biosorbent regeneration," *Journal of Hazardous Materials*, vol. 213–214, pp. 242–248, 2012.
- [21] S. Liang, X. Guo, and Q. Tian, "Adsorption of Pb²⁺, Cu²⁺ and Ni²⁺ from aqueous solutions by novel garlic peel adsorbent,"

- Desalination and Water Treatment*, vol. 51, no. 37–39, pp. 7166–7171, 2013.
- [22] F. A. Ugbe, A. A. Pam, and A. V. Ikudayisi, “Thermodynamic properties of chromium(III) ion adsorption by sweet orange (*Citrus sinensis*) peels,” *American Journal of Analytical Chemistry*, vol. 5, no. 10, pp. 666–673, 2014.
 - [23] B. I. Hussein, “Removal of copper ions from waste water by adsorption with modified and unmodified sunflower stalks,” *Journal of Engineering*, vol. 16, no. 3, pp. 5411–5421, 2010.
 - [24] M. Farnane, H. Tounsadi, R. Elmoubarki et al., “Alkaline treated carob shells as sustainable biosorbent for clean recovery of heavy metals: Kinetics, equilibrium, ions interference and process optimisation,” *Ecological Engineering*, vol. 101, pp. 9–20, 2017.
 - [25] H. Tounsadi, A. Khalidi, M. Abdennouri, and N. Barka, “Biosorption potential of *Diplotaxis harra* and *Glebionis coronaria* L. biomasses for the removal of Cd(II) and Co(II) from aqueous solutions,” *Journal of Environmental Chemical Engineering*, vol. 3, no. 2, pp. 822–830, 2015.
 - [26] H. P. Boehm, E. Diehl, W. Heck, and R. Sappok, “Surface oxides of carbon,” *Angewandte Chemie International Edition in English*, vol. 3, no. 10, pp. 669–677, 1964.
 - [27] J. S. Noh and J. A. Schwarz, “Estimation of the point of zero charge of simple oxides by mass titration,” *Journal of Colloid and Interface Science*, vol. 130, no. 1, pp. 157–164, 1989.
 - [28] C. R. Teixeira Tarley and M. A. Zezzi Arruda, “Biosorption of heavy metals using rice milling by-products. Characterisation and application for removal of metals from aqueous effluents,” *Chemosphere*, vol. 54, no. 7, pp. 987–995, 2004.
 - [29] O. E. Abdel Salam, N. A. Reiad, and M. M. ElShafei, “A study of the removal characteristics of heavy metals from wastewater by low-cost adsorbents,” *Journal of Advanced Research*, vol. 2, no. 4, pp. 297–303, 2011.
 - [30] D. Özcimen and A. Ersoy-Meriçboyu, “Removal of copper from aqueous solutions by adsorption onto chestnut shell and grape-seed activated carbons,” *Journal of Hazardous Materials*, vol. 168, no. 2–3, pp. 1118–1125, 2009.
 - [31] J. P. Chen and X. Wang, “Removing copper, zinc, and lead ion by granular activated carbon in pretreated fixed-bed columns,” *Separation and Purification Technology*, vol. 19, no. 3, pp. 157–167, 2000.
 - [32] E.-Z. El-Ashtouky, N. K. Amin, and O. Abdelwahab, “Removal of lead(II) and copper(II) from aqueous solution using pomegranate peel as a new adsorbent,” *Desalination*, vol. 223, no. 1–3, pp. 162–173, 2008.
 - [33] C. A. Rozaini, K. Jain, C. W. Oo et al., “Optimization of nickel and copper ions removal by modified mangrove barks,” *International Journal of Chemical Engineering and Applications*, vol. 1, no. 1, pp. 84–89, 2010.
 - [34] N. Barka, S. Qourzal, A. Assabane, A. Nounah, and Y. Ait-Ichou, “Removal of reactive yellow 84 from aqueous solutions by adsorption onto hydroxyapatite,” *Journal of Saudi Chemical Society*, vol. 15, no. 3, pp. 263–267, 2011.
 - [35] A. Nasrullah, H. Khan, A. S. Khan et al., “Potential biosorbent derived from calligonum polygonoides for removal of methylene blue dye from aqueous solution,” *Scientific World Journal*, vol. 2015, Article ID 562693, 11 pages, 2015.
 - [36] Y.-j. Gao, “Cadmium and Cobalt Removal from Heavy Metal Solution using Oyster Shells Adsorbent,” pp. 1098–1101, 2011.
 - [37] X. Li, Y. Tang, X. Cao, D. Lu, F. Luo, and W. Shao, “Preparation and evaluation of orange peel cellulose adsorbents for effective removal of cadmium, zinc, cobalt and nickel,” *Colloids and Surfaces A: Physicochemical and Engineering Aspects*, vol. 317, no. 1–3, pp. 512–521, 2008.
 - [38] G. Ozdemir, N. Ceyhan, and E. Manav, “Utilization of an exopolysaccharide produced by *Chryseomonas luteola* TEM05 in alginate beads for adsorption of cadmium and cobalt ions,” *Bioresource Technology*, vol. 96, no. 15, pp. 1677–1682, 2005.
 - [39] S. Lagergren, “About the theorie of so-called adsorption of soluble substance Seven Vetenskapsakad,” *Handlingar*, vol. 24, pp. 1–39, 1898.
 - [40] Y. S. Ho and G. McKay, “Pseudo-second order model for sorption processes,” *Process Biochemistry*, vol. 34, no. 5, pp. 451–465, 1999.
 - [41] B. H. Hameed, I. A. W. Tan, and A. L. Ahmad, “Adsorption isotherm, kinetic modeling and mechanism of 2,4,6-trichlorophenol on coconut husk-based activated carbon,” *Chemical Engineering Journal*, vol. 144, no. 2, pp. 235–244, 2008.
 - [42] M. H. Jnr and A. I. Spiff, “Effect of metal ion concentration on the biosorption of Pb²⁺ and Cd²⁺ by *Caladium bicolor* (wild cocoyam),” *Electronic Journal of Biotechnology*, vol. 8, no. 2, pp. 162–169, 2005.
 - [43] C. H. Giles, D. Smith, and A. Huitson, “A general treatment and classification of the solute adsorption isotherm. I. Theoretical,” *Journal of Colloid and Interface Science*, vol. 47, no. 3, pp. 755–765, 1974.
 - [44] I. Langmuir, “The constitution and fundamental properties of solids and liquids,” *Journal of the American Chemical Society*, vol. 38, no. 11, pp. 2221–2295, 1916.
 - [45] H. Freundlich and W. Heller, “The adsorption of cis- and trans-azobenzene,” *Journal of the American Chemical Society*, vol. 61, no. 8, pp. 2228–2230, 1939.
 - [46] G. D. Halsey, “The role of surface heterogeneity in adsorption,” *Advances in Catalysis*, vol. 4, pp. 259–269, 1952.
 - [47] B. Kiran and A. Kaushik, “Chromium binding capacity of Lyng by aputealisexo poly-saccharides,” *Biochemical Engineering Journal*, vol. 38, pp. 47–54, 2008.
 - [48] S. Al-Asheh and Z. Duvnjak, “Binary metal sorption by pine barks: study of equilibria and mechanisms,” *Separation Science and Technology*, vol. 33, no. 9, pp. 1303–1329, 1998.
 - [49] T. Gosset, J. L. Transcart, and D. R. Thevenot, “Batch metal removal by peat: kinetics and thermodynamics,” *Water Research*, vol. 20, no. 1, pp. 21–26, 1986.
 - [50] G. Cimino, A. Passerini, and G. Toscano, “Removal of toxic cations and Cr(VI) from aqueous solution by hazelnut shell,” *Water Research*, vol. 34, no. 11, pp. 2955–2962, 2000.
 - [51] T. W. Tee and A. R. M. Khan, “Removal of lead, cadmium and zinc by waste tea leaves,” *Environmental Technology Letters*, vol. 9, no. 11, pp. 1223–1232, 1988.
 - [52] C. L. Lee, T. C. Wang, C. K. Lin, and H. K. Mok, “Heavy metals removal by a promising locally available aquatic plant, *Najas graminea* del., in Taiwan,” *Water Science and Technology*, vol. 39, no. 10–11, pp. 177–181, 1999.
 - [53] F. Guzel, H. Yakut, and G. Topal, “Determination of kinetic and equilibrium parameters of the batch adsorption of Mn (II), Co(II), Ni(II) and Cu(II) from aqueous solution by black carrot (*Daucus carota* L.) residues,” *Journal of Hazardous Materials*, vol. 153, no. 3, pp. 1275–1287, 2008.
 - [54] H. Parab, S. Joshi, N. Shenoy, A. Lali, U. S. Sarma, and M. Sudersanan, “Determination of kinetic and equilibrium of Co(II), Cr(III), and Ni(II) onto coir pith,” *Process Biochemistry*, vol. 41, no. 3, pp. 609–615, 2006.
 - [55] M. Wael Ibrahim, “Biosorption of heavy metal ions from aqueous solution by red macroalgae,” *Journal of Hazardous Materials*, vol. 192, no. 3, pp. 1827–1835, 2011.
 - [56] T. Kumar Naiya, P. Chowdhury, A. K. Bhattacharya, and S. K. Das, “Saw dust and neem bark as low-cost natural

- biosorbent for adsorptive removal of Zn(II) and Cd(II) ions from aqueous solutions,” *Chemical Engineering Journal*, vol. 148, no. 1, pp. 68–79, 2009.
- [57] R. Zein, R. Suhaili, F. Earnestly, Indrawati, and E. Munaf, “Removal of Pb(II), Cd(II) and Co(II) from aqueous solution using *Garcinia mangostana* L. fruit shell,” *Journal of Hazardous Materials*, vol. 181, no. 1–3, pp. 52–56, 2010.
- [58] M. A. Javeda, H. N. Bhattia, M. A. Hanifa, and R. Nadeema, “Kinetic and equilibrium modeling of Pb(II) and Co(II) sorption onto rose waste biomass,” *Separation Science and Technology*, vol. 42, no. 16, pp. 3641–3656, 2007.
- [59] K. Vijayaraghavan, J. Jegan, K. Palanivelu, and M. Velan, “Biosorption of cobalt(II) and nickel(II) by seaweeds: batch and column studies,” *Separation and Purification Technology*, vol. 44, no. 1, pp. 53–59, 2005.
- [60] N. Barka, M. Abdennouri, M. El Makhfouk, and S. Qourzal, “Biosorption characteristics of cadmium and lead onto eco-friendly dried cactus (*Opuntia ficus-indica*) Cladodes,” *Journal of Environmental Chemical Engineering*, vol. 1, no. 3, pp. 144–149, 2013.
- [61] M. Saleem, T. Pirzada, and R. Qadeer, “Sorption of acid violet 17 and direct red 80 dyes on cotton fiber from aqueous solutions,” *Colloids and Surfaces A: Physicochemical and Engineering Aspects*, vol. 292, no. 2–3, pp. 246–250, 2007.
- [62] A. Sari and M. Tuzen, “Biosorption of cadmium(II) from aqueous solution by red algae (*Ceramium virgatum*): equilibrium, kinetic and thermodynamic studies,” *Journal of Hazardous Materials*, vol. 157, no. 2–3, pp. 448–454, 2008.
- [63] D. Kratochvil and B. Volesky, “Advances in the biosorption of heavy metals,” *Trends in Biotechnology*, vol. 16, no. 7, pp. 291–300, 1998.
- [64] S. Schiewer and B. Volesky, “Ionic strength and electrostatic effects in biosorption of divalent metal ions and protons,” *Environmental Science & Technology*, vol. 31, no. 9, pp. 2478–2485, 1997.
- [65] V. Murphy, “An investigation into the mechanisms of heavy metal binding by selected seaweed species,” Ph.D. Thesis, Waterford Institute of Technology, Waterford, Ireland, 2007.

Research Article

Atmospheric Nitrogen Deposition Associated with the Eutrophication of Taihu Lake

Xi Chen¹, Yan-hua Wang^{1,2}, Chun Ye³, Wei Zhou⁴, Zu-cong Cai^{1,2}, Hao Yang^{1,2}, and Xiao Han^{5,6}

¹School of Geography Science, Nanjing Normal University, Nanjing 210023, China

²Jiangsu Center for Collaborative Innovation in Geographical Information Resource Development and Application, Nanjing 210023, China

³Chinese Research Academy of Environmental Sciences, Beijing 100012, China

⁴Institute of Soil Science, Chinese Academy of Sciences, Nanjing 210008, China

⁵State Key Laboratory of Atmospheric Boundary Layer Physics and Atmospheric Chemistry, Institute of Atmospheric Physics, Chinese Academy of Sciences, Beijing 100029, China

⁶College of Earth Science, University of Chinese Academy of Sciences, Beijing 100049, China

Correspondence should be addressed to Yan-hua Wang; wangyanhua@njnu.edu.cn

Received 18 March 2018; Revised 30 May 2018; Accepted 11 June 2018; Published 25 July 2018

Academic Editor: Adina Negrea

Copyright © 2018 Xi Chen et al. This is an open access article distributed under the Creative Commons Attribution License, which permits unrestricted use, distribution, and reproduction in any medium, provided the original work is properly cited.

Environmental effects of excessive amounts of atmospheric nitrogen (N) deposition have raised a great deal of attention. In the present study, the characteristics of N deposition and its contribution to water eutrophication were investigated in the Taihu Basin. The results showed that the annual average total deposition (TN), total wet deposition (TN_W), and total dry deposition (TN_D) rates were 6154, 1142, and 5012 kg·km⁻², respectively. Moreover, seasonal fluctuations in TN, TN_W, and TN_D deposition were observed, with a higher N deposition rate occurring in spring and summer. Spatially, the distribution of TN and TN_D deposition throughout the Taihu Basin was similar. However, the TN deposition rate declined gradually from the southeast to the northwest, while the TN_W deposition rate increased. A significant positive correlation was also found between the TN deposition contents with rainfall ($R = 0.803, P = 0.01$), rainfall frequency ($R = 0.767, P < 0.01$), and rainfall intensity ($R = 0.659, P < 0.05$). The TN deposition concentration was significantly negatively correlated with rainfall ($R = -0.999, P < 0.01$), rain frequency ($R = -0.805, P < 0.01$), and rainfall intensity ($R = -0.783, P < 0.01$). The riverine input of TN was estimated to be 112,500 t·N·a⁻¹, and the main N pollutants originated from domestic sewage (accounting for 48.88%) and agriculture (accounting for 28.17%). Livestock and aquaculture contributed 90% of the agricultural pollutants. Additionally, TN deposition contributed 14,400 t·N·a⁻¹ to the lake, which accounted for 12.36% of the annual riverine TN inputs. The TN deposition load already exceeds the eutrophication critical load in theory. Furthermore, the contribution of N deposition to the lake has been increasing in recent years, which may accelerate eutrophication of Taihu Lake.

1. Introduction

Nitrogen (N) deposition mainly originates from the discharge of nitrogen oxides (NO_x), nitrate nitrogen (NO₃⁻-N), ammonia nitrogen (NH₃), and ammonium nitrogen (NH₄⁺-N) from both anthropogenic and natural sources. Ultimately, these compounds return to the surface via wet and dry deposition [1, 2]. Atmospheric N deposition represents an important source of reactive N to the ecosystems [3, 4].

However, excessive N inputs could cause adverse ecological effects, including soil acidification, plant biodiversity reduction, and eutrophication [5–7]. Many literature studies have shown that the concentration of N deposition in water N loads has increased [8–10], and the ecological effects of atmospheric N deposition have received a great deal of attention in recent years [11, 12]. Many methods have been employed to collect N deposition, including ion-exchange resin, micrometeorological integral total N input, and

minusing methods [13–16]. Due to the rapid population growth, industrialization, vehicle ownership, and fossil fuel combustion, the NO_x emissions in China have shown a marked increase of 2.8 times from 1980 to 2003 [17, 18]. It is also believed that both the excessive use of chemical N fertilizer and increasing amounts of human, aquaculture, and livestock excrement may have increased NH_3 emissions [19]. The fertilizer production in China in 2010 brought out 37.10 Tg of N. Among them, 75.74% was consumed by domestic agriculture, much more than the total world production and consumption. However, less than half of the N application was taken up by the crops [20]. The majority was discharged into the waterbody or the atmosphere by runoff and volatilization. The average total NH_3 emissions in China is 15 Tg $\text{N}\cdot\text{a}^{-1}$, approximately 90% of which is contributed by agricultural activities [21, 22]. Rapid economic development has resulted in a significant increase in reactive N creation worldwide in recent years [19]. It is estimated that the total reactive N produced by anthropogenic activities ranged from 15 Tg in 1860 to 165 Tg in 1995, and global TN deposition is expected to reach 195 Tg in 2050 [17]. In China, the total NO_x emission from anthropogenic activities increased from 8.40 Tg $\text{N}\cdot\text{a}^{-1}$ in 1990 to 11.30 Tg $\text{N}\cdot\text{a}^{-1}$ in 2000, while the total NH_3 emissions rose from 10.80 Tg $\text{N}\cdot\text{a}^{-1}$ to 13.60 Tg $\text{N}\cdot\text{a}^{-1}$ [23, 24]. Western Europe, China, and India have had the highest N deposition in the world in recent years [25].

The Taihu watershed has played an important role in the water quantity regulation, industry, agriculture, and tourism. The lake water was under the oligotrophic status in the 1950s [26]. However, it underwent more aggravated eutrophication in the mid-1980s because of the rapid industrial and agricultural development and excessive population growth [27]. Large amounts of nutrients have been discharged into the Taihu Lake via river runoff and N deposition. As a result, the natural environment of Taihu Lake has already deteriorated significantly, and water eutrophication has become a serious problem [10, 27–29]. As a result, many policies have been initiated to improve the water quality of Taihu Lake. Nevertheless, the Taihu Lake water quality has not improved remarkably. Many prior case studies have been conducted to determine the origins and forms of N entering the system [30–33]. From year 2002, a series of investigations for atmospheric N deposition in Taihu Lake have focused on more and more attention and the results were used for preliminary calculation of the contribution of N deposition to the lake [9, 10, 28]. However, studies of the temporal and spatial distribution of N deposition and the contribution to the water eutrophication of Taihu Lake need further focus. Therefore, the present study was conducted to (1) characterize the atmospheric N deposition, (2) make a unified calculation of N migration and transformation in the system, (3) calculate N loads from the inflowing rivers and explore the contribution of N deposition to the water eutrophication, and (4) provide a reference for economic development and environmental governance in the study area.

2. Materials and Methods

2.1. Study Area. The Taihu watershed ($29^{\circ}55'\sim 32^{\circ}19'\text{N}$, $118^{\circ}50'\sim 121^{\circ}55'\text{E}$) is located in the lower Yangtze River Delta

(Figure 1). The watershed extends across Jiangsu Province (53% of the watershed area), Zhejiang Province (33.40%), Anhui Province (0.1%), and Shanghai (13.50%). Taihu Lake, the third largest freshwater lake in China, is a typical large shallow lake with an area of 2338 km^2 and a mean depth of 1.90 m. More than 200 streams flow radially into the lake. The Taihu watershed is characterized by a typical subtropical monsoon climate, with an annual mean temperature of 16°C and dominant soil types of yellow-brown soil, red soil, and paddy soil. The main crops in the region are wheat and rice. Excessive use of N fertilizer is common, particularly in regions with high population densities, and the average N fertilizer application rate is 570–600 $\text{kg}\cdot\text{ha}^{-1}$ in the rice-wheat double cropping rotation system [31]. However, only $\sim 35\%$ of fertilizer is absorbed in the season [21, 31]. The rest enters into the environment. For the livestock breeding, free-range chickens and ducks mode is dominant. Approximately 65% of the livestock manure in the region is disposed by the concentrated treatment, while 35% of the undisposed manure is discharged directly into the waterbody [21], resulting in excessive N levels in local aquatic systems [21, 31].

The Taihu watershed has undergone a very high degree of urbanization and became the most important comprehensive industrial base in China [34–37]. As of 2015, the population of the region was 68.27 million, and the GDP per capita in the lake basin was USD 1,325. These increased anthropogenic activities have increased the N deposition rate and aggravated eutrophication [26–39].

2.2. Extraction N Deposition Data and Correlation Analysis.

The simulation atmospheric N deposition data (in 2015) were obtained through RAMS-CMAQ (Models 3, USA), and the horizontal resolution was 64 km. The total wet deposition (TN_w), total dry deposition (TN_D), and total nitrogen (TN) rates, which included NO_x (NO , NO_2 , NO_3 , N_2O , and N_2O_5), NH_3 , $\text{NO}_3^{-}\text{-N}$, and $\text{NH}_4^{+}\text{-N}$ were organized using the MATLAB 8.0 (The MathWorks Company, USA) software. All atmospheric TN_w and TN_D deposition rates were obtained using the Kriging interpolation and mask extraction tool of Spatial Analysis from ArcGIS 10.0 (ESRI, USA). Additionally, SPSS 18.0 (IBM, USA) was used to make a curve estimation between the concentration of TN_w , $\text{NH}_x\text{-N}$ (including $\text{NH}_4^{+}\text{-N}$ and NH_3), and $\text{NO}_3^{-}\text{-N}$ deposition rate monthly and meteorological conditions. The concentration of wet N deposition had a power-type correlation with rainfall. The Pearson correlation method was used.

2.3. Calculation of N Inputs. Calculation of the N inputs into a river from different pollutant sources is very complicated, and considerable uncertainty in the results exists because of the fluctuating emission coefficients in different regions [29, 30, 40]. Accordingly, determination of the emission coefficient is essential for calculation of the N inputs into the waterbody. In the present study, we calculated the main pollutant source of agricultural (chemical fertilizer, livestock, and aquaculture), domestic

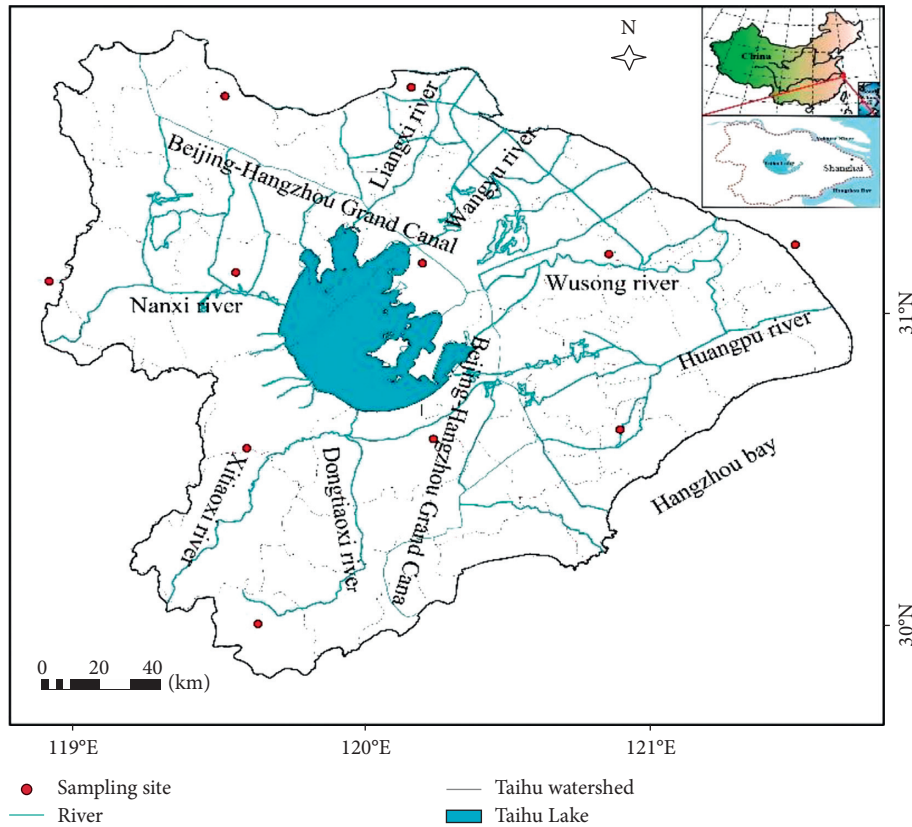


FIGURE 1: Location and administrative divisions of the Taihu watershed.

TABLE 1: Coefficients of various pollutants produced and discharged into rivers.

	Industrial effluents [41]	Urban sewage [42, 43]	Rural-domestic sewage [44]	Runoff fertilizer [38]	Aquaculture [28, 45]
Emission coefficient	—	2.92 kg·N·a ⁻¹ ·capita ⁻¹	2.19 kg·N·a ⁻¹ ·capita ⁻¹	—	1800 kg·N·(ha·a) ⁻¹
Coefficient into water	0.65	0.80	0.10	0.05	1.00

TABLE 2: Different N produced and loss coefficients by livestock.

	Pig manure [44]	Pig urine [44]	Cattle manure [42]	Cattle urine [42]	Sheep [29]	Chicken [29, 43]
Emission coefficient (kg·N·a ⁻¹ ·capita ⁻¹)	2.34	2.17	31.90	29.20	2.28	0.28
Coefficient into water	1.08	50.00	5.60	50.00	10.00	7.80

sewage (urban-domestic sewage and rural-domestic sewage), and industrial effluents (Table 1) by the following equation:

$$N_T = N_A \cdot f_A + N_B \cdot f_B + N_C \cdot f_C + N_E \cdot f_E, \quad (1)$$

where N_T (t·N·a⁻¹) is the total N discharged to surface water, N_i ($i = A, B, C$, and E) is the emission coefficient, and f_i ($i = A, B, C$, and E) is the coefficient of pollutants into the waterbody [41], where A represents industrial effluent [42], B is urban-domestic sewage [43, 44], C is rural-domestic sewage [44, 45], and E is agricultural pollution [29, 46], and the emission coefficient of livestock was determined as shown in Table 2.

3. Results and Discussion

3.1. Chemical Morphological Characteristics of N Deposition. The deposition rates of TN, TN_w, TN_D, NO₃⁻-N, and NH₄⁺-N were 6514, 1142, 5012, 878, and 1207 kg·km⁻²·a⁻¹, respectively (Table 3). The TN deposition rate was higher than that observed in previous studies [10, 19, 47]. The main N deposition is dry deposition, which accounted for 81.40%. Additionally, the NH₄⁺-N/NO₃⁻-N was 1.4 : 1, indicating that the pollution resources may originate from the agricultural activities, as well as rural and urban sewage [48]. Because of the inadequate sewage treatment system, as well as the high fertilizer application coupled with low absorption, many N nutrients were emitted into the atmosphere [21, 31].

TABLE 3: Monthly N deposition rate around the Taihu watershed ($\text{kg}\cdot\text{km}^{-2}\cdot\text{a}^{-1}$).

Deposition	Month												Total
	Jan	Feb	Mar	Apr	May	Jun	Jul	Aug	Sep	Oct	Nov	Dec	
TN	321	291	304	747	840	918	612	652	505	310	459	197	6154
$\text{NH}_4^+\text{-N}$	46	31	55	129	159	248	132	114	78	55	103	59	1207
$\text{NO}_3^-\text{-N}$	20	39	24	69	82	170	101	194	69	19	72	19	878

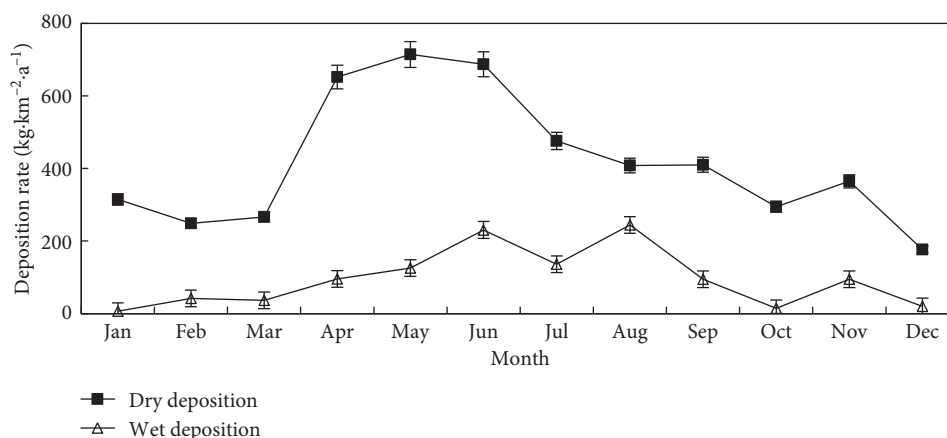


FIGURE 2: Seasonal variations in N deposition flux around the Taihu watershed.

3.2. Spatial and Temporal Distribution Characteristics of N Deposition. The TN, TN_D , and TN_W deposition rates showed seasonal variations in 2015 (Figure 2). The TN_W deposition rate was higher during summer than winter because an El Niño phenomenon occurred in 2015. Cyanobacteria usually grow rapidly in summer. At this time, the high N deposition rate may promote cyanobacterial blooms in Taihu Lake. The wet N deposition rate in July was lower than in June, which was affected by changes in rainfall. However, the continuous heavy rainfall in late June diluted the wet N deposition concentrations in the atmosphere. This phenomenon, coupled with the low rainfall in July (due to the basin being dominated by a subtropical high), caused the wet N deposition rate to decrease rapidly. The high rainfall in August and fertilizer application in the paddy field then led to a remarkable increase in the wet N deposition rate.

The TN_D deposition rate increased rapidly during spring, while it decreased in summer (Figure 2). The NH_3 volatilizing from the fertilizer application is emitted into the atmosphere and then deposited back to the ground after 15 days. Application of fertilizer and pesticides may enhance N deposition in spring. Moreover, unstable atmospheric conditions will increase the deposition rate of particulate matter [49]. Some literature studies have shown that the deposition of NO_x and $\text{NO}_3^-\text{-N}$ are both positively correlated with illumination intensity. Consequently, the dry deposition rate may increase due to the rising temperatures in spring. After fertilizer application to oilseed rape and wheat, the amount of dry N deposition increased significantly in November.

The rates of TN_W and TN_D deposition both showed significant spatial distribution in 2015 (Figure 3). Specifically, the TN_W deposition rate decreased gradually from northwest

to southeast, while the TN_D deposition rate increased. The wet deposition rates were highest ($1640 \text{ kg}\cdot\text{km}^{-2}\cdot\text{a}^{-1}$) in Changzhou and Zhenjiang, which are in the northwest of the Taihu Lake Basin. Low levels of deposition ($500\sim 770 \text{ kg}\cdot\text{km}^{-2}\cdot\text{a}^{-1}\cdot\text{TN}_W$) were observed in Shanghai. The precipitation in the northern Taihu Lake Basin was higher than that in the south in 2015, with the largest precipitation of 1186.7 mm occurring in the Wu-Cheng-Xi-Yu area. The higher rainfall which resulted in more N deposition in this area may be the reason.

The low levels of precipitation in Shanghai resulted in most of the particulate matter returning to the surface via dry deposition. Indeed, the highest dry deposition rate of $10,870 \text{ kg}\cdot\text{km}^{-2}\cdot\text{a}^{-1}$ was observed in Shanghai. Moreover, N deposition formed a high-value band in the cities of Shanghai, Suzhou, Wuxi, and Changzhou because of the higher levels of the industrialization and urbanization. The increased N nutrients accumulated through the discharges from the urban sewage and fossil fuel, especially from vehicle exhaust. Suzhou, which is located on the west of Taihu Lake, has an open terrain and high amount of green area, resulting in lower pollution, and therefore lower N deposition, than other cities.

3.3. Comparisons of N Deposition Values. Monitoring of the deposition rates of TN_W , $\text{NH}_4^+\text{-N}$, and $\text{NO}_3^-\text{-N}$ revealed values of 1647, 986, and $661 \text{ kg}\cdot\text{km}^{-2}\cdot\text{a}^{-1}$, respectively, in Nanjing from July 2015 to June 2016 (Figure 4). The simulated deposition rates of TN_W , $\text{NH}_4^+\text{-N}$, and $\text{NO}_3^-\text{-N}$ were 1653, 508, and $1144 \text{ kg}\cdot\text{km}^{-2}\cdot\text{a}^{-1}$, respectively. Both the monitored and simulated values showed significant seasonal variations in spring and summer. An obvious decrease in the monitored N

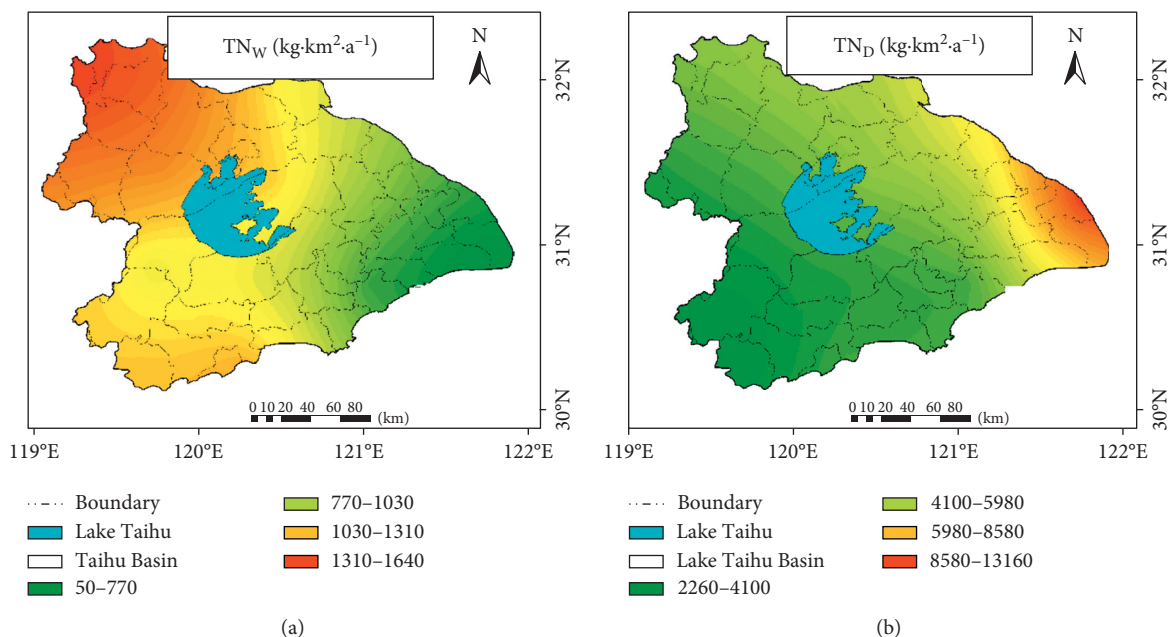


FIGURE 3: Spatial variations in N deposition (kg·km⁻²·a⁻¹) in the Taihu watershed.

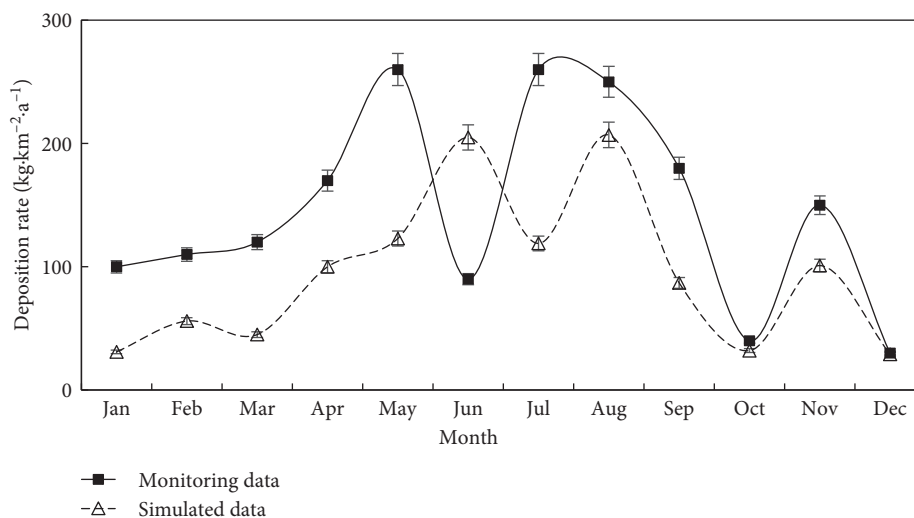


FIGURE 4: Monthly TN deposition (kg·N·km⁻²·a⁻¹) in Nanjing and the simulated value for the Taihu watershed.

deposition rate in June 2016 was observed. Less precipitation at this time may be the reason. However, the rainy season began in July. In the meantime, the N deposition rate increased remarkably. Overall, there was good consistency between the monitored and simulated values.

Atmospheric total wet inorganic nitrogen (TIN_w) deposition rates in the Taihu watershed were compared with those for other areas in China (Figure 5). The TIN_w in the Taihu watershed was higher than in other regions of China from 2001 to 2015. Specifically, the TIN_w deposition rate in the Taihu watershed increased before 2011 and then decreased obviously. The mean annual TIN_w deposition rates in the Taihu watershed, North China Plain, Pearl River Delta, and Western China were 2736, 2352, 2267, and 446 kg·km⁻² from 2001 to 2015, respectively. However, if the

dry deposition rate was considered, the North China Plain had the highest TN deposition rate because the dry deposition rate is higher in northern than in southern China. Consequently, the mean annual TN deposition rate would reach from 3908 to 4560 kg·km⁻² in the Taihu watershed. Obviously, the TN deposition load already exceeds the theoretical critical eutrophication load of 491 kg·km⁻²·a⁻¹ [9].

3.4. Influence of Meteorological Conditions on N Deposition.

Results of the Pearson correlation analysis showed that meteorological conditions were significantly correlated with TN_w deposition rate (Table 4 and Figure 6). Moreover, a significantly negative correlation was found between the concentration of TN deposition and rainfall ($Y =$

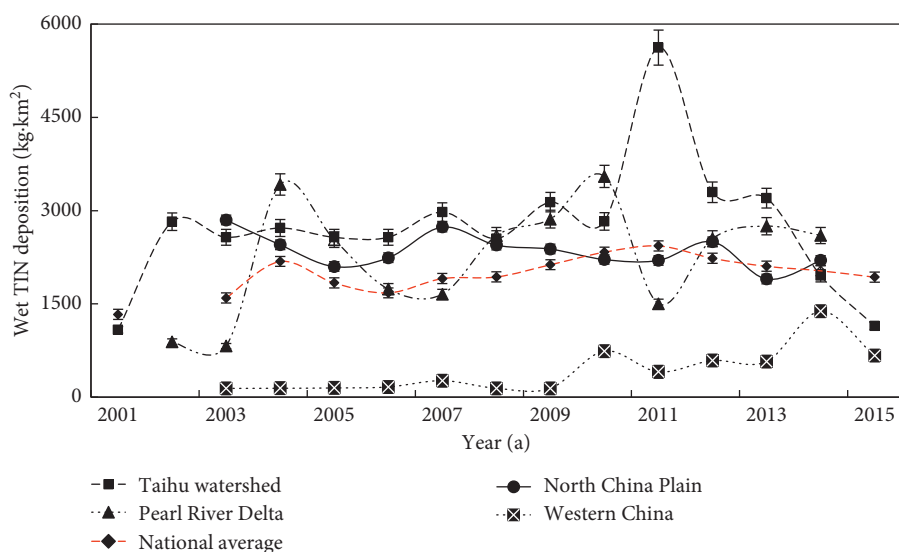


FIGURE 5: Comparisons of atmospheric TIN_w deposition rate listed with other domestic areas.

TABLE 4: Correlation (*R*) between wet N deposition and meteorological conditions.

	Rainfall	Frequency	Intensity	N deposition	Concentration
Rainfall	1	—	—	—	—
Frequency	0.646*	1	—	—	—
Intensity	0.933**	0.343	1	—	—
N deposition	0.803**	0.767**	0.659*	1	—
Concentration	-0.999**	-0.805**	-0.783**	-0.847**	1

Values are given with their level of significance: ** $p < 0.01$; * $p < 0.05$.

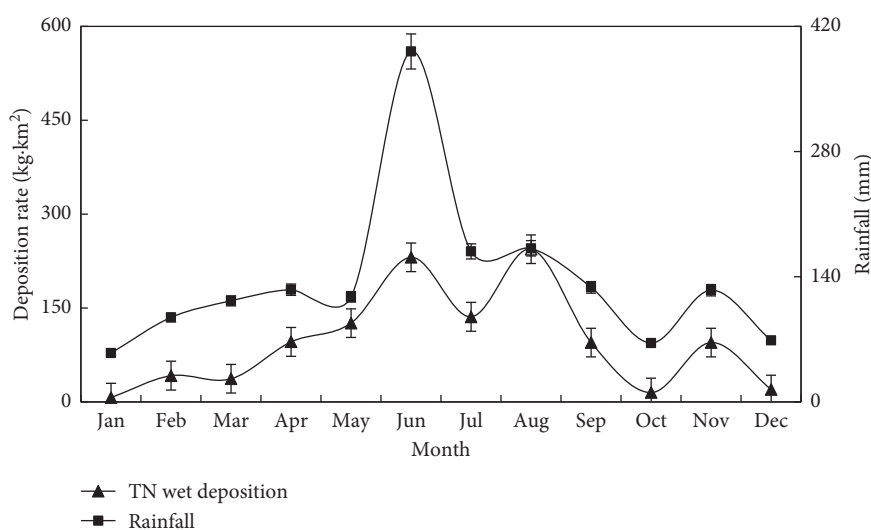


FIGURE 6: Monthly rainfall and TN_w deposition.

$189.268X^{-0.997}$, $R = -0.999$, $P < 0.01$), rainfall frequency ($R = -0.783$, $P < 0.01$), and rain intensity ($R = -0.783$, $P < 0.01$). However, it was significantly positively correlated with TN deposition. Under the same precipitation scale, the N concentration of rain may gradually decrease. The negative correlation indicates that precipitation can remove N nutrients from the atmosphere and that light rain results in greater removal than heavy rain. The positive correlation between precipitation and N deposition rate explains the

cumulative effect of N nutrients in water bodies after rainfall, as well as the dilution effect of heavy rain.

3.5. Influence of NH₃ from Agriculture on N Deposition. Agricultural activities may be the major sources of NH₃ emissions, especially from livestock and fertilizer volatilization. Changshu, which has a good agricultural base in the Taihu watershed, was investigated in this study. A remarkable

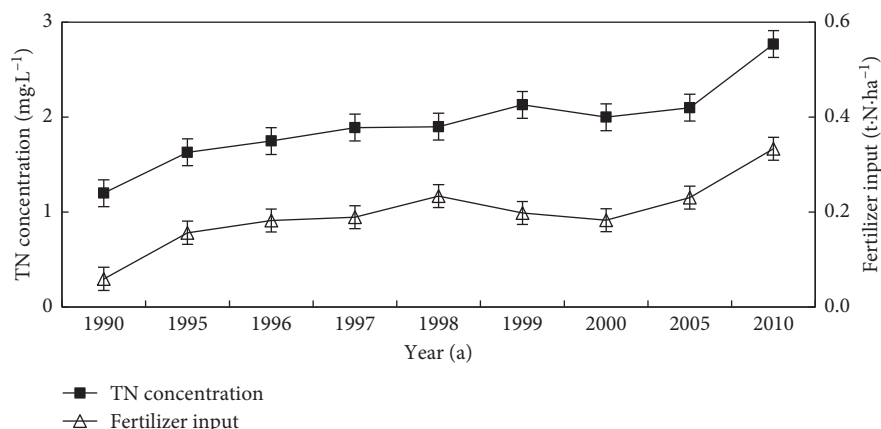


FIGURE 7: Chemical fertilizer input and TN content of water in Changshu from 1990 to 2010.

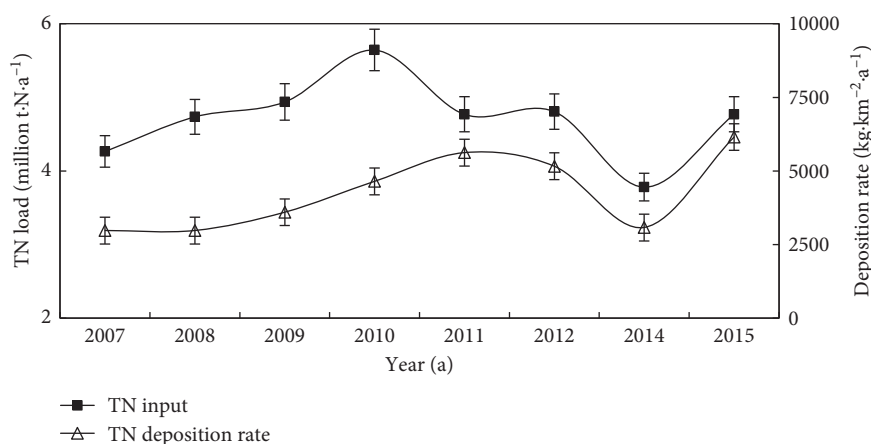


FIGURE 8: TN input into the lake and TN deposition rate in Taihu watershed from 2007 to 2015.

correlation between TN loads of water and N fertilizer applied per hectare was observed (Figure 7). Fertilizer is applied to rice paddies, wheat fields, and oilseed rape fields in March, July, and November. At that time, the wet N deposition rate increased rapidly, demonstrating that ammonia from farmland fertilizer made a significant contribution to N deposition. With the excessive fertilizer application and low absorptivity in this area, the concentration of TN in water bodies has increased in recent years. The mean NH_3 deposition rate was found to be $688 \text{ kg} \cdot \text{ha}^{-1}$, accounting for 56.80% of $\text{NH}_3^+ \cdot \text{N}$ from the simulation date. Consequently, the volatilization of NH_3 from fertilizer concentration to N deposition cannot be ignored.

The typical characteristics of livestock and aquaculture are free-ranging in or near the water bodies in this area. About 35% of the manure was discharged into the river directly from undisposed manure [21, 31]. The gross value of production of aquaculture increased from USD 0.87 billion in 2000 to USD 2.13 billion in 2015, while the gross value of livestock production increased from USD 0.5 billion to USD 1 billion. Increasing amounts of N are discharged into aquatic systems and the atmosphere under the imperfect excrement disposal system. If effective measures are not taken, NH_3 volatilized from agricultural systems will continue to increase because of

the rapid development of livestock, aquaculture, and excessive fertilizer application.

3.6. Estimated Contribution of N Deposition to N Loads of Water in the Taihu Watershed. Based on equation (1), the annual riverine input of TN was estimated to be $112,500 \text{ t} \cdot \text{N} \cdot \text{a}^{-1}$. The main N pollutants originated from domestic sewage (48.88%) and agriculture (28.17%). Among the agricultural pollutants, livestock and aquaculture contributed 90.00%. However, many studies have shown that the heavy N load in Taihu Lake originated from agricultural activities. In the present study, the TN deposition load into the lake was calculated based on an area of 2338 km^2 and an annual TN deposition load of $14,400 \text{ t} \cdot \text{N} \cdot \text{a}^{-1}$. The annual TN deposition accounted for 12.36% of the annual riverine input of TN.

When compared to the case studies conducted from 2007 to 2015 [9, 10, 28, 50–52], the contribution of N deposition to Taihu Lake showed an increasing trend (Figure 8). The eutrophication critical load of atmospheric N deposition, which is the minimal amount of N required to stimulate eutrophication, is lower than $658 \text{ kg} \cdot \text{km}^{-2} \cdot \text{a}^{-1}$ for Taihu Lake [53]. Additionally, the allowable TN load in the Taihu Lake ecosystem was estimated to be only $491 \text{ kg} \cdot \text{km}^{-2} \cdot \text{a}^{-1}$

[9], while the TN deposition rate was found to be $6514 \text{ kg} \cdot \text{km}^{-2} \cdot \text{a}^{-1}$ in the present study. Obviously, the TN deposition load already exceeds the eutrophication critical load in theory. Accordingly, this phenomenon may accelerate the eutrophication process of Taihu Lake. Overall, our results indicate that the contribution of TN deposition to water N load cannot be ignored when the pollution sources are considered.

4. Conclusions

To better understand the spatial-temporal distribution characteristics of N deposition and its estimated contributions to water eutrophication, the N deposition in the Taihu watershed was investigated. The results revealed the following:

- (1) Deposition rates of TN, wet deposition, dry deposition, $\text{NO}_3^- \cdot \text{N}$, and $\text{NH}_4^+ \cdot \text{N}$ were 6514, 1142, 5012, 878, and $1207 \text{ kg} \cdot \text{km}^{-2} \cdot \text{a}^{-1}$, respectively.
- (2) The TN, TN_w , and TN_d deposition had significant temporal and spatial distribution features. Seasonally, both deposition rates were higher in spring and summer. Spatially, the TN_w deposition rate decreased from northwest to southeast while the TN_d deposition rate increased.
- (3) Correlation analysis showed that rainfall was significantly correlated with N deposition rate. Rain could clean the atmosphere and that light rain did so more effectively than heavy rain.
- (4) The TN deposition contributed to the Taihu lake was $14,400 \text{ t N} \cdot \text{a}^{-1}$, 12.36% of the total annual N input via inflow rivers. The main N pollutants originated from urban domestic sewage and agriculture, especially fertilizer and livestock.

Data Availability

The data used to support the findings of this study are available from the corresponding author upon request.

Conflicts of Interest

The authors declare that there are no conflicts of interest regarding the publication of this paper.

Acknowledgments

This work was supported by the “973” Project of the Ministry of Science and Technology of China (Grant no. 2014CB953801) and the National Natural Science Foundation of China (Grant no. 41673107). The authors thank the Changshu Agro-Ecosystem Experimental Station, Chinese Academy of Sciences, for providing statistical data assistance.

References

- [1] Y. H. Zhao, L. Zhang, Y. F. Chen et al., “Atmospheric nitrogen deposition to China: a model analysis on nitrogen budget and critical load exceedance,” *Atmospheric Environment*, vol. 153, pp. 32–40, 2017.
- [2] K. M. Russell, J. N. Galloway, S. A. Macko, J. L. Moody, and J. R. Scudlark, “Sources of nitrogen in wet deposition to the Chesapeake-Bay region,” *Atmospheric Environment*, vol. 32, no. 14, pp. 3923–3927, 1998.
- [3] J. N. Galloway, F. J. Dentener, D. G. Capone et al., “Nitrogen cycle: past, present and future,” *Biogeochemistry*, vol. 70, no. 2, pp. 153–226, 2004.
- [4] D. Fowler, M. Coyle, U. Skiba et al., “The global nitrogen cycle in the twenty-first century,” *Philosophical Transactions of the Royal Society B: Biological Sciences*, vol. 368, no. 1621, article 20130164, 2013.
- [5] A. F. Bouwman, D. P. Van Vuuren, R. G. Derwent, and M. Posch, “A global analysis of acidification and eutrophication of terrestrial ecosystems,” *Water, Air, and Soil Pollution*, vol. 141, no. 1–4, pp. 349–382, 2002.
- [6] W. D. Bowman, C. C. Cleveland, L. Halada, J. Hresko, and J. S. Baron, “Negative impact of nitrogen deposition on soil buffering capacity,” *Nature Geoscience*, vol. 1, no. 11, pp. 767–770, 2008.
- [7] C. J. Stevens, N. B. Dise, J. O. Mountford, and D. J. Gowing, “Impact of nitrogen deposition on the species richness of grasslands,” *Science*, vol. 303, no. 5665, pp. 1876–1879, 2004.
- [8] E. W. Boyer, C. L. Goodale, and N. A. Jaworski, “Anthropogenic nitrogen sources and relationship to riverine nitrogen export in the northeastern USA,” *Biogeochemistry*, vol. 57, no. 1, pp. 137–169, 2002.
- [9] S. J. Zhai, L. Y. Yang, and W. P. Hu, “Observations of atmospheric nitrogen and phosphorus deposition during the period of algal bloom formation in northern lake Taihu, China,” *Environment Management*, vol. 44, no. 3, pp. 542–551, 2009.
- [10] H. Yu, L. L. Zhang, and S. W. Yan, “Atmospheric wet deposition characteristics of nitrogen and phosphorus nutrients in Taihu Lake and contributions to the lake,” *Research of Environmental Sciences*, vol. 24, no. 11, pp. 1210–1219, 2011.
- [11] P. M. Vitousek, J. D. Aber, and R. W. Howarth, “Human alteration of the global nitrogen cycle: sources and consequences,” *Ecological Applications*, vol. 7, no. 3, pp. 737–750, 1997.
- [12] W. Liu, X. Wang, and Y. Fan, “A review of atmospheric nitrogen deposition and its estimated contributions to nitrogen input of waters,” *Environmental Pollution and Control*, vol. 36, no. 5, pp. 88–101, 2014.
- [13] C. E. He, X. J. Liu, A. Fangmeier, and F. Zhang, “Quantifying the total airborne nitrogen input into agro-ecosystems in the north China plain,” *Agriculture, Ecosystems and Environment*, vol. 121, no. 4, pp. 395–400, 2007.
- [14] M. E. Fenn, M. A. Poth, and M. J. Arbaugh, “A through fall collection method using mixed bed ion exchange resin columns,” *Scientific World Journal*, vol. 2, pp. 122–130, 2014.
- [15] D. H. Guo and Y. Y. Zhang, “The study of atmospheric dry depositions buffer action for precipitation,” *Journal of Hubei University: Natural Science*, vol. 1, pp. 96–100, 1987.
- [16] D. Fowler, M. Coyle, C. Flechard et al., “Advances in micrometeorological methods for the measurement and interpretation of gas and particle nitrogen fluxes,” *Plant and Soil*, vol. 228, no. 1, pp. 117–129, 2011.
- [17] D. G. Streets, T. C. Bond, G. R. Carmichael et al., “An inventory of gaseous and primary aerosol emissions in Asia in the year 2000,” *Journal of Geophysical Research*, vol. 108, no. 21, pp. 1–23, 2003.

- [18] T. Ohara, H. Akimoto, J. Kurokawa et al., "An Asian emission inventory of anthropogenic emission sources for the period 1980–2020," *Atmospheric Chemistry and Physics Discussion*, vol. 7, no. 16, pp. 6843–6902, 2007.
- [19] X. Zhao, X. Y. Yan, and Z. Q. Xiong, "Spatial and temporal variation of inorganic nitrogen wet deposition to the Yangzi River Delta Region, China," *Water, Air, and Soil Pollution*, vol. 203, no. 1–4, pp. 277–298, 2009.
- [20] F. S. Zhang, J. Q. Wang, W. F. Zhang et al., "Nutrient use efficiencies of major cereal crops in China and measures for improvement," *Acta Pedologica Sinica*, vol. 45, no. 5, pp. 915–924, 2008, in Chinese.
- [21] X. T. Ju, B. J. Gu, and Z. C. Cai, "Suggestions to mitigate haze by reducing agricultural ammonia emission," *Science and Technology Review*, vol. 35, no. 13, pp. 11–12, 2017.
- [22] B. Gu, X. Ju, and J. Chang, "Integrated reactive nitrogen budgets and future trends in China," *Proceedings of the National Academy of Sciences*, vol. 112, no. 28, pp. 8792–8797, 2015.
- [23] W. Wang, W. Zhang, and S. Hong, "Geographical distribution of SO₂ and NO_x emission intensities and trends in China," *China Environmental Science*, vol. 16, pp. 161–167, 1996.
- [24] Q. R. Sun and M. R. Wang, "Ammonia emission and concentration in the atmosphere over China," *Chinese Journal of Atmospheric Sciences*, vol. 21, no. 5, pp. 590–598, 1997.
- [25] A. R. Townsend, B. H. Braswell, E. A. Holland, and J. E. Penner, "Spatial and temporal patterns in terrestrial carbon storage due to deposition of fossil fuel nitrogen," *Ecological Applications*, vol. 6, no. 3, pp. 806–814, 1996.
- [26] Y. B. Chang, "Major environmental changes since 1950 and the onset of accelerated eutrophication in Taihu Lake, China," *Acta Palaeontologica Sinica*, vol. 35, no. 2, pp. 155–174, 1995, in Chinese.
- [27] X. L. Dai, P. Q. Ye, L. Qian, and T. Song, "Changes in nitrogen and phosphorus concentrations in Lake Taihu, 1985–2015," *Journal of Lake Sciences*, vol. 28, no. 5, pp. 935–943, 2016.
- [28] Y. Z. Song, B. Q. Qin, L. Y. Yang, and W. P. Hu, "Primary estimation of atmospheric wet deposition of nitrogen to aquatic ecosystem of Lake Taihu," *Journal of Lake Sciences*, vol. 17, no. 3, pp. 226–230, 2005.
- [29] C. M. Li, S. G. Zhang, and W. P. Yao, "Study on agricultural non-point source pollution load of Taihu Lake Basin in Suzhou," *Research of Soil and Water Conservation*, vol. 23, no. 3, pp. 354–359, 2016.
- [30] Y. P. Huang, *Water Environment and its Pollution Control in Taihu Lake*, Beijing Science Press, Beijing, China, 2001.
- [31] H. J. Zhang and F. Chen, "Non-point pollution statistics and control measures in Taihu Basin," *Water Resources Protection*, vol. 26, no. 3, pp. 87–90, 2010.
- [32] X. H. Wan and H. Q. Wang, "Analysis of agricultural surface source pollution and control measures in Lake Taihu basin of Jiangsu province," *Agro-Environment and Development*, vol. 25, no. 3, pp. 69–71, 2008.
- [33] Y. Y. Shen, D. L. Hu, and Q. L. Jiang, "Characteristic of nitrogen and phosphorus load in the past three decades in the northwest of Lake Taihu basin based on the SWAT model," *Resources and Environment in the Yangtze Basin*, vol. 26, no. 6, pp. 902–914, 2017.
- [34] Jiangsu Province Statistics Bureau, *Statistical Yearbook of Jiangsu Province from 2000 to 2016*, Jiangsu province Statistics Bureau, Jiangsu, China, 2016.
- [35] Anhui Province Statistics Bureau, *Statistical Yearbook of Anhui Province from 2000 to 2016*, Anhui Province Statistics Bureau, Anhui, China, 2016.
- [36] Zhejiang Province Statistics Bureau, *Statistical Yearbook of Zhejiang Province from 2000 to 2016*, Zhejiang Province Statistics Bureau, Zhejiang, China, 2016.
- [37] Shanghai Statistics Bureau, *Statistical Yearbook of Shanghai from 2000 to 2016*, Shanghai Statistics Bureau, Shanghai, China, 2016.
- [38] Y. L. Wu, H. Xu, G. J. Yang, G. W. Zhu, and B. Q. Qin, "Progress in nitrogen pollution research in Lake Taihu," *Journal of Lake Sciences*, vol. 26, no. 1, pp. 19–28, 2014.
- [39] B. Gao, X. Y. Yan, X. S. Jiang, and C. P. Ti, "Research progress in estimation of agricultural sources pollution of the Lake Taihu region," *Journal of Lake Sciences*, vol. 26, no. 6, pp. 822–828, 2014.
- [40] C. P. Ti, Y. Q. Xia, J. J. Pan, B. J. Gu, and X. Y. Yan, "Nitrogen budget and surface water nitrogen load in Changshu a case study in the Taihu Lake region of China," *Nutrient Cycling in Agroecosystems*, vol. 91, no. 1, pp. 55–66, 2011.
- [41] Jiangsu Provincial Academy of Environmental Science, *Technical Specification of Water Environment Comprehensive Treatment Plan about the Main Rivers in Lake Taihu Basin*, Jiangsu Provincial Academy of Environmental Science, Jiangsu, China, 2008.
- [42] R. R. Yan, J. Y. Chao, L. Zhang, Y. X. Cui, and W. Zhuang, "Research on the load of industrial pollution in the Taihu Lake Basin in Jiangsu Province," *China Rural Water and Hydropower*, vol. 3, pp. 39–43, 2012.
- [43] R. G. Li, Y. L. Xia, A. Z. Wu, and Y. S. Qian, "Pollutants sources and their discharging amount in Taihu Lake area of Jiangsu Province," *Journal of Lake Science*, vol. 12, no. 2, pp. 147–153, 2000.
- [44] Z. Liu, W. X. Li, Y. M. Zhang et al., "Estimation of non-point source pollution load in Taihu Lake Basin," *Journal of Ecology and Rural Environment*, vol. 26, no. 1, pp. 45–48, 2000.
- [45] H. Zhang, H. P. Li, X. Y. Li, and Z. F. Li, "Temporal changes of nitrogen balance and their driving factors in typical agricultural area of Lake Taihu Basin," *Chinese Journal of Soil Science*, vol. 45, no. 5, pp. 1119–1129, 2014.
- [46] N. Zhang, Y. H. Wang, Y. Qiu et al., "Quantification and environmental effects of waste nitrogen in crop-livestock-household system of Suzhou city," *Soils*, vol. 49, no. 5, pp. 926–934, 2017.
- [47] X. Z. Wang, J. G. Zhu, R. Gao, and C. J. H. Bao, "Dynamics and ecological significance of nitrogen wet-deposition in Taihu Lake region—taking Changshu agro-ecological experiment station as an example," *Chinese Journal of Applied Ecology*, vol. 15, no. 9, pp. 1616–1620, 2004.
- [48] Y. Zhang, X. J. Liu, A. Fangmeier, K. T. W. Goulding, and F. S. Zhang, "Nitrogen inputs and isotopes in precipitation in the North China Plain," *Atmospheric Environment*, vol. 42, no. 7, pp. 1436–1448, 2008.
- [49] D. N. Zheng, X. S. Wang, S. D. Xie, L. Duan, and D. S. Chen, "Simulation of atmospheric nitrogen deposition in China in 2010," *China Environmental Science*, vol. 34, no. 5, pp. 1089–1097, 2014.
- [50] Y. X. Xie, Z. Q. Xiong, G. X. Xing, X. Y. Yan, and S. L. Shi, "Source of nitrogen in wet deposition to a rice agroecosystem at Tai lake region," *Atmospheric Environment*, vol. 42, no. 21, pp. 5182–5192, 2008.
- [51] Y. Wang, N. K. Liu, and J. F. Wang, "Study on atmospheric deposition of nitrogen and phosphorus in Taihu Lake,"

- Environmental Science and Management*, vol. 40, no. 5, pp. 103–105, 2011.
- [52] J. F. Wang, K. J. Zhou, and X. Q. Wang, “Atmospheric nitrogen and phosphorous deposition in Hangjiahu area,” *China Environmental Science*, vol. 35, no. 9, pp. 2754–2763, 2015.
- [53] X. M. Ye, J. M. Hao, and L. Duan, “On critical loads of nutrient nitrogen deposition for some major lakes in China,” *Environmental Pollution and Control*, vol. 24, no. 1, pp. 54–58, 2002.

Research Article

Spatial and Temporal Variations of Water Quality of Mateur Aquifer (Northeastern Tunisia): Suitability for Irrigation and Drinking Purposes

Besma Tlili-Zrelli ¹, Moncef Gueddari,¹ and Rachida Bouhlila²

¹Laboratory of Geochemistry and Environmental Geology, Department of Geology, Faculty of Sciences of Tunis, University of Tunis El Manar, 2092 Tunis, Tunisia

²Modeling in Hydraulic and Environment Laboratory, National Engineers School of Tunis, Tunis, Tunisia

Correspondence should be addressed to Besma Tlili-Zrelli; besma_fst@yahoo.fr

Received 6 February 2018; Revised 14 April 2018; Accepted 29 April 2018; Published 17 July 2018

Academic Editor: Narcis Duteanu

Copyright © 2018 Besma Tlili-Zrelli et al. This is an open access article distributed under the Creative Commons Attribution License, which permits unrestricted use, distribution, and reproduction in any medium, provided the original work is properly cited.

The present study aims to assess the spatial and temporal variations of the hydrochemical characteristics of Mateur aquifer groundwaters, a crucial water resource in the northeast of Tunisia. The aquifer was subject to water quality deterioration due to salinization and nitrate contamination, and a new assessment of water quality was needed. For this purpose, 40 groundwater samples were collected during wet and dry seasons and analyzed for salinity, pH, T, O₂, major cations and anions, and nutrient elements using standard methods and Water Quality Index (WQI). The results showed that most of the groundwater parameters were not within the permissible limits set by the World Health Organization in both seasons. The geochemical data were interpreted using WQI for drinking water. The spatial distribution maps of Water Quality Index showed that the highest quality was found, during both seasons, in the northwest and the southeast part of the aquifer, corresponding to the recharge zone, whereas the poor and very poor water quality was found in the outflow part of the aquifer. According to sodium adsorption ratio (SAR) and Na% values, most of the groundwater samples were not suitable for irrigation purposes and characterizing the eastern part of the aquifer and the outflow part of the aquifer, around the Ichkeul marshes.

1. Introduction

Groundwater is becoming the major source of water supply for domestic, industrial, and agricultural sectors of many countries all over the world. It is estimated that approximately one-third of the world's population uses groundwater for drinking [1]. Several Mediterranean countries are already facing a situation of severe water quality degradation, mainly due to anthropogenic activities (agriculture, industry, urban development, and increasing exploitation of water resources) as a direct impact of climate change. Water quality is rapidly declining worldwide, particularly in developing countries, due to natural and anthropogenic processes [2, 3]. Water pollution affects human health, economic development, and social prosperity [4]. The importance of

water quality in human health has recently attracted a great deal of interest.

An understanding of the spatial variation and processes affecting water quality is essential in sustaining usable water supplies under changing climate and local environmental pressures. Temporal changes of recharged water composition, hydrologic and human factors, may cause periodic changes in groundwater quality [5]. The quality of alluvial groundwater in rural areas is sensitive to contaminants originating from agricultural chemicals, such as, fertilizers, pesticides, and lime [6, 7]. The use of nitrogen fertilizers frequently leads to extremely high nitrate concentrations in groundwaters and may cause serious health problems [8, 9].

In such circumstances, the knowledge of temporal and spatial trends of water quality should help in the decision-making

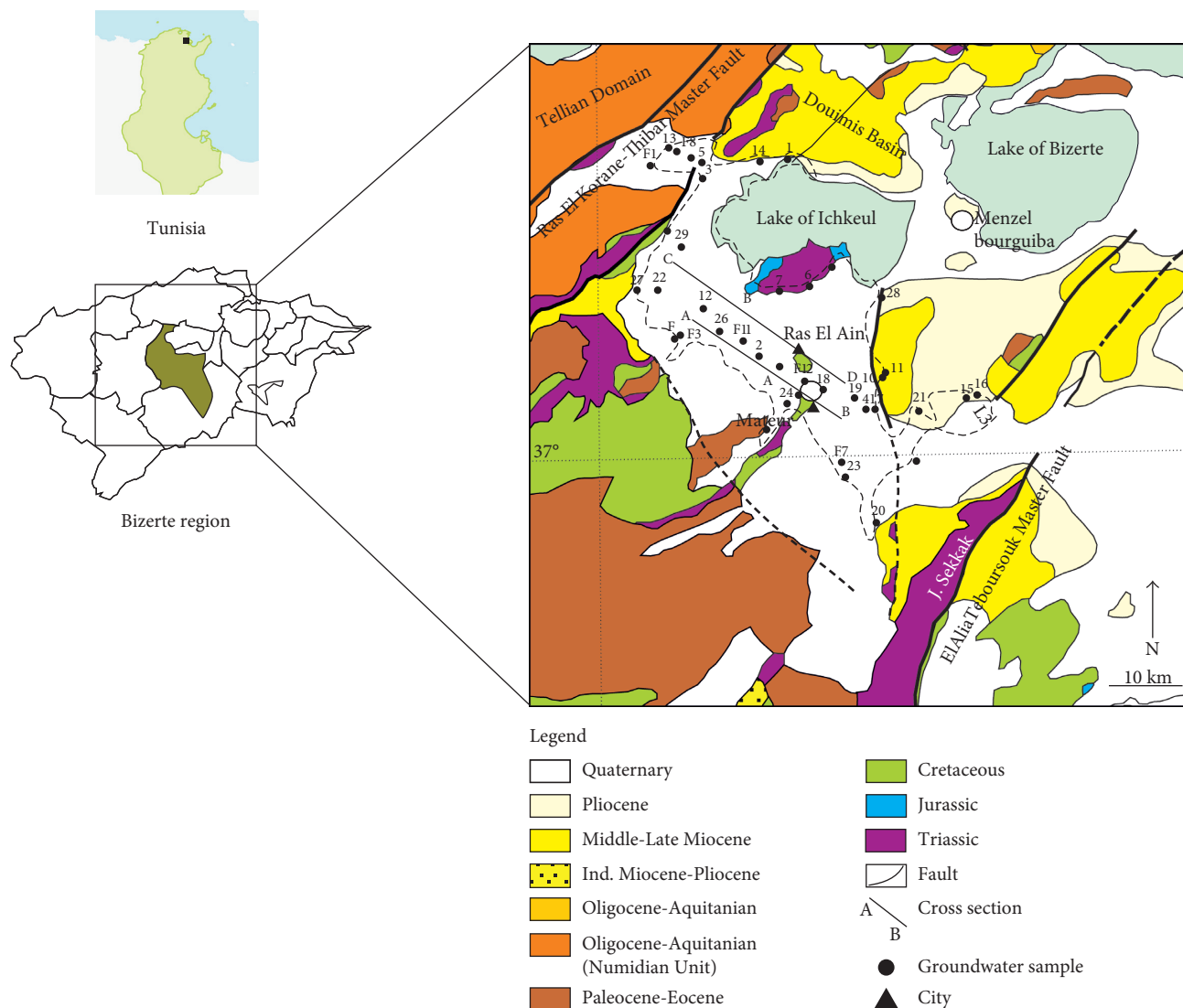


FIGURE 1: Location, geology [14], and sampling points of the study area.

process, particularly in developing countries, where there are insufficient data [10].

In Tunisia, where the climate is dry over most of its territories, water resources are both scarce and unequally distributed through time and space, with a potential decrease, due to overexploitation, exploitation of nonrenewable deep aquifer, salinization, and pollution [11]. Agriculture uses approximately 80% of all water resources [12]. Mateur alluvial plain is one of the major agricultural regions in Tunisia, and its water resources originate mainly from the alluvial aquifer, which support the local domestic and agricultural water supply with 49% and 51%, respectively [13]. Although Mateur is not a particularly water-stressed region, brine water around Ichkeul marshes and salty soils contribute to water salinization in some shallow wells. Even more, excessive agricultural activities may be the cause of its water contamination with nitrate.

This paper highlights the spatial and temporal variations in groundwater quality in an alluvial agricultural plain in Mateur region and evaluates the suitability of groundwater

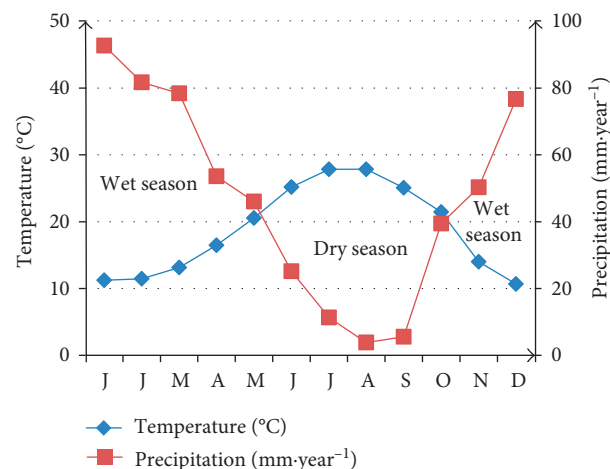


FIGURE 2: Ombrothermic diagram.

for irrigation and drinking purposes for sustainable agriculture and basic human needs. For these purposes, we used an integrated Water Quality Index (WQI), the sodium

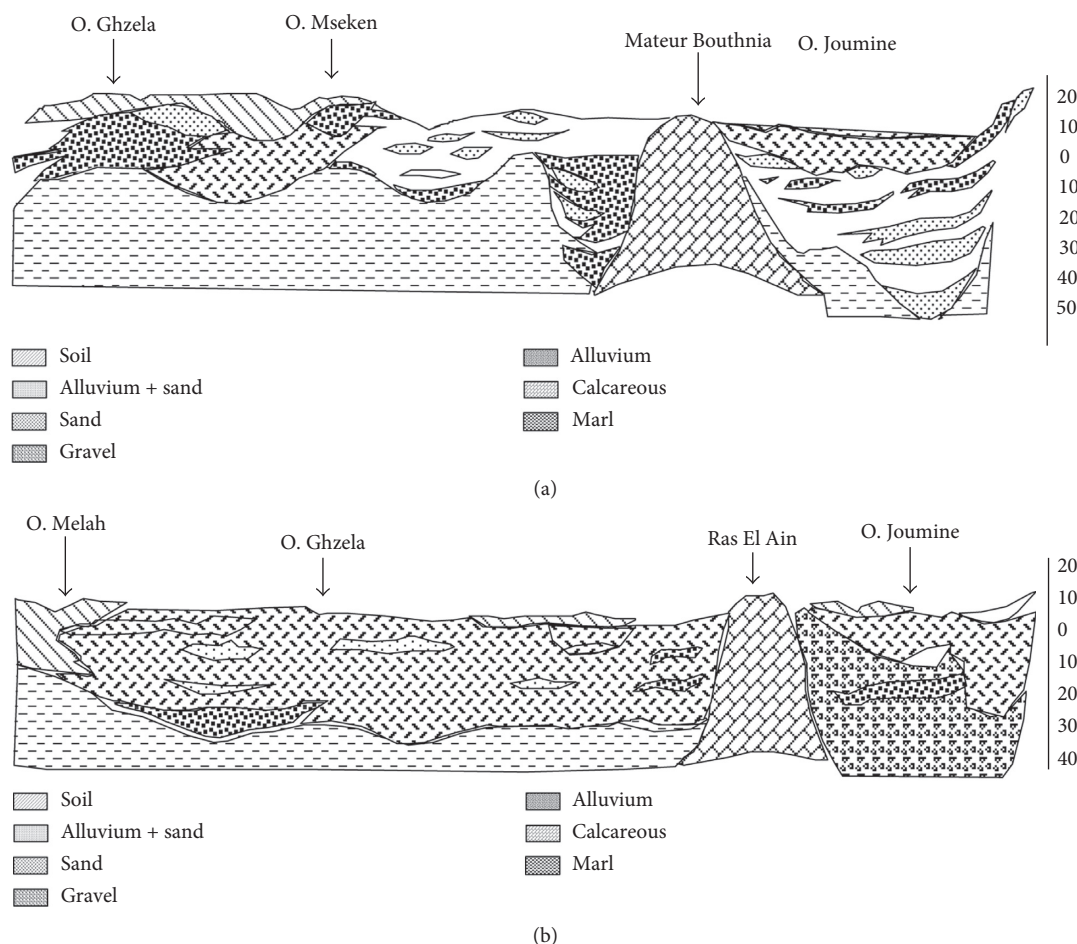


FIGURE 3: Hydrogeological cross sections: (a) Mateur and (b) Ras el Ain [15].

adsorption ratio (SAR), the sodium percentage (% Na), and the permeability index (PI).

2. Setting and Methods

2.1. Location and Climate. Mateur plain is located in Bizerte region, in the northeast of Tunisia (Figure 1) and has a surface area of 260 km² in the vast Ichkeul catchment (2600 km²). The climate is typically Mediterranean, subhumid with a considerable variation in mean monthly temperatures. The coldest month is January, with a mean temperature of 11°C, and the hottest is August, with a mean temperature of 27°C. The ombrothermic diagram (Figure 2) shows two periods: a wet period which lasts 7 months from November to May and a dry period which lasts 5 months from June to October. The mean annual precipitation (1998–2008) in the area is 518 mm and the mean annual evapotranspiration is 1074 mm.

2.2. Geological and Hydrogeological Setting. Mateur plain covers different stratigraphic units ranging from Triassic to Quaternary [14]. The stratigraphic sequence primarily consists of carbonate formations, which characterize the Tertiary deposits of Ichkeul Mountains. In the Mateur plain, outcrops prior to Quaternary are found only on the three Campanian hills of Sidi Mbarek, Mateur, and Ras El Ain.

Miocene is mainly developed in the east of Mateur plain and the north of Ichkeul lake, and it is composed of gypsum and marl. The Quaternary and recent alluvium cover the major part of the plain and are composed of silt and detrital formations. The aquifer system is made up of multilayers, which are either saturated or unsaturated [15] (Figure 3). These layers are composed of alluvial, eolian, and minor lacustrine deposits [16]. The main sources of alluvial aquifer recharge are rainfall infiltration and leakage of rivers (Joumine, Tine, Sejnane, Melah, and Rezala). According to piezometric maps (Figure 4), Mateur aquifer groundwater flow is roughly oriented northward in the upstream part of the plain, whereas in the downstream part, it is controlled by the draining action of the Joumine River.

Water loss from the aquifer is through discharge to the lake Ichkeul, evaporation, and pumping for domestic and agricultural purposes. The water table generally lies within 8–10 m of land surface, facilitating additional groundwater loss via evapotranspiration. The alluvial aquifer has transmissivity values ranging from $2 \cdot 10^{-5}$ to $20 \cdot 10^{-2}$ m²/s.

2.3. Soil Type and Agriculture Practices. According to Mori [17], two major soil types are observed in Mateur plain: fluvisol and hydromorphic and holomorphic soils with high salinity.

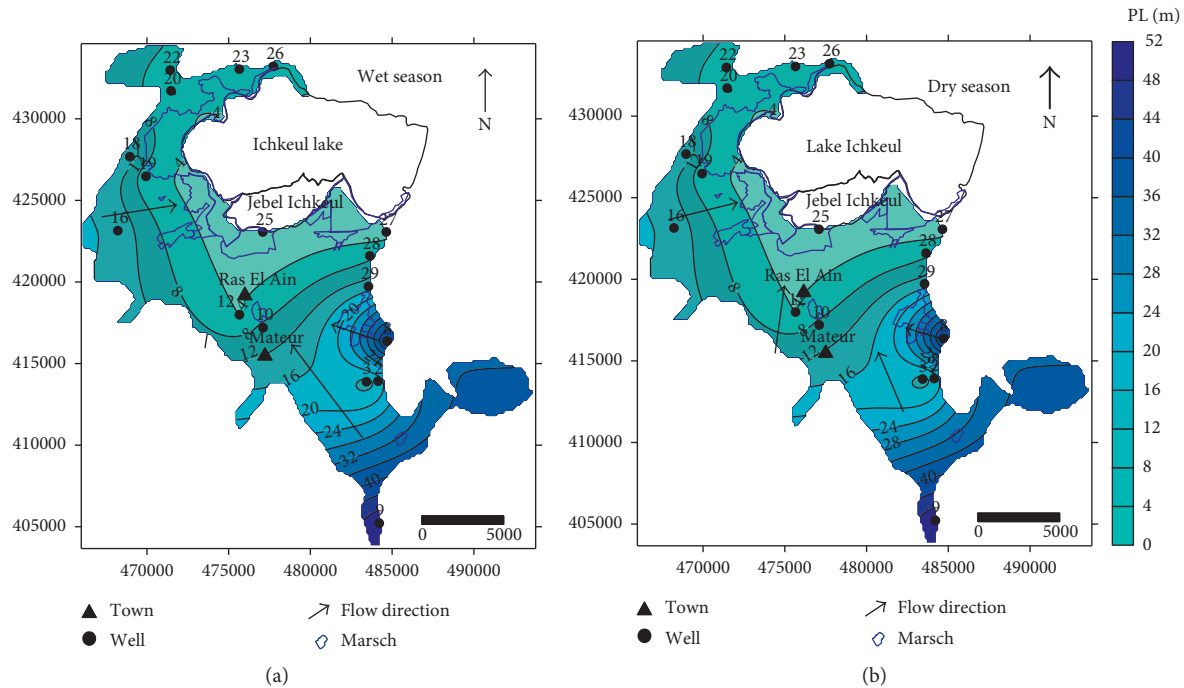


FIGURE 4: Piezometric maps of Mateur plain: (a) wet season and (b) dry season.

TABLE 1: Details of fertilizer application for different crops in the study area.

Fertilizer type (kg·ha ⁻¹)	Cereals				Fodder		Legumes		Tree crops	
	Nov	Jan	Feb	March	Sept	Jan	Dec	Jan	Oct	Feb
DAP N-P ₂ O ₅	150	—	—	—	—	—	—	200	—	—
Ammonium	—	150	150	150	—	150	—	200	—	150
Super 45 P ₂ O ₅	—	—	—	—	100	—	100	—	150	—

TABLE 2: Statistical summary of hydrochemical parameters of the study area.

Unit		Wet season (May)			Dry season (October)		
		Min	Max	SD*	Min	Max	SD*
Cl ⁻	mg/L	67.45	2406.90	524.66	106.50	4402.00	844.89
SO ₄ ²⁻	mg/L	223.53	2483.48	497.45	221.89	3591.36	583.38
HCO ₃ ⁻	mg/L	54.92	622.40	150.35	86.65	693.19	146.93
Ca ⁺⁺	mg/L	20.00	480.00	82.33	10.00	763.40	135.97
Na ⁺	mg/L	49.00	1728.00	376.45	11.25	170.13	40.30
Mg ⁺⁺	mg/L	12.70	140.00	27.33	39.33	2576.00	491.23
K ⁺	mg/L	0.78	101.60	17.84	0.00	169.00	29.88
T	°C	16.20	26.80	2.16	18.20	26.70	1.98
Conductivity	mS/cm	0.54	8.64	1.94	0.72	14.59	2.98
Salinity	g/L	0.41	6.55	1.47	0.54	11.07	2.26
pH		6.18	8.39	0.39	7.13	9.08	0.33
O ₂	mg/L	1.20	7.60	1.36	0.60	5.20	1.09
NO ₃ ⁻	mg/L	0	273.15	79.76	0.72	278.6	64.99
NH ₄ ⁺	mg/L	0	6.63	1.08	0	0.2	0.03
NO ₂ ⁻	mg/L	0	1.56	0.37	0	0.23	0.06
HPO ₄ ²⁻	μg/L	10	6.37	1.02	20	4.82	0.82

*Standard deviation.

Mateur region land is mainly used for growing cereals and fodders. A large amount of synthetic fertilizers (DAP, ammonium, and super 45) are applied during the farming season (winter through spring) [18]. Fertilizer quantities

(kg/ha) and application time are given in Table 1. Almost all farmers apply more than the recommended dose. Besides, over the last few decades, fertilizer management has been dramatically modified, and for economic considerations,

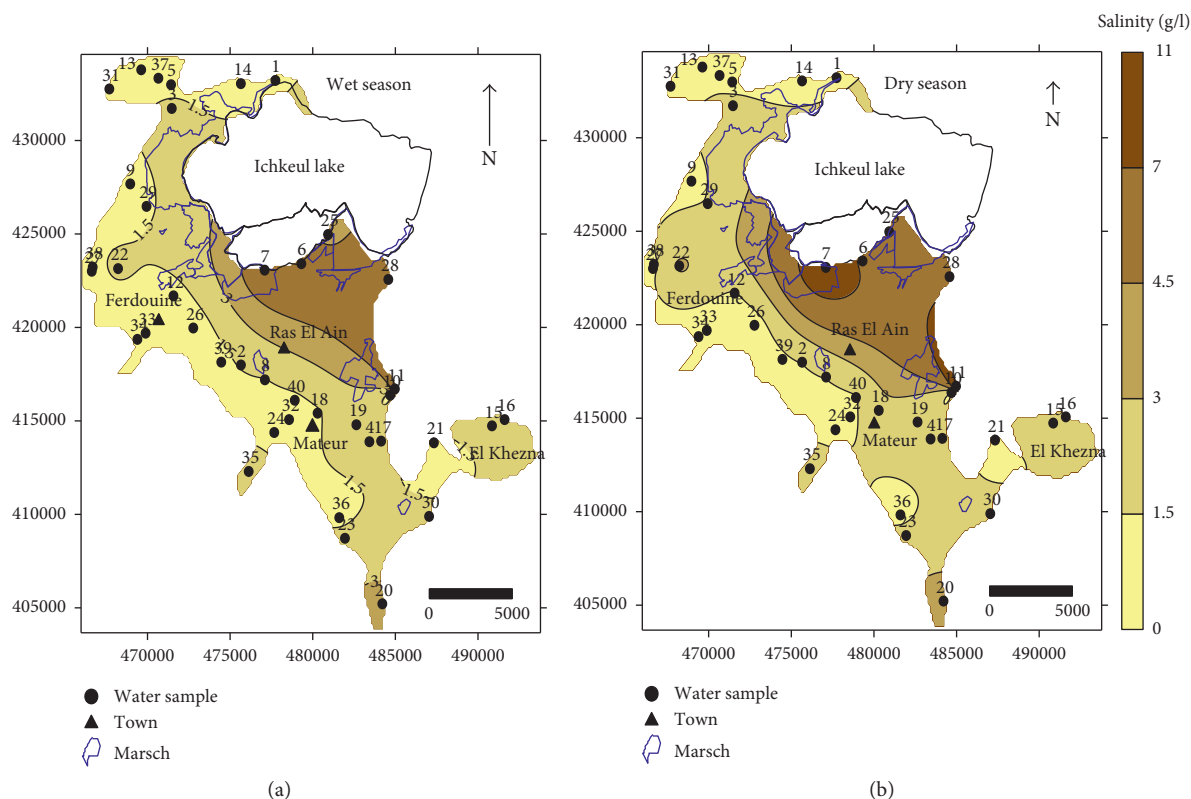


FIGURE 5: Spatial distribution maps of salinity: (a) wet season and (b) dry season.

crop rotations are rarely applied and cereals are the predominant land use for many successful agricultural years. With regard to livestock, cattle livestock is the main practice in the irrigated areas of Mateur. Animal resources are estimated for the year 2012 of around 45,627 head of sheep and 7,789 head of cattle [19]. NO_3 fluxes from farm discharges are estimated to be about 120 kg/ha/year [20].

2.4. Sampling and Analytical Methods. Groundwater samples were obtained from monitoring wells in the alluvial aquifers. A total of 70 samples were collected in wet and dry seasons in order to capture seasonal variability in water quality.

The piezometric level, pH, electrical conductivity (EC), dissolved oxygen, and temperature were measured in situ. Samples were kept at 4°C for their subsequent chemical analyses. Afterwards, the samples were filtered through a 0.45 μm Millipore filter. Chloride was determined by standard AgNO_3 [21]. Sulfate (SO_4^{2-}) content was measured by the gravimetric method using BaCl_2 . Sodium (Na^+) and potassium (K^+) were measured by flame photometry, and calcium (Ca^{2+}) and magnesium (Mg^{2+}) were measured with atomic absorption. Alkalinity was determined by titration with HCl.

The quality of chemical analysis was checked by making an ionic mass balance, accepting an error rate lower than 5%. Nitrate, nitrite, ammonium, and ortho-P were analyzed by colorimetric methods described by Rodier [21], using sodium salicylate, diazotization, blue of indophenol, and phosphomolybdate methods, respectively. The obtained

results were applied to statistical study using Andad software [22]. Statistical summaries of the parameters analyzed for this study are presented in Table 2. Data were made available in a format that is accessible via GIS. Surfer 8 was used to generate different spatial distribution maps of various chemical constituents in the study area. Water Quality Index (WQI), sodium adsorption ratio (SAR), sodium percentage (% Na), and permeability index (PI) were used to evaluate the suitability of groundwater for irrigation and drinking purposes.

3. Results and Discussion

3.1. Mateur Groundwater Geochemistry

3.1.1. pH and $T^\circ\text{C}$. The pH values of Mateur alluvial aquifer water range from 7.18 to 8.39 during the wet season and between 7.02 and 8.11 throughout the dry season.

The spatial and temporal variations of pH are controlled by the quality and the infiltration rate of recharge water, the replenishing water rate and water-rock interaction in the aquifer. These pH values are all in the desirable limits set by the World Health Organization (WHO) [23].

The temperature values of groundwater varied from 18.9°C to 25.6°C during the wet season and from 18.2°C to 26.7°C during the dry season. The highest temperature values, for the same well or borehole, are recorded during dry season. The spatial variation of temperature is a function of the recharged water and of the infiltration transfer time, which in turn both depend on porosity, lithology, and

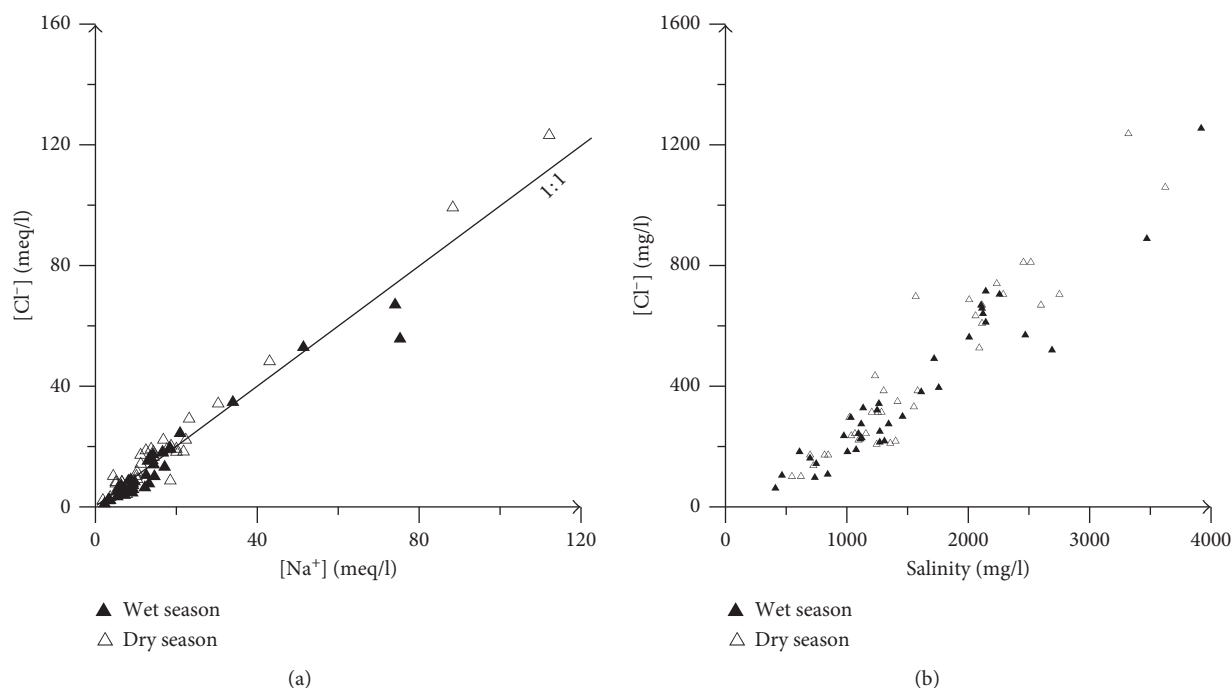


FIGURE 6: Bivariate plot of (a) Na^+ versus Cl^- and (b) salinity versus Cl^- .

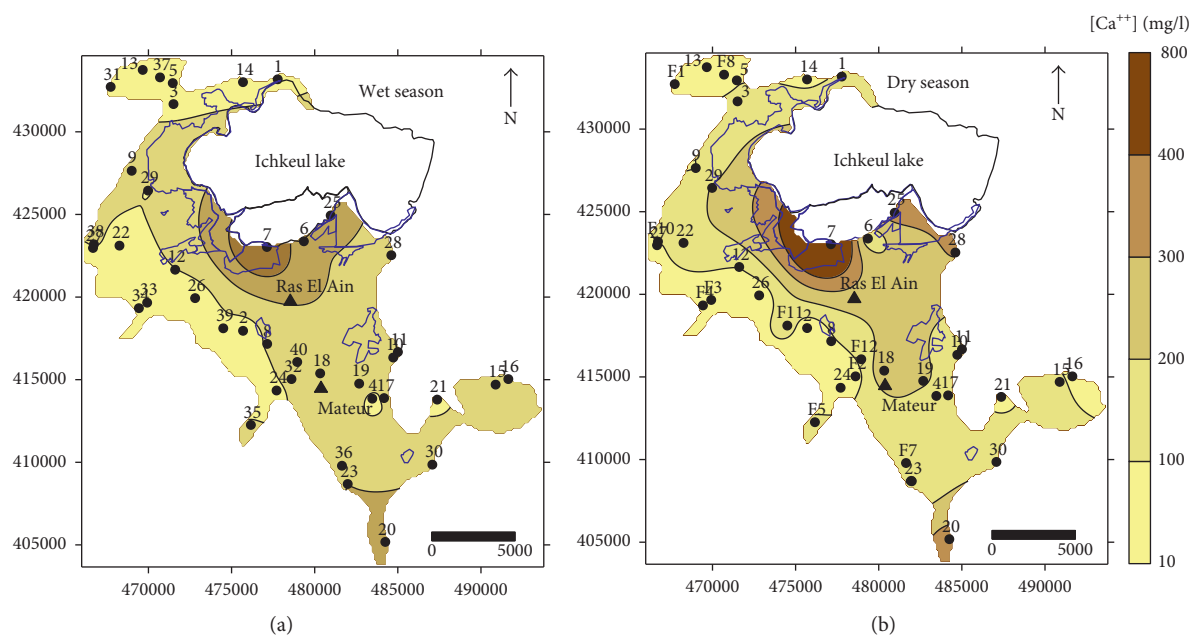


FIGURE 7: Spatial distribution maps of calcium (Ca^{++}): (a) wet season and (b) dry season.

thickness of the unsaturated zone. For the same sampling period, the spatial variation is marked by a decrease as the depth increases.

3.1.2. Salinity, Sodium, and Chloride. Water salinity of the Mateur aquifer varied from 0.1 to 4.5 g/L during the wet season and from 0.1 to 8.4 g/L throughout the dry season. The highest values were recorded during the dry season

(October), whereas the lowest values were recorded during the wet season (April). The spatial distribution maps of salinity (Figures 5(a) and 5(b)) show that the lowest values are recorded both during the wet and the dry season in the northwest and southwest parts of the aquifer. These parts correspond to the natural recharge area (dilution effect) with an increasing trend of salinity values in the water flow direction. The high salinity levels are related to the infiltration of salty water from Ichkeul marshes and of salty soil leachate

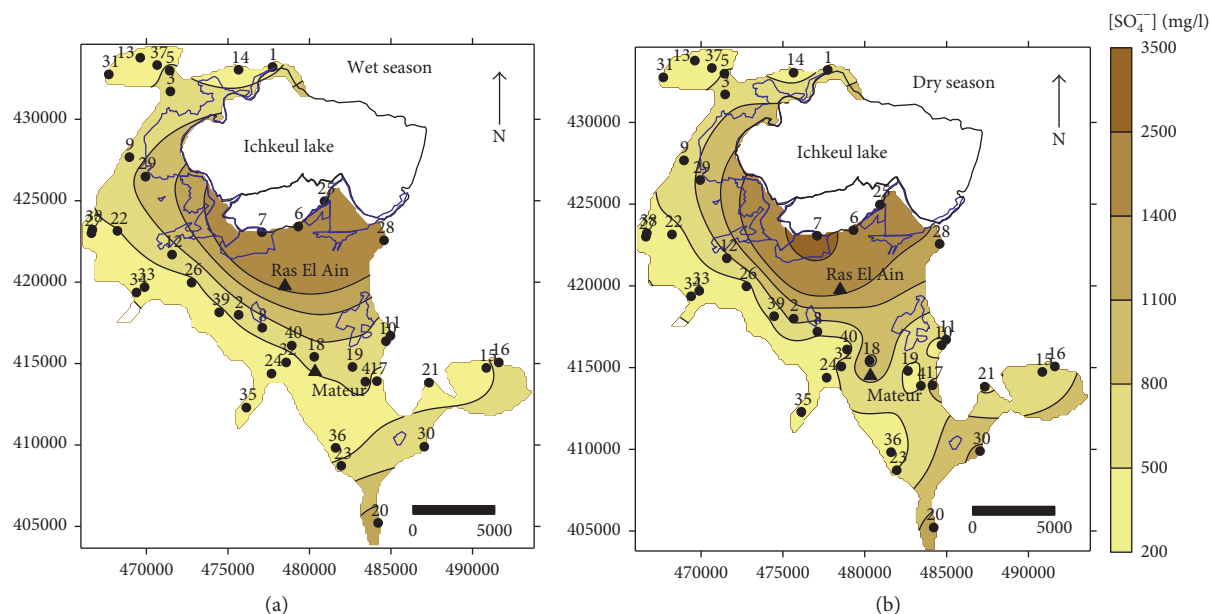


FIGURE 8: Spatial distribution maps of sulfate (SO_4^{2-}): (a) wet season and (b) dry season.

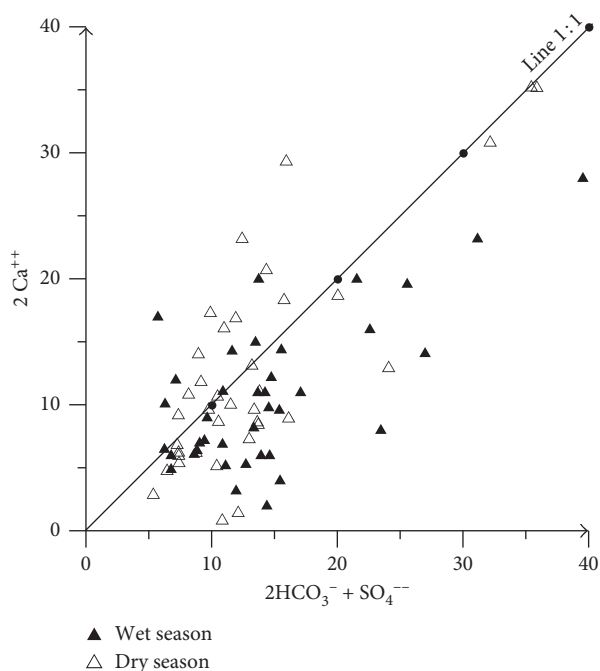


FIGURE 9: Geochemical relationship of ($2\text{HCO}_3^- + \text{SO}_4^{2-}$) versus 2Ca^{2+} .

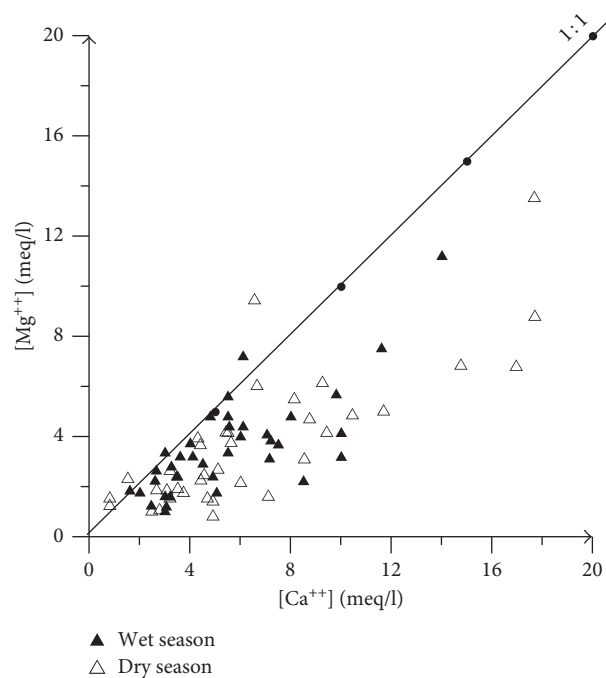


FIGURE 10: Bivariate plot of Ca^{2+} versus Mg^{2+} .

located south of Ichkeul. The main factors contributing to the groundwater salinity are dilution or evaporation, the thickness and the nature of sediments in the vadose zone, and the salty water intrusion around Ichkeul lake [11].

The concentration of chloride varied from 67 to 2406 mg/L during the wet season and from 49 to 4402 mg/L throughout the dry season. Sodium contents ranged between 49 and 1728 mg/L during wet season and between 39 and 2576 mg/L during dry season. Concentrations of chlorides and sodium show little seasonal variation. A slight decrease, more

important in the most mineralized waters, can be explained by the dilution caused by rainwater infiltration during the wet season (April), whereas evaporation contributes to ion concentration increase throughout the dry season.

Cl shows a strong positive correlation with Na (Figure 6(a)) and with salinity (Figure 6(b)), indicating that these ions seem to be dominant in the groundwater mineralization process and have the same origin: the dissolution of halite occurring in saline surface deposits and marshes around the Ichkeul lake and around salty soils.

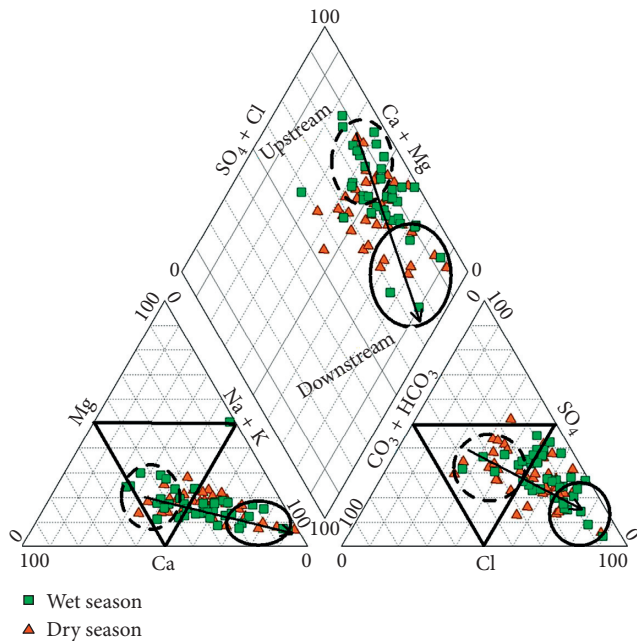
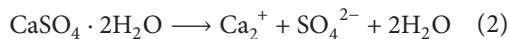
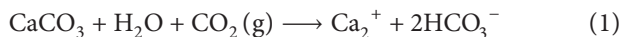


FIGURE 11: Piper diagram.

3.1.3. Ca^{2+} , Mg^{2+} , HCO_3^- , and SO_4^{2-} . The spatial distribution maps of Ca^{2+} levels show that the highest values characterize the northeastern and the outflow parts of the aquifer (Figures 7(a) and 7(b)). An increasing trend with the flow direction is registered, especially during the wet season. The spatial distribution maps of sulfate contents (Figures 8(a) and 8(b)) show that higher sulfate values characterize the northeastern and the outflow parts of the aquifer.

A good positive correlation of Ca^{2+} versus HCO_3^- and SO_4^{2-} (Figure 9) shows that the calcium originates, in addition to the dissolution of the calcite, from the dissolution of gypsum (R1 and R2), where the dissolution of one mole of calcite and one mole of gypsum was put into solution of two moles of Ca^{++} , one mole of SO_4^{2-} , and two moles of HCO_3^- :

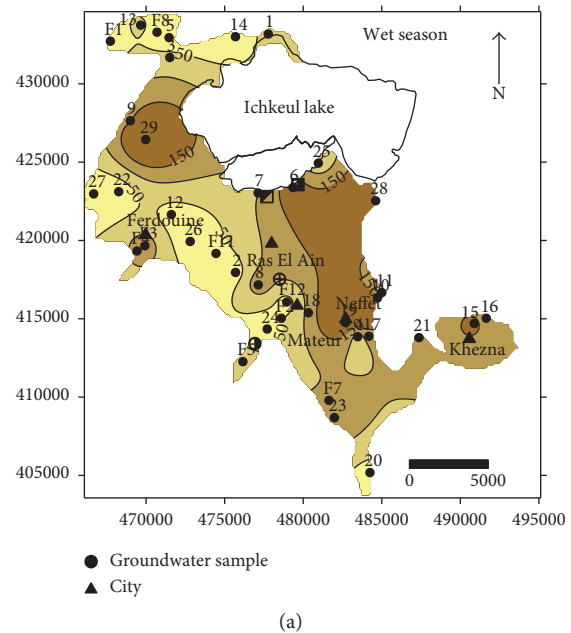


Magnesium contents in Mateur aquifer ranged from 10 to 290 mg/L during the wet season and from 11 to 170 mg/L during the dry season. The lowest values are recorded throughout the wet season, while the highest values are recorded throughout the dry season.

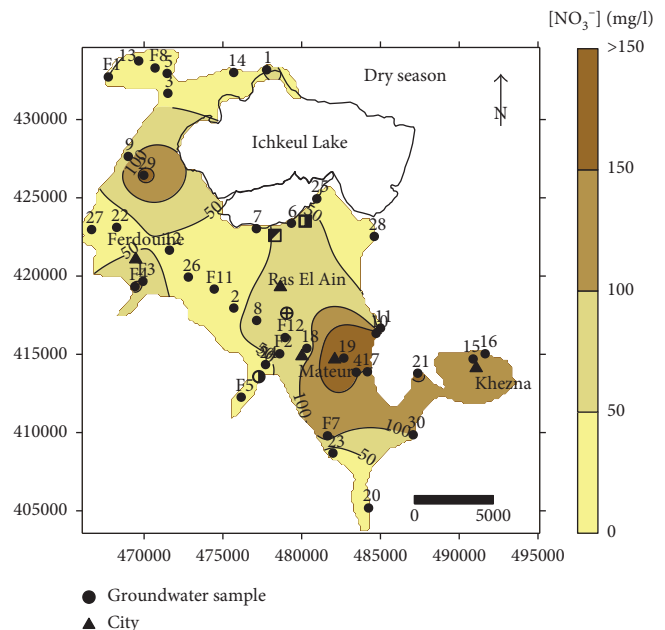
A relationship of Ca versus Mg shows a positive correlation ($R^2 = 0.59$) (Figure 10), indicating the common origin and the similar geochemical behavior of these ions, which could be derived from the dissolution of magnesium calcite $\text{Ca}_{1-x}\text{Mg}_x\text{CO}_3$.

3.1.4. *Chemical Water Types.* The Piper diagram (Figure 11) shows that groundwaters of the studied area are classified into two predominant facies:

- (i) Mixed facies: $\text{Ca-Na-SO}_4\text{-Cl}$ and $\text{Ca-Na-HCO}_3\text{-Cl}$



(a)



(b)

FIGURE 12: Spatial distribution maps of nitrate (NO_3^-): (a) wet season and (b) dry season.

- (ii) Na-Cl facies: they characterize discharge zone and are well influenced by the leaching of salty deposits.

3.1.5. NO_3^- , NO_2^- , NH_4^+ , and O_2 . To assess the possible anthropogenic effects on groundwater quality, water samples were classified into three groups based on the NO_3^- concentration during the study period as (a) below 50 mg/L, (b) 50–150 mg/L, and (c) above 150 mg/L. Figures 12(a) and 12(b) illustrate a complex spatial pattern of nitrate within the aquifer. Nitrate has a WHO (World Health organization) guideline value of 50 mg/L and exceeded this

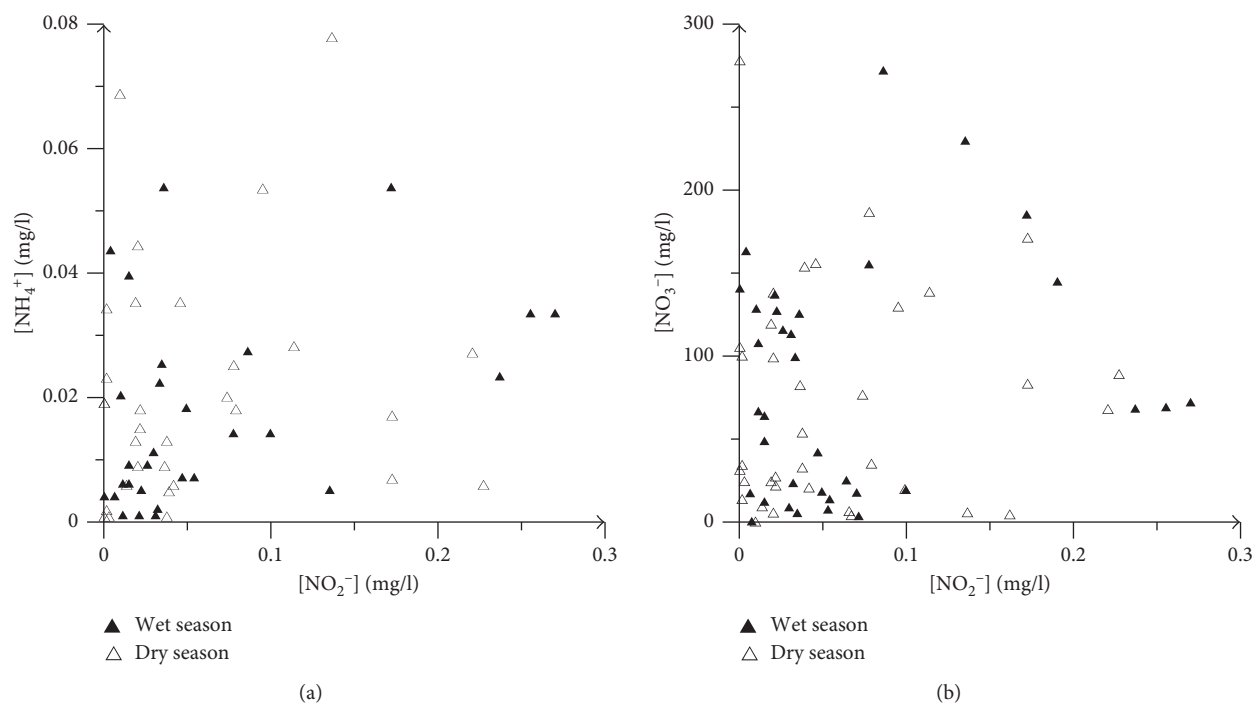


FIGURE 13: Bivariate plot of NO_2^- versus NH_4^+ (a) and NO_3^- (b).

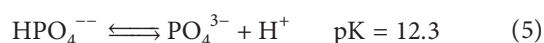
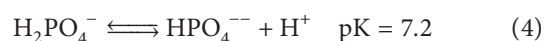
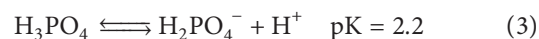
concentration in 48% and 32% of samples in wet and dry seasons, respectively. The highest values were 485 mg/L and 336 mg/L during wet and dry seasons, respectively. High concentrations of nitrate are recovered in the northwestern and central part of the aquifer. Areas where nitrate concentrations are lower than 50 mg/L are located in the western part of the aquifer, which corresponds to the natural recharge zone. Considering the temporal pattern, a similar distribution pattern was observed in the dry and the wet seasons, but the magnitude of concentration was higher during the wet season. Elevated nitrate concentration was noted during the wet season due to the combination of high nitrogen fertilizer applications from January to May and the subsequent irrigation. Throughout the dry season, elevated nitrate concentration can be explained by irrigation with NO_3^- -rich water. Indeed, fertilizer management adopted by farmers is most probably partially responsible for the observed pollution of the groundwater. This spatial distribution is also controlled by the physical, environmental, and chemical properties of the soil [24] and the particle size, lithology, and the thickness of the unsaturated zone [25]. Indeed, in spite of the position of the wells 2, 14, 26, 22, and 25 in the irrigated perimeter, they have lower nitrate concentration. This is explained by a clay unsaturated zone with a low permeability ranging between 86 and 433 mm/day. High permeabilities (4335 mm/day) with the correspondingly silty sand and silty unsaturated zone are also consistent with the higher groundwater nitrate concentrations in the wells 10, 15, 17, 19, and 28. Point nitrate groundwater pollution does not seem to be important in the studied area. Indeed, industrial and urban wastewater discharge into the Joumine River, which plays a groundwater drainage role to

the Ichkeul Lake, cause, locally, eutrophication in its southern part.

Groundwater samples in the studied area are fairly oxygenated, so NO_2^- and NH_4^+ concentrations were almost absent, except few wells which have dramatically higher values. Nitrite contamination is indicative of local and recently generated contamination [26, 27], whereas the presence of ammonium ions in groundwater is generally an indicator of groundwater pollution [28]. High nitrite values are related to wastewater leaching. The ammoniacal nitrogen may originate from the degradation of dissolved organic matter or from the infiltration of leachate water of fertilized soils.

The absence of correlation between the different inorganic nitrogen compounds (NO_3^- , NO_2^- , and NH_4^+) and O_2 (Figures 13(a) and 13(b)) and (Figures 14(a)–(c)) shows that nitrates within the Mateur aquifer waters are mainly derived from the infiltration of leaching water from cultivated land in addition to a small proportion related to nitrification.

3.1.6. Ortho-P. The solubility of inorganic forms of phosphorus, mainly represented by orthophosphates, is pH dependent. The equilibrium reactions between orthophosphates are the following [29]:



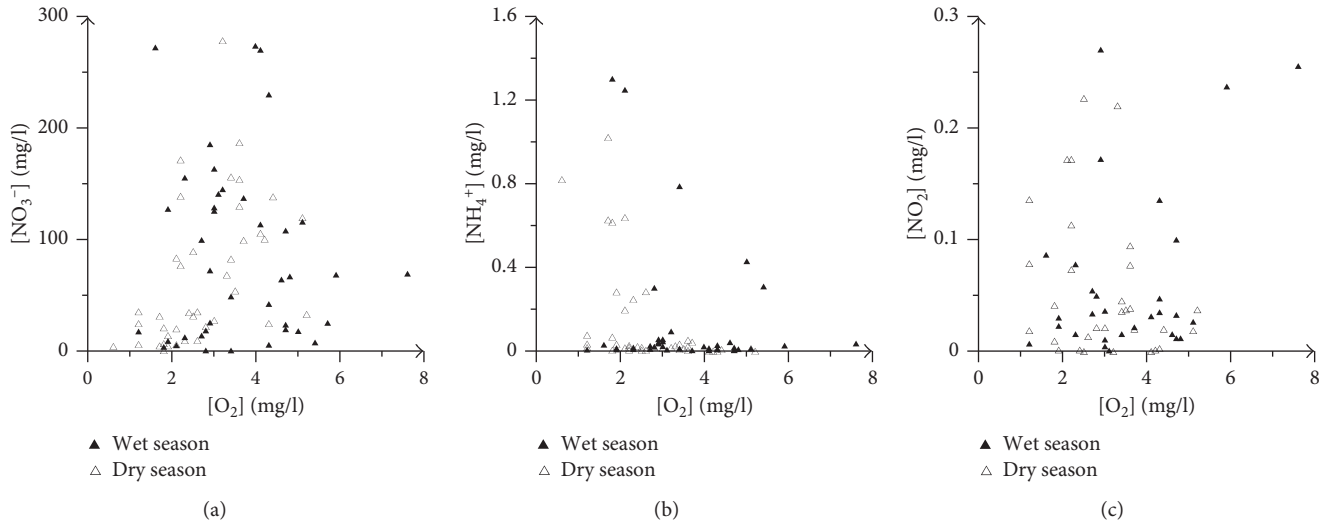
FIGURE 14: Bivariate plot of O_2 versus NO_3^- (a) NH_4^+ (b) and NO_2^- (c).

TABLE 3: Weight and relative weight of chemical parameters used for WQI computation.

	S_i	w_i	W_i
Salinity	1500	5	0.152
Bicarbonates		1	0.030
Chlorides	400	5	0.152
Sulfates	400	5	0.152
Nitrates	50	5	0.152
Calcium	300	3	0.091
Magnesium	150	3	0.091
Sodium	200	4	0.121
Potassium		2	0.061
		Total $w_i = 33$	Total $W_i = 1$

These reactions indicate that HPO_4^{2-} is the dominant form within a pH range of 7.2 and 12.5. According to the pH values of groundwater in the study area, the dominant form of orthophosphates is HPO_4^{2-} with contents between 10 and $482 \mu\text{g/L}$ during the wet season and between 20 and $637 \mu\text{g/L}$ during the dry season. The highest orthophosphate contents are recorded in the outflow parts of the aquifer and might be connected to the fertilization of agricultural land by phosphorus fertilizers (diammonium phosphate and super 45). Indeed, the repeated phosphorus fertilization increases the transfer of phosphorus to the aquifer [30, 31]. High orthophosphate levels would be related also to the discharge of urban wastewater in Joumine River.

3.2. Groundwater Suitability

3.2.1. Suitability for Drinking Purposes Using Water Quality Index (WQI). Water Quality Index is one of the most effective tools to communicate information on the quality of water to the concerned citizens and policymakers. It is an important parameter for the assessment and management of groundwater. WQI is defined as a rating reflecting the composite influence of different water quality parameters [32]. By mapping the index, the areas of high and low water

TABLE 4: Water Quality Index (WQI) ranges and percentage of samples during wet and dry seasons.

WQI range	Water quality	Wet season	Dry season
<50	Excellent	12.50	10
50–100	Good	40	45
100–200	Poor	35.50	35
200–300	Very poor	5	2.50
>300	Unsuitable for domestic purposes	7.50	7.50

quality can easily be distinguished by scientists as well as by policymakers or the general public, for treatment before various uses [33].

To compute the WQI, three steps are followed [34]. In the first step, each of the 9 parameters is assigned a weight (W_i) according to its relative importance in the overall quality of water for drinking purposes (Table 3). In the second step, the relative weight (W_i) is computed from the following equation (6):

$$W_i = \frac{w_i}{\sum_{i=1}^n w_i}, \quad (6)$$

where w_i is the weight of each parameter and n is the number of parameters.

To compute the WQI (9), the SI is first determined for each chemical parameter, which is then used to determine the WQI as in the following equation (7):

$$SI_i = W_i * q_i, \quad (7)$$

$$q_i = \left(\frac{C_i}{S_i} \right) * 100, \quad (8)$$

where C_i is the concentration of each chemical parameter in each water sample in mg/L.

S_i is a World Health Organization's standard for each of the major parameters in drinking water [23].

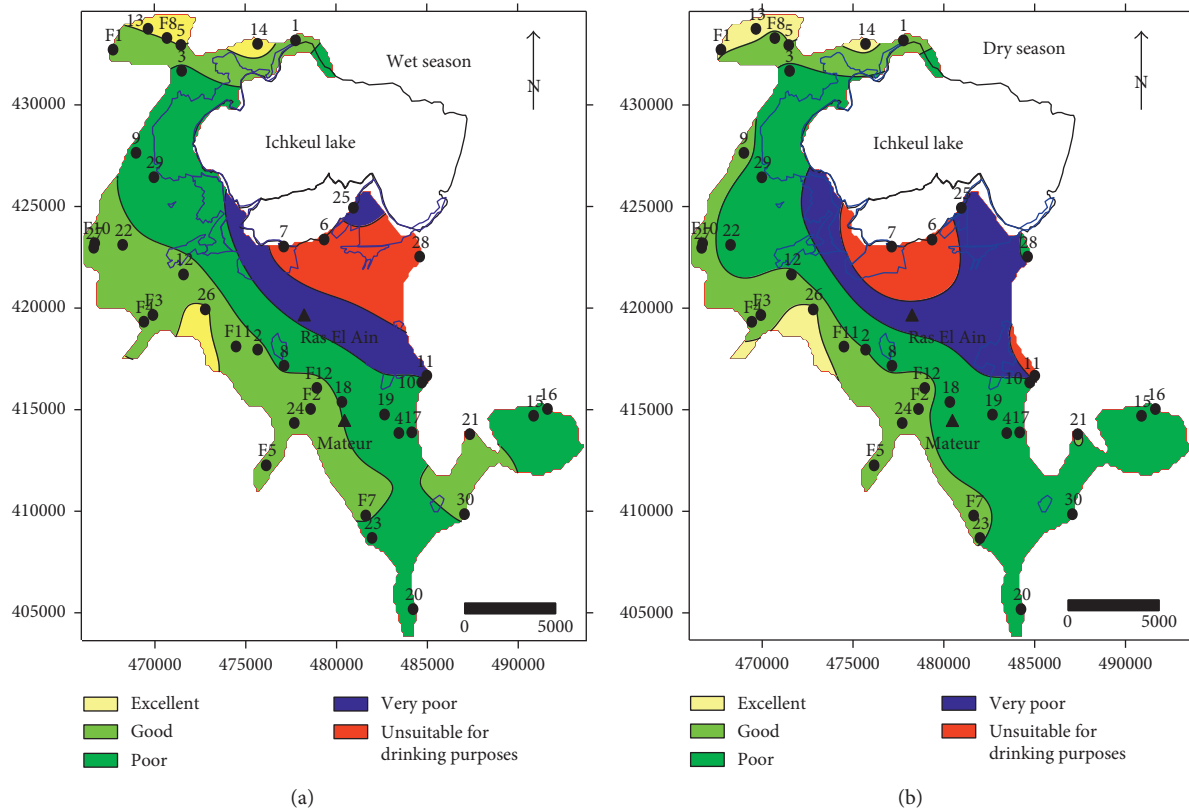


FIGURE 15: Spatial distribution maps of WQI.

$$WQI = \sum SI_i, \quad (9)$$

where SI_i is the subindex of i th parameter, q_i is the rating based on the concentration of i th parameter, and n is the number of parameters.

The computed WQI values are classified into five types, from “excellent water” to “water, unsuitable for drinking” (Table 4) [32]. In the current study, a total of nine chemical parameters (salinity, Na^+ , Cl^- , Ca^{2+} , Mg^{2+} , SO_4^{2-} , K^+ , HCO_3^- , and NO_3^-) of 40 water samples were used to calculate WQI, in order to assess the suitability of the Mateur aquifer groundwater for domestic (drinking) use. The weights assigned to the parameters ranged between 1 and 5 (Table 3) and were based on the health effects of these parameters. The highest weight (5) was assigned to salinity and nitrate due to their major importance in water quality assessment and the health implications of the high concentration of these chemical parameters in water [35, 36].

The spatial distribution of Water Quality Index (Figure 15) shows the highest quality (12.5% and 40% of groundwater samples fell into excellent to good, resp., during both seasons). These two categories characterize the northwest and the southeast part of the aquifer, corresponding to the recharge zone. The water samples within poor quality, very poor quality, and unsuitable for drinking purposes contributed 35.5%, 5%, and 7.5% of groundwater samples, respectively in the wet season with no remarkable difference in the dry season. Poor and very poor water qualities were

found in the center and east part of the aquifer and cannot be used for drinking without any treatment and conventional disinfection, whereas water “unsuitable for drinking purposes” could only be used for aquaculture, irrigation, and industrial purposes and characterizes the outflow part of the aquifer [37].

3.2.2. Suitability for Irrigation. The long-term effect of irrigation water on physical and chemical properties of soil and crop productivity depends on the conductivity and sodium contents, dissolved inorganic carbon and alkaline earth elements (Ca and Mg) of irrigation water, and initial physical properties of soil [36].

In order to assess the irrigation suitability of Mateur aquifer groundwaters, the following parameters were used: sodium percentage (% Na), sodium adsorption ratio (SAR), and permeability index (PI).

(1) Sodium Adsorption Ratio (SAR). The sodicity hazard of water is generally described by the sodium adsorption ratio. Indeed, there is a significant relationship between SAR values of irrigation water and the extent to which sodium is adsorbed by the soil [24]. If water used for irrigation is high in sodium and low in calcium, the cation exchange complex may become saturated with sodium, which can destroy the soil structure due to the dispersion of clay particles [38]. SAR is computed from the following equation (10), where the concentrations are reported in meq/L.

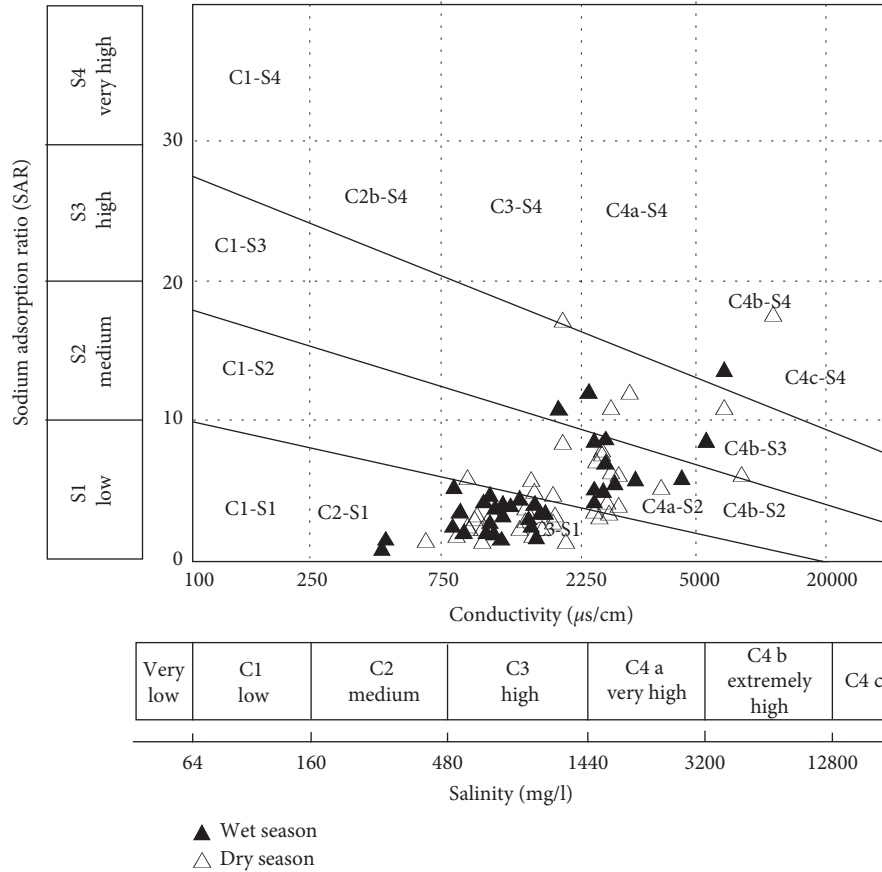


FIGURE 16: USSR diagram for the study area.

TABLE 5: Irrigation quality of groundwater based on sodium percentage.

	C2S1 (%)	C3S1 (%)	C4aS2 (%)	C4bS2 (%)	C4aS1 (%)	C4bS4 (%)	C4bS3 (%)	C3S4 (%)
Wet season	5	42	21	2	—	3	—	—
Dry season	3	36	18	3	12	—	—	3

$$SAR = \frac{Na}{\sqrt{(Ca + Mg/2)}} \quad (10)$$

The SAR values in the study area range between 4.08 and 13.9. All the sampling points on the US salinity diagram are shown in Figure 16 and summarized in Table 5. Figure 16 illustrates that the majority of water samples fall into C3S1 and C4aS2 fields during both seasons. 42% and 36% of groundwater samples fall into C3S1 during wet and dry seasons, respectively, indicating water of medium-to-high salinity and low SAR category, without risk of soil destabilization. This water falls into admissible class (C3S1) characterizing groundwater samples located in the natural recharge zone of the aquifer and can be used for irrigation of plants having a good salt tolerance, on well-drained soils or good permeability, with salinity control [39]. 23% and 21% of groundwater samples fall into C4S2 field poor class (C4S1-C4S2) in wet and dry seasons, respectively, indicating very high salinity and medium alkalinity hazards. This class is characterized by strongly mineralized water presenting

important risk of soil salinization, but with medium risk of alkalization. It is found in the center and the east part of the aquifer (Figure 17). Very high salinity waters are unsuitable for irrigation with a suitable drainage. An adequate drainage with low salinity waters and plants having good salt tolerance should be selected.

(2) *Percentage of Sodium (% Na)*. Wilcox [40] used % Na and specific conductance in evaluating the suitability of groundwater for irrigation. % Na is calculated using the following relation (11):

$$\%Na = \left(\frac{Na}{Na + Ca + Mg + K} \right) * 100, \quad (11)$$

where all the ionic concentrations are expressed in meq/L.

All groundwater samples on the Wilcox diagram are shown in Figure 18 and summarized in Table 6. Groundwater samples in the study area fall into five categories: (i) good to excellent categories, which represent 47% to 8% of

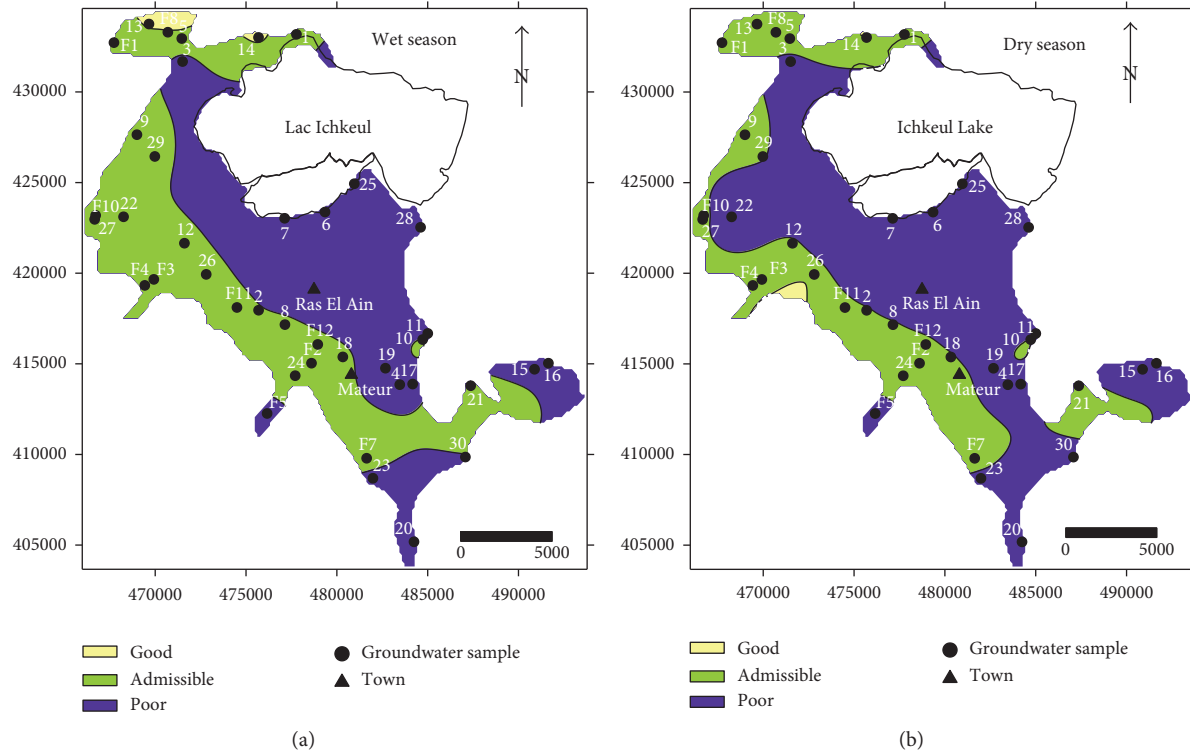


FIGURE 17: Spatial distribution maps of the irrigation suitability classes of the study area.

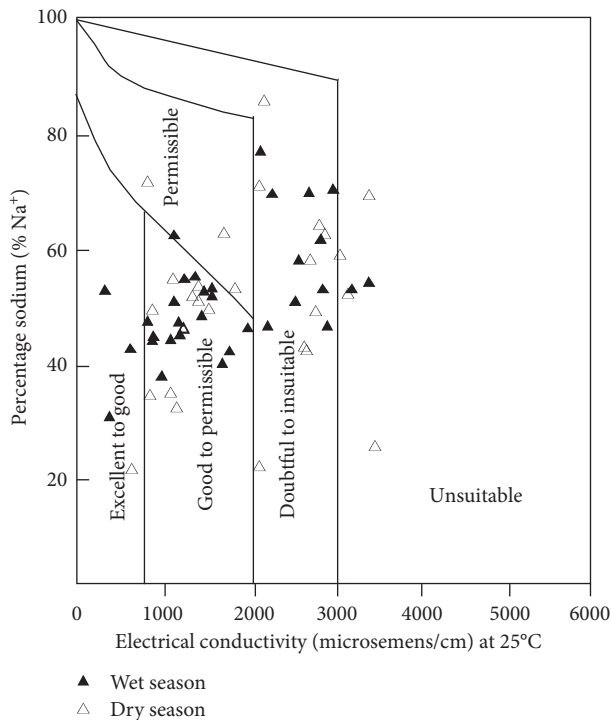


FIGURE 18: Wilcox diagram for the study area.

the groundwater samples during the wet season and 30% to 3% of the groundwater samples during the dry season, respectively; (ii) permissible categories, which are moderately mineralized and represent 2% of groundwater samples during the wet season and 9% throughout the dry season;

TABLE 6: Salinity and alkalinity hazards of irrigation water in US salinity diagram.

	Excellent (%)	Good (%)	Permissible (%)	Doubtful (%)	Unsuitable (%)
Wet season	8	47	2	26	10
Dry season	3	30	9	21	18

and (iii) from poor to very poor quality water, which are the most mineralized, with the highest percentage of sodium. These waters represent 26% to 10% of all water during the wet season and 21% to 18% during the dry season and are located mainly in the eastern part of the web and in the discharge area, in the marshes of Ichkeul.

It is noteworthy that when the sodium content is high in irrigation water, this element tends to replace the Ca and Mg ions in the interlayer space of soil clays, reducing its permeability, and thus, causing poor internal drainage [36, 41].

(3) *Permeability Index*. The permeability index is an important factor, which influences the quality of irrigation water in relation to the soil for development in agriculture [42].

The permeability index (PI) of a water sample is computed from the following equation (12), where concentrations are in meq/L.

$$PI = \left(\frac{Na + \sqrt{HCO_3}}{(Na + Ca + Mg)} \right) * 100. \quad (12)$$

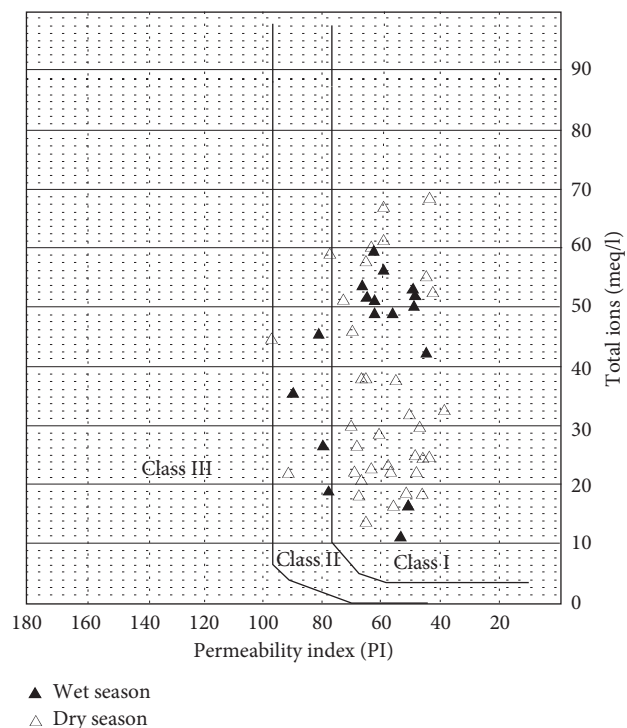


FIGURE 19: A Doneen's chart for the study area.

Permeability indices were plotted with the total ionic content of the groundwater samples on a Doneen's chart [42], which represent three different classes: CI with the best water type for irrigation, CII water generally acceptable, and CIII waters unacceptable [44].

In the study area, the PI ranged from 52.44 to 64.09 with an average of 56.13, Figure 19 shows that all the samples fall within the CI best water type for irrigation purposes.

4. Conclusions

The objective of this study is to assess the seasonal variation in the physicochemical characteristics of water supply wells in the Mateur plain, Northern Tunisia. The WQI was applied to investigate the seasonal changes and the factors influencing groundwater hydrochemistry and hence its suitability for irrigation and domestic purposes. The investigation results suggest the following: (i) The highest quality was found, during both the wet and dry season, in the northwest and southeast part of the aquifer, corresponding to the recharge zone where 12.5% and 40% of groundwater samples fell into excellent to good categories, respectively. Toward the flow direction, groundwaters become poor to very poor and need treatment before consumption. (ii) Most of the groundwater samples fell in doubtful to unsuitable categories, characterizing the eastern part of the aquifer and the outflow part, around the Ichkeul marshes. These waters with high to very high salinity are unsuitable for irrigation purposes in ordinary conditions, an adequate drainage with low salinity waters and plants having good salt tolerance should be selected. (iii) The little seasonal change of groundwaters' quality of Mateur aquifer is mainly related to

dilution in the wet season, evaporation throughout the dry season, and agricultural activities.

Data Availability

The data used to support the findings of this study are available from the corresponding author upon request.

Conflicts of Interest

The authors declare that they have no conflicts of interest.

Supplementary Materials

A table showing the subindex of i th parameter (SI_i) values during wet and dry seasons was added as supplementary material. (*Supplementary Materials*)

References

- [1] R. T. Nickson, J. M. McArthur, B. Shrestha, T. O. Kyaw-Nyint, and D. Lowry, "Arsenic and other drinking water quality issues, Muzaffargarh District, Pakistan," *Applied Geochemistry*, vol. 20, no. 1, pp. 55–68, 2005.
- [2] S. R. Carpenter, N. F. Caraco, D. L. Correll, R. W. Howarth, A. N. Sharpley, and V. H. Smith, "Non-point pollution of surface waters with phosphorus and nitrogen," *Ecological Applications*, vol. 8, no. 3, pp. 559–568, 1998.
- [3] J. Chen, F. Wang, X. Xia, and L. Zhang, "Major element chemistry of the Changjiang (Yangtze River)," *Chemical Geology*, vol. 187, no. 3–4, pp. 231–255, 2002.
- [4] M. Milovanovic, "Water quality assessment and determination of pollution sources along the Axios/Vardar River, Southeastern Europe," *Desalination*, vol. 213, no. 1–3, pp. 159–173, 2007.
- [5] M. Vasanthaviga, K. Srinivasamoorthy, R. Vijayaragavan et al., "Application of water quality index for groundwater quality assessment: Thirumanimuttar sub-basin, Tamilnadu, India," *Environmental Monitoring and Assessment*, vol. 171, no. 1–4, pp. 595–609, 2010.
- [6] W. R. Kelly, "Heterogeneities in ground-water geochemistry in a sand aquifer beneath an irrigated field," *Journal of Hydrology*, vol. 198, no. 1–4, pp. 154–176, 1997.
- [7] T. Y. Stigter, S. P. J. van Ooijen, V. E. A. Post, C. A. J. Appello, and A. M. M. Carvalho Dill, "A hydrogeological and hydrochemical explanation of the groundwater composition under irrigated land in a Mediterranean environment, Algarve, Portugal," *Journal of Hydrology*, vol. 208, no. 3–4, pp. 262–279, 1998.
- [8] E. E. Cey, D. L. Rudolf, R. Aravena, and G. Parkin, "Role of the riparian zone in controlling the distribution and fate of agricultural nitrogen near a small stream in southern Ontario," *Journal of Contaminant Hydrology*, vol. 37, no. 1–2, pp. 45–67, 1999.
- [9] T. Peterson, G. Folland, W. Gruza et al., *Report of the Activities of the Working Group on Climate Change Detection and Related Rapports 1998–2001*, National Oceanography Centre, Southampton, UK, 2001.
- [10] M. Massoud, M. D. Scrimshaw, and J. N. Lester, "Qualitative assessment of the effectiveness of the mediterranean action plan: wastewater management in the Mediterranean Region," *Ocean and Coastal Management*, vol. 46, no. 9–10, pp. 875–899, 2003.
- [11] B. Tlili-Zrelli, M. Gueddari, R. Bouhlila, and M. N. Oueslati, "Groundwater hydrogeochemistry of Mateur alluvial aquifer

- (Northern Tunisia)," *Journal of Hydrogeology & Hydrologic Engineering*, vol. 5, no. 1, 2016.
- [12] DGRE, *Annuaire d'Exploitation des Nappes Profondes*, Direction Générale des Ressources en Eaux, Tunis, Tunisia, 2010.
 - [13] DGRE, *Annuaire d'Exploitation des Nappes Phréatiques*, Direction Générale des Ressources en Eaux, Tunis, Tunisia, 2005.
 - [14] F. Melki, T. Zouaghi, S. Harraba, A. Z. Sainez, M. Bédir, and F. Zargouni, "Structuring and evolution of Neogene transcurrent basins in the Tellian foreland domain, north-eastern Tunisia," *Journal of Geodynamics*, vol. 52, no. 1, pp. 57–69, 2011.
 - [15] M. Ennabli, "Etude hydrogéologique des aquifères du Nord-Est de la Tunisie pour une gestion intégrée des ressources en eau," Thèse de Doctorat d'Etat, Université de Paris, Nice, France, 1980.
 - [16] M. Ennabli, "Contribution à l'étude Hydrogéologique de la Plaine de Mateur," Thèse de 3ème Cycle, Faculté des Sciences de Paris, Tunis, Tunisia, 1967.
 - [17] A. Mori, *Etude Pédologique du Périmètre de Mateur Oued Melah et Oued Sejnane*, OROSTOM, Service du sol Ministère de l'Agriculture et des Ressources en eau, Dubai, UAE, 1962.
 - [18] CRDA, *Commissariat Régional de Développement Agricole Rpp. Int*, 2007.
 - [19] CRDR, *Commissariat Régional de Développement Régional: Gouvernorat de Bizerte en Chiffres*, 2012, ISSN 1737-8790.
 - [20] A. Jendoubi and R. Bouhlila, "Modelling of nitrate transport in the Mateur aquifer (Tunisia)," in *Proceedings of the Conference on Impact of Human Activity on Groundwater Dynamics*, Maastricht, Netherlands, July 2001.
 - [21] J. Rodier, *L'Analyse de l'Eau: Eaux Naturelles, Eaux Résiduelles, Eaux de Mer*, Editions Dunod, Paris, France, 1984.
 - [22] CVRM, *Programa ANDAD. Manual do Utilizador*, CVRM-Centro de Geosistemas, Instituto Superior Técnico, Lisboa, Portugal, 2000.
 - [23] WHO, *Guidelines for Drinking-Water Quality*, World Health Organization, Geneva, Switzerland, 3rd edition, 2004.
 - [24] G. V. Subbarao, O. Ito, K. L. Sahrawat et al., "Scope and strategies for regulation of nitrification in agricultural systems-challenges and opportunities," *Critical Reviews in Plant Sciences*, vol. 25, no. 4, pp. 303–335, 2006.
 - [25] A. Landreau and J. C. Roux, *Répartition et Évolution des Teneurs en Nitrates dans les Eaux Souterraines en France*, Note Technique, BRGM, Orléans, France, 1981.
 - [26] J. D. Hem, *Study and Interpretation of the Chemical Characteristics of Natural Water*, U. S. Geological Survey, Water Supply Paper 2254, University of Virginia, Charlottesville, VA, USA, 1985.
 - [27] S. Fertouani, M. Sbaa, M. Vanclooster, and B. Bendra, "Assessing groundwater quality in the irrigated plain of Triffa (north-east Morocco)," *Agricultural Water Management*, vol. 95, no. 2, pp. 133–142, 2008.
 - [28] I. Idrissi, M. Zeraoui, M. Addou, A. Mokhtari, and I. A. Soulaymani, "Évaluation de la pollution nitrrique de la nappe phréatique de la," *Afrique Science: Revue Internationale des Sciences et Technologie*, vol. 3, no. 3, pp. 378–390, 2007.
 - [29] W. Stumm and I. J. Morgn, *Aquatic Chemistry: An Introduction Emphasizing Chemical Equilibria in Natural Waters*, John Wiley & Sons, Hoboken, NJ, USA, 2nd edition, 1981.
 - [30] M. Mozaffari and J. T. Sims, "Phosphorus availability and sorption in an Atlantic coastal plain watershed dominated by animal-based agriculture," *Soil Science*, vol. 157, no. 2, pp. 97–107, 1994.
 - [31] T. Q. Zhang, A. F. Mackenzie, and B. C. Liang, "Long-term changes in Mehlich-3 extractable P and K in a sandy clay loam soil under continuous corn (*Zea mays* L.)," *Canadian Journal of Soil Science*, vol. 75, no. 3, pp. 361–367, 1995.
 - [32] C. R. Ramkrisahniah, C. Sadashivaiah, and G. Ranganna, "Assessment of water quality index for the groundwater in Tumkur Taluk, Karnataka State, India," *E-Journal of Chemistry*, vol. 6, no. 2, pp. 523–530, 2009.
 - [33] M. Saeedi, O. Abess, F. Sharifi, and H. Meraji, "Development of groundwater quality index," *Environmental Monitoring and Assessment*, vol. 163, no. 1–4, pp. 327–335, 2010.
 - [34] F. Hamzaoui-Azaza, B. Tlili-Zrelli, M. Gueddari, and R. Bouhlila, "Suitability of groundwater of Zeuss-Koutine aquifer (Southern of Tunisia) for domestic and agricultural use," in *Water Quality: Indicators, Human Impact and Environmental Health*, Chapter 5, pp. 109–130, Nova Science Publishers, Hauppauge, NY, USA, 2012.
 - [35] K. Srinivasamoorthy, M. Chidambaram, M. V. Prasanna, M. Vasanthavignar, A. John Peter, and P. Anandha, "Identification of major sources controlling groundwater chemistry from a hard rock terrain a case study from Mettur taluk, Salem district, Tamil Nadu, India," *Journal of Earth System Sciences*, vol. 117, no. 1, pp. 49–58, 2008.
 - [36] S. M. Yidana, B. Banoeng-Yakubo, and T. M. Akabzaa, "Analysis of groundwater quality using multivariate and spatial analyses in the Keta Basin, Ghana," *Journal of African Earth Sciences*, vol. 58, no. 2, pp. 220–234, 2010.
 - [37] R. Jindal and C. Sharma, "Studies on water quality of Sutlej River around Ludhiana with reference to physicochemical parameters," *Environmental Monitoring and Assessment*, vol. 174, no. 1–4, pp. 417–425, 2011.
 - [38] D. K. Todd, *Groundwater Hydrology*, Wiley, New York, NY, USA, 2nd edition, 1980.
 - [39] L. Gouaidia, O. Gueffiafia, A. Boudoukha, M. L. Hemila, and C. Martin, "Evaluation de la salinité des eaux souterraines utilisées en irrigation et risques de dégradation des sols: exemple de la plaine de Meskiana (Nord-Est Algérien)," *Physio-Géo*, vol. 6, pp. 141–160, 2012.
 - [40] M. N. Tijani, "Hydrochemical assessment of groundwater in Moro area, Kwara State, Nigeria," *Environmental Geology*, vol. 24, no. 3, pp. 194–202, 1994.
 - [41] L. V. Wilcox, *Classification and Use of Irrigation Water*, US Department of Agriculture, Circular, Washington, DC, USA, 1955.
 - [42] K. Srinivasamoorthy, M. Vasanthavignar, K. Vijayaraghavan, R. Sarathidasan, and S. Gopinath, "Hydrochemistry of groundwater in a coastal region of Cuddalore district, Tamil Nadu, India: implication for quality assessment," *Arabian Journal of Geosciences*, vol. 6, no. 2, pp. 441–454, 2013.
 - [43] P. A. Domenico and F. W. Schwartz, *Physical and Chemical Hydrogeology*, Wiley, New York, NY, USA, 1990.
 - [44] B. Tlili-Zrelli, F. Hamzaoui-Azaza, M. Gueddari, and R. Bouhlila, "Geochemistry and quality assessment of groundwater using graphical and multivariate statistical methods. A case study: Grombalia phreatic aquifer (Northeastern Tunisia)," *Arabian Journal of Geosciences*, vol. 6, no. 9, pp. 3545–3561, 2013.

Research Article

Assessment of the Trophic Status of the South Lagoon of Tunis (Tunisia, Mediterranean Sea): Geochemical and Statistical Approaches

Myriam Abidi , Rim Ben Amor, and Moncef Gueddari

R.U. Geochemistry and Environmental Geology, Department of Geology, Faculty of Sciences of Tunis, University of Tunis El Manar, 2092 Tunis, Tunisia

Correspondence should be addressed to Myriam Abidi; bidi.myriam@gmail.com

Received 6 February 2018; Revised 2 April 2018; Accepted 9 May 2018; Published 24 June 2018

Academic Editor: Adina Negrea

Copyright © 2018 Myriam Abidi et al. This is an open access article distributed under the Creative Commons Attribution License, which permits unrestricted use, distribution, and reproduction in any medium, provided the original work is properly cited.

The trophic status assessment of the South Lagoon of Tunis, a shallow Mediterranean coastal area after its restoration, is addressed herein with respect to its various environmental settings which are taken as indicators of water quality. The lagoon had, in the past, witnessed severe environmental quality issues. To resolve these problems, a large restoration project of the lagoon was undertaken which consisted of dredging the bottom sediments removing areas of water stagnation and improving water circulation. After this restoration work, the lagoon morphology has radically changed. In this paper, we attempt to evaluate the lagoon water's trophic state to analyze the eutrophication risk after almost 16 years. In order to achieve these purposes, two water quality monitoring campaigns were conducted (July 2013 and February 2014). Natural and anthropogenic factors controlling the nutrient content of the lagoon water have been assessed through both geochemical methods and multivariate statistical tools. The results show that the nutrients are from external sources due to the discharge of municipal and industrial wastewater from the surrounding city of the catchment in the lagoon's south side. According to the TRIX index, the lagoon remains eutrophic presenting a "poor" water quality, notwithstanding the engineering project due to the high level of nutrients.

1. Introduction

Coastal lagoons are very important for the ecological preservation of biodiversity [1]. However, they are fast turning into threatened ecosystems around the world [2]. The intense anthropogenic development around this area also has negative effects. Recently, the water quality of coastal lagoons in many areas of the world has deteriorated due to massive discharge of nitrogen and phosphorous from domestic and industrial wastewater as well as urban drainage [3–5]. Consequently, there has been a growing interest in eutrophication as one of the most pertinent disturbance processes on aquatic ecosystems caused by humans [6]. Due to increasing human pressure including fisheries, tourism, demographic expansion, and global climate change, the preservation of biodiversity and natural processes in coastal lagoons has become a challenge in recent decades [7].

The Tunisian coastline on the Mediterranean Sea is about 1300 km long. Because of the development of its industrial, touristic, and agricultural activities, Tunisian marine resources began to get contaminated. These activities, together with the expansion of its population had affected the quality of the aquatic environment in the long term.

The present study is integrated in this framework. The Lagoon of Tunis, one of the four major lagoons in Tunisia, is located near the capital and close to the most populated region. This Mediterranean lagoon is characterized by an anthropogenic catchment. Its geographical location had made it, over many decades, as a site of domestic and industrial discharge, causing a massive introduction of nutrients and organic matter. The combination of hydrodynamic and anthropogenic factors (poor circulation, shallow depth (average of 1 meter)) and very high nutrient pollution have led the ecosystem to the state of eutrophication. It has been

considered as the most eutrophicated lagoon on the Tunisian coast [8–10].

In order to resolve the pollution problem and to improve the water quality of the South Lagoon of Tunis (the south basin of the lagoon of Tunis being the subject of our studies) for ecological and economical purposes, an environmental restoration project was conducted from April 1998 to July 2001 [11, 12]. The overall aim of the project was to achieve a good ecological status in the lagoon and to realize substantial land reclamation all around. After this restoration work, the lagoon morphology has radically changed.

The general aspect of the project was to increase the flushing power of the lagoon water with marine water from the Gulf of Tunis and to reduce the water residence time. These purposes were reached by setting two groups of locks in order to allow water exchange between the Gulf of Tunis and the lagoon. In order to avoid water stagnation, different areas located in both the Southeast and the southwest side of the lagoon were removed (reducing the lagoon area from 13 km² to 7 km²), and the shoreline was rectified to be straightened. Moreover, polluted sediments were dredged and removed from the north area of the lagoon. To improve water circulation, fishery was removed, and the Canal of Rades and the Canal of Tunis were restored [13, 14].

Understanding the ecosystem response to this restoration project is essential to assess its rehabilitation. The time elapsed after restoration is a critical indicator of the real restoration success [15]. Indeed, this coastal ecosystem recovery requires a continuous survey through an ecological trophic state evaluation.

The assessment of the status of the lagoon after 16 years of the installation of the restoration works is much needed in order to project further solutions for the decision makers. In this study, this assessment targets mainly the nutrient elements and the trophic index to see if the eutrophication of the lagoon has been improved or otherwise. To our knowledge, this is the unique study which is addressing such problematic related to nutrient elements in relation to eutrophication within the Lagoon of Tunis as previous investigations were conducted from a biological and hydrodynamic point of view only (algae, mussels, etc.). However, the trophic status has received little attention, and this research aims to overcome this gap.

In this paper, these investigations were conducted throughout the lagoon to assess the restoration level and improvement of water quality. Furthermore, we attempt to evaluate the trophic state of lagoon water for eutrophication's risk analysis after almost 16 years.

Surface water samples were collected in wet and dry seasons (July/February) and then were analyzed. Distribution maps and plots of chemical parameters were used to determine the geochemical characteristics of the lagoon water and to identify major natural and anthropogenic processes governing water geochemistry.

In addition, multivariate statistical analysis, such as principal component analysis (PCA) and hierarchical cluster analysis (HCA) were used, in order to help interpreting the complex data matrices for better understanding of the water quality and to allow the identification of possible factors that influence the water system [16–18].

It is widely recognized that the water quality assessment in coastal ecosystems is complicated since a great number of variables, including cause (nutrients) and response (chlorophyll *a*) variables are interrelated [19, 20]. Several methods are thus used to characterize water quality and to assess eutrophication. In this study, the TRIX developed by Volenweider et al. [21] is used to estimate the trophic status of the lagoon water.

2. Materials and Methods

2.1. Study Area. The lagoon of Tunis is located in the northeast of Tunisia. Cutting across the lagoon and connecting the Mediterranean with the old port of Tunis, the Canal of Tunis divides the lagoon into two basins, commonly known as the South Lake and the North Lake of Tunis.

The South Lagoon of Tunis coordinates extend from 12' to 10°16'E longitudes and from 36°46' to 36°48'N latitudes (Figure 1). This area was used to be heavily polluted [8, 22], but it has recently been rehabilitated [23]. After the restoration program, the lagoon appears shaped as an eclipse stretching in a SW-NE direction with about 10 km long and 3.5 km wide (Figure 1). It extends over an area of 720 ha with a regular depth of about 2.1 m, except in some restricted areas, on the east side, where it reaches a maximum of 5 m. Its shores are rectilinear and protected by large rockery stones.

The lagoon is characterized by a semiarid Mediterranean climate. The annual temperature ranges between 7 and 30°C. The mean annual rainfall is 528 mm with interannual variations. The luminosity is about 6 h per day, with 155 h in December and 359 h in July. Evaporation ranges between 62 and 201 mm, respectively, in January and July [24].

Coastal lagoons maintain a connection to the sea through a restricted inlet. At the South Lagoon, the water flow between the lagoon and the Gulf of Tunis is impeded by two inlets (or outlets): seawater generally flows into the lagoon from the east side through the Canal of Rades (2 km length and 4 m deep) and goes out from the western side through the Canal of Tunis (10 km length and 4.5 m deep).

The hydrodynamic of the lagoon is mainly controlled by wind and tide which is semidiurnal [23, 25]. The locks at Rades and Tunis are opened and closed in an alternative way, imposing a one-way water flow going from the east to the west. The average water residence time in the lagoon varies from 6.6 to 8.2 days [25]. The total exchange of water volume with the sea via the Canal of Rades is about 2.57 million·m³/day. The water speed of the lagoon is not homogenous. It varies from 65 cm/s, to no more than 5 cm/s, going from the Canal of Rades to the canal of Navigation, leading to the appearance of little stagnation zones in the northwestern part of the lagoon [26] (Figure 2).

The South Lagoon of Tunis has a drainage watershed of 4000 ha where more than 1500 ha are industrial areas (food industries, wholesale, etc.) [23]. Rapid urbanization around the lagoon during the past decade has resulted in a substantial increase in the volume and pollutant load of the storm-water and wastewater flowing into the lagoon. The lagoon receives water from draining the urban area of

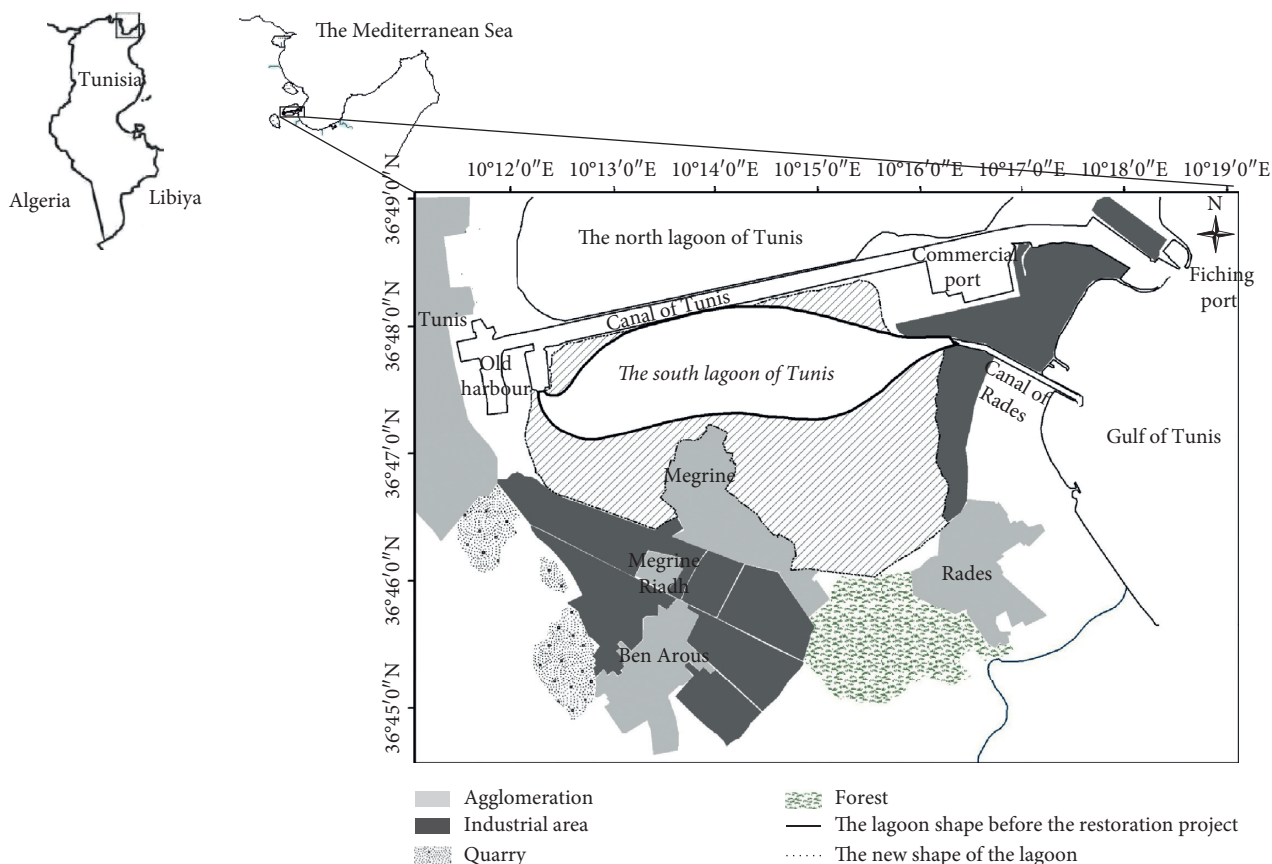


FIGURE 1: Map showing the study area.

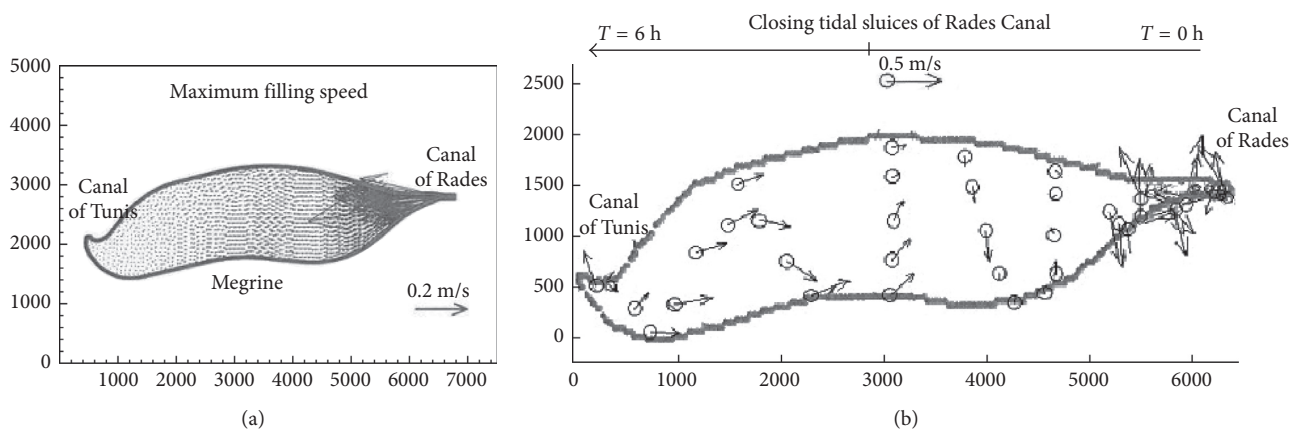


FIGURE 2: Water circulation in the South Lagoon of Tunis: (a) filling speed of the lagoon [25] and (b) the direction of water circulation on the lagoon [26].

Megrine, runoff of newly developed areas after their planning, as well as a channel called the belt channel, which protects the city of Megrine from flooding [27]. Whereas, the industrial and domestic water of Jbel Jloud, Ben Arous, and Megrine, located in the west side of the lagoon, are discharged to the catchment area of the oueds (Oued Essalaas and canal of Ben Arous) and transported to the lagoon. During the rainy season, they are mixed by runoff [27]. It received about $5500 \text{ m}^3/\text{day}$ of untreated industrial wastewater, enriched with nutrients and heavy metals [23].

2.1.1. Sampling and Analysis. A spatiotemporal monitoring of nutrients concentrations was carried out in July 2013 and in February 2014. Samples were taken from 14 sites, which cover most of the surface area (Figure 3). In order to estimate the anthropogenic nutrient intake of the lagoon water, samples collected from manholes dumped into the lagoon, presented in the map (Figure 3) as point and non-point sources, are also taken. On the other hand, other samples were taken from the Canal of Rades in order to see the water quality coming from the Gulf.

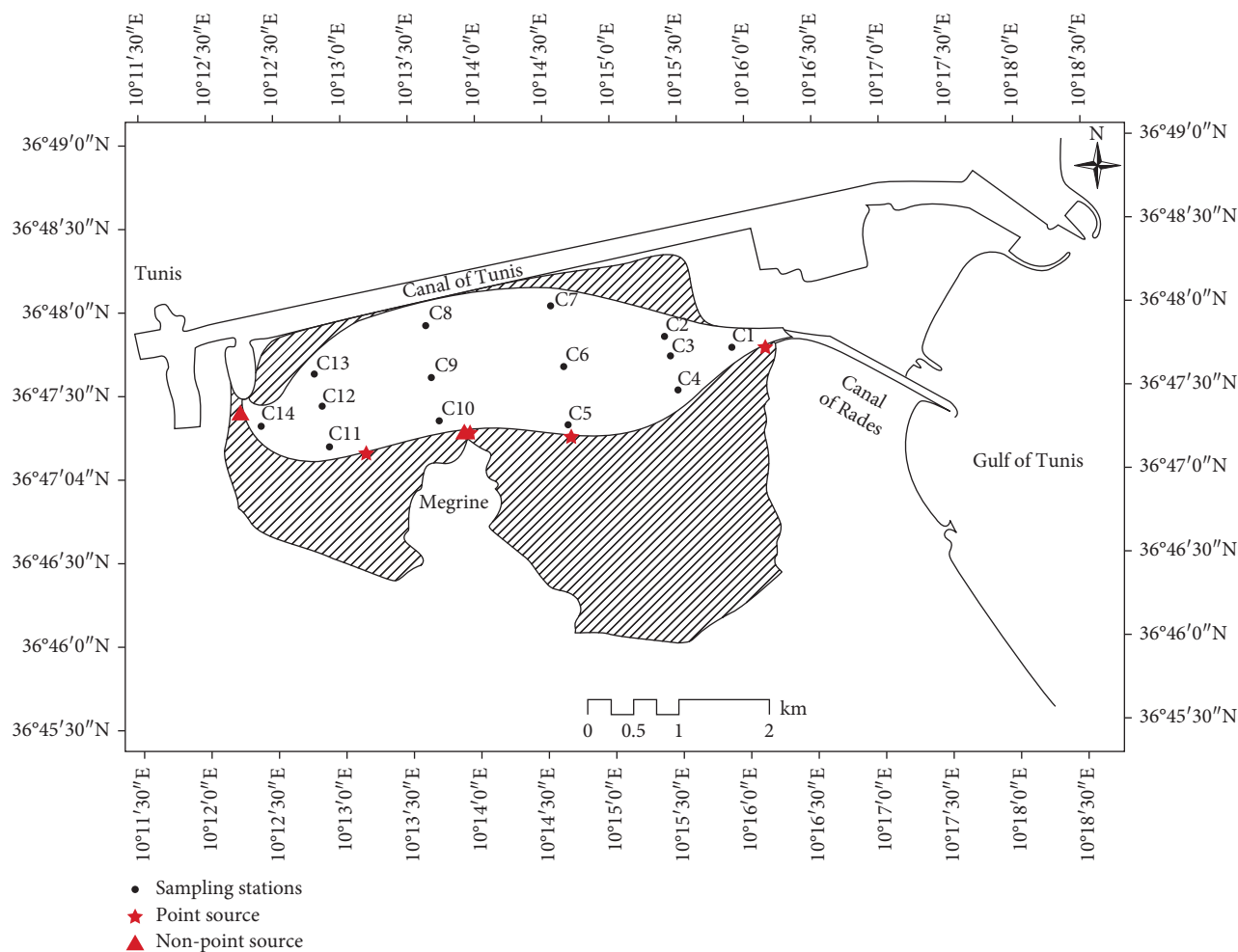


FIGURE 3: Map showing the location of sampling stations.

Temperature, pH, dissolved oxygen content, salinity, and transparency were measured in the field using calibrated portable digital meters. All water samples were filtered through a 45 μm millipore cellulose member and were stored at 4°C in the laboratory until their subsequent analysis. Those membranes are dried and weighed before and after filtration. The difference in weight allows knowing the total dry mass of suspended particulate matter (SPM) [28].

Dissolved inorganic nutrients (nitrate, nitrite, ammonium, and orthophosphate) were measured by standard Rodier [29] colorimetric method using UV-Vis spectrophotometer. Nitrate (NO_3^-) was measured colorimetry on 420 nm. Sulfosalicylic acid forms with nitrate in anhydrous environment and releases in basic environment a nitrosalicylate complex which is yellow. A colorimetric determination of this ion allows to determine the concentration of nitrate ions in a solution [29]. The nitrite (NO_2^-) was determined by complexation with the diazotization of sulfanilamide in and with N (1-naphthyl) ethylene diamine in acidic pH, which gave a purple-colored complex. Nitrite was measured colorimetry on 540 nm [29]. The ammonium ions (NH_4^+) are treated, in an alkaline pH, with sodium hypochlorite and phenol giving indophenol blue coloration. This reaction is catalyzed by

nitroprusside. Ammonium was measured colorimetry on 640 nm [29]. Orthophosphates react in the presence of antimony molybdate to give phosphomolybdic acid compounds that were reduced by ascorbic acid, giving a blue coloration. Ortho-P was measured colorimetry on 720 nm [29].

Turbidity measurements (expressed in Nephelometric Turbidity Unit, NTU) were performed using a HACH 2100P turbidimeter.

The chlorophyll a (chl a) contents were determined using the spectrophotometric method of Lorenzen [30] and following the procedure given by Parsons et al. [31] after 24 h extractions in 90% acetone at -5°C in the dark.

Spatial distribution maps of these water quality parameters were carried out through GIS 9.3.

2.2. Statistical Analysis. Multivariate statistical analysis of the experimental data has been performed using the XLstat. Two multivariate statistical techniques were used: the hierarchical cluster analysis (HCA) and the principal component analysis (PCA). In addition, Pearson's correlation analysis was, also, performed. These methods are considered as good tools to classify water samples according to their geochemical characteristics [32].

2.3. Trophic State Assessment

2.3.1. Trophic Index (TRIX). The TRIX proposed by Vollenweider et al. [21], which can be considered as an adaptation of Carlson's TSI to transitional waters, is used in order to assess the trophic state of the lagoon. The TRIX is frequently used to characterize the ecosystem trophic status. The TRIX has been applied to many ecosystems of coastal marine waters, such as the Tyrrhenian [33] and the Caspian Seas [34], Bizerte Lagoon in Tunisia [35], and the Greek coastal lagoon [36] are among others.

It is a mathematical tool derived from the combination of dissolved inorganic nitrogen, inorganic phosphorus, dissolved oxygen, and chlorophyll *a*. The TRIX analytical expression is given as follows:

$$\text{TRIX} = \frac{[\log_{10}(\text{DIN} * \text{DIP} * |\text{D\%DO}| * \text{chl}(a)) + a]}{b}, \quad (1)$$

where $\text{chl}(a)$ represents the chlorophyll *a* concentration (in $\mu\text{g/L}$), while $|\text{D\%DO}|$ represents the absolute value percentage deviation of the oxygen concentration from saturation conditions (in %). DIN and DIP represent dissolved inorganic nitrogen (in $\mu\text{g/L}$) and dissolved inorganic phosphorus (in $\mu\text{g/L}$), respectively. The parameters $a=1.5$ and $b=1.2$ are scale coefficients used to fix the index lower limit and the scale ranges from 0 to 10 [33].

According to Vollenweider et al. [21], the scores are as follows:

- (i) $\text{TRIX} < 4$ indicates high state of water quality with low eutrophication.
- (ii) $4 < \text{TRIX} < 5$ indicates good state of water quality with medium eutrophication.
- (iii) $5 < \text{TRIX} < 6$ indicates bad state of water quality with high eutrophication.
- (iv) $6 < \text{TRIX}$ indicates poor state of water quality with high eutrophication levels.

3. Results and Discussion

Descriptive statistics for the minimum, maximum, and average concentrations for each variable at each sampling period are reported in Table 1.

3.1. Physicochemical Parameters. The collected water from the Southern lagoon of Tunis were characterized by a temperature ranging between 28.8 and 30°C and between 15.1 and 17.5°C, respectively, in July 2013 and February 2014, with salinity values that range between 48.3 to 49.1‰ and 47.5 to 48.5‰, respectively, in summer and in hibernal seasons (Table 1). These parameters undergo wide seasonal variations.

pH values vary from 8.48 to 8.95 in July and from 8.5 to 8.94 in February.

These parameters show a progressive increase in the water flow direction, going from the east to the west (Figure 4). This variation is supported by evaporation and

by the hydrodynamic regime of the lagoon driven by seawater circulation from the inlet gates to the outlet ones from the east to the west.

Dissolved oxygen values in the lagoon, varied between 2.9 and 4.4 mg/L (51.4 and 75.6% of saturation) in July and between 6.5 and 11 mg/L (86.5 and 148.3% saturation) in February. Dissolved oxygen in aquatic ecosystems is the function of many physicochemical parameters, which govern their solubility. Obviously, oxygen solubility increases as salinity and temperature decrease, which could be the reason of the low DO concentration in summer.

The important biological processes associated with oxygen distribution are photosynthesis, respiration, and decomposition [37]. In the South Lagoon of Tunis, the lowest values of DO are measured in July mainly due to the high rate of bacterial degradation of organic matter and the highest values of the algae population presented during this season. In contrast, the lagoon water is well oxygenated and even oversaturated in February due to wind agitation especially in low depth as well as the decrease of biomass production.

The compilation of the distribution maps of dissolved oxygen contents (Figure 5) with the algal distribution of the lagoon (Figure 6) shows that the most oxygenated water is in the west side of the lagoon, where the water depth is low and rich in algae.

SPM ranges from 0.025 to 0.043 mg/L and from 0.018 to 0.032 mg/L, respectively, in July 2013 and February 2014. The highest values could be attributed to the low depth of the water where the particle resuspension is much easier and to the decomposition/release of organic particles from the macrophytes in summer. The turbidity varies between 8 and 20 (100 NTU) in July, due to the high rate of chlorophyll *a*. In the other hand, the lagoon is almost transparent, and the turbidity ranges between 1 and 9 (100 NTU) in February. The Secchi disk transparency values vary between 1.3 and 2 m in July and between 1.5 and 1.8 m in February which indicating a generally moderate water visibility. The lowest values of transparency were recorded in July due to the growth of chlorophyll *a*.

3.2. Nutrients. For the lagoon water samples, the nitrogen inorganic compounds are mainly composed by nitrates (90%).

Nitrite contents range between 0.08 and 0.09 mg/L in July and between 0.53 and 0.76 mg/L in February. Ammonium varies between 0.071 and 0.117 mg/L in July and from 0.042 to 0.052 mg/L in February. Nitrate contents vary between 8.06 and 13 mg/L in July, and from 2.08 to 15.58 mg/L in February (Table 1). These values are close to those found by Saccon et al. in the Marano lagoon (Italy) [39]. As shown in Table 1, the lagoon water is richer in nutrient compared to seawater.

Rapid mobilization resulted in low values of ammonium and nitrite. In fact, these elements are transitory and unstable in water, having very weak dissolved oxygen concentrations [40]. Ammonium may differ from steady-state conditions reflecting the balance between production through mineralization of organic matter [41], nitrification/denitrification,

TABLE 1: Statistical summary of physicochemical parameters and nutrients in South Lagoon of Tunis.

	Depth (m)	T (°C)	pH	DO (mg/L)	Salinity (‰)	Conductivity (S/cm)	SPM (mg/L)	NH ₄ ⁺ (mg/L)	NO ₂ ⁻ (mg/L)	NO ₃ ⁻ (mg/L)	Ortho-P (mg/L)	Chl-a (µg/L)	Pheo (µg/L)	Turbidity (100 NTU)	Transparency (m)
July campaign	Minimum	28.8	8.48	3	48.3	56.8	0.025	0.071	0.079	9.295	2.129	1.108	4.424	8	1.3
	Maximum	30	8.95	4.4	49.1	57.7	0.043	0.117	0.095	14.429	2.409	3.324	8.759	24	2
	Average	29.5	8.72	3.5	48.6	57.1	0.034	0.088	0.087	11.593	2.275	2.137	6.230	15.7	1.5
February campaign	Minimum	15.1	8.5	6.2	47.5	55.9	0.019	0.043	0.550	3.070	1.601	0.997	0.598	1	1.5
	Maximum	17.5	8.94	11	48.4	56.9	0.032	0.052	0.901	15.580	2.958	2.659	2.726	9	1.8
	Average	15.9	8.73	8	48.1	56.6	0.027	0.046	0.643	9.423	1.790	1.994	1.612	4	1.6
Gulf of Tunis (July)	—	22.7	7.57	6.9	43.5	51.1		0.244	0.11	1.375	0.465				
Nonpoint source	—	24.7	7.55	3.9	6.1	7.12		0.291	0.399	11.063	1.283				
Point sources	—	24.7	7.63	3.9	51.8	51.8		0.018	0.063	11.265	1.243				

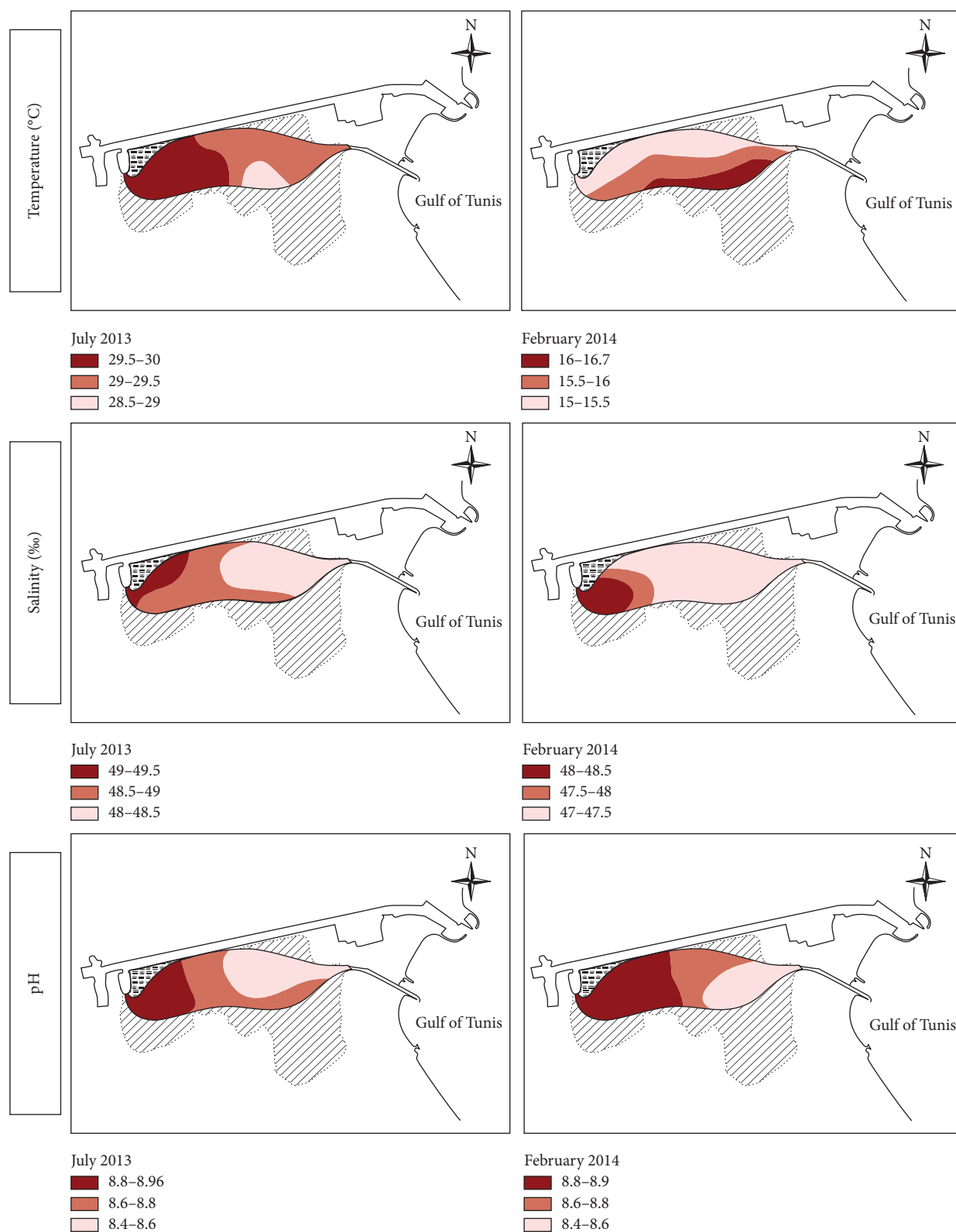


FIGURE 4: Physicochemical distribution maps of the South Lagoon of Tunis.

and consumption by the abundant primary producers living near the sediment-water interface [42].

As for nitrate, the characterization of its origins in the lagoon is much more difficult to achieve because of complex mixing

processes among different water types like seawater, rainwater, and wastewater charges from the catchment area [39]. Generally, nitrate can be originated from airborne (atmospheric), nitrification process, or agricultural (leaching of agricultural land).

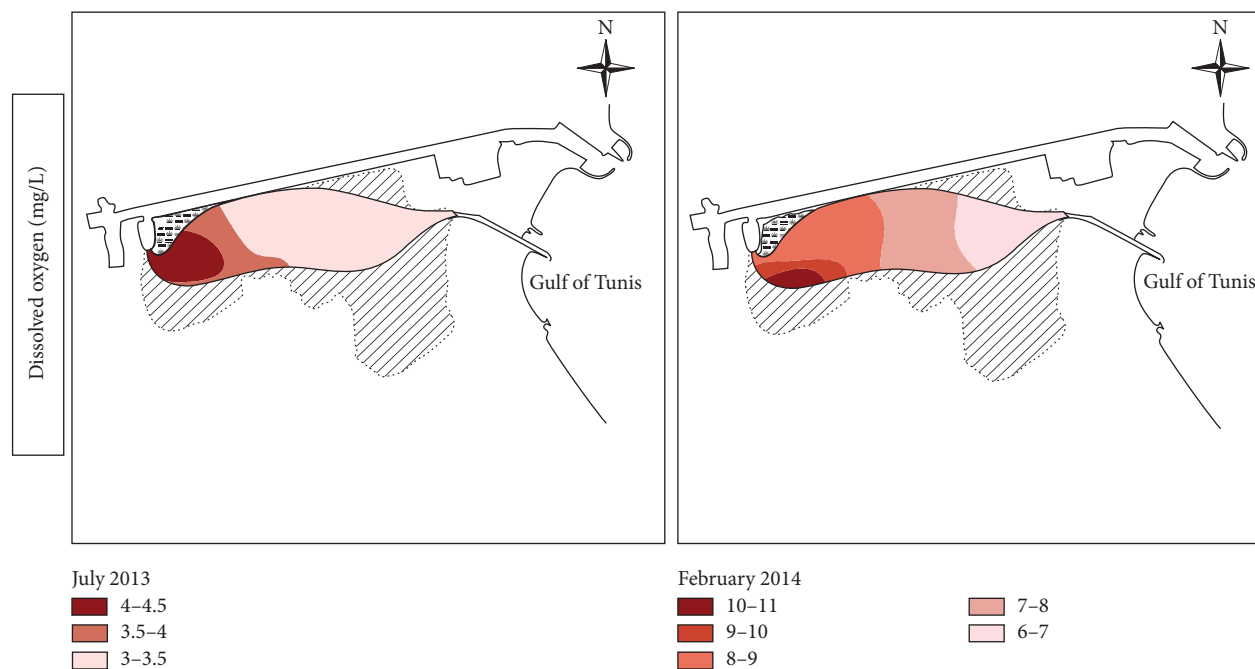


FIGURE 5: Dissolved oxygen distribution map of the South Lagoon of Tunis.

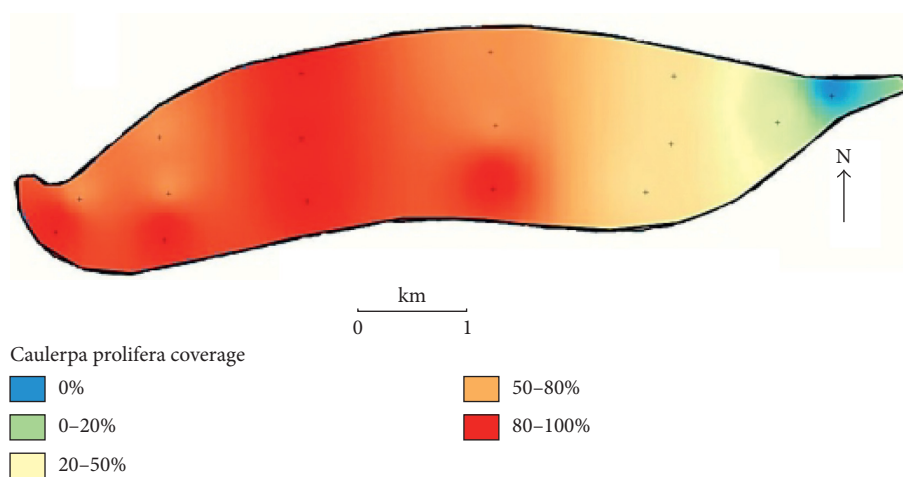


FIGURE 6: The distribution of *Caulerpa prolifera* in the South Lagoon of Tunis in summer 2014 [38].

In our case, the lagoon catchment area is exclusively occupied by urban or industrial zones which mean that the high rate of nitrate intake in the lagoon is not derived from agricultural activities. Therefore, the nitrate is formed in the lagoon by nitrification of NH_4^+ that may enter the lagoon directly, from urban or industrial N-bearing wastewater as anthropogenic sources, or could be produced in situ by remineralization of organic matter.

Spatial variation maps of nitrate contents show that the distributions are influenced by liquid discharges on the south side of the lagoon, showing a positive gradient from south to north. The highest levels are those sampled near the discharge site. As they move away, the contents decrease and become homogenous in the rest of the study area which means the western and eastern parts of the lagoon (Figure 7).

Furthermore, it is important to stress that NH_4^+ and NO_2^- nitrification can start even towards the lagoon and will consequently increase the NO_3^- concentration intake in the sampled water [39, 43].

The orthophosphate contents vary from 1.60 mg/L to 2.4 mg/L in July and from 1.6 mg/L to 2.94 mg/L in February (Table 1). Orthophosphate content variations are caused by primary production uptake and can be affected by various processes like adsorption and phosphate desorption and buffering action of sediments under environmental condition change (temperature and dissolved oxygen) [44, 45].

The cross-plot orthophosphate-total dissolved inorganic nitrogen (DIN) did not show any correlation ($r^2 = 0.13$ for July campaign and $r^2 = 0.40$ for February campaign) for sampled water (Figure 8). In shallow coastal ecosystems such

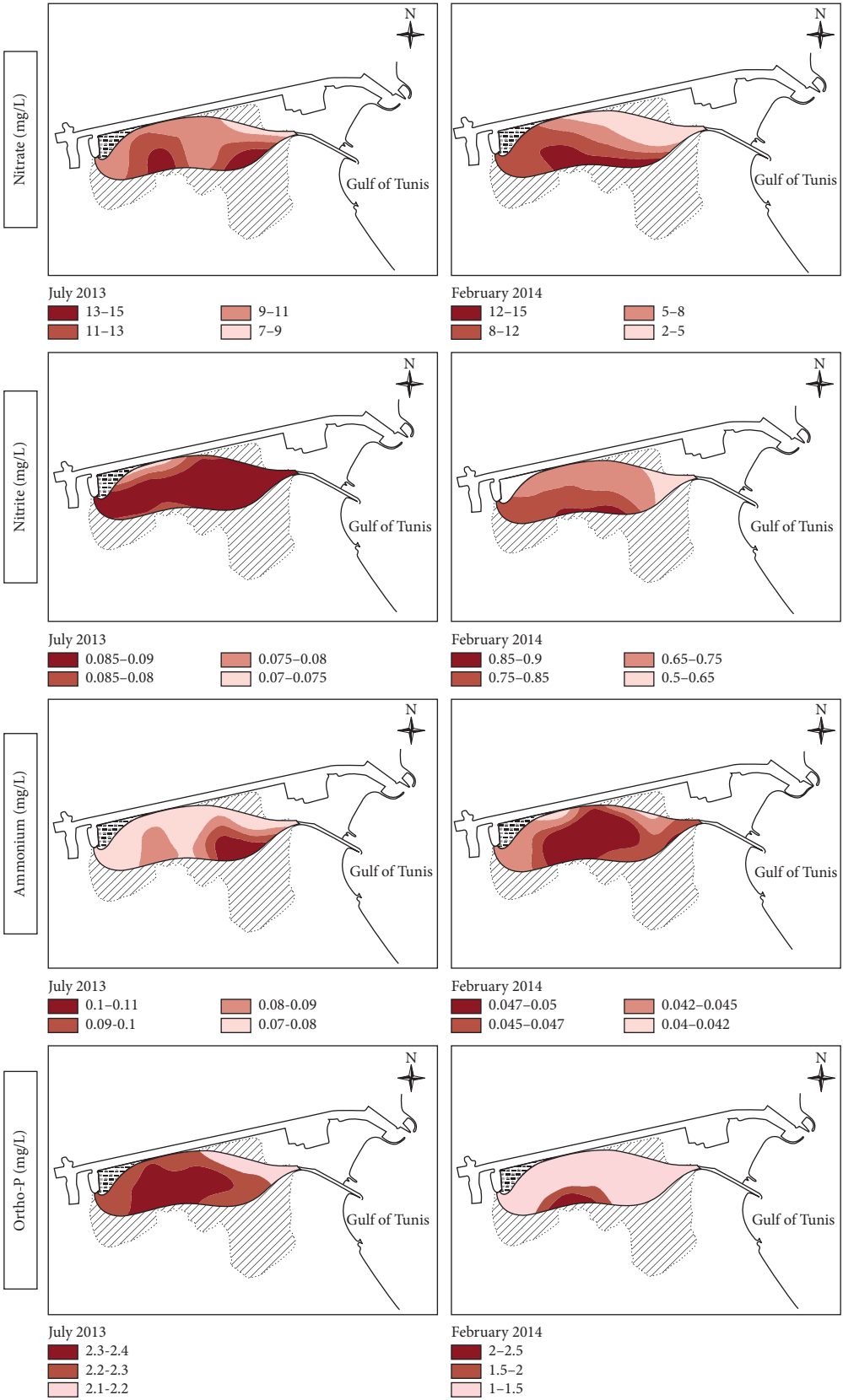


FIGURE 7: Nutrient distribution maps of the South Lagoon of Tunis.

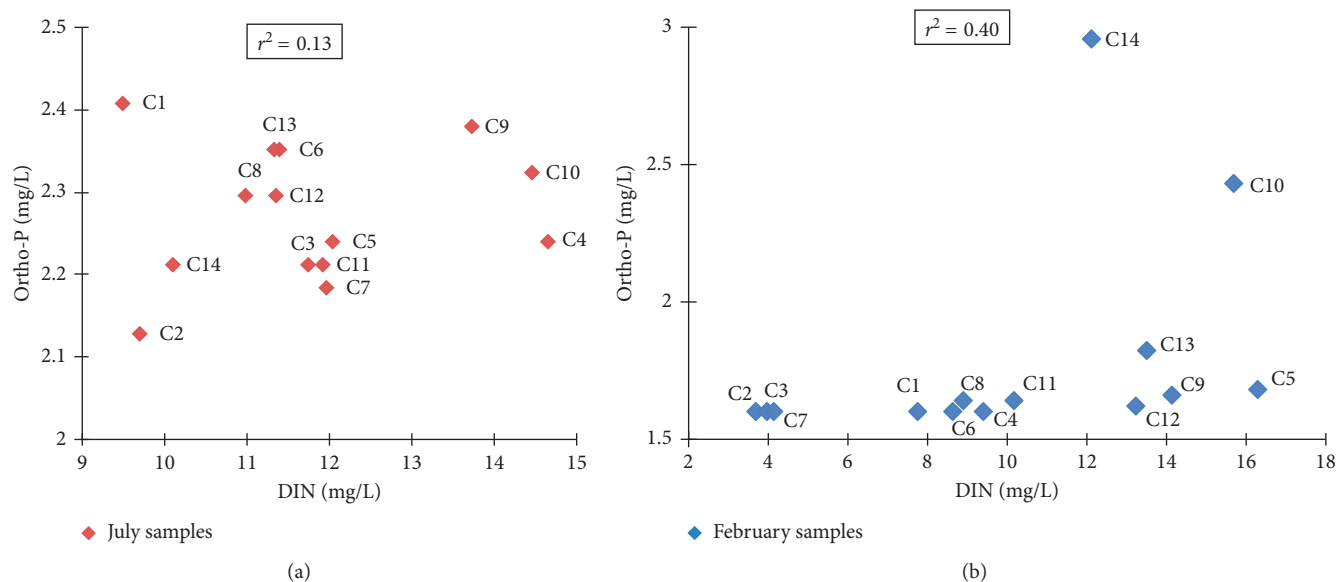


FIGURE 8: Plot of ortho-P by NID.

as the South Lagoon of Tunis, remineralization of the organic matter in the sediment and/or in suspended particles could often be a major source of dissolved inorganic nutrients in the water column [46–48]. Although this study was not designed to investigate the role of sediments as an internal source of nutrients to the water column, their influence in the nutrient's regeneration was apparent. In summer, mineralizing of organic matter at the sediment interface is accelerated, leading to a supplementary nutrient release to the water column [49–52].

Just like nitrate, the spatial distributions of ammonium and ortho-P contents show that the highest levels are recorded in the south side of the lagoon. Nitrite contents are homogeneous in July, whereas a positive gradient is noticed going from the south part to the north part in February. This distribution can be attributed mostly to urban wastewater and runoff (Figure 7).

3.2.1. Ratio NID/Ortho-P. The N/P ratio is often used in the prediction of the limiting nutrient for phytoplankton production. Despite the advances, nutrients limitation in coastal water is still an open question. There is an ongoing debate regarding the choice of the form of phosphorus and nitrogen used for calculating Redfield ratio [53], using the total form or just the inorganic form.

For the present study, in N/P ratio computation, the dissolved inorganic nitrogen (DIN) and orthophosphorus (ortho-P) are used [54–56]. In algal cells, the approximate ratio of nitrogen to phosphorus mass (Redfield ratio) is 7.2 : 1 (grams) or 16 : 1 (atoms).

Figure 9 shows the calculated molar ratios of DIN/ortho-P for all data. It varies between 3 and 4.9 for the July campaign and between 1.7 and 7.3 for the February campaign. The low N:P molar ratios (less than 16:1) suggest N-limitation in the sampled water. Nonetheless the N-limitation of coastal ecosystems (lagoon) might not

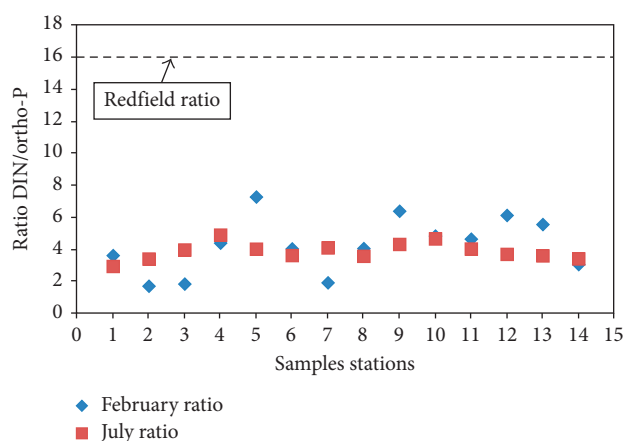


FIGURE 9: Ratio N/P for the South Lagoon of Tunis water samples.

necessarily be applied, especially when they are under high anthropic pressure [57].

3.3. Chlorophyll a. The chlorophyll a contents range from 1.11 to 3.32 $\mu\text{g/L}$ in July and from 0.99 to 2.66 $\mu\text{g/L}$ in February. Pheopigment contents vary from 4.42 to 8.76 $\mu\text{g/L}$ and from 0.6 to 2.72 $\mu\text{g/L}$, respectively, in July and February. Pheopigment contents are higher than the chlorophyll a in July, which coincide with the end of the growth cycle of macroalgae and seagrass and their decomposition.

The spatial distribution of pheopigments in the same period is almost the opposite distribution of the chlorophyll a. The highest concentrations of chl a are in the west and the southeastern part of the lagoon where the depth varies from 1.8 to 2.4 m. However, the lowest concentrations are in the East side of the lagoon where the water depth varies from 3.8 to 5.1 m (Figure 10). Positive gradient is established with the incoming water from the east side of the lagoon to the west side.

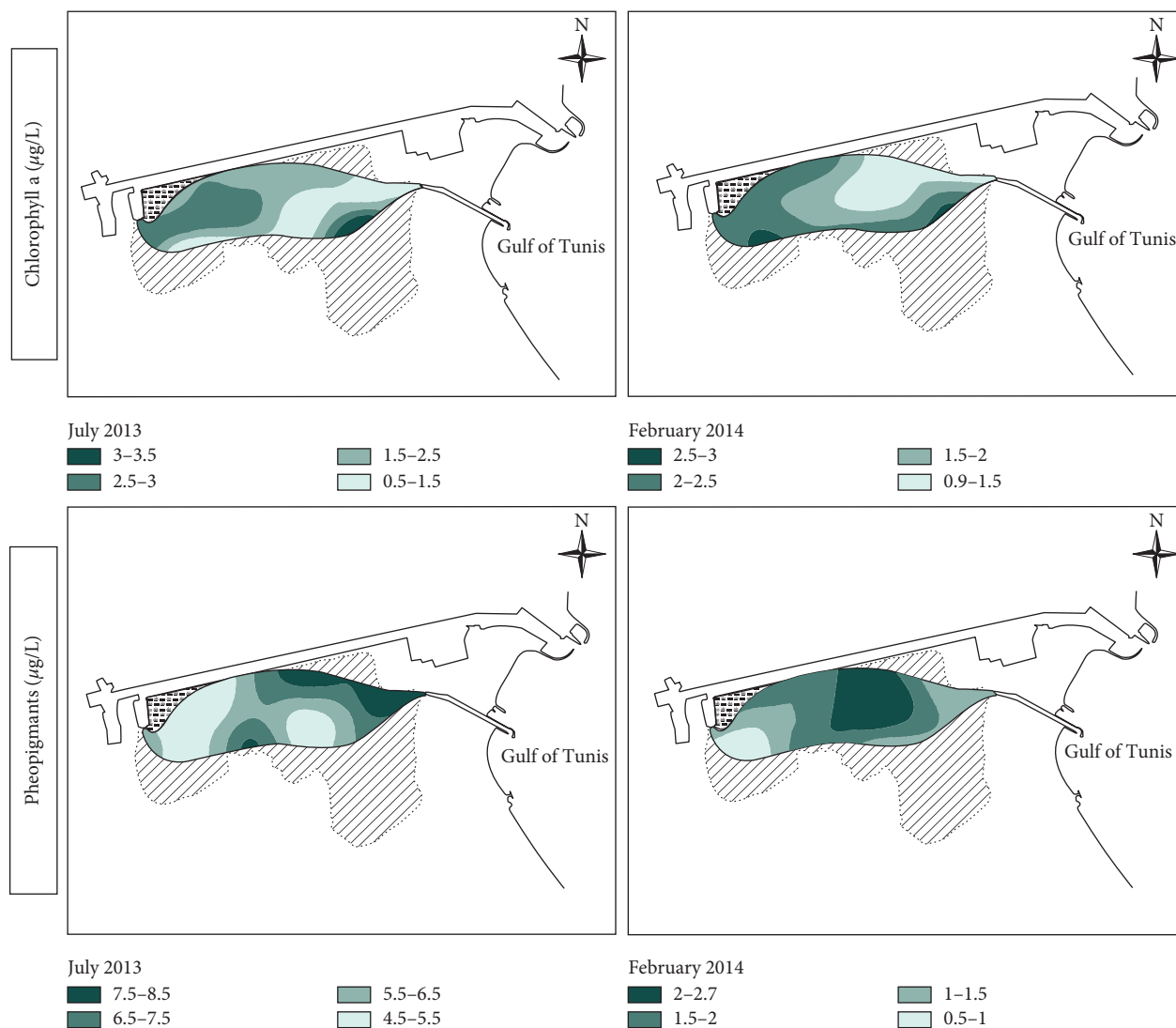


FIGURE 10: Spatial distribution maps of chlorophyll a ($\mu\text{g/L}$) and pheopigments ($\mu\text{g/L}$) in surface water of the South Lagoon of Tunis.

3.4. Statistic Study. In order to classify the trends of this coastal lagoon, a detection of significant relationships between indices (differences of environmental parameters and nutrients) and samples was tested.

3.4.1. Correlation Matrix. Pearson's correlation coefficient matrix of the physicochemical parameters, nutrients, chlorophyll a, and pheopigment contents was calculated (Table 2). The following results are drawn:

- Significant negative correlation between ammonium and dissolved oxygen contents ($r^2 = -0.87$), which conclude that ammonium is controlled by ammonification.
- Negative correlation between nitrite and ammonium ($r^2 = -0.87$) and positive correlation between dissolved oxygen and nitrite ($r^2 = 0.79$), which indicates a continuous process of nitrosation.
- Nitrate does not show any correlation with nitrite, ammonium, and dissolved oxygen that can be

explained by an external input of nitrate in the lagoon water from urban/industrial water discharge.

- Ortho-P concentrations were positively correlated with temperature ($r^2 = 0.64$), indicating phosphate release from sediments of the lagoon.
- Significant positive correlation between pheopigments and temperature ($r^2 = 0.91$) and negative correlation with dissolved oxygen ($r^2 = -0.88$) show a high rate of pheopigments in July matching the end of algal growth cycle. Those parameters correspond to the eutrophic condition in the dry season.
- Turbidity presents a positive correlation with temperature ($r^2 = 0.85$), SPM ($r^2 = 0.85$), and pheopigments ($r^2 = 0.78$). These parameters correspond to the eutrophic condition in the dry season. On the contrary, turbidity and transparency have an antagonist behavior ($r^2 = -0.45$) and high value of turbidity causes low visibility of lagoon water.

TABLE 2: Pearson correlation matrix of water quality variables of the South Lagoon of Tunis.

Variables	T°C	pH	O ₂	Salinity	SPM	NH ₄ ⁺	NO ₂ ⁻	NO ₃ ⁻	Ortho-P	Chl a	Pheo	Turbidity	Transparency
T°C	1	-0.04	-0.93	0.74	0.68	0.90	-0.97	0.31	0.64	0.12	0.91	0.85	-0.39
pH		1	0.32	0.32	0.02	-0.18	-0.02	0.41	0.27	0.20	-0.09	0.12	-0.09
O ₂			1	-0.57	-0.65	-0.87	0.89	-0.15	-0.54	-0.06	-0.88	-0.78	0.35
Salinity				1	0.50	0.64	-0.72	0.41	0.66	0.10	0.72	0.58	-0.42
SPM					1	0.49	-0.60	0.04	0.23	0.11	0.63	0.85	-0.51
NH ₄ ⁺						1	-0.87	0.31	0.57	0.07	0.87	0.70	-0.37
NO ₂ ⁻							1	-0.38	-0.65	-0.14	-0.87	-0.79	0.34
NO ₃ ⁻								1	0.48	0.12	0.31	0.23	0.07
Ortho-P									1	0.07	0.61	0.46	-0.07
Chl a										1	0.20	0.15	0.12
Pheo											1	0.78	-0.31
Turbidity												1	-0.45
Transparency													1

3.4.2. *Principal Components Analysis: PCA.* To evaluate the temporal and spatial variations of the studied parameters (physicochemical parameters and nutrients) in the Southern lagoon of Tunis, a principal component analysis (PCA) was applied.

The used variables are temperature, pH, dissolved oxygen content, salinity, suspended particulate matter (SPM), turbidity, transparency, NH₄⁺, NO₂⁻, NO₃⁻, ortho-P, chlorophyll a (chl a), and pheopigments (pheog).

Three components were extracted, which explained 75.57% of the total variance. The first factor (PC1) accounting for 54.65% of the total variance is strongly correlated primarily with dissolved oxygen (0.91) and nitrite (0.95) on the positive side and negatively correlated with water temperature (-0.99) and with ammonium (-0.89) and pheopigments (-0.93), showing the inverse relationship between temperature and dissolved oxygen and between nitrite and ammonium (Table 3). It is also defined by less important salinity and SPM. HPO₄ is also correlated with PC1 (Table 3). Therefore, PC1 mainly represents the seawater marine influence from the gulf of Tunis, which has an important effect on the lagoon with continuous flushing, buffering, and dilution effect.

PC2 explained that 13.97% of the total variance was principally represented by pH and nitrate (Table 3). Additional 9.52% of the total variance was explained in PC3 and was represented by transparency.

The correlation circles of both components (PC1 and PC2) (Figure 11) show that chlorophyll a and nitrate have the same behavior explaining that the nutrient intake stimulates algae growth. Then, pheopigments-temperature-ammonium-SPM and turbidity have the same behavior, indicating the eutrophic state in the July campaign.

The loading plot of the two factors (PC1/PC2) (Figure 11) shows the presence of two different groups:

- (i) Group I included the July samples. They are dominated by ammonium, turbidity, SPM, pheopigments, temperature, and salinity.
- (ii) Group II included the February samples, at which the dominance of dissolved oxygen is determined.

PCA analysis shows a clear seasonal variation. Indeed, February samples are well oxygenated and the July samples present eutrophicated characters.

TABLE 3: Results of principal component analysis are shown as correlation values between the variables and the principal components for the first three principal components (PC1–PC3).

	PC1	PC2	PC3
T°C	-0.99	-0.07	0.08
pH	-0.04	0.81	-0.51
O ₂	0.91	0.31	-0.21
Salinity	-0.79	0.30	-0.16
SPM	-0.72	-0.26	-0.43
NH ₄ ⁺	-0.89	-0.13	0.23
NO ₂ ⁻	0.95	-0.02	-0.12
NO ₃ ⁻	-0.37	0.71	0.18
Ortho-P	-0.68	0.44	0.25
Chl a	-0.14	0.31	-0.05
Pheo	-0.93	-0.06	0.16
Turbidity	-0.88	-0.08	-0.24
Transparency	0.45	0.27	0.68

3.4.3. *Cluster Analysis.* Hierarchical clustering based on the Euclidean distances as similarity coefficient allows the relationship investigation between the observations of the variables of a dataset, in order to recognize the existence of groups. It is applied to detect spatial similarity for sampling site grouping. In our study, 3 clusters that present similar characteristic features are identified (Figure 12):

- (i) *Cluster I* is represented by samples taken from the west side of the lagoon in the July campaign (S4, S8, S9, S11, S12, and S14).
- (ii) *Cluster II* concerns the July samples taken in the east side of the lagoon (S1, S2, S3, S5, S6, S7, S10, and S13).
- (iii) *Cluster III* characterizes the samples collected in the February campaign, that can be subsided in two subclusters:
 - (i) Samples located in the eastern part of the lagoon (S1, S2, S3, S6, and S7).
 - (ii) Samples collected in the western part of the lagoon (S4, S5, S8, S9, S10, S11, S12, S13, and S14).

This classification allow us to divide the lagoon in two parts according to the physicochemical parameters: the eastern part under the influence of seawater coming from the gulf characterized by the lowest levels of temperature, pH,

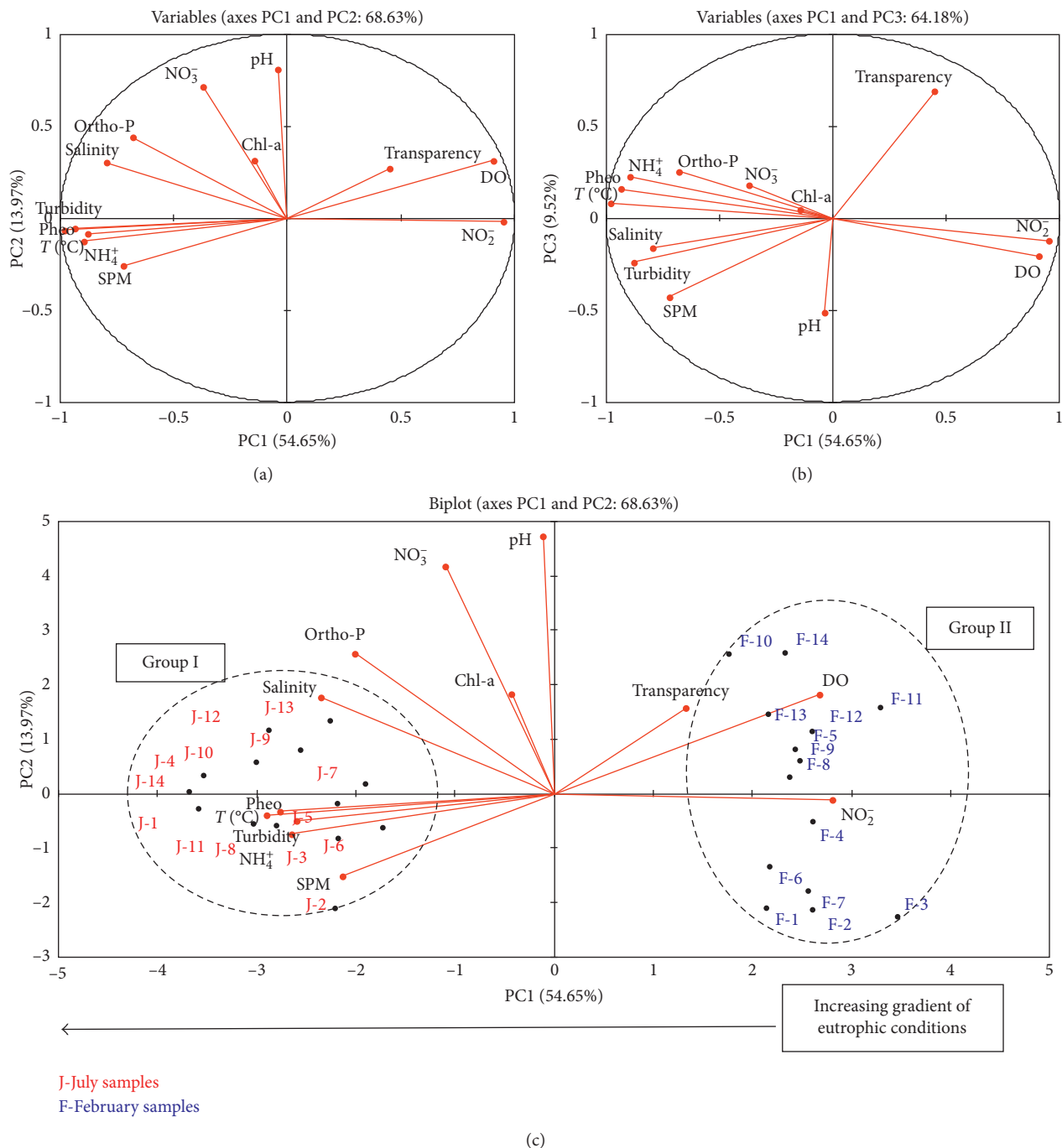


FIGURE 11: Circle of correlation on (PC1 and PC2) and (PC1 and PC3) and spatial distribution of variables and individuals in the axes system PC1 and PC2.

salinity, and dissolved oxygen contents and the western part with the highest levels of these parameters.

Water coming from the Canal of Rades exerts a continuous flushing on the lagoon. However, this dilution effect is limited in the east side of the lagoon. To road the outlet gate (on the west) the lagoon water are enriched.

3.5. Trophic State Assessment. In these last years, the concern of managers and scientists has grown and

different classifications of the trophic state of coastal water based on nutrients and oxygen thresholds have been settled [58–60].

The morphology of the South Lagoon of Tunis has totally changed during the last decades (before and after the restoration project). For this propose, a comparative analysis, evaluating the restoration project impact on physico-chemical parameters and the nutrient contents of the lagoon, seems to be extremely interesting to check the good functioning of the restored ecosystem. In order to track the

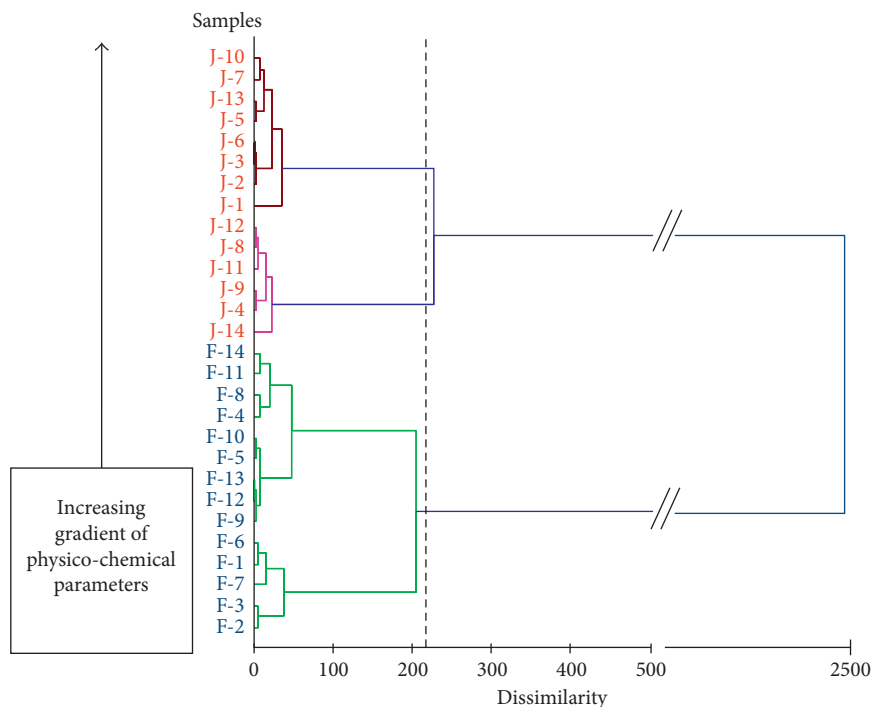


FIGURE 12: Dendrogram for the South Lagoon of Tunis samples.

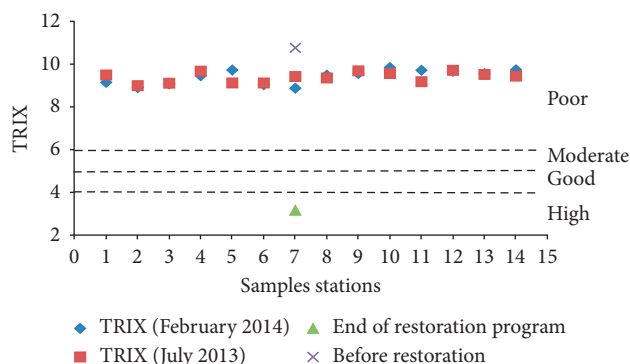


FIGURE 13: Variation of TRIX index [21] for the South Lagoon of Tunis.

evolution of the trophic conditions in the South Lagoon of Tunis, the TRIX [21] was selected.

Figure 13 shows the water trophic status in the South Lagoon of Tunis before, during, and after the restoration work. Before restoration, Ben Souissi [22] showed that nitrates/phosphorus and chl a rates reached high levels in the South Lagoon of Tunis. The lagoon water quality was categorized as “poor” according to TRIX index calculated from the mean monthly values. The best trophic state was registered during the restoration work; the lagoon was categorized as “high”. In the present work, the TRIX values ranged from 8.9 to 9.9. Despite the hydrodynamic system improvement in the lagoon, the lagoon water quality was categorized as “poor”.

The trophic status of marine coastal ecosystem assessment is based on measurements of combinations of biotic and abiotic variables [21] as well as the main

elements (e.g., inorganic and organic N and P) and molecules (organic matter, chlorophyll a concentrations) that had been used as indicators of biomass in the water column [61]. However, the increase in the primary production levels is not the only factor controlling the trophic status of a marine ecosystem. There is also transparency, sunshine, and water circulation which are considered as important factors too [62]. For example, increased levels of primary production can also be associated with the accumulation of large amounts of detrital organic materials [63].

During the restoration of the South Lagoon of Tunis, a new hydraulic design was required. The hydrological parameters show an improvement of the physicochemical parameters, due to the newly produced hydrodynamic, permanent seawater exchanges, the water residence time reduction, the lagoon water volume increase, and a continuous flushing.

The engineering work improved the quality but did not fully reach the expected results. The South Lagoon of Tunis still records a poor water quality classification. As shallow marine ecosystems, the arid climate (characterized by a high evaporation rate and temperature) and the continuous intake of nutrients can modify the structure and the biology of the water column at very short time intervals (from minutes to hours). Despite dredging the bottom sediment of the lagoon, the South Lagoon of Tunis is still contaminated by organic matter and records a high rate of nutrients even after management work. These elements may, under precise conditions [64–66], be released and might be diffused from the water-sediment interface.

Moreover, in the anoxic phase that could happen in the lagoon due to the high summer temperature; the exchange

with the sea seems to be ineffective for flushing to decrease nutrient contents.

4. Conclusion

The purpose of this manuscript was to give an assessment of the lagoon status using geochemical and statistical approaches. The results indicate that the spatial distribution of temperature, salinity, and pH is under the control of water circulation in the Southern lagoon of Tunis. They show a slight increase from the east to the west.

The lagoon water shows a high level of nutrients (NO_3^- , NO_2^- , NH_4^+ , and ortho-P) compared to the incoming water from the sea. This is essentially due to natural (nitrification, release from the sediments, and primary production) and anthropogenic (wastewater and runoff) sources.

Based on nutrient contents, DO, and chlorophyll a, TRIX proposed by Vollenweider et al. [21] was calculated. It demonstrated that the lagoon has reached the eutrophic status with a poor water quality index. The trophic status of the South Lagoon of Tunis is worrying and requires a serious intervention.

PCA identified two groups (winter sampling campaign/summer sampling campaign), the eutrophic status of the lagoon water is highlighted in July campaign. The CHA analysis allowed us to divide the lagoon into two parts (east and the west parts) where the west side is richer in nutrients and in physical-chemical parameters compared to the east side.

The current status of the lagoon requires serious interest, given its vulnerability and fragile balance, in order to avoid the failure of the engineering works (if a status-quo is maintained).

Data Availability

The data used to support the findings of this study are available from the corresponding author upon request.

Disclosure

This work was partially presented in international conference days: ICEWE 2017.

Conflicts of Interest

The authors wish to confirm that there are no known conflicts of interest associated with this publication and there has been no significant financial support for this work that could have influenced its outcome.

Acknowledgments

The authors would like to thank Pr. Amina Mabrouk, Faculty of Sciences of Tunis, University Tunis El Manar, for her helpful assistance to improve the manuscript.

References

- [1] S. Cataudella, D. Crosetti, and F. Massa, *Studies and Review No. 95 General Fisheries Commission for the Mediterranean Coastal Lagoons: Sustainable Management and Interactions among Aquaculture, Capture Fisheries and the Environment*, Food and Agriculture Organization of the United Nations, Rome, Italy, 2015.
- [2] J. J. Berzas, L. F. Garcia, R. C. Rodríguez, and M. Alvarez, "Evolution of the water quality of a managed natural wetland: Tablas De Dimiel National Park (Spain)," *Water Research*, vol. 34, no. 12, pp. 3161–3170, 2002.
- [3] G. Cabçadas, M. Nogueira, and M. J. Brogueira, "Nutrient dynamics and productivity in three European estuaries," *Marine Pollution Bulletin*, vol. 38, no. 12, pp. 1092–1096, 1999.
- [4] J. E. Cloern, "Our evolving conceptual model of the coastal eutrophication problem," *Marine Ecology Progress Series*, vol. 210, pp. 235–265, 2001.
- [5] C. B. Lopes, A. I. Lillebø, J. M. Dias, E. Pereira, C. Vale, and A. C. Duarte, "Nutrient dynamics and seasonal succession of phytoplankton assemblages in a Southern European Estuary: Ria de Aveiro, Portugal," *Estuarine, Coastal and Shelf Science*, vol. 71, no. 3–4, pp. 480–490, 2007.
- [6] European Commission, "Directive 91/271/EEC concerning urban waste water treatment," *Official Journal of the European Communities*, pp. 40–52, 1991.
- [7] J. E. Graham, R. L. Peter, S. B. Neville, G.-H. Karen, D. Michael, and M. Peter, "Conservation of natural wilderness values in the Port Davey marine and estuarine protected area, south-western Tasmania," *Aquatic Conservation: Marine and Freshwater Ecosystems*, vol. 20, no. 3, pp. 297–311, 2010.
- [8] J. Zaouali, "Lac de Tunis: 3000 years of engineering and pollution: a bibliographical study with comments," *UNESCO Reports in Marine Science*, vol. 26, pp. 30–47, 1983.
- [9] OCDE, *Eutrophisation des Eaux; Méthodes de Surveillance, D'évaluation et de Lutte*, Organisation for Economic Co-operation and Development, Paris, France, 1982.
- [10] Z. Armi, E. Trabelsi, S. Turki, B. Bejaoui, and N. Ben Maïz, "Seasonal phytoplankton responses to environmental factors in a shallow Mediterranean lagoon," *Journal of Marine Science and Technology*, vol. 15, no. 4, pp. 417–426, 2010.
- [11] J. Vandenbroeck and R. Ben Charrada, "Restoration and development project of South Lake of Tunis and its shores," *Terra et Aqua*, vol. 85, pp. 11–20, 2001.
- [12] S. Souissi, O. Daly Yahia-Kéfi, and M. N. Daly Yahia, "Spatial characterization of nutrient dynamics in the Bay of Tunis (south-Western Mediterranean) using multivariate analyses: consequences for phyto-and zooplankton distribution," *Journal of Plankton Research*, vol. 22, no. 11, pp. 2039–2059, 2000.
- [13] SPLT, STUDI/SOGREAH, *Société d'étude et de Promotion de Tunis Sud (Etude de la marée, Travaux de Restauration du lac sud de Tunis et de ses Berges)*, 1998.
- [14] SERAH, *Etude d'aménagement du lac sud—Rapport Analyse des eaux du lac sud. Etude réalisée pour le compte de la Société d'Etude et de Promotion de Tunis Sud*, 1992.
- [15] M. Abidi, R. Ben Amor, and M. Gueddari, "Geochemistry of nutrients in the South lagoon of Tunis, Northeast of Tunisia, using multivariable methods," in *Proceedings of the 19th International Conference on Energy, Water and Environmental, World Academy of Science, Engineering and Technology, International Scientific Committees, and Editorial Review Boards*, Istanbul, Turkey, July 2017.
- [16] Y. Ouyanga, P. Nkedi-Kizza, Q. T. Wuc, D. C. H. Shinde, and C. H. Huang, "Assessment of seasonal variations in surface water quality," *Water Research*, vol. 40, no. 20, pp. 3800–3810, 2006.
- [17] S. Shrestha and F. Kazama, "Assessment of surface water quality using multivariate statistical techniques: a case study

- of the Fuji river basin, Japan," *Environmental Modelling & Software*, vol. 22, no. 4, pp. 464–475, 2007.
- [18] E. L. Bahri Trabelsi, Z. Armi, N. Trabelsi-Annabi, A. Shili, and N. Ben Maiz, "Water quality variables as indicators in the restoration impact assessment of the north lagoon of Tunis, South Mediterranean," *Journal of Sea Research*, vol. 79, pp. 12–19, 2013.
 - [19] L. Ignatiadis, M. Karydis, and P. Vounatsou, "A possible method for evaluating oligotrophy and eutrophication based on nutrient concentration scales," *Marine Pollution Bulletin*, vol. 24, no. 5, pp. 238–243, 1992.
 - [20] R. A. Vollenweider, R. Marchetti, and R. Viviani, "Marine coastal eutrophication," in *Proceedings of an International Conference, Bologna, Italy*, p. 1310, March 1990.
 - [21] R. A. Vollenweider, F. Giovanardi, G. Montanari, and A. Rinaldi, "Characterization of the trophic conditions of marine coastal waters with special reference to the NW Adriatic Sea: proposal for a trophic scale, turbidity and a generalized water quality index," *Environmetrics*, vol. 9, no. 3, pp. 329–357, 1998.
 - [22] J. Ben Souissi, *Impact de la Pollution sur les Communautés Macro benthiques du Lac Sud de Tunis avant sa Restauration Environnementale*, Ph.D. thesis, Faculté des sciences de Tunis, Tunis, Tunisia, 2002.
 - [23] Z. Jouini, R. Ben Charrada, and M. Moussa, "Caractéristiques du Lac Sud de Tunis après sa restauration," *Marine*, vol. 15, no. 1-2, pp. 3–11, 2005.
 - [24] National Institute of Meteorology, INM, *Climate Data Report for the Period 2007–2011*, 2012.
 - [25] Z. Jouini, *Le Fonctionnement Hydrodynamique et Écologique du lac sud de Tunis après les Aménagements*, DEA, ENIT, Springfield, VA, USA, 2003.
 - [26] M. Kochlef, *Contribution à L'étude du Fonctionnement Hydrodynamique du lac Sud Tunis après les Travaux D'aménagement*, DEA, National Agronomy Institute of Tunisia, Carthage University, Tunis, Tunisia, 2003.
 - [27] Département Hydraulique Urbaine (DHU), *Etude de Protection du Grand Tunis contre les inondations—Phase 1—1ère Partie Juin 2006*, Ministère d'Équipement, Département Hydraulique Urbaine (DHU), Rabat, Morocco, 2015.
 - [28] A. Aminot and R. Kérouel, "Dosage automatique des nutriments dans les eaux marines: méthodes en flux continu," in *Méthodes D'analyse en Milieu Marin*, p. 188, Ifremer, Issy-les-Moulineaux, France, 2007.
 - [29] J. Rodier, *L'Analyse de l'eau: Eaux Naturelles, Aux Résiduares, Eau de Mer ; Chimie, Physico-Chimie, Bactériologie, Biologie*, Dunod, Paris, France, 2006.
 - [30] C. J. Lorenzen, "Determination of chlorophyll and pheopigments by spectrophotometric equations," *Limnology and Oceanography*, vol. 12, no. 2, pp. 343–346, 1967.
 - [31] T. R. Parsons, "A manual of chemical and biological methods for seawater analysis. Pergamon, Oxford sized algae and natural seston size fractions," *Marine Ecology Progress Series*, vol. 199, pp. 43–53, 1984.
 - [32] B. Tlili-Zrelli, F. Hamzaoui-Azaza, M. Gueddari, and R. Bouhlila, "Geochemistry and quality assessment of groundwater using graphical and multivariate statistical methods. A case study: Grombalia phreatic aquifer (North-eastern Tunisia)," *Arabian Journal of Geosciences*, vol. 6, no. 9, pp. 3545–3561, 2013.
 - [33] F. Giovanardi and R. A. Vollenweider, "Trophic conditions of marine coastal waters: experience in applying the Trophic Index TRIx to two areas of the Adriatic and Tyrrhenian seas," *Journal of Limnology*, vol. 63, no. 2, pp. 199–218, 2004.
 - [34] M. Shahrban and A. Etemad-Shahidi, "Classification of the Caspian Sea coastal waters based on trophic index and numerical analysis," *Environmental Monitoring and Assessment*, vol. 164, no. 1–4, pp. 349–356, 2010.
 - [35] B. Béjaoui, Z. Armi, E. Ottaviani et al., "Random forest model and TRIx used in combination to assess and diagnose the trophic status of Bizerte lagoon, southern Mediterranean," *Ecological Indicators*, vol. 71, pp. 293–301, 2016.
 - [36] C. Chrysoula, G. Giordani, and E. Papastergiadou, "Assessment of ecological quality of coastal lagoons with a combination of phytobenthic and water quality indices," *Marine Pollution Bulletin*, vol. 86, pp. 411–423, 2014.
 - [37] S. R. Aston, "Nutrients, dissolved gases and general biogeochemistry in estuaries," in *Chemistry and Biogeochemistry of Estuaries*, E. Olausson and I. Cato, Eds., pp. 233–262, John Wiley and Sons, New York, NY, USA, 1980.
 - [38] A. Yahyaoui, *Distribution, Biomass and Meadow Structure of Caulerpa prolifera in the Southern Lagoon of Tunis*, National Agronomy Institute of Tunisia, Carthage University, Tunis, Tunisia, 2014.
 - [39] P. Saccon, A. Leis, A. Marca et al., "Determination of nitrate pollution sources in the Marano lagoon (Italy) by using a combined approach of and isotopic techniques," *Procedia Earth and Planetary Science*, vol. 7, pp. 758–761, 2013.
 - [40] G. Copin-Montégut, *Chemistry of Seawater Oceanographic*, Oceanographic Institute, Kerala, India, 1996.
 - [41] G. Bally, V. Mesnage, J. Deloffre, O. Clarisse, R. Lafite, and J. P. Dupont, "Chemical characterization of porewaters in an intertidal mudflat of the Seine estuary: relationship to erosion-deposition cycles," *Marine Pollution Bulletin*, vol. 49, no. 3, pp. 163–173, 2004.
 - [42] M. Vidal and J. A. Morguí, "Short-term pore water ammonium variability coupled to benthic boundary layer dynamics in Alfacs bay, Spain (Ebro Delta, NW Mediterranean)," *Marine Ecology Progress Series*, vol. 118, pp. 229–236, 1995.
 - [43] P. Saccon, A. Leis, A. Marca et al., "Multi-isotope approach for the identification and characterisation of nitrate pollution sources in the Marano lagoon (Italy) and parts of its catchment area," *Applied Geochemistry*, vol. 34, pp. 75–89, 2013.
 - [44] C. R. Pomeroy, E. E. Smith, and C. M. Grant, "The exchange of phosphate between estuarine water and sediments," *Limnology and Oceanography*, vol. 10, no. 2, pp. 167–172, 1965.
 - [45] H. Jamila, B. Mouldi, and G. Moncef, "Assessment of the water quality of Bizerte lagoon of Tunisia by use of statistical analyses," *Journal of Waste Water Treatment & Analysis*, vol. 7, no. 2, p. 237, 2016.
 - [46] D. Ganguly, S. Patra, P. R. Muduli et al., "Influence of nutrient input on the trophic state of a tropical brackish water lagoon," *Journal of Earth System Science*, vol. 124, no. 5, pp. 1005–1017, 2015.
 - [47] J. F. Lopes, N. Vaz, L. Vaz, J. A. Ferreira, and J. M. Dias, "Assessing the state of the lower level of the trophic web of a temperate lagoon, in situations of light or nutrient stress: a modeling study," *Ecological Modelling*, vol. 313, pp. 59–76, 2015.
 - [48] N. Zaaboub, A. Ounis, M. A. Helali et al., "Phosphorus speciation in sediments and assessment of nutrient exchange at the water-sediment interface in a Mediterranean lagoon: implications for management and restoration," *Ecological Engineering*, vol. 73, pp. 115–125, 2014.
 - [49] A. Sfriso, A. Marcomini, and B. Pavoni, "Relationships between macroalgal biomass and nutrient concentrations in a hypertrophic area of the Venice lagoon," *Marine Environmental Research*, vol. 22, no. 4, pp. 297–312, 1987.

- [50] K. Reddy, M. M. Fisher, H. Pant, P. Inglett, and J. R. White, *Indian River Lagoon Hydrodynamics and Water Quality Model: Nutrient Storage and Transformations in Sediments. Final Report*, Florida Department of Environmental Regulation, Gainesville, FL, USA, 2001.
- [51] A. C. Tyler, K. J. McGlathery, and I. C. Anderson, "Macroalgae mediation of dissolved organic nitrogen fluxes in a temperate coastal lagoon," *Estuarine, Coastal and Shelf Science*, vol. 53, no. 2, pp. 155–168, 2001.
- [52] C. Gilbert, C. Sigua, and W. A. Tweedale, "Watershed scale assessment of nitrogen and phosphorus loadings in the Indian River lagoon basin, Florida," *Journal of Environmental Management*, vol. 67, no. 4, pp. 363–372, 2003.
- [53] A. C. Redfield, "The biological control of chemical factors in the environment," *American Scientist*, vol. 46, pp. 205–222, 1958.
- [54] C. L. Schelske, M. F. Coveney, F. J. Aldridge, W. F. Kenney, and J. E. Cable, "Wind or nutrients: historic development of hypereutrophy in Lake Apopka, Florida. Limnology and lake management," *Archiv für Hydrobiologie—Advances in Limnology*, vol. 55, pp. 543–563, 2000.
- [55] W. K. Dodds, "Misuse of inorganic N and soluble reactive P concentrations to indicate nutrient status of surface waters," *Journal of the North American Benthological Society*, vol. 22, no. 2, pp. 171–181, 2003.
- [56] G. D. Gikas, T. Giannakopoulou, and V. Tsihrintzis, "Water quality trends in a lagoon impacted by non-point source pollution after implementation of protective measures," *Hydrobiologia*, vol. 563, no. 1, pp. 385–406, 2006.
- [57] M. Cañedo-Argüelles and M. Rieradevall, "Disturbance caused by freshwater releases of different magnitude on the aquatic macro invertebrate communities of two coastal lagoons," *Estuarine, Coastal and Shelf Science*, vol. 88, no. 2, pp. 190–198, 2010.
- [58] M. A. Best, A. W. Wither, and S. Coates, "Dissolved oxygen as a physico-chemical supporting element in the water framework directive," *Marine Pollution Bulletin*, vol. 55, no. 1–6, pp. 53–64, 2007.
- [59] M. Devlin, S. Painting, and M. Best, "Setting nutrient thresholds to support an ecological assessment based on nutrient enrichment, potential primary production and undesirable disturbance," *Marine Pollution Bulletin*, vol. 55, no. 1–6, pp. 65–73, 2007.
- [60] European Environmental Agency, *Nutrients in Transitional, Coastal and Marine Waters*, Office for official publications of the European Communities, Luxembourg, 2009.
- [61] S. Coelho, S. Gamito, and A. Pérez-Ruzafa, "Trophic state of Foz de Almargem coastal lagoon (Algarve, South Portugal) based on the water quality and the phytoplankton community," *Estuarine, Coastal and Shelf Science*, vol. 71, no. 1–2, pp. 218–231, 2007.
- [62] H. K. Lotze, H. S. Lenihan, B. J. Bourque et al., "Depletion, degradation, and recovery potential of estuaries and coastal seas," *Science*, vol. 312, no. 5781, pp. 1806–1809, 2006.
- [63] A. Pusceddu, A. Dell'Anno, M. Fabiano, and R. Danovaro, "Quantity and bioavailability of sediment organic matter as signatures of benthic trophic status," *Marine Ecology Progress Series*, vol. 375, pp. 41–52, 2009.
- [64] M. M. Alaoui and L. Aleya, "Assessment of the eutrophication of Al Massira reservoir (Morocco) by means of a survey of the biogeochemical balance of phosphorus," *Hydrobiologia*, vol. 297, no. 1, pp. 75–82, 1995.
- [65] F. Andrieux-Loyer, X. Philippon, G. Bally, R. Kérouel, A. Youenou, and J. Le Grand, "Phosphorus dynamics and bioavailability in sediments of the Penzé Estuary (NW France): in relation to annual P-fluxes and occurrences of *Alexandrium Minutum*," *Biogeochemistry*, vol. 88, no. 3, pp. 213–231, 2008.
- [66] M. A. Helali, N. Zaaboub, W. Oueslati, A. Ayed, and L. Aleya, "Nutrient exchange and oxygen demand at the sediment-water interface during dry and wet seasons off the Medjerda River Delta (Tunis Gulf, Tunisia)," *Environmental Earth Sciences*, vol. 75, no. 1, p. 25, 2016.

Research Article

Removal of Colored Organic Pollutants from Wastewaters by Magnetite/Carbon Nanocomposites: Single and Binary Systems

Simona Gabriela Muntean ¹, Maria Andreea Nistor,¹ Eliza Muntean ²,
Anamaria Todea,² Robert Ianoș,² and Cornelia Păcurariu²

¹Institute of Chemistry Timișoara of Romanian Academy, 24 Mihai Viteazul Str., 300223 Timișoara, Romania

²Faculty of Industrial Chemistry and Environmental Engineering, Politehnica University of Timișoara, 6 Pirvan Blv., 300223 Timișoara, Romania

Correspondence should be addressed to Simona Gabriela Muntean; sgmuntean@yahoo.com and Eliza Muntean; eliza.muntean@yahoo.ro

Received 13 January 2018; Accepted 19 March 2018; Published 20 May 2018

Academic Editor: Alina Barbulescu

Copyright © 2018 Simona Gabriela Muntean et al. This is an open access article distributed under the Creative Commons Attribution License, which permits unrestricted use, distribution, and reproduction in any medium, provided the original work is properly cited.

This work develops a methodology for selective removal of industrial dyes from wastewaters using adsorption technology based on magnetic adsorbents. The magnetic nanoparticles embedded within a matrix of activated carbon were tested as adsorbents for removal of industrial dyes from aqueous solutions. The effects of four independent variables, solution pH, initial concentration of pollutant, adsorbent dose, contact time, and their interactions on the adsorption capacity of the nanocomposite were investigated in order to optimize the process. The removal efficiency of pollutants depends on solution pH and increases with increasing the carbon content, with initial concentration of the pollutants, the temperature, and the dose of magnetite/carbon nanocomposites. Pseudo-second-order kinetic model was fitted to the kinetic data, and adsorption isotherm analysis and thermodynamics were used to elucidate the adsorption mechanism. The maximum adsorption capacities were 223.82 mg g⁻¹ for Nylosan Blue, 114.68 mg g⁻¹ for Chromazurol S, and 286.91 mg g⁻¹ for Basic Red 2. The regeneration and reuse of the sorbent were evaluated in seven adsorption/desorption cycles. The optimum conditions obtained for individual adsorption were selected as starting conditions for simultaneous adsorption of dyes. In binary systems, in normal conditions, selectivity decreases in the order: Red Basic 2 > Nylosan Blue > Chromazurol S.

1. Introduction

Progress of various industries from the past decade led to a drastic increase in industrial effluent discharge, causing dramatically environmental pollution as well as serious life-threatening problems for environment. With regard to organic pollutants, dyes possess a high capacity to modify the environment due to their strong color and visual pollution and also cause changes in biological cycles mainly affecting photosynthesis processes. More than 10,000 tons of dyes are used in different industries, and approximately 100 tons are released into water streams, annually. Their concentration in wastewaters usually varies from 10 to 200 mg L⁻¹ [1].

Release of industrial effluent without proper and prior treatment into the environment is one of the major causes

leading to a burden of healthcare issues worldwide. For water purification, there is a need for technologies that have the ability to remove toxic contaminants from the environment to a safe level and to do so rapidly, efficiently, and within a reasonable costs framework. Adsorption process provides an attractive alternative for the treatment of colored wastewaters due to its simplicity, selectivity, and efficiency [2–5].

In recent years, magnetic nanoparticles (NPs) have attracted much interest in many environmental engineering related applications. With reported sizes ranging from 1 to 100 nm, high surface-to-volume ratio, and high loading capacity, NPs were successfully used as strong adsorptive materials for pollutants adsorption from contaminated water [6, 7].

TABLE 1: Features of magnetite/carbon nanocomposites prepared by combustion synthesis [9].

Sample	Fe ₃ O ₄ /C mass ratio	SSA (m ² /g)	ESA (m ² /g)	Micropore volume (cm ³ /g)	M _s (emu/g)
PM-1	1/0	75	71.2	0.001	59.7
PM-2	1/1	360	148.4	0.096	34.1
PM-3	1/2	522	204.5	0.144	21.9
PM-4	1/5	706	245.5	0.212	12.4
PM-5	1/10	814	307.9	0.234	7.8
PM-6	0/1	890	321.1	0.264	0.4

SSA: BET specific surface area, ESA: external surface area, and M_s: specific saturation magnetization.

The key to adsorption technology lies in the effectiveness and efficiency of adsorbent. Although commercial activated carbon has been most widely applied in adsorption, its microporous nature has limited the pore utility and adsorption capacity for large molecules [8].

In this work, three industrial dyes have been selected as pollutants. As adsorbent in this work a combination of active carbon and magnetic nanocomposite synthesized by combustion method has been selected.

The adsorption processes were first in detail investigated for single component solutions in terms of pH, initial concentration, adsorbent dose, contact time, and temperature effect, completed by kinetics, equilibrium, and thermodynamics studies.

Subsequently the adsorption studies were performed for six combinations of the selected dyes mixed as binary systems.

The obtained results were compared with the previously reported data on different adsorbents for the same dyes and the selected magnetite nanocomposite from this work demonstrates its superiority and the potential as a new efficient adsorbent for the removal of dyes in binary systems from aqueous solutions.

2. Experimental

2.1. Materials. The starting raw materials for nanocomposites synthesis were activated carbon (Utchim), iron nitrate nonahydrate (Fe(NO₃)₃·9H₂O, Roth), and tartaric acid (C₄H₆O₆, Merck).

Investigated dyes were supplied by Chemical Romania and Colorom Codlea. Chromazurol S (C.I. 43825, ChS) is used as indicator for metal titration, Nylosan Blue (Acid Blue 129, C.I. 62058, NB) is an antraquinonic dye mainly used for wool, silk, polyamide fiber, and leather dyeing but is a skin and eye irritant, and Safranin T (Basic Red 2, C.I. 50240, BR2) is a water soluble organic dye, used in textile industries. Safranin can cause eye burns which may be responsible for permanent injury to the cornea and conjunctiva in human and rabbit eyes. Contact with Safranin dye also causes skin and respiratory tract irritation [17]. The industrial applications of these dyes in different fields confirm the necessity for development of efficient adsorbents.

All reagents were used as received, without further purification. Working dye solutions were prepared with distilled

water. The solution pH was adjusted to the desired values using HCl (0.1 mol L⁻¹) or NaOH (0.1 mol L⁻¹) solutions.

2.2. Preparation of Magnetite/Carbon Nanocomposites. Magnetite/carbon nanocomposites (MNC) having different Fe₃O₄/C mass ratios, ranging from 1/1 to 1/10 (Table 1), were prepared by solution combustion synthesis. The detailed procedure about the preparation route and sample characterization is presented in a previous paper [9]. Briefly, activated carbon impregnated with the precursor solution of iron nitrate nonahydrate (0.09 mol) and tartaric acid (0.138 mol) was heated to 400°C inside a flask, in the absence of air. In order to conduct the combustion reaction in the absence of air, the starting raw materials were placed inside a round bottom flask and heated to 400°C, as described elsewhere. During heating, water evaporates and the air from the flask expands. Driven by the increasing pressure, this mixture of gases is bubbled in a Berzelius glass filled with water, so that the air partial pressure decreased. This way, the atmospheric oxygen is prevented from getting inside the flask during the combustion process. After water evaporation, a smouldering combustion reaction began, accompanied by the release of large amounts of gases. The reaction product was hand-ground, washed with distilled water, and dried [9].

2.3. Adsorption Experiments. The prepared magnetite/carbon nanocomposites were introduced in dye solutions in flat-bottom glass flasks, and adsorption experiments were performed in a thermostat shaker with a constant shaking speed of 180 rpm. The adsorbent synthesis and the adsorption process are schematically presented in Figure 1.

At previously defined time intervals, the sorbent was separated via an external magnetic field, and the samples were collected for dye concentration measurements. For the dye desorption, the dye-loaded MNC were dispersed in 50 mL of ethanol solution (anhydrous alcohol : water = 1 : 1) and shaken for 60 min. After magnetic separation, the concentration of the released dye in the supernatant was spectrophotometrically determined by measuring dye absorbance at maximum wavelength, using a calibration curve (SuppFig. 1).

After desorption, the magnetic sorbent was washed for three times with distilled water, dried at 70°C for 1 h, and reused for adsorption in the next cycle. To validate the reusability of the magnetic sorbent, seven cycles of consecutive adsorption-desorption were carried out at 25°C.

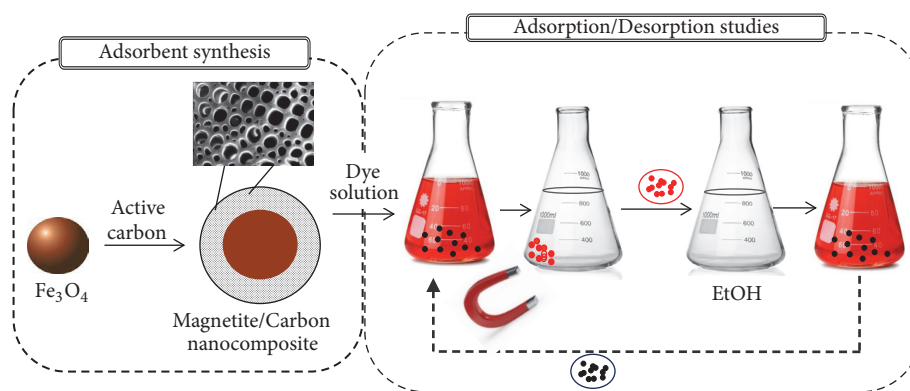


FIGURE 1: Route of synthesis of MNC and their application for dyes removal.

The optimum adsorption conditions were determined by studying several experimental variables, including pH value (2.6–14.0), sorbent dose ($0.25\text{--}3.0\text{ g L}^{-1}$), dye initial concentration ($10\text{--}250\text{ mg L}^{-1}$), and temperature (25, 40, and 60°C). The dyes concentration was measured using a UV-Vis JASCO V-730 spectrophotometer, by monitoring the absorbance changes at the wavelength of maximum absorbance: 465.7 nm (ChS), 629.5 nm (NB), and 516 nm (BR2).

Using these experimental values, the adsorption capacity (1) and the percentage of dye removal (2) were calculated.

$$q_t = \frac{(C_0 - C_t) \cdot V}{W} \quad (1)$$

$$R = \frac{C_0 - C_e}{C_0} \cdot 100, \quad (2)$$

where q_t represents the amount of dye adsorbed per unit of adsorbent (mg g^{-1}), R is the percentage of dye removal (%), C_0 , C_t , and C_e are the concentrations of the dye solution at initial time, at different periods of time, and at equilibrium (mg L^{-1}), V is the volume of solution (L), and W is the mass of the sorbent (g).

3. Results and Discussion

3.1. Characterization of Magnetite/Carbon Nanocomposites (MNC). Our goal was to obtain a new sorbent that combines good adsorption capacity given by activated carbon with good sorbent separation out of solution, given by magnetite. The structure and morphology of the MNC nanocomposites were investigated by X-ray diffraction (XRD), FTIR spectroscopy, scanning electron microscopy- (SEM-) energy dispersive X-ray (EDX), thermal analysis, and N_2 adsorption-desorption technique. The sample characterization is presented in a previous paper [9].

By comparing the specific surface area of the magnetite ($75\text{ m}^2/\text{g}$) with that of the activated carbon ($890\text{ m}^2/\text{g}$) and that of the samples, it is clear that the high specific surface area of the composites is due to the presence of activated carbon in all the samples. As the mass ratio of activated carbon increases, the BET surfaces increased from $360\text{ m}^2/\text{g}$

to $814\text{ m}^2/\text{g}$ (Table 1) which is closed to activated carbon specific surface area. The average size of the crystallites of magnetite, calculated by the Sherrer equation, varied between 12 and 21 nm. The thermal behavior and textural properties of the samples are significantly influenced by the carbon content.

The endothermic effect at about 100°C on the DSC curves (Figure 2), accompanied by weight loss on the TG curves, was attributed to the evaporation of the water present in the samples. The large exothermic effect between 400 and 800°C , accompanied by a significant mass loss on the TG curve, is obvious in the overlap of two exothermic effects, due to combustion of both, fuel residues and carbon. The values of the saturation magnetization of the samples are in accordance with their phase composition, decreasing with the decrease of magnetite content, from 59.7 to 7.8 emu/g . The MNC nanocomposites exhibited a ferrimagnetic behavior. All MNC samples exhibit similar isotherm shape that can be explained by the large amount of carbon content present in their composition (SuppFig. 2) [9].

3.2. Adsorption Studies. A promising adsorbent for large-scale wastewater treatment must present a very good adsorption capacity, easy separation, and high stability. In this vein, the magnetite/carbon nanocomposites (MNC) were tested as adsorbents for removal of two anionic dyes, Chromazurol S (ChS) and Nylosan Blue (NB), and a cationic dye, Safranin T (Basic Red 2, BR2). Molecular structures of investigated dyes are presented in Figure 3.

3.2.1. Effect of pH. Solution pH is an important parameter of adsorption process which affects the adsorbent's surface charge as well as molecular stability of dyes (anionic or cationic molecule) [18]. The influence of pH was evaluated in the range of 2.6–14.0, using MNC sample PM-4, keeping all other variables constant. The results presented in Figure 4 indicate a direct dependence between the dyes removal yield and solution pH.

The efficiency of anionic dyes (NB, ChS) removal was higher than 85% at pH 2.6 and decreased when the pH increased to 13.2. This can be explained by the fact that the

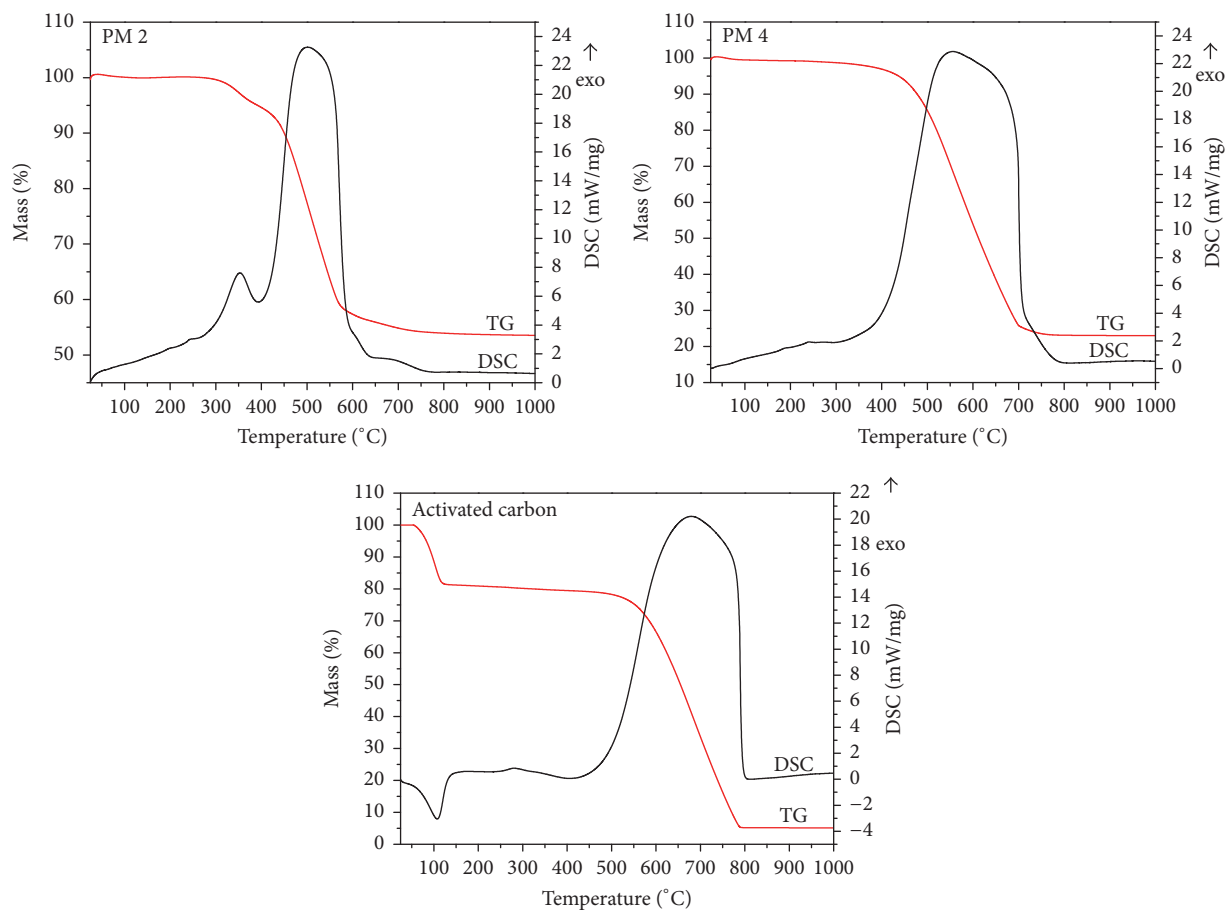


FIGURE 2: TG-DTA curves of samples PM-2, PM-4, and P-6 (activated carbon).

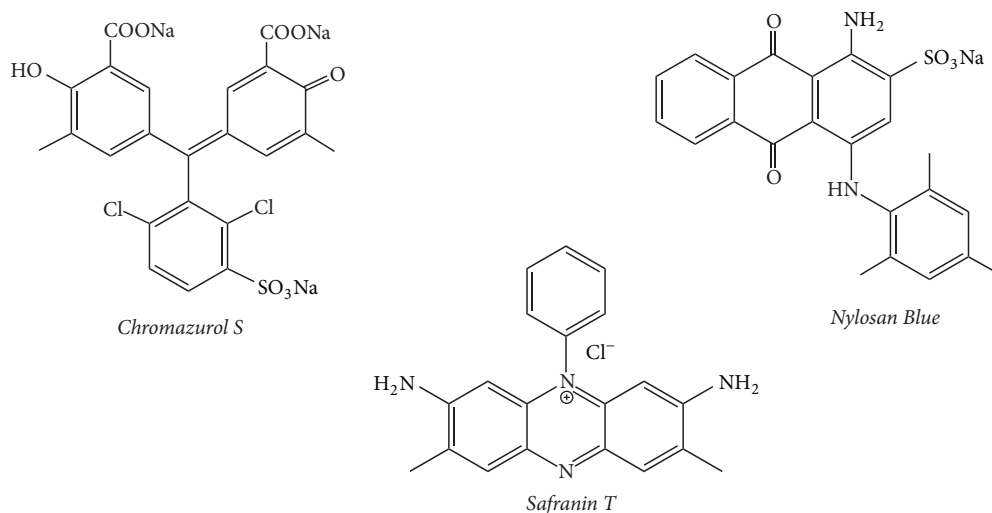


FIGURE 3: Molecular structure of investigated dyes.

adsorption mechanism of anionic dyes at low pH value is controlled by electrostatic attractions between the positively charged surface of adsorbent, as a result of the protonation process, and the negatively charged dyes molecules. In the case of BR2, the removal percentage increased from 70.19%

to 96.84% as the solution pH increases. At pH values higher than magnetite pH_{PZC} (7.9) [19], the adsorption of cationic dye is enhanced due to electrostatic forces of attraction between the negatively charged surface of adsorbent and the positively charged dyes molecules. It is important to note the

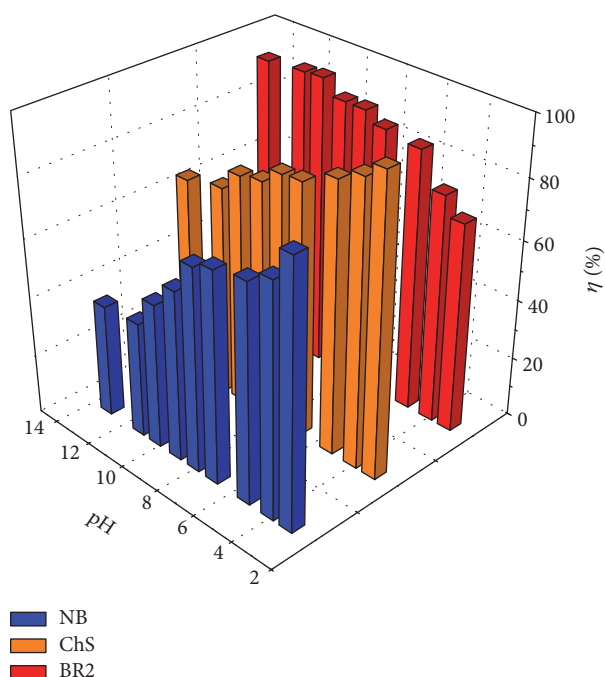


FIGURE 4: Effect of pH on dyes adsorption onto PM-4 adsorbent: contact time 120 min, initial concentration 100 mg L^{-1} , 1 g L^{-1} , and 25°C .

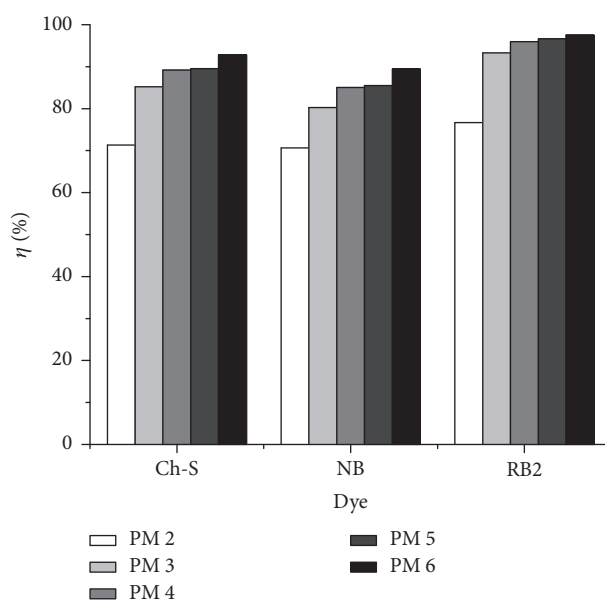


FIGURE 5: Influence of magnetite/carbon ratio on removal efficiency (dyes concentration 100 mg L^{-1} , 25°C , pH 7.4 for NB, 7.1 for ChS, and 6.7 for BR2).

high removal efficiency even at neutral pH (67.89% for NB, 82.95% for ChS, and 89.29% for BR2), which suggests another mechanism involving nonelectrostatic interactions between free electrons of the dye molecule present in aromatic ring and the delocalized π -electrons on the surface of adsorbent as previously mentioned by Istratie et al. [20]. Further experiments were carried out at the natural pH of each dye solution: 7.4 for NB, 7.1 in case of ChS, and 6.7 for BR2.

3.2.2. Effect of the Magnetite/Carbon Ratio on Removal Efficiency. The obtained results from the study of the effect of magnetite/carbon ratio on the removal efficiency are presented in Figure 5.

Sample 6 containing only activated carbon showed the best adsorption capacity. Activated carbon is a well-known and used sorbent for wastewater treatment, with high adsorption capacity [21, 22], but also with many disadvantages,

TABLE 2: Effect of sorbent dose on dyes removal.

PM-4 dose (g L ⁻¹)	R (%)		
	NB	ChS	BR2
0.25	23.58	33.68	19.70
0.5	48.66	40.30	39.94
1	79.90	68.91	91.07
2	85.97	79.63	95.98
3	94.21	85.31	96.50

such as high cost production, poor mechanical properties, and problems in separation, regeneration, and reuse [23–25]. This led to the search for new materials with an adsorption capacity close to that of activated carbon and with good regeneration and reuse. In this idea, we tested four samples which contain different magnetite/carbon ratio. As can be observed, the removal percentage increases from sample 2 to sample 5 due to the increase of the carbon content. The differences among the results obtained by using PM-4, PM-5, and P-6 as adsorbent were in the range of 5% which demonstrates the high efficiency of investigated materials. In order to combine the good adsorption capacity (given by carbon) with the good separation and reutilization of the adsorbent (given by magnetite) the further studies were performed using PM-4.

3.2.3. Effect of Sorbent Dose. The influence of the sorbent dose towards the dye adsorption was studied at different quantities of PM-4 ranging from 0.25 g L⁻¹ to 3 g L⁻¹, at natural pH of dyes solutions, and at 25°C, and results are presented in Table 2.

Removal efficiency of investigated dyes increases rapidly with an increasing amount from 0.25 to 1.0 g L⁻¹ of PM-4 nanocomposite. At the same time, further increasing the adsorbent dose from 1 to 3.0 g L⁻¹ leads to only a small increase of the removal efficiency. This can be attributed to the availability of more adsorption sites as the adsorbent dose increased [26–28]. To get good removal efficiency, but still using as less sorbent, subsequent studies were conducted using 1 g L⁻¹ PM-4 dose.

3.2.4. Effect of Initial Dye Concentration and Contact Time. We investigated the effect of the initial concentration of the dye adsorption process, in a wide range of concentrations between 10 and 250 mg L⁻¹ at 25°C and natural pH values (7.4 for NB, 7.1 for ChS, and 6.7 for BR2). The concentration of the dye at λ_{\max} was obtained using a standard calibration curve (SuppFig. 1).

As can be seen in Figure 6, the adsorption is very rapid in the initial stages of the adsorption, and it remained constant after reaching the equilibrium time. This can be explained by a large number of active centers at the beginning of adsorption and saturation of these centers on the surface of the adsorbent with achieving equilibrium. The necessary time for reaching the equilibrium increases with increasing the concentration due to the fact that adsorption involves film

diffusion and internal diffusion [29]. The surface diffusion is rapid but the pore diffusion is slower, and the rate of diffusion in the internal adsorption sites decreased with increasing the initial dye concentration.

Very good results (higher than 95%) for the dye removal percentage were obtained at low concentrations (Table 3), but even at high concentrations the removal percentage is high in case of BR2 (>93%) and higher than 50% for NB and ChS dyes. The amount of dye adsorbed increased while the percentage removal decreased, with the increase in the initial dye concentration, which is in accordance with the literature data [30, 31].

3.2.5. Effect of Temperature. The effect of temperature on the sorption process was studied at three different temperatures (i.e., 25, 40, and 60°C) at natural pH values (7.4 for NB, 7.1 for ChS, and 6.7 for BR2). The amount of dyes adsorbed onto PM-4 as a function of contact time for different temperatures is presented in Table 3.

A comparison of experimental data shows for all investigated dyes that the rise of temperature induced a positive effect on the removal percentage (Table 3). The adsorption capacity increases as the temperature increases [32], suggesting that dyes adsorption onto PM-4 is an endothermic process [30, 33]. This can be explained by the fact that by increasing the temperature the dye aggregation is reduced and the diffusion of dye molecules into the pores of the absorber is facilitated [34, 35]. On the other hand, there was a decrease of the necessary time for reaching the equilibrium as the temperature increases from 25°C to 60°C. Within the first 40 min, approximately 80% of the dyes are rapidly adsorbed. Later, the adsorption process slows as the system approaches equilibrium. The shorter the contact time in adsorption process, the lower the operational costs that recommend the adsorbent for large-scale industrial application.

These adsorption studies indicate that colored pollutants, such as NB, ChS, and BR2, can be easily removed from wastewaters by adsorption onto magnetite/carbon nanocomposites (SuppFig. 3). Due to their saturation magnetization, these adsorbents can be simply separable from the parent solution using a magnetic field, resulting in clean water.

3.3. Kinetics Studies. In the kinetic experiment, the changes of absorbance were determined at certain time intervals during the adsorption process. The experimental results obtained for the influence of initial concentration were analyzed using the pseudo-first-order Lagergren (3), pseudo-second-order (4), and intraparticle diffusion (5) models.

$$\ln(q_e - q_t) = \ln q_e - k_1 t \quad (3)$$

$$\frac{t}{q_t} = \frac{1}{k_2 q_e^2} + \frac{t}{q_e} \quad (4)$$

$$q_t = k_i t^{0.5} + l, \quad (5)$$

where q_e and q_t are the amount of solute adsorbed at equilibrium and at time t , respectively, per unit weight of adsorbent (mg g⁻¹), k_1 is Lagergren rate constant (min⁻¹), k_2

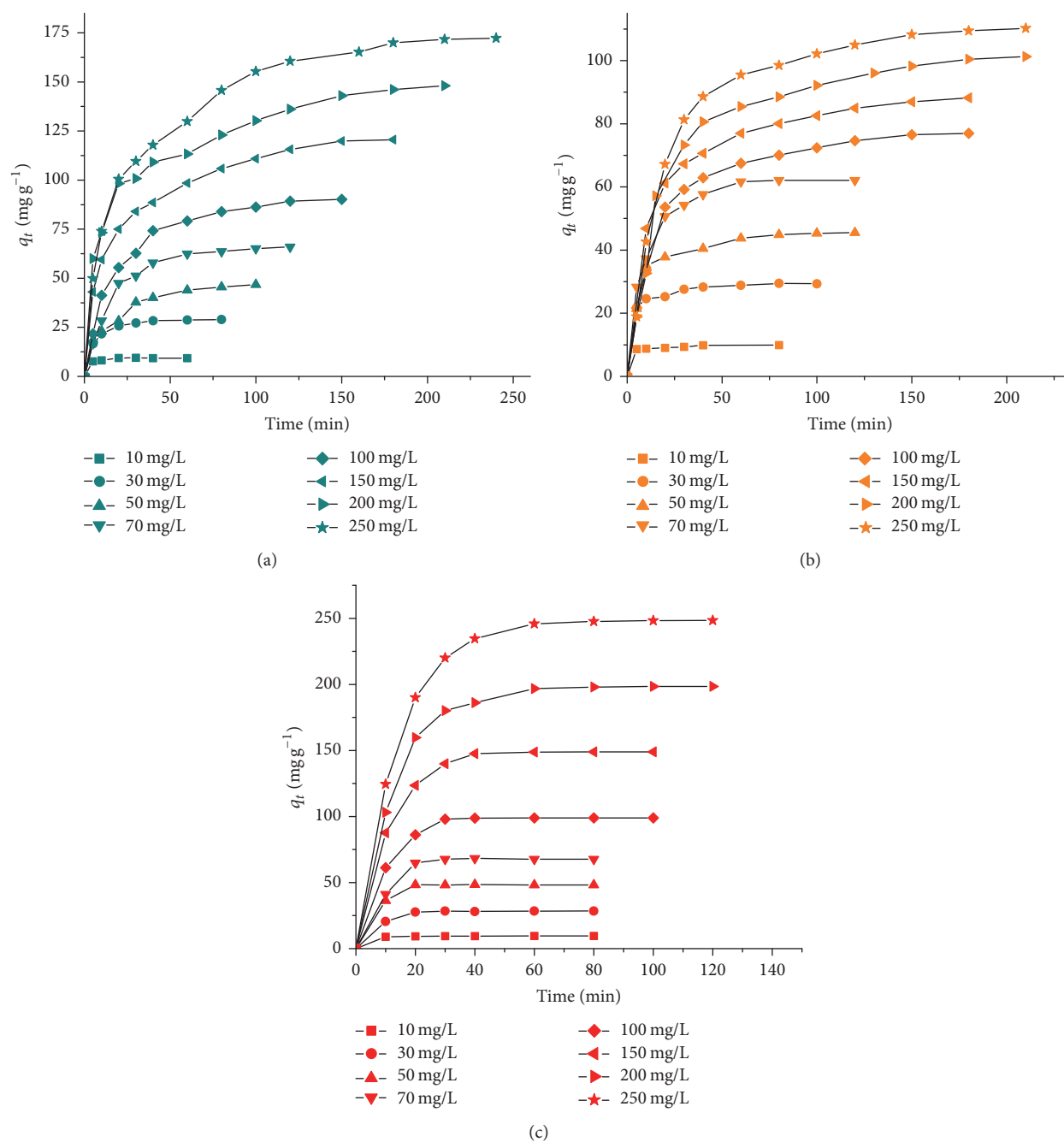


FIGURE 6: The effect of initial concentration on (a) NB, (b) ChS, and (c) BR2 dyes removal (1 g L^{-1} PM-4, 25°C , pH 7.4 for NB, 7.1 for ChS, and 6.7 for BR2).

is the intraparticle diffusion rate constant ($\text{g mg}^{-1} \text{ min}^{-1}$), and k_i is the intraparticle diffusion rate constant ($\text{mg g}^{-1} \text{ min}^{-0.5}$) and l is the effect of boundary layer thickness.

The statistical criteria used to determine the best fitting kinetic model were the standard deviation (SD) and the squared multiple regression coefficient (R^2). The comparison of experimental (obtained for the influence of temperature) and calculated adsorption capacities and the kinetic parameters estimated from (3), (4), and (5) are presented in Table 4.

The pseudo-second-order model was the best applicable kinetic model for the investigated dyes removal kinetics, emphasized by the accordance between the experimental and calculated q_e values. With increasing the temperature, an increase of the pseudo-second-order rate constant k_2 was observed, pointing out that the necessary time for reaching the equilibrium decreased with increasing temperature. Similar results were obtained for the application of modified magnetic nanocomposites for dye removal [28, 36, 37].

TABLE 3: Influence of the process variables on the adsorption process.

	NB			ChS			BR2		
	q_e (mg g ⁻¹)	R (%)	t_e (min)	q_e (mg g ⁻¹)	R (%)	t_e (min)	q_e (mg g ⁻¹)	R (%)	t_e (min)
Dye concentration (mg L ⁻¹)									
10	9.51	95.13	30	9.86	98.57	40	9.83	98.27	20
30	28.36	94.52	40	28.80	96.01	60	29.40	97.99	30
50	47.77	93.54	95	45.35	90.71	70	48.87	97.74	40
70	65.11	93.02	110	62.06	88.65	80	68.27	97.73	50
100	89.22	89.22	120	78.97	78.97	130	96.86	96.86	65
150	119.87	79.91	150	86.95	57.97	140	144.93	96.62	100
200	146.14	73.07	180	96.07	56.90	150	190.06	95.03	150
250	171.67	68.67	210	108.72	51.29	170	234.64	93.85	190
Temperature (°C)									
25	89.22	89.22	120	78.97	78.97	130	96.86	96.86	65
40	95.84	95.84	100	94.77	94.77	100	98.84	98.84	40
60	98.91	98.81	60	97.86	97.86	60	99.45	99.45	20

TABLE 4: Comparison of experimental and calculated q_e values and rate constants for adsorption of NB, ChS, and BR2 dyes on PM-4 nanocomposites.

Dye	Temp (°C)	$q_{e,exp}$ (mgg ⁻¹)	First-order kinetic model			Second-order kinetic model			Intraparticle diffusion		
			$q_{e,calc}$ (mg·g ⁻¹)	$k_1 \cdot 10^3$ (min ⁻¹)	R^2	$q_{e,calc}$ (mg·g ⁻¹)	$k_2 \cdot 10^4$ (g·mg ⁻¹ ·min ⁻¹)	R^2	k_i (mg·g ⁻¹ ·min ^{-0.5})	L	R^2
NB	25	89.22	83.27	30.77	0.9851	93.63	5.45	0.9994	9.71	5.40	0.9603
	40	95.84	69.51	38.17	0.9491	102.99	9.57	0.9987	10.07	12.75	0.9435
	60	98.91	59.65	63.56	0.9579	104.28	21.11	0.9996	10.27	33.95	0.9822
ChS	25	79.49	68.06	28.95	0.9753	80.81	7.85	0.9992	5.67	37.15	0.9866
	40	94.77	48.33	25.75	0.9501	100.81	13.78	0.9996	6.79	40.29	0.9629
	60	97.86	28.87	52.97	0.9219	101.21	66.36	0.9999	7.01	58.67	0.9765
BR2	25	96.86	33.78	57.02	0.8747	99.80	39.69	0.9996	17.99	5.58	0.9540
	40	98.84	15.51	49.84	0.6774	100.00	82.24	0.9999	29.17	1.94	0.9845
	60	99.45	8.071	50.36	0.6212	101.21	843.7	0.9999	32.70	4.55	0.9673

In adsorption systems, there is the possibility of intraparticle diffusion being the rate-limiting step. When applying intraparticle diffusion model, the plots had two portions which means that the intraparticle diffusion is not the rate determining step of the adsorption [38].

The plots had the same shapes (Figure 7), a linear initial portion in which the intraparticle diffusion is the rate-controlling step, followed by a plateau where intraparticle diffusion slows down [23].

The plots did not pass through the origin and the values of the intercept were significantly different from zero, and larger intercepts indicate that contribution of surface adsorption was higher in rate-controlling step. Moreover, the value of intraparticle parameter k_i increases with increasing temperature. All these results suggest that adsorption involved diffusion of the particles and film diffusion but was not the only rate-controlling step.

3.4. Adsorption Isotherms. Equilibrium adsorption studies were carried out for a better understanding of the adsorption process.

The experimental data obtained at equilibrium was analyzed with Freundlich, Langmuir, Sips, and Redlich-Peterson adsorption models.

$$\begin{aligned}
 q_e &= K_F C_e^{1/n} \\
 q_e &= \frac{q_m K_L C_e}{1 + K_L C_e} \\
 q_e &= \frac{q_m K_S C_e^{1/n}}{1 + K_S C_e^{1/n}} \\
 q_e &= \frac{K_{RP} C_e}{1 + \alpha_{RP} C_e^\beta},
 \end{aligned} \tag{6}$$

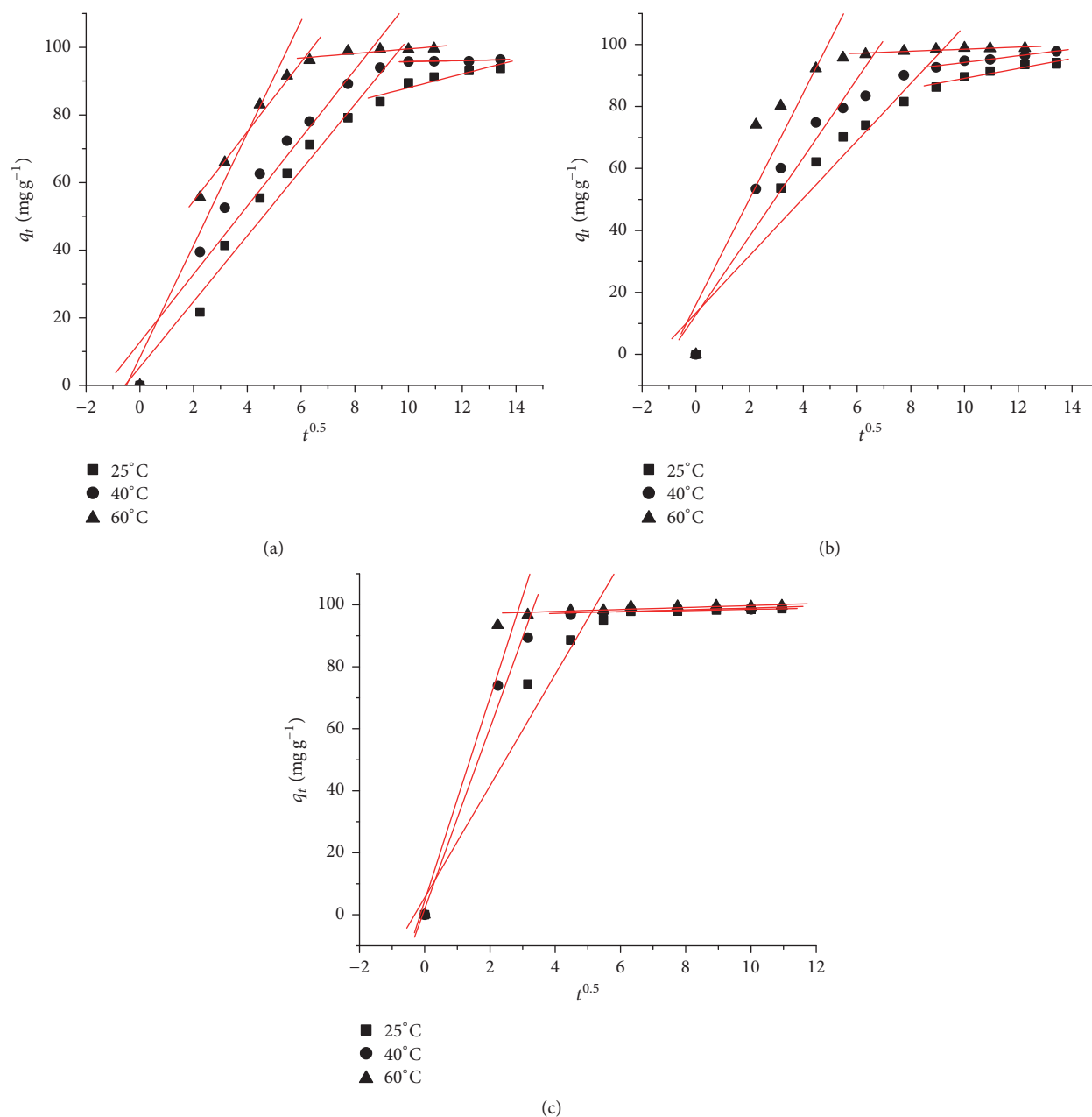


FIGURE 7: Intraparticle diffusion model applied for adsorption of (a) NB, (b) ChS, and (c) BR2 on PM-4 nanocomposites.

where q_e is the equilibrium solid phase concentration, C_e is the dye concentration at equilibrium, K_F is the constant of Freundlich isotherm, the Freundlich exponent (dimensionless), K_L is the constant of Langmuir isotherm, q_m is the maximum adsorption capacity of adsorbent, K_S is Sips constant related to affinity constant, K_{RP} is the constant of Redlich-Peterson isotherm, α_{RP} is the Redlich-Peterson constant, and β is the Redlich-Peterson exponent (dimensionless) ($0 < \beta < 1$).

The analysis of the experimental data and determination of the parameters which describe the theoretical models were performed, and the main statistical criteria were the

squared multiple regression coefficient (R^2) and the chi-square analysis (χ^2) [38]:

$$\chi^2 = \sum \frac{(q_e - q_{e,m})^2}{q_{e,m}}, \quad (7)$$

where q_e is the equilibrium capacity (mg/g) obtained from experimental data and $q_{e,m}$ is the equilibrium capacity obtained by calculating from the model (mg/g).

The calculated parameters based on the isotherms models are listed in Table 5.

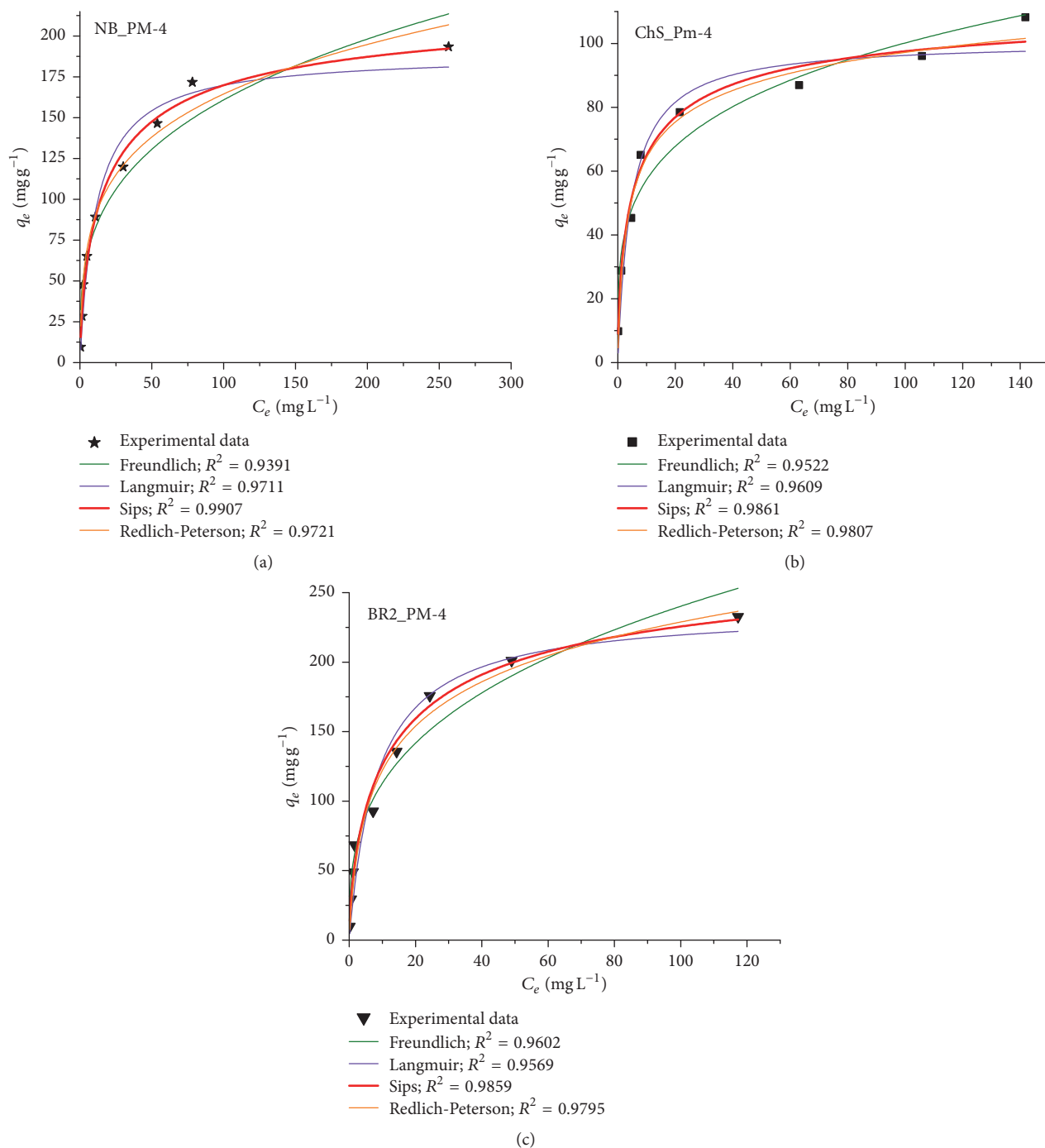


FIGURE 8: Isotherms plots for the adsorption of (a) NB, (b) ChS, and (c) BR2 on PM-4.

The best isotherm model that fits with the experimental data was the Sips isotherm model (Figure 8).

That means that an adsorption process is going on after a combined model of Freundlich and Langmuir: diffused adsorption on low dye concentration and a monomolecular adsorption with a saturation value, at high adsorbate concentrations [38]. The maximum adsorption capacity of the PM-4 was determined from the sorption isotherms curves and compared with other results in Table 6.

The magnetite/carbon nanocomposites PM-4 showed a higher affinity for BR2 adsorption than that of NB and ChS in single dye solution.

Thermodynamic Studies. The results obtained using the Sips model were used to calculate the thermodynamic parameters for the adsorption process [18]. Gibb's free energy (ΔG^0) was calculated using the following equation:

$$\Delta G^0 = -RT \ln K_s \quad (8)$$

TABLE 5: Constants and correlation coefficients of adsorption isotherm models.

Models	Parameter	Dyes		
		NB	ChS	BR2
<i>Freundlich</i>	K_F ($\text{mg g}^{-1} (\text{mg L}^{-1})^{-1/n}$)	40.28	32.76	53.05
	n	3.326	4.121	3.049
	R^2	0.9391	0.9522	0.9602
	χ^2	292.77	65.62	287.58
<i>Langmuir</i>	q_m (mg g^{-1})	188.96	100.77	238.17
	K_L (L mg^{-1})	0.089	0.213	0.118
	R^2	0.9711	0.9609	0.9569
	χ^2	138.98	53.59	311.63
<i>Sips</i>	q_m (mg g^{-1})	223.82	114.68	286.91
	$K_S ((\text{mg L}^{-1})^{-1/n})$	0.051	0.152	0.069
	n	1.424	1.563	1.489
	R^2	0.9907	0.9861	0.9859
<i>Redlich-Peterson</i>	χ^2	52.57	29.59	118.98
	K_{RP} (L g^{-1})	85.37	35.46	50.11
	α_{RP} (mg L^{-1}) $^{-\beta}$	1.486	0.577	0.462
	β	0.767	0.895	0.828
	R^2	0.9721	0.9807	0.9795
	χ^2	157.21	31.75	172.32

TABLE 6: Adsorption capacities of magnetic nanocomposites for the adsorption of dyes from aqueous solutions.

Dye	Adsorbent	q_t (mg/g)	Reference
Chromazurol S	PEI-Halloysite	68.40	[10]
Chromazurol S	Halloysite nanotubes	20.40	[11]
Nylosan Blue	Thermally treated rice husk	30.00	[12]
Nylosan Blue	Acid-activated Bentonite	119.10	[13]
Safranin T	Kaolinite clay	16.23	[14]
Metyl Orange	CoFe ₂ O ₄ -reduced graphene oxide nanocomposites	263.00	[15]
Safranin T	G-SO ₃ H/Fe ₃ O ₄	199.30	[16]
Nylosan Blue	Magnetite/carbon nanocomposites	223.82	[This study]
Chromazurol S	Magnetite/carbon nanocomposites	114.68	[This study]
Safranin T	Magnetite/carbon nanocomposites	286.91	[This study]

and both enthalpy (ΔH^0) and entropy (ΔS^0) were determined from van' Hoff equation:

$$\Delta G^0 = \Delta H^0 - T\Delta S^0, \quad (9)$$

where R is the universal gas constant ($8.314 \text{ J K}^{-1} \text{ mol}^{-1}$), T is the absolute temperature, and K_S represents the Sips equilibrium constant, obtained from the isotherm plots. ΔH^0 and ΔS^0 values can be calculated from the slope and intercept of the linear plot of $\ln K_S$ versus $1/T$.

The ΔG^0 values are negative indicating that the adsorption is a spontaneous process (Table 7). The positive values of ΔH^0 suggest the endothermic nature of the process and indicate that the amount adsorbed at equilibrium is increased with increasing temperature. The positive values of ΔS^0 reflect an increase in randomness at the solid-solution interface during the dyes adsorption onto PM-4 [39].

Adsorbent Stability and Reusability. A promising adsorbent for large-scale wastewater treatment must present a very good adsorption capacity, easy separation, and high stability. To validate the reusability of the magnetic adsorbent, seven cycles of consecutive adsorption-desorption were carried out at 25°C (Figure 9).

The removal efficiency decreased continuously, but it still remained at 68% in the seventh cycle, indicating the good recycling performance of the used adsorbent (PM-4). The adsorption-desorption studies revealed a greater preference for BR2 compared with other two dyes.

Adsorption in Binary Systems. The optimum conditions obtained for individual adsorption were selected as starting conditions for simultaneous adsorption of dyes from bisorbate systems.

In binary adsorption systems, the primary and coexisting sorbate had the same initial concentration, a mass ratio of 1 : 1,

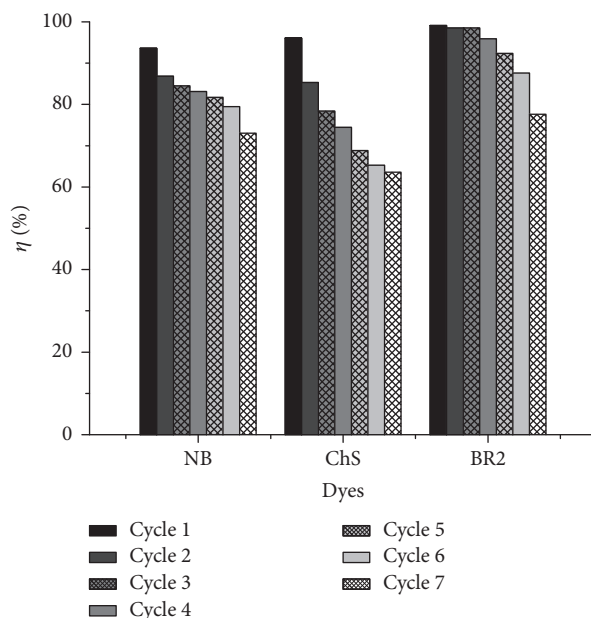


FIGURE 9: Removal efficiency of PM-4 in seven adsorption-desorption cycles.

TABLE 7: Thermodynamic parameters for the adsorption of investigated dyes on PM-4 nanocomposites.

Dye	Temp. (°C)	ΔG^0 (J/mol)	ΔH^0 (J/mol)	ΔS^0 (J/mol·K)
NB	25	-7373.08	6053.50	432.99
	40	-7744.21		
	60	-8239.05		
ChS	25	-4667.44	3832.12	274.09
	40	-4902.37		
	60	-5215.62		
BR2	25	-6624.16	5438.63	389
	40	-6957.59		
	60	-7402.16		

and the experimental studies followed the same procedure as for the single sorbate adsorption experiments.

The concentration of each dye in binary systems was calculated using the following equations [40]:

$$C_A = \frac{k_{B2} \cdot A_1 - k_{B1} \cdot A_2}{k_{A1} \cdot k_{B2} - k_{A2} \cdot k_{B1}} \quad (10)$$

$$C_B = \frac{k_{A1} \cdot A_2 - k_{A2} \cdot A_1}{k_{A1} \cdot k_{B2} - k_{A2} \cdot k_{B1}},$$

where A_1 , A_2 represent the total absorbance at wavelengths $\lambda_{1\max}$ and $\lambda_{2\max}$ and k_{A1} , k_{B1} , k_{A2} , k_{B2} are the calibration constants for components A and B at $\lambda_{1\max}$ and $\lambda_{2\max}$.

Each individual dye spectrum and spectra of binary mixtures of dyes are shown in supplementary file SupFig. 4.

Effect of solution pH on removal percentage in case of binary systems studied for 100 mg/L dye concentration, at 25°C, is presented in Table 8.

TABLE 8: Effect of solution pH on dyes removal efficiency in the case of binary system.

Dye	pH		
	2.84	6.90	10.14
	R (%)		
NB (NB + ChS)	87.38	77.21	51.11
NB (NB + BR2)	87.98	96.52	94.00
ChS (ChS + NB)	63.50	59.17	22.60
ChS (ChS + BR2)	73.08	52.82	52.37
BR2 (BR2 + NB)	95.48	97.83	98.92
BR2 (BR2 + ChS)	88.29	91.76	92.82

Even in case of binary systems, in acidic medium, the removal efficiency of PM-4 is higher for anionic dyes: NB and ChS due to electrostatic attraction between negatively charged dye molecules and positively charged surface of PM-4. At a pH ~10, which was the optimum pH for removal of

TABLE 9: Effect of initial concentration on dyes removal efficiency for binary systems.

Conc (mg L ⁻¹)	<i>R</i> sin. (%)	<i>R</i> bin. (%)	
	NB	NB (NB + RB2)*	NB (NB + ChS)*
30	94.52	94.24	86.40
100	89.22	93.98	87.38
200	73.07	84.50	66.08
	ChS	ChS (ChS + BR2)*	ChS (ChS + NB)*
30	96.01	92.72	90.18
100	78.97	90.08	70.33
200	56.90	89.20	63.50
	BR2	BR2 (BR2 + NB)**	BR2 (BR2 + ChS)**
30	97.99	94.30	93.80
100	96.86	92.82	93.92
200	95.03	88.30	93.18

* Determined at pH 2.68. ** Determined at pH 10.14.

BR2 dye in single system, the adsorption of BR2 (cationic dye) from binary systems is favored in comparison with adsorption of NB or ChS (anionic dyes).

The effect of the initial dye concentrations on the percentage removal in case of binary (bin.) systems was investigated using 20 ml of dye solution and 20 mg/L PM-4 at 25°C, for 200 min, and results are presented in Table 9. Three different binary mixtures were investigated NB + BR2, ChS + BR2, and NB + ChS, at three different concentrations: a lower one consists of 30 mg L⁻¹ of both dyes, a higher initial concentration consists of 200 mg L⁻¹ of both dyes, and a middle concentration value is 100 mg L⁻¹ of both dyes.

As it was expected, the removal percentage of dyes decreased in binary systems when compared with the adsorption in single-solute systems. By increasing concentration of dyes in binary systems, the removal efficiency decreased, similar with the case of single component. It is seen that adsorption of BR2 was slightly affected by the presence of NB or ChS in BR2 + NB and BR2 + ChS binary solutions. The adsorption of NB and ChS dyes in binary systems containing BR2 as copollutant was improved compared with the single systems. Similar results were obtained for other binary systems by Deng et al. [41], Yang et al. [42], and An et al. [28].

In order to determine the effectiveness of the absorbent investigated (PM-4) under field conditions, that is, pH of the solutions (6.90 for NB + BR2, 7.09 for ChS + BR2, and 7.90 for NB + ChS) at 25°C, we have extended the analysis for the dye concentration of 100 mg/L. Results are presented in Figure 10.

As can be observed even at the natural pH of the BR2 dye solution, sorbent PM-4 demonstrates a high selectivity for BR2 in binary systems. The removal percentage of NB decreased in binary system NB + ChS compared with its removal in single system indicated that NB was affected by the presence of ChS during the competitive adsorption. The most affected in binary system was ChS dye, the removal efficiency

of ChS decreasing due to competition between the ChS and NB or BR2 onto MNC PM-4.

4. Conclusions

In this paper, magnetic nanoparticles embedded within a matrix of activated carbon were tested as adsorbent for dyes removal from single and binary systems.

The adsorption capacities decreased for NB and ChS and increased for BR2 with increasing pH value. The removal efficiency of pollutants increased with increasing the carbon content, with initial concentration of the pollutants, the dose of MNC, and temperature. Kinetic studies revealed that adsorption of investigated dyes followed a pseudo-second-order kinetic in single dye solution. The application of intraparticle diffusion model demonstrates that the surface diffusion and the intraparticle diffusion occur in parallel during the adsorption process. The experimental data were well correlated by the Sips adsorption model, and in single systems, the maximum adsorption capacities were 223.82 mg g⁻¹ for NB, 114.68 mg g⁻¹ for ChS, and 286.91 mg g⁻¹ for BR2, respectively. Thermodynamic analysis showed that adsorption of investigated dyes on MNC was favorable, spontaneous, and endothermic. Even after seven adsorption-desorption cycles, the magnetite/carbon nanocomposites still present a good efficiency (greater than 65%) for dyes removal from aqueous solution, indicating the possible industrial application of MNC. In binary systems, the removal efficiency decreased due to competitive effect, but still sorbent PM-4 demonstrates a high selectivity for BR2 in binary systems. The obtained results were compared with the previously reported data on different adsorbents for the same dyes and the selected magnetite nanocomposite from this work demonstrates its superiority and the potential as a new efficient adsorbent for the removal of dyes in binary systems from aqueous solutions.

Considering the facile and low-cost characteristics of the synthesis method, magnetic separation efficiency and simplicity, and the stability and reusability in several adsorptions-desorption cycles, the magnetite/carbon nanocomposites

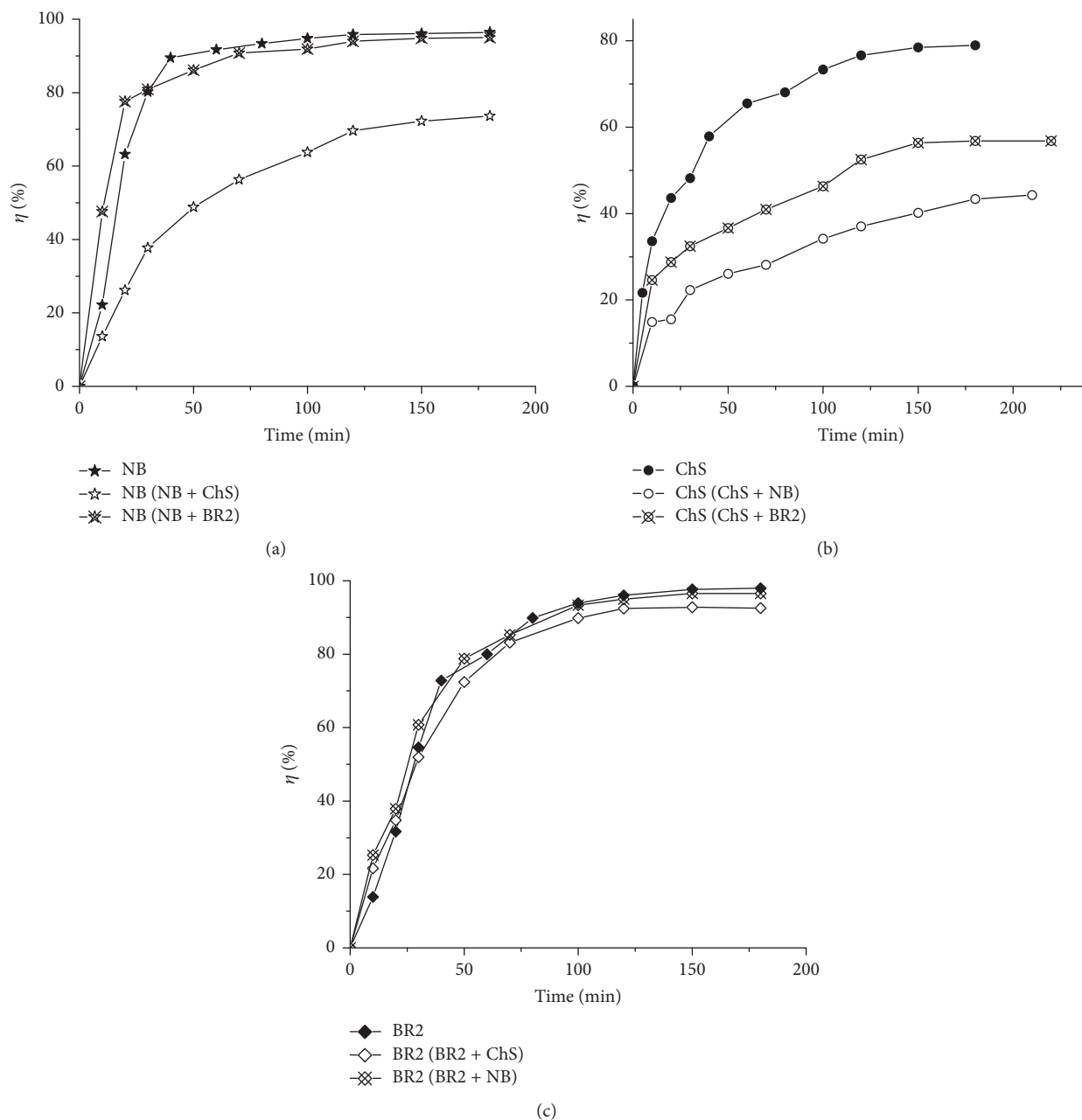


FIGURE 10: The kinetics of competitive adsorption of NB, ChS, and BR2 in single- and binary-solute systems (100 mg/L, adsorbent 2 g/L, 25°C, pH 7.4 for NB, 7.1 for ChS, and 6.7 for BR2).

used in this study are versatile and promising candidates for the removal of dyes from aqueous solutions.

Conflicts of Interest

The authors declare that they have no conflicts of interest.

Acknowledgments

This work was supported by a grant of the Romanian National Authority for Scientific Research and Innovation, CNCS-UEFISCDI, Project no. PN-II-RU-TE-2014-4-1319, and by

Program 2 of the Institute of Chemistry Timișoara of Romanian Academy (Research Project 2.4.)

Supplementary Materials

SuppFig. 1: calibration curve for ChS, NB, and BR2 dyes. SuppFig. 2: adsorption-desorption isotherms of samples PM-1, PM-3, PM-4, PM-5, and P-6 [10]. SuppFig. 3: samples of dyes solution before and after adsorption. SuppFig. 4: individual dye spectra and spectra of binary mixtures of dyes. (*Supplementary Materials*)

References

- [1] M. Ashrafi, M. Arab Chamjangali, G. Bagherian, and N. Goudarzi, "Application of linear and non-linear methods for modeling removal efficiency of textile dyes from aqueous solutions using magnetic Fe₃O₄ impregnated onto walnut shell," *Spectrochimica Acta Part A: Molecular and Biomolecular Spectroscopy*, vol. 171, pp. 268–279, 2017.
- [2] R. K. Vital, K. V. N. Saibaba, K. B. Shaik, and R. Gopinath, "Gopinath, Dye removal by adsorption: a review," *Journal of Bioremediation & Biodegradation*, vol. 7, no. 371, 2016.
- [3] N. M. Mahmoodi and S. Soltani-Gordefaramarzi, "Dye removal from single and quaternary systems using surface modified nanoparticles: Isotherm and kinetics studies," *Progress in Color, Colorants and Coatings*, vol. 9, no. 2, pp. 85–97, 2016.
- [4] R. Tang, C. Dai, C. Li, W. Liu, S. Gao, and C. Wang, "Removal of Methylene Blue from Aqueous Solution Using Agricultural Residue Walnut Shell: Equilibrium, Kinetic, and Thermodynamic Studies," *Journal of Chemistry*, vol. 2017, Article ID 8404965, 2017.
- [5] W. T. Al-Rubayee, O. F. Abdul-Rasheed, and N. M. Ali, "Preparation of a Modified Nanoalumina Sorbent for the Removal of Alizarin Yellow R and Methylene Blue Dyes from Aqueous Solutions," *Journal of Chemistry*, vol. 2016, Article ID 4683859, 2016.
- [6] L. Kong, X. Gan, A. L. B. Ahmad et al., "Design and synthesis of magnetic nanoparticles augmented microcapsule with catalytic and magnetic bifunctionalities for dye removal," *Chemical Engineering Journal*, vol. 197, pp. 350–358, 2012.
- [7] H. R. Lotfi Zadeh Zhad, F. Aboufazel, O. Sadeghi, V. Amani, E. Najafi, and N. Tavassoli, "Tris(2-Aminoethyl)amine-functionalized Femagnetic nanoparticles as a selective sorbent for separation of silver and gold ions in different pHs," *Journal of Chemistry*, Article ID 482793, 2013.
- [8] Y. Liu, G. Zeng, L. Tang et al., "Highly effective adsorption of cationic and anionic dyes on magnetic Fe/Ni nanoparticles doped bimodal mesoporous carbon," *Journal of Colloid and Interface Science*, vol. 448, pp. 451–549, 2015.
- [9] R. Ianoş, C. Păcurariu, and G. Mihoc, "Magnetite/carbon nanocomposites prepared by an innovative combustion synthesis technique - Excellent adsorbent materials," *Ceramics International*, vol. 40, no. 8, pp. 13649–13657, 2014.
- [10] Y. Zhao, E. Abdullayev, A. Vasiliev, and Y. Lvov, "Halloysite nanotubule clay for efficient water purification," *Journal of Colloid and Interface Science*, vol. 406, no. 15, pp. 121–129, 2013.
- [11] Y. Zhao, E. Abdullayev, and Y. Lvov, "Nanotubular halloysite clay as efficient water filtration system for removal of cationic and anionic dyes," in *Proceedings of the 2nd International Conference on Structural Nano Composites, NANOSTRUC 2014*, May 2014.
- [12] G. K. Jayatunga, "Rice husk based adsorbents for dye removal from wastewater," 2009, <http://dl.lib.mrt.ac.lk/handle/123/1832>.
- [13] A. S. Özcan and A. Özcan, "Adsorption of acid dyes from aqueous solutions onto acid-activated bentonite," *Journal of Colloid and Interface Science*, vol. 276, no. 1, pp. 39–46, 2004.
- [14] K. O. Adebawale, B. I. Olu-Owolabi, and E. C. Chigbundu, "Removal of Safranin-O from Aqueous Solution by Adsorption onto Kaolinite Clay," *Journal of Encapsulation and Adsorption Sciences (JEAS)*, vol. 04, no. 03, pp. 89–104, 2014.
- [15] Z. J. Song, W. Ran, and F. Y. Wei, "One-step approach for the synthesis of CoFe₂O₄@rGO core-shell nanocomposites as efficient adsorbent for removal of organic pollutants," *Water Science and Technology*, vol. 75, no. 2, pp. 397–405, 2017.
- [16] R. K. Gautam and M. C. Chattopadhyaya, *Nanomaterials for wastewater remediation (Butterworth-Heinemann, vol. cap 6*, Taylor & Francis Group, 2016.
- [17] M. Fayazi, D. Afzali, M. A. Taher, A. Mostafavi, and V. K. Gupta, "Removal of Safranin dye from aqueous solution using magnetic mesoporous clay: Optimization study," *Journal of Molecular Liquids*, vol. 212, pp. 675–685, 2015.
- [18] S. G. Muntean, O. Paska, S. Coseri, G. M. Simu, M. E. Grad, and G. Ilia, "Evaluation of a functionalized copolymer as adsorbent on direct dyes removal process: Kinetics and equilibrium studies," *Journal of Applied Polymer Science*, vol. 127, no. 6, pp. 4409–4421, 2013.
- [19] E. Tombácz, E. Illés, A. Majzik, A. Hajdú, N. Rideg, and M. Szekeres, "Ageing in the inorganic nanoworld: Example of magnetite nanoparticles in aqueous medium," *Croatica Chemica Acta*, vol. 80, no. 3-4, pp. 503–515, 2007.
- [20] R. Istratie, M. Stoia, C. Păcurariu, and C. Locovei, "Single and simultaneous adsorption of methyl orange and phenol onto magnetic iron oxide/carbon nanocomposites," *Arabian Journal of Chemistry*, 2015.
- [21] P. K. Malik, "Dye removal from wastewater using activated carbon developed from sawdust: adsorption equilibrium and kinetics," *Journal of Hazardous Materials*, vol. 113, no. 1–3, pp. 81–88, 2004.
- [22] D. Schimmel, K. C. Fagnani, J. B. O. Dos Santos, M. A. S. D. Barros, and E. A. Da Silva, "Adsorption of turquoise blue qg reactive dye on commercial activated carbon in batch reactor: Kinetic and equilibrium studies," *Brazilian Journal of Chemical Engineering*, vol. 27, no. 2, pp. 289–298, 2010.
- [23] C. Păcurariu, O. Paşka, R. Ianoş, and S. G. Muntean, "Effective removal of methylene blue from aqueous solution using a new magnetic iron oxide nanosorbent prepared by combustion synthesis," *Clean Technologies and Environmental Policy*, vol. 18, no. 3, pp. 705–715, 2016.
- [24] I. Shah, R. Adnan, W. S. W. Ngah, and N. Mohamed, "Iron impregnated activated carbon as an efficient adsorbent for the removal of methylene blue: Regeneration and kinetics studies," *PLoS ONE*, vol. 10, no. 4, Article ID e0122603, 2015.
- [25] H. Sun, L. Cao, and L. Lu, "Magnetite/reduced graphene oxide nanocomposites: one step solvothermal synthesis and use as a novel platform for removal of dye pollutants," *Nano Research*, vol. 4, no. 6, pp. 550–562, 2011.
- [26] M. R. Patil and V. S. Shrivastava, "Adsorption of malachite green by polyaniline–nickel ferrite magnetic nanocomposite: an isotherm and kinetic study," *Applied Nanoscience*, vol. 5, no. 7, pp. 809–816, 2015.
- [27] S. D. Abkenar, "Application of magnetic-modified Fe₃O₄ nanoparticles for removal of crystal violet from aqueous solution: kinetic, equilibrium and thermodynamic studies," *J. Appl. Chem. Res.*, vol. 10, no. 1, pp. 65–74, 2016.
- [28] S. An, X. Liu, L. Yang, and L. Zhang, "Enhancement removal of crystal violet dye using magnetic calcium ferrite nanoparticle: Study in single- and binary-solute systems," *Chemical Engineering Research and Design*, vol. 94, pp. 726–735, 2015.
- [29] S. G. Muntean, M. E. Rădulescu-Grad, and P. Sfârloagă, "Dye adsorbed on copolymer, possible specific sorbent for metal ions removal," *RSC Advances*, vol. 4, no. 52, pp. 27354–27362, 2014.
- [30] M. K. Satapathy, P. Banerjee, and P. Das, "Plant-mediated synthesis of silver-nanocomposite as novel effective azo dye adsorbent," *Applied Nanoscience*, vol. 5, no. 1, pp. 1–9, 2015.
- [31] C. Vîrlan, R. G. Ciocârlan, T. Roman, D. Gherca, N. Cornei, and A. Pui, "Studies on adsorption capacity of cationic dyes on

- several magnetic nanoparticles,” *Acta Chemica Iasi*, vol. 21, no. 1, 2013.
- [32] D. Robati, B. Mirza, M. Rajabi et al., “Removal of hazardous dyes-BR 12 and methyl orange using graphene oxide as an adsorbent from aqueous phase,” *Chemical Engineering Journal*, vol. 284, pp. 687–697, 2016.
- [33] X. Zhao, S. Liu, Z. Tang et al., “Synthesis of magnetic metal-organic framework (MOF) for efficient removal of organic dyes from water,” *Scientific Reports*, vol. 5, Article ID 11849, 2015.
- [34] S. G. Muntean, G. M. Simu, L. Kurunczi, and Z. Szabadai, “Investigation of the aggregation of three disazo direct dyes by UV-vis spectroscopy and mathematical analysis,” *CHEMISTRY MAGAZINE*, vol. 60, no. 2, pp. 152–155, 2009.
- [35] S. G. Muntean, G. M. Simu, L. Kurunczi, and Z. Szabadai, “Experimental and mathematical study of the aggregation of a green trisazo direct dye,” *CHEMISTRY MAGAZINE*, vol. 59, no. 8, pp. 894–897, 2008.
- [36] T. Wang, P. Zhao, N. Lu, H. Chen, C. Zhang, and X. Hou, “Facile fabrication of Fe₃O₄/MIL-101(Cr) for effective removal of acid red 1 and orange G from aqueous solution,” *Chemical Engineering Journal*, vol. 295, pp. 403–413, 2016.
- [37] D. Chen, Z. Zeng, Y. Zeng, F. Zhang, and M. Wang, “Removal of methylene blue and mechanism on magnetic γ -Fe₂O₃/SiO₂ nanocomposite from aqueous solution,” *Water Resources and Industry*, vol. 15, pp. 1–13, 2016.
- [38] S. G. Muntean, A. Todea, M. E. Radulescu-Grad, and A. Popa, “Decontamination of colored wastewater using synthetic sorbents,” *Pure and Applied Chemistry*, vol. 86, no. 11, pp. 1771–1780, 2014.
- [39] R. Ahmad and R. Kumar, “Kinetic and thermodynamic studies of brilliant green adsorption onto carbon/iron oxide nanocomposite,” *Journal of the Korean Chemical Society*, vol. 54, no. 1, pp. 125–130, 2010.
- [40] N. M. Mahmoodi, R. Salehi, and M. Arami, “Binary system dye removal from colored textile wastewater using activated carbon: Kinetic and isotherm studies,” *Desalination*, vol. 272, no. 1-3, pp. 187–195, 2011.
- [41] J.-H. Deng, X.-R. Zhang, G.-M. Zeng, J.-L. Gong, Q.-Y. Niu, and J. Liang, “Simultaneous removal of Cd(II) and ionic dyes from aqueous solution using magnetic graphene oxide nanocomposite as an adsorbent,” *Chemical Engineering Journal*, vol. 226, pp. 189–200, 2013.
- [42] L. Yang, Y. Zhang, X. Liu et al., “The investigation of synergistic and competitive interaction between dye Congo red and methyl blue on magnetic MnFe₂O₄,” *Chemical Engineering Journal*, vol. 246, pp. 88–96, 2014.

Research Article

Water Pollution and Water Quality Assessment of Major Transboundary Rivers from Banat (Romania)

Andreea-Mihaela Dunca 

Department of Geography, Faculty of Chemistry, Biology, Geography, West University of Timișoara,
Blvd. V. Pârvan No. 4, Timișoara, 300223 Timiș, Romania

Correspondence should be addressed to Andreea-Mihaela Dunca; andreea.dunca@e-uvr.ro

Received 13 November 2017; Revised 23 January 2018; Accepted 6 February 2018; Published 5 March 2018

Academic Editor: Narcis Duteanu

Copyright © 2018 Andreea-Mihaela Dunca. This is an open access article distributed under the Creative Commons Attribution License, which permits unrestricted use, distribution, and reproduction in any medium, provided the original work is properly cited.

This study focuses on water resources management and shows the need to enforce the existing international bilateral agreements and to implement the Water Framework Directive of the European Union in order to improve the water quantity and quality received by a downstream country of a common watershed, like Timiș-Bega hydrographical basin, shared by two countries (Romania and Serbia). The spatial trend of water quality index (*WQI*) and its subindexes are important for determining the locations of major pollutant sources that contribute to water quality depletion in this basin. We compared the values of *WQI* obtained for 10 sections of the two most important rivers from Banat, which have a great importance for socioeconomic life in southwestern part of Romania and in northeastern part of Serbia. In order to assess the water quality, we calculated the *WQI* for a long period of time (2004–2014), taking into account the maximum, minimum, and the mean annual values of physical, chemical, and biological parameters (*DO*, *pH*, *BOD₅*, *temperature*, *total P*, *N-NO₂⁻*, and *turbidity*). This article highlights the importance of using the water quality index which has not been sufficiently explored in Romania and for transboundary rivers and which is very useful in improving rivers water quality.

1. Introduction

The water quality from the rivers has a considerable importance for the reason that these water resources are generally used for multiple matters such as: drinking domestic and residential water supplies, agriculture (irrigation), hydroelectric power plants, transportation and infrastructure, tourism, recreation, and other human or economic ways to use water [1].

For a given river the water quality is the result of several interrelated parameters with a local and temporal variation which are influenced by the water flow rate during the year [2].

In the context of sustainable water management, many hydrological studies have been published around the world, which highlights the ecological role of water from the rivers. Moreover, there have been more researches based upon water quality evaluation [3–5]. This category of studies is related to the quality of watercourses which generally use many statistical and mathematical models.

Most of the studies related to the assessment of the water resources quality use several water quality indices among

the most important are water quality index (*WQI*), water pollution index (*WPI*), and river habitat survey (*RHS*) [6, 7].

Studies focusing on water quality of water bodies from Romanian territory and especially of major transboundary rivers from Banat hydrographical area are scarce, so this study has a great importance for the reason that it describes the suitability of surface water sources from this hydrographical area for human consumption being useful for communication of overall water quality information to the concerned citizens and policy makers.

To determine the locations of major polluting sources that contribute to water quality depletion in the Timiș-Bega hydrographical basin and its tributaries, an analysis has been made in order to evaluate the two largest waterways from Banat (Timiș and Bega transboundary rivers), using the water quality index (*WQI*) method, which is one of the most reliable indicators of the watercourses pollution and the most convenient way to express the water quality at the same time [8].

Timiș-Bega hydrographical system is located in the western part of Romania, overlapping the hydrographical basins

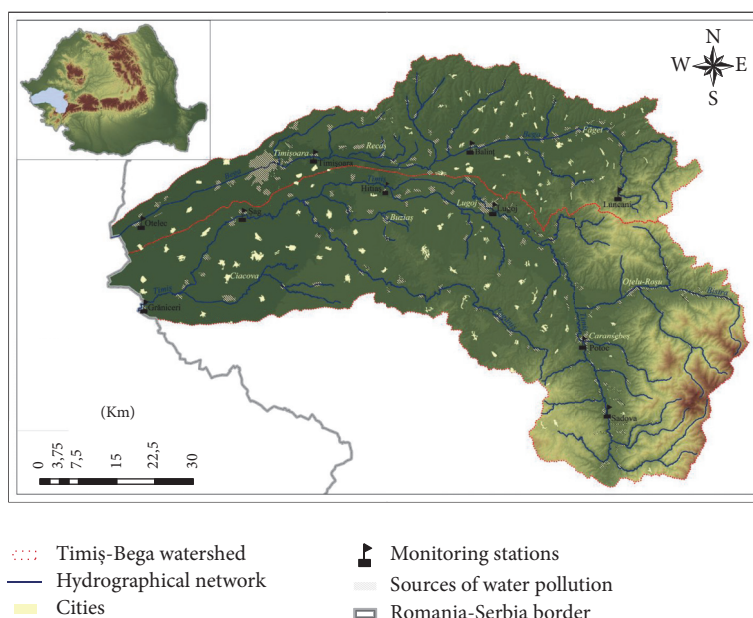


FIGURE 1: The geographical position of the Timiș-Bega hydrographical basin within Romania.

of Timiș and Bega rivers, named after the hydrotechnical works constructed in the two basins. These works are meant to ease the better management of the water resources within them, interconnecting the two rivers, through the Coștei-Chizătău Supply Channel and Topolovăț-Hitiaș Discharge Channel (Figure 1).

Timiș River is the most important river of Banat historical region, springing from the crystalline massif of Semenice, under the Piatra Goznei Peak, from the approximate altitude of 1135 m, and it discharges on a total length of 249 km up to the confluence point with the Danube, located in the South of Pancevo locality, on the current territory of Serbia [9, as amended]. The river gathers its tributaries that spring from the Banat Mountains, Țarcu Mountains, Poiana Ruscă Mountains, and, finally, the piedmont hills of Lugoj and Pogăniș, summing up a total length of the watercourses of approximately 462 km and a watershed surface of 5505 km² on the territory of Romania, representing approximately 2.31% from the total surface of Romania (238391 km²) [10].

Bega River springs from Poiana Ruscă Mountains, under Padeș Peak (1359 m), from an altitude of 1150 m, discharging into Tisa River, near Titel locality, found on the current territory of Serbia where it collects its tributaries from Poiana Ruscă Mountains, Lipova Piedmont, the pied mountainous, and divagation field of Banat that are summing up a length of 176 km and a surface of 2675 km² on the territory of Romania (almost 1.12% from the total surface) [10].

Human activities in the basin of the two most important rivers from Banat have a great importance for socioeconomic life in southwestern part of Romania and in northeastern part of Serbia. Moreover, these human activities have an important influence in the geographical environment generally speaking with a particularity in what concerns the water resources, their quantity, and quality.

The problems involving the water resources management activity from Timiș-Bega hydrographical system consist of the assurance of the required water demand by the various social-economic objectives, the prevention of damaging effects of the waters, and the maintenance of a good environmental quality.

The water intakes from Timiș-Bega hydrographical system are providing the drinkable water supply or the use of water for industrial purposes, which can influence the river hydromorphological level, changing the features of the natural water discharge regime on their courses.

In Timiș-Bega hydrographical system the river monitoring activity started in the 19th century, when the achievement of drainage works of great amplitude was started, in the subsidence area of the Western Plain, where several swamps and frequent floods took place, and when several hydrotechnical works were performed, based on studies and projects, for which several observations and hydrological measurements were necessary.

According to the Water Framework Directive of European Union (WFD 2000), Timiș-Bega watershed has been selected several watercourses, well-delimited in the territory, for the operational monitoring of the surface and ground waters and for the determination of water quality status, as follows: 14 surface water bodies found in natural status, 12 surface water bodies which are heavily modified and artificial, 3 surface reservoirs, and 8 monitored ground water bodies [10].

2. Materials and Methods

The water quality index (WQI) is a numeric expression used to evaluate the quality of a given water body meant to be easily understood by managers from many countries [11].

TABLE 1: Index value intervals and the corresponding quality category [17].

Value intervals (%)	Water quality status
90–100	Excellent
70–90	Good
50–70	Medium
25–50	Bad
0–25	Very bad

In order to calculate the water quality index, Horton proposed in 1965 the first formula which takes into account all parameters necessary for determining the quality of the surface waters and which reflects the composite influence of different parameters important for the assessment and management of water quality [12, 13].

This index was for the first time used to highlight the physical-chemical changes that may occur during the year on the flowing water quality [14, 15].

Most often, the water quality index is used in the evaluation of surface water quality. This index incorporates data from multiple parameters into a mathematical equation that rates the quality of water bodies with numbers from 1 to 100 which can be separated in five classes, each class with a different quality state and with a different usage domain [13, 16].

One of the most computation formulas used to determine the water quality index can be noticed in the following arithmetic expression:

$$WQI = \frac{1}{100} \left(\sum_{i=1}^9 q_i w_i \right)^2, \quad (1)$$

where i is the quality parameter, q_i is the registered value, and w_i is the rank of implication of the parameter in the computation formula [12].

Seven factors have been chosen, in order to rate this index; each of them is more important than others, so weighted mean is used to combine the values of these factors.

The classes of the water quality status obtained according to the quality intervals of the WQI are presented in Table 1.

WQI scores above 80 represent stations of “lowest concern” that generally meet state water quality standards, WQI scores between 40 and 80 indicate stations of “marginal concern,” and WQI scores below 40 did not meet expectations and are of “highest concern” [18].

In order to obtain the WQI values a selection of the parameters has been made according to the Global Quality Classes established through the norms regarding the classification of surface water quality towards the determination the ecological status of the water bodies.

Thereby, some of the most important parameters of water quality index have been taken into account with the impossibility of considering two of these parameters (total coliforms and turbidity), for the reason that, first of all, the total coliforms parameter is monitored only in the sections where the water is targeted for the potable use and secondly

because turbidity was not considered from sampling stations analyzed.

The results have been further analyzed using current Romanian legislation (the Water Law number 107/1996, as amended and supplemented, the Law number 310/2004, and Order number 161/2006 approving the norms concerning the classification of surface water quality to determine the ecological status of water bodies) which complies with WFD 2000 [19–22].

This directive has been adopted by European Parliament and Council (Directive 2000/60/EC) on establishing a framework for European Community action in the field of water, and it contains for each parameter the limit values for corresponding chemical status of all five classes set, namely, very good (1st grade of quality), good condition (2nd grade of quality), moderate condition (3rd grade of quality), poor condition (4th grade of quality), and bad condition (5th grade of quality) [23].

Another step in calculating the values of water quality index from each sampling sections analyzed has been the one that brings all the measurement units at the same reference scale.

Determining the degree of involvement of the parameters has been accomplished in correspondence with the specific methodology, which takes into account the role of each analyzed parameter in defining the status of the water bodies and of the aquatic ecosystems [12]. Afterward the last step has been completed using an online calculator of the water quality index advanced by Mr. Brian Oram in 2010, according to the Field Manual for Water Quality Monitoring book [12, 17].

The computation of the WQI for two of the most important rivers from Banat (Timiș and Bega) has been performed taking into account the mean annual values of each quality parameter, which were registered at the six monitoring stations on the Timiș River (Sadova Veche, Potoc, Lugoj, Hitiaș, Șag, and Grăniceri) and at the four monitoring stations on the Bega River (Luncanii de Jos, Balinț, Timișoara, and Otelec).

3. Results and Discussions

In order to assess the water quality of Timiș and Bega rivers the water quality index for a long period of time (2004–2014) has been calculated which has been applied also for 10 sampling sections, along the Timiș (6) and Bega (4) rivers, taking into account the maximum annual, the minimum annual, and the mean annual values of 7 following physical, chemical, and biological parameters: *DO* (oxygen saturation in percent), *pH* (in pH units), *BOD5* (biochemical oxygen demand in mg O₂/L), temperature (°C), *total P* (total phosphorus in mg P/L), *N-NO₂⁻* (total nitrates in mg N/L), and *turbidity* (mg/L), with units of measurement adapted according to International Union of Pure and Applied Chemistry (IUPAC).

The average values of physical (*temperature* and *turbidity*), chemical (*pH*, *total phosphorus* and *nitrates*), and biologic/organic (*oxygen saturation* and *biochemical oxygen demand*) parameters of water from Timiș and Bega rivers

TABLE 2: Water quality status and WQI values at sampling stations from the Timiș River.

Water quality parameters (unit)	Water sampling station								
	Sadova Veche			Potoc			Lugoj		
	Max.	Min.	Mean	Max.	Min.	Mean	Max.	Min.	Mean
DO (%)	125.9	56.1	84.5	128	57.7	85.7	163.8	54.1	98.1
pH (U pH)	7.9	7.1	7.5	7.9	7.2	7.6	9	6.8	7.6
BOD5 (mg O ₂ /L)	3	1.2	1.9	3	1.1	1.9	5.8	1.2	2.8
Temperature (°C)	17.3	1	7.9	17	1.9	8.6	24.5	1.5	12.9
Total P (mg P/L)	0.075	0.032	0.050	0.106	0.026	0.052	0.298	0.028	0.106
N-NO ₂ ⁻ (mg N/L)	0.021	0.004	0.010	0.037	0.008	0.017	0.041	0.004	0.016
Turbidity (mg/L)	37.2	18.7	26.1	41.4	17.9	27.1	198.3	4.6	37.5
Overall WQI	79	83	86	78	84	86	58	81	83
Class	II	II	II	II	II	II	III	II	II
Water quality status	Good	Good	Good	Good	Good	Good	Medium	Good	Good
Water quality concern	Marginal concern	Lowest concern		Marginal concern	Lowest concern		Marginal concern	Lowest concern	

Source. Data processed by the Banat Water Basin Administration (ABAB) Archives, Timișoara.

TABLE 3: Water quality status and WQI values at sampling stations from the Timiș River.

Water quality parameters (unit)	Water sampling station								
	Hitiaș			Șag			Grăniceri		
	Max.	Min.	Mean	Max.	Min.	Mean	Max.	Min.	Mean
DO (%)	130.9	40	79.1	147.7	51.2	89.3	144.7	47.4	86.7
pH (U pH)	7.7	6.8	7.3	7.7	7	7.4	8	7.2	7.6
BOD5 (mg O ₂ /L)	10.8	1.3	4.2	4.8	1.1	2.4	6	1.6	3.7
Temperature (°C)	23.6	2.7	12.6	23.6	2.1	12.1	23.3	3.1	12.7
Total P (mg P/L)	0.437	0.042	0.145	0.263	0.041	0.123	0.434	0.058	0.171
N-NO ₂ ⁻ (mg N/L)	0.078	0.009	0.030	0.042	0.007	0.021	0.046	0.006	0.021
Turbidity (mg/L)	291.4	8.9	68	185.2	6.2	44.9	124.9	11.5	46.8
Overall WQI	66	76	79	66	81	83	62	79	81
Class	III	II	II	III	II	II	III	II	II
Water quality status	Medium	Good	Good	Medium	Good	Good	Medium	Good	Good
Water quality concern	Marginal concern			Marginal concern	Lowest concern		Marginal concern		Lowest concern

Source. Data processed by the Banat Water Basin Administration (ABAB) Archives, Timișoara.

and the results of water quality data analysis are presented in Tables 2, 3, 4, and 5.

At Sadova Veche and Potoc monitoring stations, located on the upper course of Timiș River, the water quality status is good (70–90%), according to the average, maximum, and minimum annual values of the analyzed parameters during the period under review (2004–2014), which make these sampling stations fall into the “lowest concern” category (Table 2).

Downstream on the Timiș River beginning with Lugoj monitoring section until the border between Romania and Serbia the water quality is preserved in good condition according to the mean and minimum annual values. Only the maximum annual values decreased, which cause the medium status of water quality (50–70%) at all other sections (Lugoj,

Hitiaș, Șag, and Grăniceri), fitting them into the “marginal concern” category (Table 3).

The values of the water quality index from these stations correspond to the moderate class, which are influenced by the nutrients, respectively, by the high values of the nitrates from Timiș river water, as a result of the agricultural practices, municipal and industrial wastewaters, manure from farms, and so on.

The water quality of the Timiș River is influenced by many factors including the quantitative variation of biogenic and organic substances. All biogenic elements within the water bodies are the result of the decomposition process of the organic substances therefore the regime of the biogenic elements depends directly on the vital activity of the organisms from the rivers. Moreover this river is characterized

TABLE 4: Water quality status and WQI values at sampling stations from the Bega River.

Water quality parameters (unit)	Water sampling station					
	Luncanii de Jos			Balint		
	Max.	Min.	Mean	Max.	Min.	Mean
DO (%)	146.3	60.6	97.6	154.1	48.3	89.1
pH (U pH)	8.3	7.6	8	8.1	7.2	7.7
BOD5 (mg O ₂ /L)	3.7	0.8	2	6.1	1.5	3.4
Temperature (°C)	19.8	2.2	10	23	1.7	11.4
Total P (mg P/L)	0.242	0.032	0.099	0.381	0.037	0.128
N-NO ₂ ⁻ (mg N/L)	0.015	0.002	0.007	0.041	0.006	0.017
Turbidity (mg/L)	54.9	4.4	18.8	232.4	5.2	55.5
Overall WQI	66	84	85	61	80	82
Class	III	II	II	III	II	II
Water quality status	Medium	Good		Medium	Good	
Water quality concern	Marginal concern	Lowest concern		Marginal concern	Lowest concern	

Source. Data processed by the Banat Water Basin Administration (ABAB) Archives, Timișoara.

TABLE 5: Water quality status and WQI values at sampling stations from the Bega River.

Water quality parameters (unit)	Water sampling station					
	Timișoara			Otelec		
	Max.	Min.	Mean	Max.	Min.	Mean
DO (%)	148.9	44.9	85.6	136.9	23.8	61.9
pH (U pH)	7.8	7	7.4	7.7	6.9	7.3
BOD5 (mg O ₂ /L)	3.8	0.8	1.8	10.3	3.2	5.7
Temperature (°C)	23.9	1.4	12.2	24.7	1.5	13.1
Total P (mg P/L)	0.395	0.026	0.117	0.881	0.161	0.418
N-NO ₂ ⁻ (mg N/L)	0.041	0.004	0.013	0.268	0.011	0.056
Turbidity (mg/L)	132.1	5.7	30.1	134.8	5.2	28.9
Overall WQI	65	80	84	64	69	68
Class	III	II	II	III	III	III
Water quality status	Med.	Good		Medium		
Water quality concern	Marginal concern	Lowest concern		Marginal concern		

Source. Data processed by the Banat Water Basin Administration (ABAB) Archives, Timișoara.

by the presence of several impurities in natural state with a composition which depends on the types of soils from the reception basin, waste water spills from different kind of users, and the dissolving capacity of the gases in the atmosphere [24, 25].

Within the water of unpolluted rivers, the concentration of nitrates often oscillates between the limits of a few tenths of mg/l. The main cause for the loading of the flowing waters with nitrates consists in the eviction of the urban waste waters [26]. This is the reason why the content in N-NO₂⁻ of the river water is almost double at Lugoj station and the reason why the water quality is changing from good to a moderate status according to the maximum annual values.

Generally, the best water quality status from Bega River concerning average and minimum annual is centralized in the sections from the upper course, which falls into the “lowest concern” category (Tables 4 and 5).

Downstream from Timișoara until the Romanian Serbian border the water quality status is deteriorated according to the average annual, maximum annual, and minimum annual

values of the water quality index (50–70% – medium state), so the water quality of Bega River has a moderate status at the exit of our country, weaker compared with Timiș River, which causes Grăniceri station to have a “marginal concern” regarding water quality.

Water quality of the most important rivers from Timiș-Bega hydrographical basin is a result of human activity and demographic characteristics on one side and urbanization and industrialization on the other side. Discharging of untreated waste waters from industry, households, and pollution from agriculture (sewage water from rural localities, from animal farms and from industry) are the main causes of pollution on surface water resources and groundwater in this region [27, 28].

The human stress on the surface water within Timiș and Bega catchments is induced by the total number of inhabitants (almost 700000 people) and the urban inhabitants (428168 people, by National Institute of Statistics (INS) from Romania, 2011) from cities like Timișoara, Lugoj, Buziaș, Făget, Recaș, Ciacova, Caransebeș, and Oțelu Roșu, by the

organic loading that they generate through the industrial activities, land use, and animal husbandry in animal farming complexes, and finally through the degree of improvement of the hydrographical network, as a result of human activity.

At the monitoring sections situated downstream of the wastewater discharge high values of nitrogen compounds have been identified, more exactly of the nitrate, nitrite, and ammonium ions, which influence the quality of the watercourses, especially Timiș and Bega that flow into the Tisa River and Danube River on the territory of Serbia.

The waters of Timiș River and Bega River at the exit from Romania country are much polluted because the rivers quality state suffers a slight depreciations downstream thanks to effects of the urban sewage, of the urban wastewaters, of the agricultural wastes, and of the natural causes such as erosion in the hydrographical basins of these main rivers from Banat [29].

Water pollution by nitrates reaches high levels due to the introduction of intensive farming methods, with increased use of chemical fertilizers and higher concentrations of animals in smaller areas, especially in animal farming complexes from the Timiș-Bega hydrographical basin. In this basin the values of these parameters vary from one monitoring station to another due to the hydrological regime of the surface water but also to the origin and the behavior of the physical, chemical, and biological parameters.

The anthropogenic factor has an important role in the formation and the influence of leakage water processes on the rivers of this hydrographical system. Starting from 1716 and up to the present, it has mostly influenced the water discharge, by achieving several types of hydraulic structures, among which the most important are the regulation of maximum discharges on the main rivers and the most important tributaries, the performance of flood mitigation works, and river bed regulation, damming works on the most important rivers and tributaries, within the proximity of the most important localities [30, 31].

More than that, in Timiș-Bega hydrographical basin several significant water intakes and two secondary intakes (Slatina and Borlova) have been identified. The most important units that require large amounts of water within the basin are S.C. Aquacaraș S.A. from Caransebeș and Oțelu Roșu, S.C. Meridian 22 S.A. from Lugoj, S.C. Aquatim S.A. from Timișoara, and the National Administration for Land Improvement from Romania (ANIF).

The company which represents the main economic actor in the water supply field from the Timiș-Bega hydrographical basin is S.C. Aquatim S.A. This company operates with public water and wastewater services for Timișoara Municipality and many other localities [32].

During the analyzed period (2004–2014) the evaluation of the ecological status of surface water courses (rivers), existing within Timiș-Bega hydrographical system has revealed the fact that the most rivers have been found in good ecological status.

Concerning the evaluation of the chemical status, one could notice that most rivers have been found in good chemical status and only some of them have been characterized by a

bad chemical status (ANPM-Timiș Environment Protection Agency, Timișoara).

Regarding the surface water courses that are heavily modified (rivers), which exist within this basin, it has been found that most of the water courses have had a moderate ecological potential, the difference being represented by the water courses that have had a good ecological potential; and from a chemical status point of view, more than half had a good chemical status and less than half have had a bad ecological status.

Also in the same period, the evaluation of the ecological potential of the three surface reservoirs existing within the basin analyzed has revealed the fact that all these have had a moderate ecological potential and that all have been found in a good chemical status.

However, the evolution trend within the last few years of the pollutant concentrations recorded at the monitoring stations on the basin rivers has had a significant decrease, due to the measures introduced by the national and European legislation, referring especially to the treatment of the urban waste waters and to the reduction of the pollution with nitrogen and phosphorous from the agricultural practices.

In the analyzed period, the limited excess on the water quality according to the Law 311/2004 was due to the zootechnical complexes (Recaș, Peciu Nou, Pădureni, Parța, Ciacova, Voiteni, etc., some of them owned by COMTIM, currently S.C. Smithfield Ferme S.R.L.) within the Timiș-Bega hydrographical basin, as well as to the spray irrigation of the fields with phenolic waters from S.C. Solventul S.A. from Margina, which at the moment, although it has suspended its activity, continues to influence the quality of ground waters from this region.

Another source which influences quite a lot the surface and underground waters quality from this hydrographical area is Waste Deposit Parța, which does not have environment factor protection equipment [29].

4. Conclusions

The results of this paper present the water polluting and quality assessment of two transboundary rivers (Timiș and Bega) from two different hydrographical basins and show that *WQI* values of the Timiș River ranging from 86 to 58 and *WQI* values of the Bega River ranging from 85 to 61 denote degradation of water quality downstream of the rivers.

Water quality in the upstream sections of the Timiș and Bega has been in a better condition than the downstream river sections. There have been significant deterioration in values of the most important water quality parameters (*DO*, *pH*, *BOD5*, *temperature*, *total P*, *N-NO₂⁻*, and *slurry*) downstream of the rivers, which indicates that the local pollutants may be contributing incrementally to the degradation of river quality.

The given *WQI* values control sections of the studied area are distributed on quality classes as follows: 90% in the 2nd class of quality (good) and 10% in the 3rd class of quality (medium) taking into account the mean annual values; 20% in the 2nd class of quality (good) and 80% in the 3rd class of quality (medium) taking into account the maximum annual; 90% in the 2nd class of quality (good) and 10% in the 3rd

class of quality (medium) taking into account the minimum annual values.

The trend in the water quality index is determined by the economic activities in the agriculture, industrial, and residential areas in the sampling stations vicinity in the Timiș-Bega hydrographical basin. For these reasons a constant monitoring is necessary in order to ensure water quality of Timiș and Bega rivers at the optimum level according to the Water Framework Directive (2000/60/EC), especially because these rivers flow further through the territory of Serbia where they are discharging into Tisa and Danube rivers.

This article focuses on water resources management and shows the need to enforce the existing international bilateral agreements and to implement this European directive in order to improve the water quantity and quality received by the downstream country of a shared watershed, like Timiș-Bega hydrographical basin, shared by two countries, Romania (EU country) and Serbia (non-EU country).

According to the Water Framework Directive requirements, knowledge of anthropogenic pressure formed on water resources is highly imperative, in order to identify the quality of water bodies and ultimately for adopting appropriate measures to protect and conserve the water in this region of Romania which have so many transboundary rivers.

In order to protect the environment in general and preserve a good water quality in particularly, especially of the transboundary rivers from Banat, shared by two countries and by so many communities, it is necessary to implement an adequate wastewater management through the construction of modern and efficient waste water treatment plants.

Conflicts of Interest

The author declares that he has no conflicts of interest.

References

- [1] S. Venkatramanan, S. Y. Chung, S. Y. Lee, and N. Park, "Assessment of river water quality via environmentric multivariate statistical tools and water quality index: A case study of Nakdong River Basin, Korea," *Carpathian Journal of Earth and Environmental Sciences*, vol. 9, no. 2, pp. 125–132, 2014.
- [2] P. Mandal, R. Upadhyay, and A. Hasan, "Seasonal and spatial variation of Yamuna River water quality in Delhi, India," *Environmental Modeling & Assessment*, vol. 170, no. 1–4, pp. 661–670, 2010.
- [3] L. Ferencz and A. Balog, "A Pesticide survey in soil, water and foodstuffs from Central Romania," *Carpathian Journal of Earth and Environmental Sciences*, vol. 5, no. 1, pp. 111–118, 2010.
- [4] L. Părvulescu and C. Hamchevici, "The relation between water quality and the distribution of *Gammarus balcanicus schäferna* 1922 (Amphipoda: Gammaridae) in the Anina mountains," *Carpathian Journal of Earth and Environmental Sciences*, vol. 5, no. 2, pp. 161–168, 2010.
- [5] M. Pantelić, D. Dragan, S. Savić, V. Stojanović, and I. Nađ, "Statistical analysis of water quality parameters of Veliki Bački canal (Vojvodina, Serbia) in the period 2000–2009," *Carpathian Journal of Earth and Environmental Sciences*, vol. 7, no. 2, pp. 255–264, 2012.
- [6] A. Milanović, M. Urošev, and D. Milijašević, "Use of the RHS method in Golijška Moravica river basin," *Bulletin of the Serbian Geographical Society*, vol. 86, no. 2, pp. 53–61, 2006.
- [7] A. Milanović, D. Milijašević, and J. Brankov, "Assessment of polluting effects and surface water quality using water pollution index: a case study of hydro-system Danube-Tisa-Danube, Serbia," *Carpathian Journal of Earth and Environmental Sciences*, vol. 6, no. 2, pp. 269–277, 2011.
- [8] M. Paiu and I. G. Breabăn, "Water quality index—an instrument for water resources management," in *Air and Water—Components of the Environment Conference*, G. Pandi and F. Moldovan, Eds., pp. 391–398, Presa Universitară Clujeană Press, Cluj Napoca, Romania.
- [9] R. Munteanu, *Hydrographical Basin of Timiș River—Hydrological Study*, Mirton Publishing, Timișoara, Romania, 1998 (Romanian).
- [10] A. M. Arba, *Water Resources from the Timiș-Bega Hydrographical System: Genesis, Hydrological Regime and Hydrological Risks*, West University of Timișoara Publishing, Timișoara, Romania, 2016 (Romanian).
- [11] O. Ionus, "Water quality index—assessment method of the Motru River water quality (Oltenia, Romania)," *Annals of the University of Craiova, Series Geography*, vol. 13, pp. 74–83, 2010.
- [12] S.-M. Liou, S.-L. Lo, and S.-H. Wang, "A generalized water quality index for Taiwan," *Environmental Modeling & Assessment*, vol. 96, no. 1–3, pp. 35–52, 2004.
- [13] S. Tyagi, B. Sharma, P. Singh, and R. Dobhal, "Water quality assessment in terms of water quality index," *American Journal of Water Resources*, vol. 1, no. 3, pp. 34–38, 2013.
- [14] M. A. House and J. B. Ellis, "The development of water quality indices for operational management," *Water Science and Technology*, vol. 19, no. 9, pp. 145–154, 1987.
- [15] M. A. House, "Water quality indices as indicators of ecosystem change," *Environmental Modeling & Assessment*, vol. 15, no. 3, pp. 255–263, 1990.
- [16] A. A. Bordalo, R. W. Teixeira, and W. J. Wiebe, "A water quality index applied to an international shared river basin: the case of the Douro River," *Journal of Environmental Management*, vol. 38, no. 6, pp. 910–920, 2006.
- [17] B. Oram, Water Quality Index Calculator, According to the book Field Manual for Water Quality Monitoring, 2010, <http://www.water-research.net/index.php/water-treatment/water-monitoring/monitoring-the-quality-of-surfacewaters>.
- [18] D. Hallock, *A Water Quality Index for Ecology's Stream Monitoring Program*, Washington State Department of Ecology, Olympia, Wash, USA, 2002.
- [19] The Water Law 107 of 25 September 1996, Official Monitor of Romania, no. 244 of 08/10/1996.
- [20] The Law 310 of 30 June 2004, amending and supplementing The Water Law no. 107/1996, Official Monitor of Romania, no. 584 of 30/06/2004.
- [21] The Law 311 of 28 June 2004, amending and supplementing Law no. 458/2002 on drinking water quality, Official Monitor of Romania, 1st part, no. 582 of 30/06/2004.
- [22] The Order no. 161 of 16 February 2006, approving the Norms concerning the classification of surface water quality to determine the ecological status of water bodies, the Ministry of Environment and Water, Official Monitor, no. 511 of 13/06/2006.

- [23] Water Framework Directive (2000/60/EC), *Official Journal of the European Community*, vol. L327, pp. 1–73, 2000.
- [24] V. Trufaş and C. Trufaş, *Hydrochemistry*, University of Bucharest Press, Bucharest, Romania, 1975 (Romanian).
- [25] L. Oprean, E. Lengyel, and R. Iancu, “Monitoring and evaluation of Timiş River (Banat, Romania) water quality based on physicochemical and microbiological analysis,” *Transylvanian Review of Systematical and Ecological Research*, vol. 15, no. 3, pp. 33–42, 2013.
- [26] L. Şmuleac, S. Oncia, A. Ienciu, and R. Bertici, “Quality indices of the water in the middle Timiş River basin,” *Annals of the University of Oradea, Environmental Protection Fascicle*, vol. 21, pp. 757–764, 2013.
- [27] A. Ienciu, S. Oncia, L. Şmuleac, P. Fazakas, and C. A. Nicolici, “The quality of the Timis River Waters,” *Research Journal of Agricultural Science*, vol. 45, no. 2, pp. 146–151, 2013.
- [28] A. Balint, G. Cîrciu, E. Alexa, and A. Cozma, “Monitoring of nitrogen compound long ways Timis River basin,” *Journal of Horticulture, Forestry and Biotechnology*, vol. 18, no. 1, pp. 144–150, 2014.
- [29] I. Both, I. Borza, L. Copăcean, and P. Mergheş, “The impact of the antropic activities on the water quality of the rivers Timiş and Bega in the inferior sector,” *Research Journal of Agricultural Science*, vol. 46, no. 2, pp. 38–45, 2014.
- [30] A. M. Dunca, “Chronological study of the water resources management within the Banat historical region (1716–2016),” *Review of Historical Geography and Toponomastics, West University of Timişoara Press, Timişoara*, vol. 12, pp. 83–94, 2017.
- [31] A. M. Dunca, “The history of hydraulic structures realized in Banat hydrographical area (Romania),” *Transactions on Hydrotechnics, Scientific Bulletin of Politehnica University of Timişoara*, vol. 61, no. 75, 1, pp. 53–60, 2017.
- [32] B. Mitrică and I. Mocanu, “Drinking water supply and consumption territorial disparities in the Timiş Plain,” *Annals of the University of Oradea, Geography Series*, vol. 21, no. 2, pp. 239–247, 2011.

Research Article

Impact Assessment of Phosphogypsum Leachate on Groundwater of Sfax-Agareb (Southeast of Tunisia): Using Geochemical and Isotopic Investigation

Samira Melki  and Moncef Gueddari

Laboratory of Geochemistry and Environmental Geology, Department of Geology, Faculty of Sciences of Tunis, University of Tunis El Manar, 2092 Tunis, Tunisia

Correspondence should be addressed to Samira Melki; melkisamiralefi@hotmail.fr

Received 12 November 2017; Accepted 8 January 2018; Published 31 January 2018

Academic Editor: Adina Negrea

Copyright © 2018 Samira Melki and Moncef Gueddari. This is an open access article distributed under the Creative Commons Attribution License, which permits unrestricted use, distribution, and reproduction in any medium, provided the original work is properly cited.

The production of phosphoric acid by the Tunisian Chemical Group, in Sfax, Tunisia, led to the degradation of the groundwater quality of the Sfax-Agareb aquifer mainly by the phosphogypsum leachates infiltration. Spatiotemporal monitoring of the quality of groundwater was carried out by performing bimonthly sampling between October 2013 and October 2014. Samples culled in the current study were subject to physicochemical parameters measurements and analysis of the major elements, orthophosphates, fluorine, trace metals, and stable isotopes (^{18}O , ^2H). The obtained results show that the phosphogypsum leachates infiltration has a major effect on the downstream part of the aquifer, where the highest values of conductivity, SO_4^{2-} , Ortho-P, and F^- , and the lowest pH were recorded. In addition, these results indicated that phosphogypsum leachates contained much higher amount of Cr, Cd, Zn, Cu, Fe, and Al compared to the groundwater. Spatiotemporal variation of the conductivity and concentrations of major elements is linked to the phosphogypsum leachates infiltration as well as to a wide range of factors such as the natural conditions of feeding and the water residence time. Contents of ^{18}O and ^2H showed that the water of the Sfax-Agareb aquifer undergoes a large scale evaporation process originated from recent rainfall.

1. Introduction

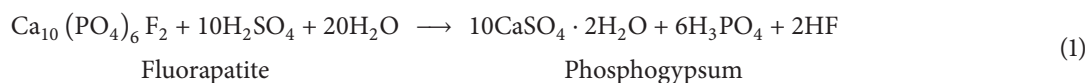
Groundwater pollution proves to be potentially threatening as it puts at jeopardy the hygienic integrity of a huge water reserve. The intensification of industrial activities, as well as the diversification of the storage modes of by-products production, makes groundwater resources vulnerable and can be considered as the main factors responsible for groundwater pollution. The groundwater quality is equally important as its quantity to the suitability of water for various purposes [1]. Variation of groundwater quality in different regions is a function of physical and chemical parameters that are greatly influenced by geological formations and anthropogenic activities [2]. Groundwater resources of the Mediterranean coastal plains in the southern bank of the basin (Middle East and North Africa) show a qualitative and quantitative deterioration developing in time [3–5] resulting in natural constraints and anthropological activities.

In Tunisia, climatic constraints, with a moderate rainfall contribution, which are unequally distributed in the space and irregular in time, as well as a strong evaporation power, make water resources limited. Socioeconomic development and the spread of industrialization have led to pressuring the resources and increasing the demand. Thus, the water supply, estimated at $472 \text{ m}^3/\text{inhabitant}$ in 2010, will decrease to $315 \text{ m}^3/\text{inhabitant}$ in 20 years [6]. In addition, water pollution related to the increased water use, urban and industrial areas, and agricultural intensification is increasingly threatening both the quality and the amount of groundwater resources. This phenomenon's implications are felt in the satisfaction of water demand as well as water cost.

Urban, industrial, and tourist centers have been developing along the eastern coast of Tunisia. Several industries are located in Sfax area, especially those of the Tunisian Chemical Group (TCG) for the enrichment and transformation of natural phosphate. The TCG activity focuses primarily on

the chemical fertilizers and phosphoric acid production, by the fluorapatite transformation. This production model generates gaseous emissions, liquid discharges, and huge

amounts of phosphogypsum (PG), issued from the treatment of phosphate rock with sulfuric acid [7–14]. This chemical reaction is illustrated in the equation below:



The main environmental contamination associated with PG dump is fluoride, sulfate, calcium, phosphate, and trace elements or radionuclides movement into groundwater [7]. The scope of this study is to appreciate the PG leachates infiltration effect on the Sfax-Agareb aquifer and to identify the factors and the phenomena, which explain the spatial and the temporal variation of the groundwater quality's assessment parameters.

2. Description of the Study Area

The study area is situated in the coast of Sfax, where the TCG plant, a discharge of domestic waste, and a station of wastewater treatment are located (Figure 1). The study area is under the influence of the Mediterranean climate, relatively humid and temperate, with cold and rainy seasons, between December and March, and dry and hot seasons, between June and October. The average annual precipitation is around 250 mm [15]. The mean annual temperature is 20°C [16]. The outcropping geological formations (Figure 2) are composed of sandy clays rich in gypsum and silty sand [17], of Mio-Pliocene to lower Quaternary age [18]. The TCG site takes place in an area covered by recent alluvium, made up by sand and calcareous gypsum crusts. The Sfax-Agareb aquifer, in this case study, is constituted by two sandy levels, ranging from 2 to 5 m in terms of thickness (Figure 3), separated by clay and sandy layers [19]. This aquifer is recharged by meteoric water. Groundwater flow in the study area is Northwest to Southeast.

3. Materials and Methods

3.1. Groundwater Sampling and Analysis. Groundwater samples were culled bimonthly from ten piezometers in the phreatic aquifer of Sfax-Agareb, between October 2013 and October 2014 (Figure 1). Monitoring piezometers purging was accomplished by using a submersible pump. The purge was achieved when the pH and the electrical conductivity (EC) of the ground water have been stabilized. Samples taken were acidified using 0.1 N HNO₃ and kept at 4°C until the analysis was thoroughly carried out aiming to optimize the accuracy of the obtained findings. The samples were analyzed for the following parameters, which include EC, pH, T, dissolved O₂, Cl[−], SO₄^{2−}, HCO₃[−], Na⁺, K⁺, Mg²⁺, Ca²⁺, F[−], and orthophosphates (Ortho-P). EC, pH, and dissolved oxygen were measured in the field using calibrated portable digital meters. Calcium, magnesium, sodium, and potassium were identified using atomic absorption spectrometer. Carbonate, bicarbonate, chloride, and sulfate were determined

by standard titration methods [21]. Orthophosphates were analyzed by absorption colorimeter [21] and fluoride ion concentrations were measured by specific electrode [21]. The accuracy of the chemical analysis was determined by calculating the ionic balance error, which was generally less than 5%. The trace elements were analyzed using inductivity coupled plasma-atomic emission spectrophotometer (ICP-AES). A summary of the physicochemical and chemical data of all the investigated groundwater during the period 2013–2014 is presented in Table 1. Stable isotope analysis of δ²H and δ¹⁸O was performed by cavity ring down spectrometry using a Picarro L2120 [22] at the laboratory of Applied Geology and Geo-Environment, Ibn Zohr University, Morocco.

3.2. Multivariate Statistical Analysis. The application of multivariate statistical analysis offers a clearer understanding of water quality and enables comparison of the different water samples [23] and making of correlations between chemical parameters and groundwater samples, respectively. The different elements combination (samples and parameters) is used in order to characterize the hydrogeochemical variation of the Sfax-Agareb aquifer, in the site of TCG, in order to predict the future of the PG leachate percolation as well as to assess the spatial variation of the groundwater chemical composition. In this study, only the principal component analysis (PCA) was carried. PCA of the experimental data has been performed using the Xlstat.

4. Results and Discussion

4.1. Characterization of PG Leachate. On global scale, 15% of the PG production is recycled while large quantities are stored in the factories vicinity, which are disposed mostly in big piles. They are located in coastal areas with phosphoric acid plants nearby, both as dry or wet staking and without treatment [24]. Since PG waste is generally transported and disposed as an aqueous slurry, dissolution/leaching of the chemical elements present in the PG can occur. Dissolved elements may be deposited in nearby soils or transferred to groundwater [25]. Thus, it is important to know the characteristics of leachate obtained from the PG waste dump. Table 2 lists the chemical composition of a typical sample of PG leachate sampling from the GCT site of Sfax. The leachate has a very low pH (1.3) and high concentrations of fluoride (3500 mg/L), orthophosphate H₂PO₄[−] (6730 mg/L), and toxic elements (Cd, Cr, and Zn). For all the analyzed elements, the levels exceeded the Tunisian standard for liquid discharge (NT 106-002).

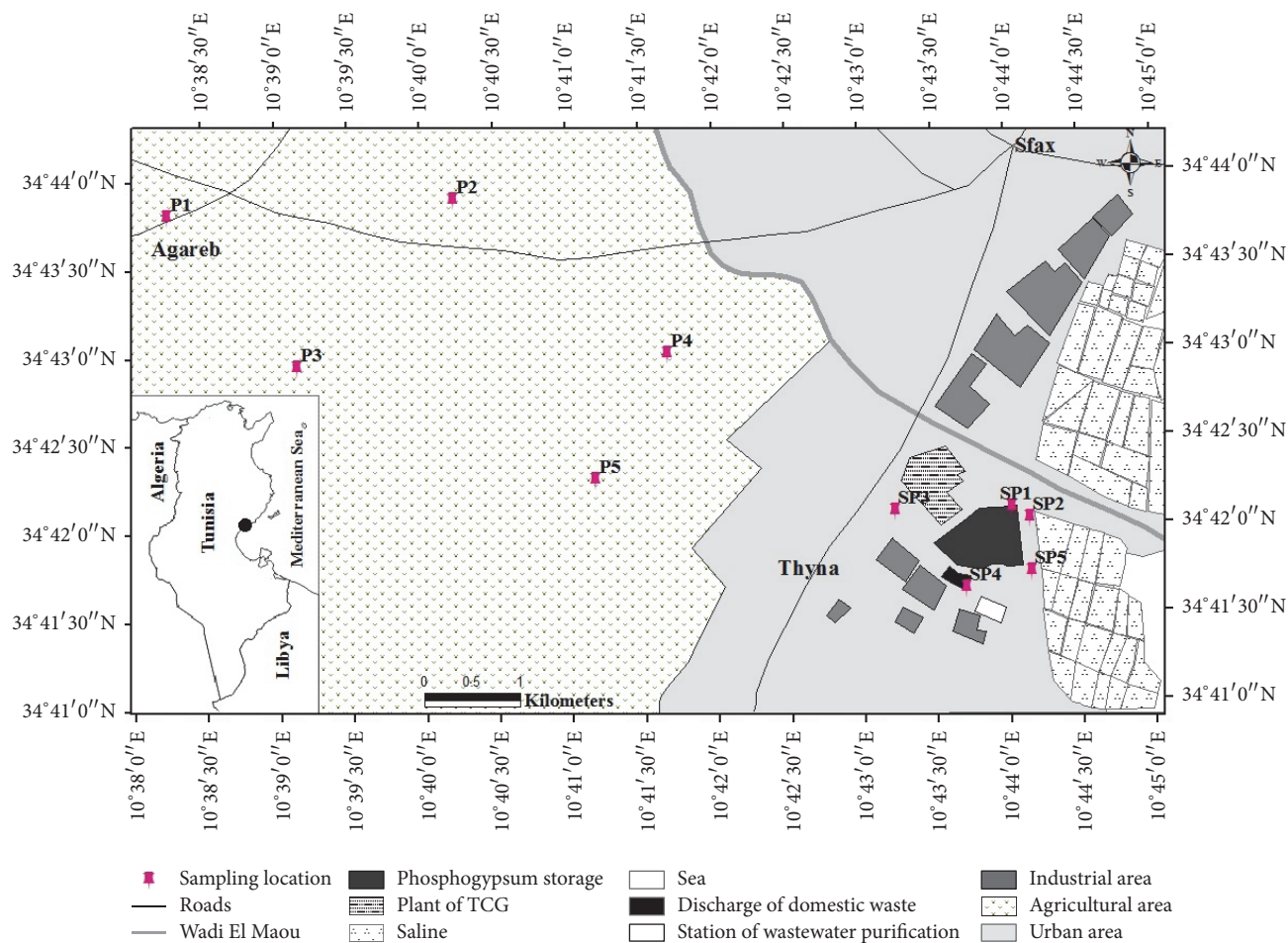


FIGURE 1: Location map of the study area showing piezometers and reference well sampled for groundwater analysis.

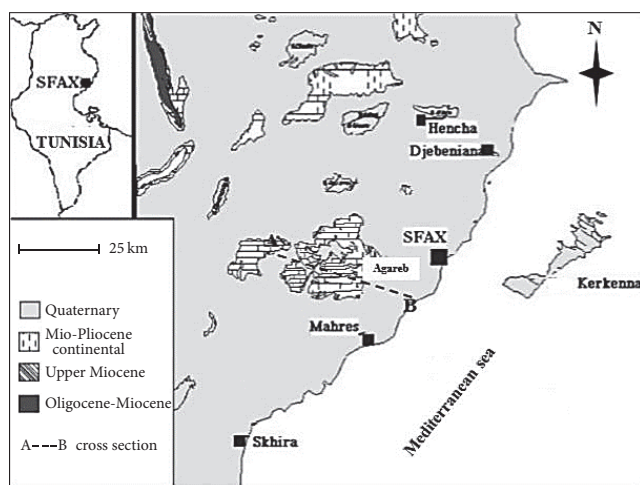


FIGURE 2: Geological map of Sfax [20].

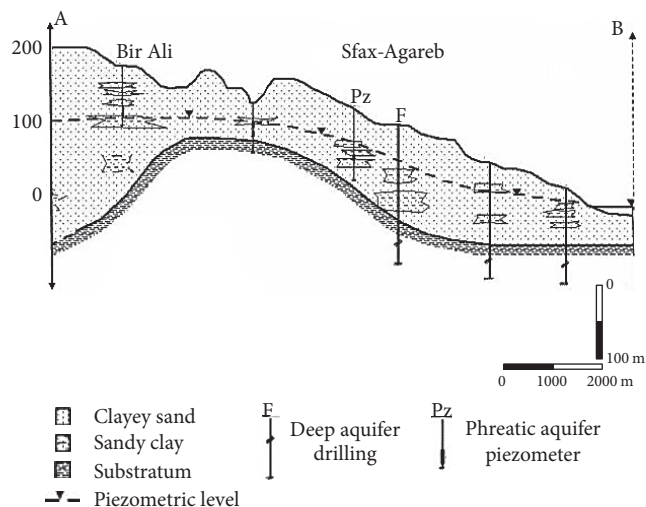


FIGURE 3: Hydrogeological cross-section along transect AB, as indicated in Figure 2 [19].

4.2. Groundwater Geochemical Characteristics and Evolution

4.2.1. Physicochemical Parameters. Groundwater temperature tends to vary from 10.1 to 13.9°C. The spatiotemporal variation of this parameter did not show any audible alternation during the whole period of testing (Figure 4(a)). The pH

values remain in the range of 5.18–7.95 as detailed. The lowest values were measured near PG storage site (SP1 and SP4), whereas in the upstream part of the study area (P1, P2, P3, P4, P5, and SP1) they were mainly neutral to slightly alkaline

TABLE 1: Chemical composition of groundwater samples

Months	Unit	Oct 13		Jan 14		Mar 14		May 14		Aug 14		Oct 14	
Parameters		Min	Max	Min	Max	Min	Max	Min	Max	Min	Max	Min	Max
T	°C	12.1	13.9	10.1	12.8	11	11.7	11.10	12.20	12.2	13.2	12.00	13.1
pH	mg/L	5.18	7.74	5.75	8.1	5.58	7.95	5.56	7.85	5.2	7.79	5.50	7.76
O ₂ dissolved	mg/L	0.9	2.15	0.9	4.2	0.8	3.5	0.80	3.12	0.7	2.9	0.50	2.8
EC	μs/cm	2100	33200	1590	33000	1650	32600	1680	34300	1800	34700	1900	34900
K ⁺	mg/L	2.7	22.70	2.25	19	2.15	19.6	2.60	19.50	2.5	21.2	2.7	23.68
Na ⁺	mg/L	111.5	6965	139.4	6760	142	6300	115.16	6124	198	6600	195	6515
Ca ²⁺	mg/L	59	986	49	904	50	851	54.36	1075	51	1080	58	1020
Mg ²⁺	mg/L	37	945	22.5	920	24	940	29.75	1085	25	1050	35	1080
Cl ⁻	mg/L	110.6	5480	104.3	5396	101	5372.5	151	5475	135.5	5810	112	5632.5
HCO ₃ ⁻	mg/L	256.4	9143.9	195.2	9661.5	271	9533.9	199.20	8533.9	245	9313.9	255	9973
SO ₄ ²⁻	mg/L	215	4396.1	201.5	4295.7	204	4352.9	261.25	4543.7	210	4857.3	210	4948.5
Ortho-P	mg/L	2.15	67.3	2.5	81.7	2.7	71.00	1.90	136.65	1.5	92	1.25	114.95
F ⁻	mg/L	0.6	26	0.6	27	0.50	19.00	0.50	29.00	0.5	17	0.6	19
Al	mg/L	0.02	1.8	0.03	1.57	0.03	0.90	0.06	0.98	0.02	0.96	0.03	0.97
Zn	mg/L	0.03	1.46	0.02	1.41	0.02	1.44	0.03	1.47	0.04	1.51	0.03	1.05

(Figure 4(b)). The contents of dissolved O₂ fluctuate between 0.5 and 4.2 mg/L. The spatial distribution of these values shows an increase as we move further from the site of PG storage, in the direction of groundwater flow (Figure 4(c)). The temporal variation of this parameter depends on the control of the depth of the water table, the recharge rate, the transfer speed of oxygenated water from the upstream to the downstream, and the temperature. The electrical conductivity (EC) ranged from 1590 μs/cm to 34900 μs/cm at 25°C. The highest value characterizes sampled water in the southwest (SP4) and in the southeast (SP5) of the study area, whereas the lowest EC was the main feature of the P1, P2, and P3 piezometers (Figure 4(d)). This spatial variation in the flow direction of the phreatic aquifer (North-West to Southeast) is related to sea water intrusion and to the infiltration of both PG leachate and saline brines. The highest values are recorded during the dry season (May, August, and October), while the lowest values are recorded during the wet season (January and March). The temporal variation is due to the dilution effect with fresh water in the recharge areas during the wet season and the direct evaporation, during the dry season, in areas with low hydraulic gradient and poor permeability [26].

4.2.2. Origin and Geochemical Behavior of Major Elements.

Concentrations of SO₄²⁻, HCO₃⁻, and Ca²⁺ ranged from 201.5 to 4948.5 mg/L, from 195.2 to 9973 mg/L, and from 49 to 1080 mg/L, respectively. During the study period, the higher contents of HCO₃⁻ and Ca²⁺ were registered in SP4 piezometer, whereas the optimal concentrations of SO₄²⁻ were measured in SP5 piezometer, which is located in the east of the PG storage.

Understanding of the water-rock interaction and the associated reactions in the aquifer is essential to identify the variability of Ca²⁺, HCO₃⁻, and SO₄²⁻ concentrations. The calculation of ions activities and the appreciation of the saturation state with respect to calcite and gypsum help

TABLE 2: Chemical composition of PG leachate in May 2014.

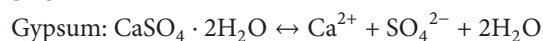
Parameters	Leachate PG	Tunisian standard for liquid discharge (NT 106-002)
EC	22700	
pH	1.3	6.5–8.5
F	3500	3
H ₂ PO ₄ ⁻	6730	0.05
Ca ²⁺	1357	500
SO ₄ ²⁻	3240	600
Mg ²⁺	198	200
Cl ⁻	1560	600
Na ⁺	2000	500
K ⁺	139	50
Cr	1.2	0.5
Cd	0.8	0.005
Zn	4	5
Al	4	5
Cu	0.5	0.5
Fe	6	1

Units in mg/L except pH and EC (μS/cm).

to assess the chemical composition of the groundwater and to identify the controlling geochemical reactions [27]. The flowing dissolution reactions ($T = 25^{\circ}\text{C}$ and $P = 1\text{ atm}$) are considered:



$$\log K_{\text{ps}} = \log a[\text{Ca}^{2+}] + \log a[\text{HCO}_3^-] + \text{pH} = 1.71 \quad [28]$$



$$\log K_{\text{ps}} = \log a[\text{Ca}^{2+}] + \log a[\text{SO}_4^{2-}] + 2 \log a[\text{H}_2\text{O}] = -4.61 \quad [29]$$

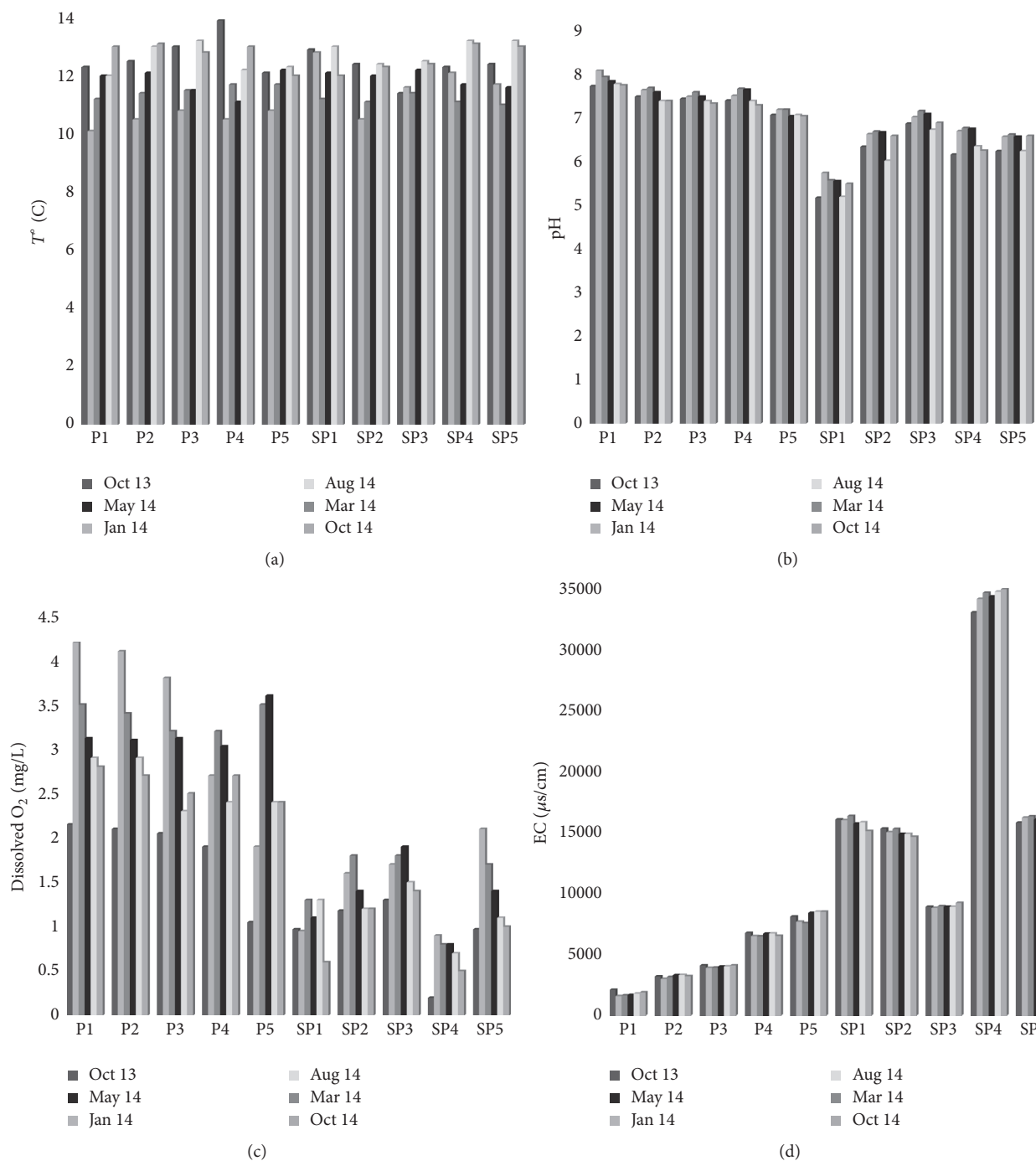


FIGURE 4: Distribution of temperature (a), pH (b), dissolved O_2 (c), and EC (d) in groundwater of Sfax-Agareb aquifer.

In order to calculate activities and ion activity product, the computer code PHREEQC [30] is used. The relation between the solubility product constant (K_{ps}) and the ion activities product (IAP) is given by the saturation index (SI) defined as

$$SI = \log \left(\frac{IAP}{K_{ps}} \right). \quad (2)$$

When $SI < 0$ water is considered undersaturated, whereas when $SI > 0$ water is considered oversaturated compared to the mineral.

The results show that the groundwater of the upstream zone of the phreatic aquifer (P1, P2, P3, P4, P5, and SP3) is undersaturated compared to gypsum (Figure 5), while, in the downstream zone, water with low pH (SP1, SP2, SP4, and SP5) is oversaturated. Compared to this mineral, the

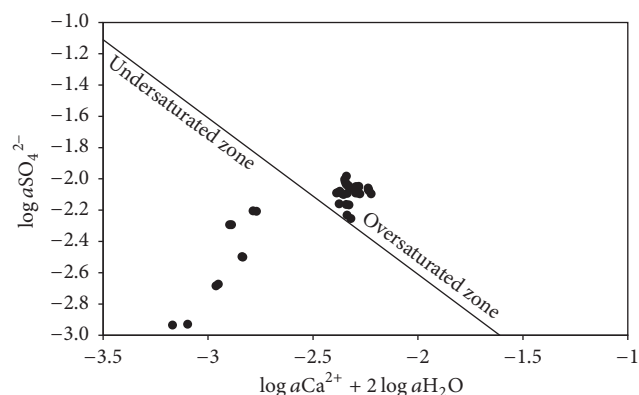


FIGURE 5: Equilibrium diagram of gypsum.

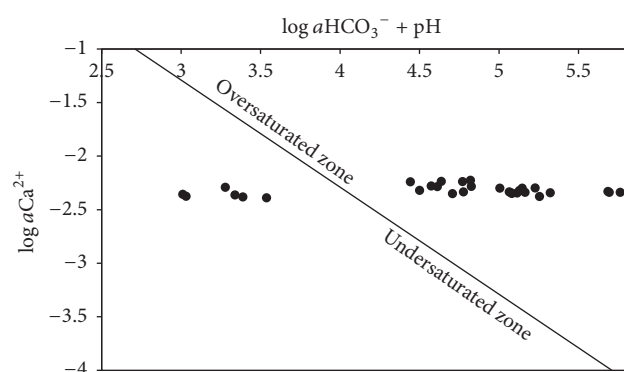
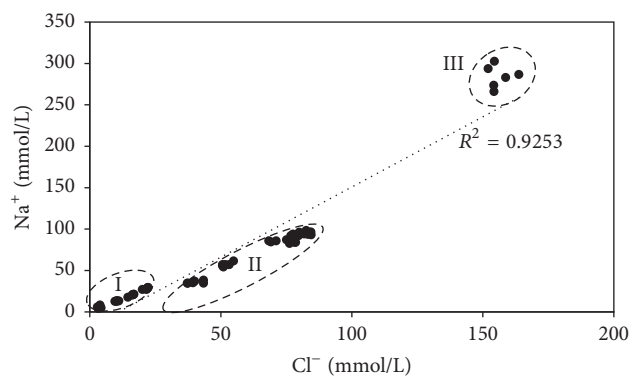
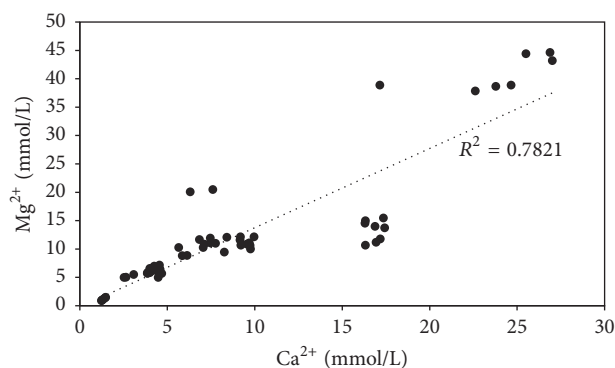


FIGURE 6: Equilibrium diagram of calcite.

groundwater oversaturation, in the TCG site, is explained by the acid PG leachate infiltration, which promotes the dissolution of gypsum and the complexation of Ca^{2+} and SO_4^{2-} ions. The equilibrium diagram Ca^{2+} - HCO_3^- (Figure 6) shows that groundwater, except for SP1 near the PG dump, is widely oversaturated compared to calcite. SP1 water is highly acidic, which prevents saturation with respect to calcite.

The sodium and chloride concentrations varied from 111.5 to 6965 mg/L and from 101 to 5810 mg/L, respectively. The Na^+ - Cl^- plot exhibits three water groups (Figure 7):

- (i) Group I: Na^+ and Cl^- contents are less than 50 mmol/L and 30 mmol/L, respectively. It concerns water of the upstream part of the study area (P1, P2, P3, and P4).
- (ii) Group II: Na^+ and Cl^- concentrations range from 50 to 120 mmol/L and from 30 to 100 mmol/L, respectively. This group encompasses water of the downstream zone, near the evaporation ponds (SP1, SP2, SP3, and SP5).
- (iii) Group III: Na^+ and Cl^- contents are greater than 250 mmol/L and 150 mmol/L, respectively. It includes water of SP4 piezometer, affected by the wastewater and the infiltration of PG leachate relatively rich in Na^+ and Cl^- (Table 2).

FIGURE 7: Plot of Na^+ against Cl^- .FIGURE 8: Plot of Ca^{2+} against Mg^{2+} .

The enrichment in Na^+ and Cl^- , from the upstream to the downstream, would be related to water-reservoir rock interaction, saline water infiltration from the evaporation ponds, and marine intrusion. During the study period, potassium concentrations are almost homogeneous at the same sampling location, with values ranging from 2.15 to 23.68 mg/L. The concentrations of Mg^{2+} , which fluctuate between 22.5 and 1085 mg/L, are positively correlated to Ca^{2+} contents, with a determination coefficient of 0.78, suggesting the same origin, which is the magnesian calcite dissolution (Figure 8). The highest values of the different majors elements are recorded during the dry season (October, August, and May), while the lowest values are recorded during the wet season (January and March). The slight variation is due to the dilution effect with fresh water in the recharge areas during the wet season and evaporation, during the dry season.

4.2.3. Orthophosphates and Fluorine Concentrations. Ortho-P and fluorine concentrations fluctuate between 1.5 and 136.65 mg/L and between 0.5 and 29 mg/L, respectively. Groundwater sampled near the PG discharge site showed high concentration levels of Ortho-P, which are larger in terms of extent and impact than those taken from the upstream part (Figure 9(a)). The highest levels of fluorine were measured in SP4 groundwater (Figure 9(b)). All shallow groundwater samples except P1, P2, and P3 contain $\text{F}^- > 1.5$ mg/L, which is the WHO drinking water standard. The

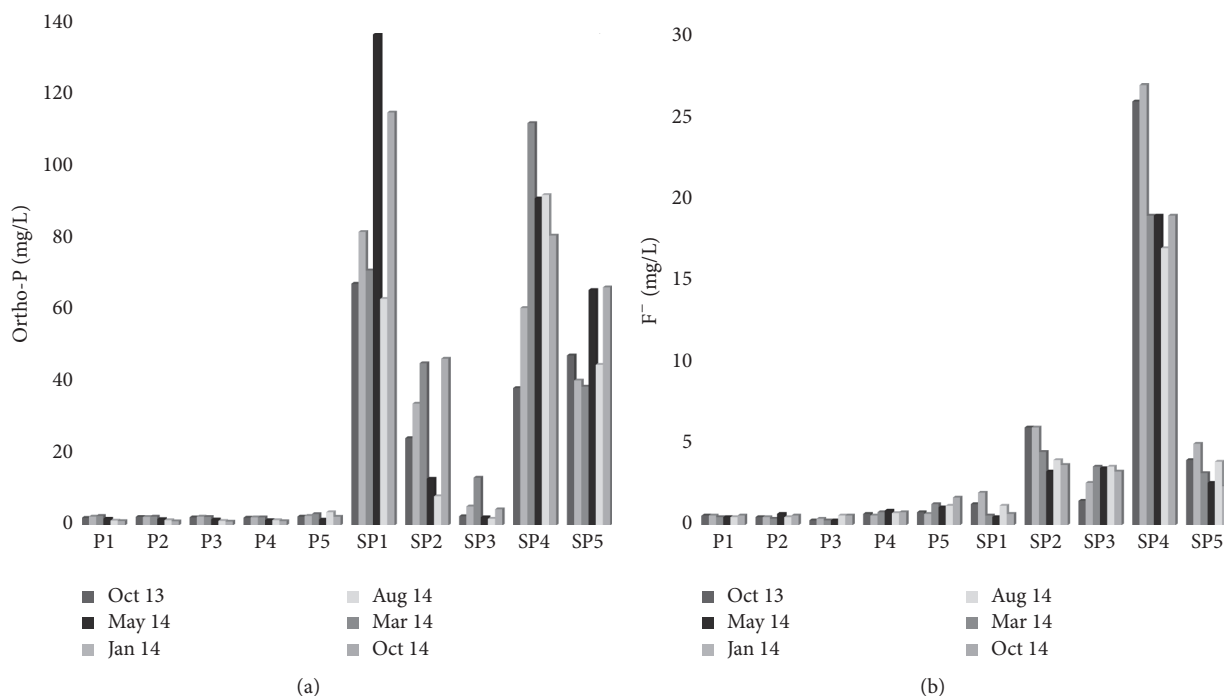


FIGURE 9: Distribution of orthophosphates (a) and fluorine (b) in Sfax-Agareb groundwater.

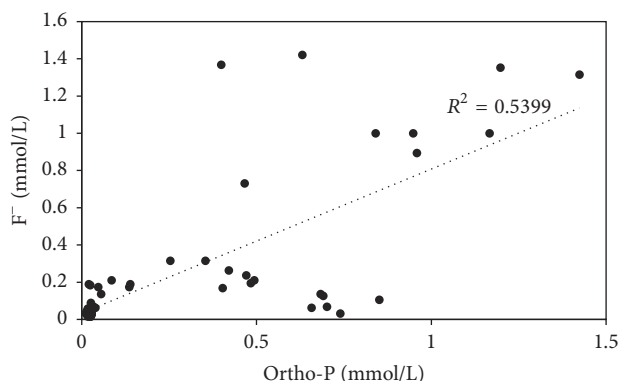


FIGURE 10: Plot of Ortho-P against fluoride.

spatial distribution of F⁻ and Ortho-P contents is related to the diffusion resulting from the flow direction of the aquifer as well as the chemical transformations of the PG leachates in the unsaturated zone. A significant temporal variation was recorded, due to the dilution during the recharging period. Plot of Ortho-P against fluoride (Figure 10) shows tremendous correlation, around the PG dump, suggesting that these elements originate from PG leachate, which are highly concentrated in Ortho-P and F⁻ (Table 2). On the other hand, groundwater of the upstream part does not show an evident correlation, which confirms the natural origin of these elements in this zone [31].

4.2.4. Trace Elements. The source of trace metals in the groundwater could be geogenic, but high concentrations

above the permissible limit of drinking water standards raise the suspicions of industrial contamination sources [32]. The concentrations of Zn and Al in the study area varied from 0.02 to 1.51 mg/L and from 0.02 to 1.8 mg/L, respectively. The higher contents of Zn were registered in SP4 piezometer, whereas the optimal concentrations of Al were measured in SP1 piezometer, which is located near the PG storage. For the majority of the sampled water, the Cr, Cd, and Cu contents do not exceed 0.05 mg/L. Low levels of trace elements noticed in the majority of the analyzed water, despite the gypsum water contamination, are linked to the purifying function of soils. The mechanisms that allow transforming charged surface water with dissolved, mineral, or organic matter into less charged water form the purifying functions of the soil [33].

4.3. Statistical Analysis. To discuss the relationships between the physicochemical parameters, major elements, Ortho-P, and fluorine in groundwater samples, PCA was used to distinguish the contributions of the natural and anthropogenic processes to the Sfax-Agareb aquifer, in the site of TCG.

Two independent factors were extracted, which explain 83.77% of the total variance. The first factor (F1) presents 72.34% of the total inertia. It is defined by EC and the Ca²⁺, Cl⁻, Na⁺, K⁺, Mg²⁺, HCO₃⁻, and SO₄²⁻ contents in a less important measurement by Ortho-P and F⁻. These elements contribute to the mineralization of the groundwater in TCG site. The second factor (F2) explains 11.43% of the total variance with a strong loading with pH and dissolved O₂ (Table 3). The spatial distribution of the variables (chemical parameters) and individuals (samples) in the axe systems F1-F2 shows the presence of two water groups (Figure 11).

TABLE 3: Summary of the PCA results including the loadings and the eigenvalues.

Variables	Axe F1	Axe F2
Na ⁺	0.9902	0.0400
Cl ⁻	0.9537	0.2568
K ⁺	0.9646	-0.0319
Ca ²⁺	0.9162	0.2195
SO ₄ ²⁻	0.7810	-0.3565
Mg ²⁺	0.8930	0.3142
HCO ₃ ²⁺	0.8782	0.4375
T°	0.1665	-0.3803
pH	-0.7253	0.6316
H ₂ PO ₄ ⁻	0.8026	-0.3231
F ⁻	0.8387	0.4741
Dissolved O ₂	-0.8304	0.3433
EC	0.9894	0.1067
Al	0.7383	-0.4214
Zn	0.9474	0.0343
Eigenvalues	10.8513	1.7147
% variance explained	72.3422	11.4312
% cumulative variance	72.3422	83.7734

TABLE 4: Isotopic and chloride composition of selected groundwater samples in October 2014.

	$\delta^{18}\text{O}$ (‰)	$\delta^2\text{H}$ (‰)	Cl ⁻ (mg/L)
P1	-5.97	-36.01	151
P2	-5.88	-35.98	356
P3	-5.64	-35.37	581
P4	-5.61	-35.22	776
P5	-5.57	-32.18	1739.5
SP1	-3.58	-26.80	2627
SP2	-4.12	-27.20	2130
SP3	-5.50	-34.47	745.5
SP4	-3.65	-26.10	5475
SP5	-4.10	-26.88	2094.5
Sfax rainwater	-4.60		10
Seawater	0.00		19000

The PCA confirm the different geochemical correlation and classification of the Sfax-Agareb groundwater, in TCG site, into two types: groundwater samples collected from the downstream part, which are influenced by the anthropogenic processes, largely controlled by the PG leachate percolation and the seawater intrusion. Samples collected from the upstream part of the study area were principally controlled by the natural recharge, with no evidence of high anthropogenic impacts.

4.4. Stable Isotopes (^{18}O , ^2H). The stable isotope composition of water in the study area varies from -5.97‰ to -3.58‰ V-SMOW for $\delta^{18}\text{O}$ and from -36.01‰ to 26.1‰ V-SMOW for $\delta^2\text{H}$. The $\delta^{18}\text{O}$ and $\delta^2\text{H}$ values (Table 4), plotted in Figure 12 in relation to the Global Meteoric Water Line

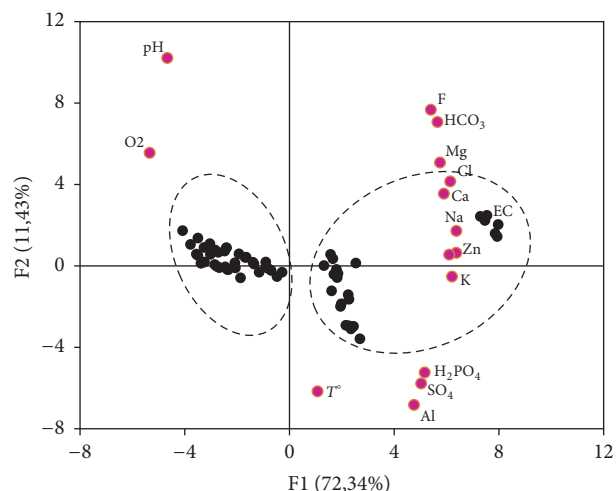
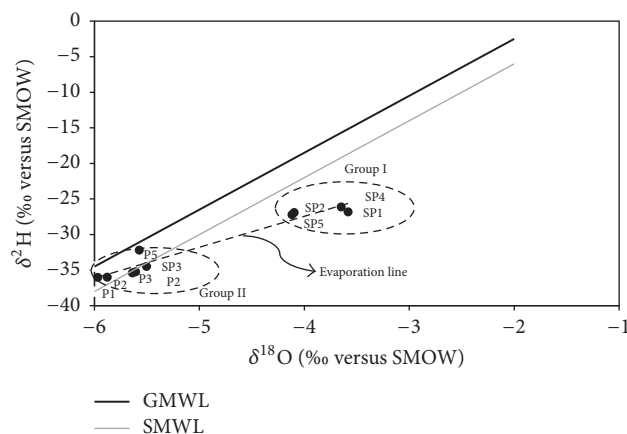


FIGURE 11: Spatial distribution of the variables and individuals in the axes system F.

FIGURE 12: $\delta^2\text{H}$ - $\delta^{18}\text{O}$ relationship of Sfax-Agareb groundwater.

(GMWL: $\delta^2\text{H} = 8\delta^{18}\text{O} + 10$) [34] and the Regional Meteoric Water Line of Sfax, Tunisia (SMWL: $\delta^2\text{H} = 8\delta^{18}\text{O} + 13.5$) [35, 36], show that most of the groundwater samples are located below the GMWL and near the SMWL which indicates water evaporation in the unsaturated zone. Therefore, groundwater isotopic enrichment might be the outcome from evaporation of recent precipitation. This is facilitated by the sandy clay lithology of the unsaturated zone and the low depth of the piezometric level, which is less than 10 m. The stable isotope signature of groundwater, in the study area, has identified two groups (Figure 12):

Group I is generated by the most enriched water in isotopes: SP1, SP2, SP4, and SP5 in the downstream part of the water table.

Group II involves water characterized by the lowest levels of $\delta^{18}\text{O}$ and $\delta^2\text{H}$: P1, P2, P3, P4, and SP3 in the upstream part of the water table.

The $\delta^{18}\text{O}/\text{Cl}^-$ diagram [37] confirms the groundwater distribution into two groups (Figure 13), weakly or strongly

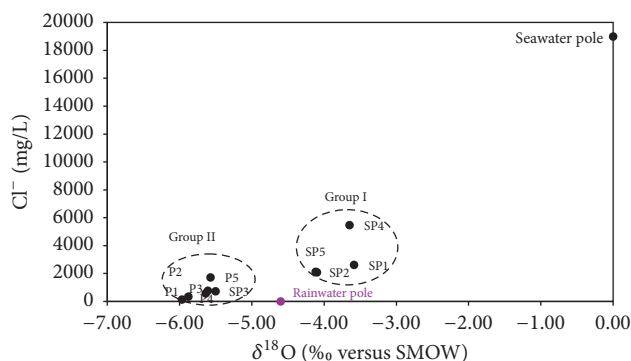


FIGURE 13: Cl^- - $\delta^{18}\text{O}$ relationship of Sfax-Agareb groundwater.

evaporated, which are distinguished by their chlorides and oxygen-18 contents. Indeed, the representative points of these two groups are located on either side of the rainwater pole, characterized by Cl^- and $\delta^{18}\text{O}$ contents, respectively, of 10 mg/L and 4, 6‰ V-SMOW.

The total dissolved solids of group I water, which are characterized by higher contents of Cl^- and $\delta^{18}\text{O}$ than those of rainwater, but lower than those of seawater, are related, in part, to evaporation.

5. Conclusion

The geochemical study of the major elements, Ortho-P, F^- , trace elements, and stable isotopes, elucidated the influence of PG leachates and laid emphasis upon the natural factors intervening in altering the groundwater chemistry of the Sfax-Agareb aquifer. Temporal variation was recorded due to dilution during the recharging period in winter. The groundwater mineralization is related to water-rock interaction processes, saline water, and PG leachates infiltration coupled with marine intrusion. Groundwater below the PG dump and in the downstream part of the aquifer showed the highest concentrations of Ortho-P, F^- , SO_4^{2-} , acidity, and total dissolved solids, which significantly exceed those relevant to the upstream water. Spatial distribution of these contents is presumably related to the diffusion that ensues the flow direction of the aquifer and the water-rock interaction. The groundwater quality is severely deteriorating in the downstream part of the Sfax-Agareb aquifer especially by Zn and Al. The stable isotope data attests that water of the Sfax-Agareb aquifer originated from recent rainwater has evaporated in the unsaturated zone. The result of this study will be helpful for a proper water development and for remediation of strategies to decrease the pollution source.

Conflicts of Interest

The authors declare that they have no conflicts of interest.

References

- [1] S. M. Yidana and A. Yidana, "Assessing water quality using water quality index and multivariate analysis," *Environmental Earth Sciences*, vol. 59, no. 7, pp. 1461–1473, 2009.
- [2] H. Vijith and R. Satheesh, "Geographical Information System based assessment of spatiotemporal characteristics of groundwater quality of upland sub-watersheds of Meenachil River, parts of Western Ghats, Kottayam District, Kerala, India," *Environmental Geology*, vol. 53, no. 1, pp. 1–9, 2007.
- [3] E. Custodio and G. A. Bruggeman, "Groundwater Problems in Coastal Areas," in *Studies and Reports in Hydrology*, vol. 45, UNESCO, 1987.
- [4] W. M. Edmunds, A. H. Guendouz, A. Mamou, A. Moulla, P. Shand, and K. Zouari, "Groundwater evolution in the Continental Intercalaire aquifer of southern Algeria and Tunisia: trace element and isotopic indicators," *Applied Geochemistry*, vol. 18, no. 6, pp. 805–822, 2003.
- [5] M. Ketata, F. Hamzaoui, M. Gueddari, R. Bouhlila, and L. Ribeiro, "Hydrochemical and statistical study of groundwaters in Gabes-south deep aquifer (south-eastern Tunisia)," *Physics and Chemistry of the Earth*, vol. 36, no. 5–6, pp. 187–196, 2011.
- [6] A. Sherif and D. Dadi, *Tunisia- Degradation Cost of water resources of the Medjerda Basin. Sustainable Water Integrated Management (SWIM) Support Mechanism*, Project funded by the European Union, 2012.
- [7] P. M. Rutherford, M. J. Dudas, and R. A. Samek, "Environmental impacts of phosphogypsum," *Science of the Total Environment*, vol. 149, no. 1–2, pp. 1–38, 1994.
- [8] H. T. Fukuma, E. A. N. Fernandes, and A. L. Quinelato, "Distribution of natural radionuclides during the processing of phosphate rock from Itataia-Brazil for production of phosphoric acid and uranium concentrate," *Radiochimica Acta*, vol. 88, no. 9–11, pp. 809–812, 2000.
- [9] P. P. Haridasan, C. G. Maniyan, P. M. B. Pillai, and A. H. Khan, "Dissolution characteristics of ^{226}Ra from phosphogypsum," *Journal of Environmental Radioactivity*, vol. 62, no. 3, pp. 287–294, 2002.
- [10] E. A. Abdel-Aal, "Crystallization of phosphogypsum in continuous phosphoric acid industrial plant," *Crystal Research and Technology*, vol. 39, no. 2, pp. 123–130, 2004.
- [11] C. Papastefanou, S. Stoulos, A. Ioannidou, and M. Manolopoulou, "The application of phosphogypsum in agriculture and the radiological impact," *Journal of Environmental Radioactivity*, vol. 89, no. 2, pp. 188–198, 2006.
- [12] T. Bituh, G. Marovic, Z. Franic, J. Sencar, and M. Bronzovic, "Radioactive contamination in Croatia by phosphate fertilizer production," *Journal of Hazardous Materials*, vol. 162, no. 2–3, pp. 1199–1203, 2009.
- [13] C. Roselli, D. Desideri, and M. A. Meli, "Radiological characterization of phosphate fertilizers: Comparison between alpha and gamma spectrometry," *Microchemical Journal*, vol. 91, no. 2, pp. 181–186, 2009.
- [14] P. Chauhan, R. P. Chauhan, and M. Gupta, "Estimation of naturally occurring radionuclides in fertilizers using gamma spectrometry and elemental analysis by XRF and XRD techniques," *Microchemical Journal*, vol. 106, pp. 73–78, 2013.
- [15] R. Trabelsi, M. Zairi, and H. B. Dhia, "Groundwater salinization of the Sfax superficial aquifer, Tunisia," *Hydrogeology Journal*, vol. 15, no. 7, pp. 1341–1355, 2007.
- [16] INM, "National Institute of Meteorology, climate data report for the period 2005–2015," 2015.
- [17] M. Ben Akacha, *Etude géologique de la région d'Agareb-Sfax Evolution géomorphologique, néotectonique et paléogéologique [Master, thesis]*, University of Sfax, Sfax, Tunisia, 2001.

- [18] P. F. Burollet, "Contribution à l'étude stratigraphique de la Tunisie Centrale., Tunisia," *Annuaire Géologique des Mines*, 1956.
- [19] R. Trabelsi, *Contribution à l'étude de la salinisation des nappes phréatiques côtières. Cas du système de Sfax-Mahdia [Ph.D. thesis]*, 2008.
- [20] M. Takrouni and J. Michelot, "Relation entre aquifère profond, nappes superficielles et intrusion marine dans le bassin de Sfax (Tunisie)," *Hydrogeology of the Mediterranean and Semi-arid Regions*, vol. 278, pp. 477–483, 2003.
- [21] J. Rodier, *L'analyse de l'eau. Eaux naturelles, eaux résiduaires, eau de mer*. Dunod, 8th edition, 2005.
- [22] Y. Ait Brahim, A. Benkaddour, M. Agoussine, A. Ait Lemkadem, L. A. Yacoubi, and L. Bouchaou, "Origin and salinity of groundwater from interpretation of analysis data in the mining area of Oumjrane, Southeastern Morocco," *Environmental Earth Sciences*, vol. 74, no. 6, pp. 4787–4802, 2015.
- [23] R. Ben Amor and M. Gueddari, "Major ion geochemistry of Ghannouch-Gabes coastline (at Southeast Tunisia, Mediterranean Sea): study of the impact of phosphogypsum discharges by geochemical modeling and statistical analysis," *Environmental Earth Sciences*, vol. 75, no. 10, article no. 851, 2016.
- [24] S. Sahu, P. Ajmal, R. Bhangare, M. Tiwari, and G. Pandit, "Natural radioactivity assessment of a phosphate fertilizer plant area," *Journal of Radiation Research and Applied Sciences*, vol. 7, no. 1, pp. 123–128, 2014.
- [25] L. Å. Reijnders, "Cleaner phosphogypsum, coal combustion ashes and waste incineration ashes for application in building materials: a review," *Building and Environment*, vol. 42, no. 2, pp. 1036–1042, 2007.
- [26] B. Tlili Zrelli and M. Gueddari, "Groundwater hydro-geochemistry of Mateur Alluvial Aquifer (Northern Tunisia)," *Journal of Hydrogeology and Hydrologic Engineering*, vol. 05, no. 01, 2016.
- [27] C. Appelo and D. Postma, *Geochemistry, Groundwater and Pollution, Second Edition*, Taylor & Francis, 2005.
- [28] H. C. Helgeson and D. H. Kirkham, "Theoretical prediction of the thermodynamic behavior of aqueous electrolytes at high pressures and temperatures; II, Debye-Huckel parameters for activity coefficients and relative partial molal properties," *American Journal of Science*, vol. 274, no. 10, pp. 1199–1261, 1974.
- [29] M. Gueddari, *Géochimie et thermodynamique des évaporites continentales, étude du lac Natron en Tanzanie et du Chott El Jrid en Tunisie. Thesis*, University of Louis Pasteur, Strasbourg, 1984.
- [30] D. L. Parkhurst and C. A. J. Appelo, "Description of input and examples for PHREEQC version 3-a computer program for speciation, batch-reaction, one-dimensional transport," in *and inverse geochemical calculations: U.S. Geological Survey Techniques and Methods, Book 6, Chap. A43*, p. 497, and inverse geochemical calculations, U.S. Geological Survey Techniques and Methods, 2013.
- [31] S. Melki and M. Gueddari, "Impact Assessment of Phosphogypsum on the Groundwater of Sfax-Agareb Aquifer," in *Proceedings of the in Southeast of Tunisia. ICEWE 2017 : 19th International Conference on Energy, Water and Environment. World Academy of Science, Engineering and Technology International Journal of Energy and Power Engineering Vol:11*, 2017.
- [32] A. G. S. Reddy, B. Saibaba, and G. Sudarshan, "Hydrogeochemical characterization of contaminated groundwater in Patancheru industrial area, southern India," *Environmental Modeling & Assessment*, vol. 184, no. 6, pp. 3557–3576, 2012.
- [33] B. J. Alloway, *Heavy metals in soils*, Blackie Academic & Professional, London, 2nd edition, 1995.
- [34] H. Craig, "Isotopic variation in meteoric waters. Science," in *Groundwater Problems in Coastal Areas*, vol. 45 of *Studies and Reports in Hydrology*, pp. 1702–1703, 1987.
- [35] A. Maliki, *Etude hydrogéologique, hydrochimique et isotopique de la nappe profonde de Sfax [Ph.D. thesis]*, University of Sfax, Sfax, Tunisia, 2000.
- [36] H. Jeanton, K. Zouari, Y. Travi, and A. Daoud, "Caractérisation isotopique des pluies en Tunisie. Essai de typologie dans la région de Sfax," *Earth and Planetary Science Letters*, vol. 333, pp. 625–631, 2001.
- [37] I. D. Clark and p. p. Fritz, *Environmental isotopes in hydrology*, CRC Lewis, Boca Raton, FL, USA, 1997.